Some Embedding Problems In 4-Dimensional Topology

by

Giulia Carfora

A thesis submitted in fulfilment of the requirements
for the degree of

Doctor of Philosophy

at the

School of Mathematics & Statistics
College of Science & Engineering
University of Glasgow

March 2026

Abstract

This thesis consists of two independent parts addressing problems related to smooth embeddings in 4-dimensional manifolds. In the first part, we consider embeddings of 3-dimensional lens spaces in the complex projective plane. Using an obstruction derived by Owens [59] and relying on Donaldson's Diagonalisation Theorem [16], we obtain a complete classification of lens spaces of Lisca type (2) or (3) [49] that are unobstructed from embedding in $\mathbb{C}P^2$. This classification is further refined for lens spaces $L(p,q)$ of Lisca type (2) or (3) with p even, using an obstruction due to Lidman–Moore–Vazquez [47].

In the second part, we consider a real projective plane smoothly embedded in $\mathbb{R}^4$, on which a height function restricts to a Morse function with five critical points. The aim is to generalise the work by Bleiler–Scharlemann [10] and prove that any such embedding of $\mathbb{R}P^2$ is standard, using 3-dimensional topological techniques and graphs of intersection. As the scope was not reached, the second part of the thesis presents an account of the approach undertaken.

Contents

Acknowledgements

First and foremost, I would like to thank my supervisor, Brendan Owens, for his guidance, support, and patience over the years. I also thank my second supervisor, Andy Wand, and the entire topology group at the University of Glasgow. I thank Rachael Boyd, Marco Golla, Ian Hambleton, Gordana Matić, Ana Lecuona, Mark Powell, Arunima Ray, and Martin Scharlemann for helpful conversations and advice.

The people, past and present, at the maths department in Glasgow truly shaped my PhD experience, and I want to thank all of them for their friendship and mathematical help. In particular, I would like to thank Alessandro, Clayton, Daniel, Franco, JJ, Livio, Marina, Miguel, Parth, Pasha, Paula, Sara, Sarah, Simone, and Xiaoqi. A special thank you goes to the Gym Gang, who rarely went to the gym together, and mostly spent time cooking and eating: Robin, Riccardo, and Francesco. Robin, thank you for helping me discover more about Glasgow and for being a supportive friend. I treasure all the food trips, karaokes, and chats together. Riccardo, thank you for all the laughs, gossip sessions, and weekend plans. You are one of the most empathetic people I know, and I truly cherish our friendship. Francesco, thank you for all the office crosswords, shared obsessions, and for trying to push me to reach my athletic peak. You are a really fun person to be around, and I hope we can have many more adventures together.

A heartfelt thank you goes to all the people from the Sandyford Henderson Community, who have been like a second family to me ever since I moved to Glasgow in 2016. In particular, I want to say thank you to Marta. It has been great to be your friend since our early days in Glasgow, and to go through our PhDs together.

Un ringraziamento speciale va a Ilaria, Pierpaolo, Marco e Valentina. Ilaria, è sempre bello vedere che nonostante gli anni e la distanza il nostro neurone in comune continui ad essere attivo. Spero che ci saranno molti altri giretti casoriani e serie trash da vedere insieme in futuro. Pierpaolo, grazie per tutti i rantini, le chiamate e i K-drama. Sono felice di poter contare sulla tua amicizia. MarcoRu, grazie per la tua amicizia in questi anni, per le chiacchierate, gli sfottò e i momenti di serietà quando necessario. Valentina, grazie per la tua amicizia fin dall'infanzia, so di potermi sempre aprire con te. Grazie per tutte le chiamate, gli anime, le ossessioni e i viaggi insieme.

Vorrei ringraziare la mia famiglia per il loro supporto durante gli anni a Glasgow, soprattutto Lorenzo, mio fratello e coinquilino. Grazie a Nonna Marro e a Davide, il QG.

Finally, thank you, Philipp, for your affection, support, patience and kindness. Thank you for always being there during difficult moments and for all your invaluable help.

Author's declaration

I declare that, except where explicit reference is made to the contribution of others, this dissertation is the result of my own work and has not been submitted for any other degree at the University of Glasgow or any other institution.

Chapter 1

Introduction

This thesis addresses two problems about smooth embeddings in a 4-manifold. It consists of two entirely independent projects and is divided into two parts. In the first, we discuss an obstruction to embeddings of 3-dimensional lens spaces in the complex projective plane. In the second part, we focus on embeddings of the real projective plane in the Euclidean 4-space. These problems are approached using very different techniques. We shall now present an overview of both projects, but each part of this thesis contains a thorough introduction to the relevant problem and methodology employed.

Let $L(p,q)$ be a 3-dimensional lens space that embeds in $\mathbb{C}P^2$. Using standard homology arguments, it can be shown that given such an embedding, $L(p,q)$ must separate $\mathbb{C}P^2$ into two 4-manifolds, which we may call M and B. Since $\mathbb{C}P^2$ is a positive definite manifold, we deduce that M is also positive definite, and furthermore $H_1(M;\mathbb{Z}) = 0$ and $H_2(M;\mathbb{Z}) \cong \mathbb{Z}$. The manifold B is a rational homology 4-ball; this indicates that to work with embeddings in $\mathbb{C}P^2$ we need to restrict our interest to lens spaces that bound rational homology 4-balls, which have been classified by Lisca in [49]. The classification is presented in Theorem 3.2, and can be divided into three families of lens spaces.

A lens space $L(p,q)$ can also be described as the boundary of a positive definite plumbing, a 4-manifold whose construction is presented in Chapter 3. Let X be the manifold obtained by gluing M and P, the canonical positive definite plumbing bounded by $-L(p,q)$, along their common boundary. Observe that X is a smooth closed positive definite manifold, hence by Donaldson's Diagonalisation Theorem 3.8, its intersection lattice is isomorphic to the standard lattice on $\mathbb{Z}^{n+1}$, where $n = b_2(P)$. It follows that the intersection lattices on M and P embed in this standard lattice on $\mathbb{Z}^{n+1}$. Based on

the assumption that $L(p,q) = \partial M$ and $-L(p,q) = \partial P$ as above, Owens in [59] derives some constraints on the aforementioned lattice embeddings. The result is presented in Proposition 3.9, which provides an obstruction to embedding $L(p,q)$ in $\mathbb{C}P^2$. We shall call lens spaces that satisfy the conditions of Proposition 3.9 *DO-unobstructed*.

In the first part of this thesis, we focus on lens spaces of Lisca type (2) and (3) from Theorem 3.2, and derive a complete classification of which ones are DO-unobstructed from embedding in $\mathbb{C}P^2$, using Donaldson's Diagonalisation Theorem 3.8 and Proposition 3.9.

Theorem 1 *Any lens space $L(m^2,q)$, up to diffeomorphism and orientation reversal, that embeds in $\mathbb{C}P^2$ and is of Lisca type (2) or (3) must have m and q of one of the following forms:*

(1) $m = (2s+3)k^2+1$ *and* $q = m^2-(2s+3)(m-1)$, *with* $s \geq 0$ *and* $k \neq 0, \pm 1$;

(2) $m = 24k^2+12k+2$ *and* $q = (m+1)(8k^2+4k+1)$, *with* $k \neq 0$;

(3) $m = 81k^2-72k+17$ *and* $q = 9(m+1)$, *with* $k \in \mathbb{Z}$;

(4) $m = 3k^2-1$ *and* $q = 6k^4-3k^2$, *with* $k \neq 0, \pm 1$;

(5) $m = 18k+23$ *and* $q = (m+1)(4k+5)$, *with* $k \geq 0$;

(6) $m = 81k^2+36k+5$ *and* $q = 9(m+1)$, *with* $k \neq 0$;

(7) $m = (2t+5)k^2-1$ *and* $q = (2m-1)k^2$, *with* $t \geq 0$ *and* $k \neq 0, \pm 1$;

(8) $m = 18k+17$ *and* $q = (2m-1)(2k+2)$, *with* $k \geq 0$;

(9) $m = 18k+31$ *and* $q = (4k+7)(m-1)$, *with* $k \geq 1$;

(10) $m = 128k^2+48k+5$ *and* $q = 4(32k^2+12k+1)^2$, *with* $k \neq 0$;

(11) $m = 128k^2-80k+13$ *and* $q = 4(32k^2-20k+3)^2$, *with* $k \in \mathbb{Z}$;

(12) $m = 18k+19$ *and* $q = 162(k+1)$, *with* $k \geq 0$;

(13) *either of* $L(7^2,31)$, $L(9^2,50)$, $L(31^2,270)$ *or* $L(11^2,50)$.

Furthermore, we also consider an obstruction due to Lidman–Moore–Vazquez, presented in Theorem 5.2, concerning the d-invariants of a lens space $L(m^2,q)$ bounding a spin Kollár manifold M: from Theorem 5.1 we shall see that this obstruction is only defined for lens spaces with m even. We shall call lens spaces that satisfy the conditions of

Theorems 5.2 and 5.1 *LMV-unobstructed*. The analysis carried out yields additional constraints on which lens spaces with even m are LMV-unobstructed from embedding in $\mathbb{C}P^2$, presented below.

Theorem 2 *Any lens space $L(m^2, q)$ that embeds into $\mathbb{C}P^2$, and is of Lisca type (2) or (3) with m even, must be, up to diffeomorphism and orientation reversal, either $L(26^2, 243)$, or $L((24k^2+12k+2)^2, 3(8k^2+4k+1)^2)$ with $k \neq 0$.*

The results from Theorems 1 and 2 can be combined as follows.

Main Theorem. *Any lens space $L(m^2, q)$, up to diffeomorphism and orientation reversal, that embeds in $\mathbb{C}P^2$ and is of Lisca type (2) or (3) must have m and q of one of the following forms:*

(1) $m = (2s+3)k^2+1$ *and* $q = m^2-(2s+3)(m-1)$, *with* $s \geq 0$ *and* $k \neq 0, \pm 1$ *even;*

(2) $m = 24k^2+12k+2$ *and* $q = (m+1)(8k^2+4k+1)$, *with* $k \neq 0$;

(3) $m = 81k^2-72k+17$ *and* $q = 9(m+1)$, *with* $k = 1$ *or* k *even;*

(4) $m = 3k^2-1$ *and* $q = 6k^4-3k^2$, *with* $k \neq 0, \pm 1$ *even;*

(5) $m = 18k+23$ *and* $q = (m+1)(4k+5)$, *with* $k \geq 0$;

(6) $m = 81k^2+36k+5$ *and* $q = 9(m+1)$, *with* $k \neq 0$ *even;*

(7) $m = (2t+5)k^2-1$ *and* $q = (2m-1)k^2$, *with* $t \geq 0$ *and* $k \neq 0, \pm 1$ *even;*

(8) $m = 18k+17$ *and* $q = (2m-1)(2k+2)$, *with* $k \geq 0$;

(9) $m = 18k+31$ *and* $q = (4k+7)(m-1)$, *with* $k \geq 1$;

(10) $m = 128k^2+48k+5$ *and* $q = 4(32k^2+12k+1)^2$, *with* $k \neq 0$;

(11) $m = 128k^2-80k+13$ *and* $q = 4(32k^2-20k+3)^2$, *with* $k \in \mathbb{Z}$;

(12) $m = 18k+19$ *and* $q = 162(k+1)$, *with* $k \geq 0$;

(13) *either of* $L(7^2, 31)$, $L(9^2, 50)$, $L(31^2, 270)$ *or* $L(11^2, 50)$.

Using methods by Golla–Owens in [28, Propositions 6.3, 6.5], it is possible to construct embeddings of triples of lens spaces in a homotopy $\mathbb{C}P^2$ or $\overline{\mathbb{C}P^2}$, which include lens spaces of Lisca type (2) or (3) from the Main Theorem. For instance, one may show that the lens spaces $L(5^2, 11)$, $L(26^2, 243)$, and $L(3^2, 4)$ disjointly embed in a homotopy $\mathbb{C}P^2$ or

$\overline{\mathbb{C}P^2}$. Note that the lens space $L(26^2, 243)$ is of Lisca type (3).

In the second part of the thesis, we consider a smooth embedding of $\mathbb{R}P^2$ in $\mathbb{R}^4$ on which a height function from $\mathbb{R}^4$ to $\mathbb{R}$ restricts to a Morse function with five critical points. The work undertaken aims to show that any such embedding is isotopic to the standard embedding of $\mathbb{R}P^2$ in $\mathbb{R}^4$: unfortunately, the scope was not reached, but we present the approach employed and what was understood about this problem along the way. By standard embedding of $\mathbb{R}P^2$ in $\mathbb{R}^4$ we shall mean the real projective plane obtained by gluing an unknotted disc sitting in $\mathbb{R}^3 \times [0, \infty)$ to the unknotted Möbius band in $\mathbb{R}^3 \times \{0\}$ along S^1 [10]. The problem considered is a direct generalisation of the one in [10], in which Bleiler–Scharlemann prove that any real projective plane embedded in $\mathbb{R}^4$ with three critical points is standard.

Movie pictures and graphs of intersection are the main tools employed to tackle this problem. Given an embedding of a surface in 4-space, movie pictures were developed by Fox [23] and offer a way to visualise the embedding. The rough idea is to slice the embedded surface via 3-dimensional hyperplanes that are "perpendicular" to it (the precise definition is presented in Chapter 7): the intersection of the hyperplanes with the surface will correspond to a collection of knots and links, with singular intersections represented by band moves. The collection of hyperplanes that have a non-empty intersection with the surface is called a movie picture. This tool allows us to reduce questions about smooth embeddings of surfaces in 4-space to questions about knots and links in 3-space with bands attached. We may assume that a movie decomposition of $\mathbb{R}P^2$ with five critical points consists of a 2-component unlink with two bands attached, yielding an unknot (see Chapter 8 for a detailed explanation). In particular, the aim of our project can be rephrased in knot-theoretical terms: this is done in Objective 8.1.1, which says that up to isotopy and interaction of the bands, there is a unique way to obtain this movie picture.

To prove Objective 8.1.1, we wish to prove an intermediate statement. Consider the aforementioned movie picture. Let $\hat{P}$ be a sphere separating the components of the unlink and $\hat{Q}$ be the disc bounded by the unknot. We wish to understand how these surfaces can intersect, and in particular, would like to prove that these intersections can always be reduced in an appropriate sense, made clear in Objective 8.1.2. The intersections of these surfaces with each other and with the bands from the movie picture above are studied using graphs of intersection, which were first introduced by Litherland in [52]. On each surface, it is possible to construct a graph: the vertices correspond to intersections with

the bands, while the edges are arcs in the punctured $\hat{P} \cap \hat{Q}$. The edges of the two graphs constructed on $\hat{P}$ and $\hat{Q}$ are in bijection. Using classical methods from graph theory, one aims to understand and control the punctured $\hat{P} \cap \hat{Q}$.

Given the overarching theme of smooth embeddings in 4-dimensional manifolds, this thesis showcases how different tools can be employed to tackle problems in low-dimensional topology.

Part I

Embeddings of Lens Spaces in $\mathbb{C}P^2$

Chapter 2

Introduction

In this part of the thesis, we address the historically rich issue of smooth embeddings of orientable manifolds. In the early 1960s, Wall built on Hirsch's earlier work ([37]) and proved that any 3-manifold embeds smoothly in 5-space [72]. As in this result we talk about codimension 2 embeddings, the next step is to ask whether this holds for codimension 1 embeddings as well. Do all 3-manifolds smoothly embed in 4-space? The answer to this question has been known to be negative for a long time.

Let Y be a rational homology 3-sphere (i.e. a 3-manifold whose rational homology groups are the same as those of S^3) that smoothly embeds in S^4. Using Mayer-Vietoris it can be seen that such an embedding separates the 4-sphere in two sub-manifolds A and B such that $S^4 = A \bigcup_Y B$ (a similar argument will be presented in detail in the next chapter concerning embeddings in $\mathbb{C}P^2$). In the late 1930s, Hantzsche argued that such a manifold Y must have $H_1(Y;\mathbb{Z}) \cong G \oplus G$, where G is a finite abelian group [36]. Indeed, the Mayer-Vietoris sequence for cohomology tells us that

$$H^2(Y;\mathbb{Z}) \cong H^2(A;\mathbb{Z}) \oplus H^2(B;\mathbb{Z}),$$

while by Alexander duality we have $H^2(A;\mathbb{Z}) \cong H_1(S^4 \backslash A;\mathbb{Z}) \cong H_1(B;\mathbb{Z})$ and similarly $H^2(B;\mathbb{Z}) \cong H_1(A;\mathbb{Z})$. By the Universal Coefficient Theorem, the torsion subgroups of $H^2(A;\mathbb{Z})$ and $H^2(B;\mathbb{Z})$ are isomorphic and shall be denoted by G. Hence, $H_1(Y;\mathbb{Z}) \cong H^2(Y;\mathbb{Z}) \cong G \oplus G$.

After S^3, lens spaces are the next simplest manifolds in terms of handle decomposition. For $p > q > 0$ coprime integers, one may define the lens space $L(p,q)$ as the result of $-\frac{p}{q}$ surgery on the unknot in S^3. Different definitions of this manifold will be discussed in

greater detail in the next chapter. Lens spaces are known to be rational homology 3-spheres and $H_1(L(p,q);\mathbb{Z}) = \mathbb{Z}/p\mathbb{Z}$. Therefore, Hantzsche's argument above proves that lens spaces are manifolds that do not embed in S^4, thus showing that matters are more complicated for codimension 1 embeddings.

Embeddings of lens spaces in 4-space have attracted considerable attention over the years, yielding many interesting results. Let $L_0(p,q)$ denote a punctured lens space. In [18], Epstein proved that when p is odd there exists a smooth embedding of $L_0(p,q)$ in S^4. This was also confirmed by Zeeman in [73], who employed a construction called k-twist spinning. Roughly speaking, from a given knot $K \subset S^3$ we may remove a small segment and spin the remaining arc while twisting the knot k times; this will yield a 2-knot $S_k(K) \subset S^4$. When $k = 1$, $S_1(K)$ is unknotted for any K, and has a section $K\# - K$ whose double branched cover $\Sigma_2(S^3, K\# - K) \cong \Sigma_2(S^3,K)\# - \Sigma_2(S^3,K)$ smoothly embeds in S^4. When K is a 2-bridge knot, the lens space $L(p,q)$ with odd p is its double branched cover; hence $L(p,q)\# - L(p,q)$ embeds smoothly in S^4. This is equivalent to Epstein's result since the tubular neighbourhood of $L_0(p,q)$ is $L_0(p,q)\times I$ with boundary $L(p,q)\# - L(p,q)$ [3].

The question of which connected sums of lens spaces smoothly embed in S^4 was settled by Donald in 2015 [14]. Let $L = \#_{i=1}^{h} L(p_i,q_i)$; then L embeds smoothly in S^4 if and only if each p_i is odd and there exists Y such that $L \cong Y\# - Y$ [14].

Many intermediate results were obtained concerning embeddings of connected sums of lens spaces into S^4, both in the smooth and topological categories. More can be found in [14, 27, 63], and [3] provides a comprehensive survey.

The study of smooth embeddings of lens spaces (and of orientable 3-manifolds in general) into 4-manifolds did not stop at S^4. In fact, Edmonds–Livingston in [17] showed that any punctured lens space smoothly embeds in $S^2 \times S^2$, and that for any non-punctured lens space $L(p,q)$ there exists $n \in \mathbb{N}$ such that $L(p,q)$ embeds smoothly in $\#_n S^2 \times S^2$. In fact, the latter statement is true for any closed, orientable 3-manifold. Achieving a lower bound on n for different such 3-manifolds is an interesting problem on its own, and it was tackled in [1].

It is also interesting to study embeddings of orientable 3-manifolds in definite 4-manifolds,

although we shall focus on lens spaces. Again in [17], it was proved that every lens space embeds smoothly in $\#_n\mathbb{C}P^2$ for some $n \in \mathbb{N}$. The paper presents many results on such embeddings of $L(p,q)$, both in the topological and smooth category, which yield restrictions on n, p and q. These are nicely summarised in a table at the end of [17].

In this thesis we address obstructions to smooth embeddings of individual lens spaces in $\mathbb{C}P^2$. The reason for focusing on $\mathbb{C}P^2$ is that it is a (positive) definite manifold and it has a simple structure in terms of handle decomposition, making it the most natural manifold to consider for such embeddings after S^4. Moreover, note that proving that a lens space is obstructed from embedding in $\mathbb{C}P^2$ implies that $n \geq 2$ in the problem mentioned above.

In Proposition 3.1, we show that a lens space embedding in $\mathbb{C}P^2$ must separate it into two components, one of which is a rational homology ball. In [49], Lisca completely classified which lens spaces bound a rational homology ball. The problem of embedding a single lens space in $\mathbb{C}P^2$ is then equivalent to that of embedding a rational homology ball it bounds. This leads us to an intersection with a wider issue in algebraic geometry.

Let (m_1, m_2, m_3) be a *Markov triple*, that is, a triple of positive integers forming a solution to $m_1^2 + m_2^2 + m_3^2 = 3m_1m_2m_3$. Such a triple gives rise to an embedding

$$\bigsqcup_{i=1}^{3} B_{m_i,k_i} \hookrightarrow \mathbb{C}P^2,$$

where each B_{m_i,k_i} is a rational homology ball obtained as the Milnor fiber of a smoothing of the corresponding cyclic quotient singularity $\frac{1}{m_i^2}(1, m_ik_i{-}1)$ with $\gcd(m_i, k_i) = 1$; B_{m_i,k_i} has boundary $L(m_i^2, m_ik_i{-}1)$. This embedding arises from the smoothing of three singular points in the weighted projective space $\mathbb{P}(m_1^2, m_2^2, m_3^2)$ [59]. Hacking–Prokhorov showed in [35] that any projective surface X admitting a smoothing to $\mathbb{C}P^2$ is $\mathbb{Q}$-Gorenstein deformation equivalent to some $\mathbb{P}(m_1^2, m_2^2, m_3^2)$, thus giving rise to an embedding of disjoint rational homology balls as above. Evans–Smith in [20] generalised this result to the symplectic case. In [59], Owens provided smooth non-symplectic embeddings of such rational homology balls. This work was later extended to disjoint triples of rational homology balls by Lisca–Parma in [51], and again by Golla–Owens in [28]. Much of this work concerning triples of rational homology balls was motivated by a conjecture by Kollár, which we shall discuss at a later stage.

Let us now return to individual lens spaces bounding rational homology balls; Lisca's classification is presented in Theorem 3.2 in the next chapter. Much of the work mentioned up to now, especially by Owens [59] and Golla–Owens [28], provides smooth embeddings in $\mathbb{C}P^2$ of lens spaces of type (1) from Theorem 3.2. This thesis addresses embeddings of lens spaces of type (2) and (3) from the same theorem, using an obstruction derived by Owens in [59]. This obstruction relies on Donaldson's Diagonalisation Theorem from [16] (presented in Theorem 3.8), which states that the intersection lattice of a closed, oriented, smooth, positive definite 4-manifold is equivalent to the standard integer lattice over $\mathbb{Z}^n$.

Let us outline the obstruction work presented in this part of the thesis. A lens space that embeds in $\mathbb{C}P^2$ splits off a rational homology ball B and a positive definite manifold M such that $H_1(M;\mathbb{Z}) = 0$ and $H_2(M;\mathbb{Z}) \cong \mathbb{Z}$. We construct a new positive definite manifold X by gluing M and P, the canonical positive definite plumbing bounded by $-L(p,q)$, along their common boundary. By Donaldson's Diagonalisation Theorem, this manifold has intersection lattice isomorphic to the standard one on $\mathbb{Z}^{n+1}$, where $n = b_2(P)$. The intersection lattices of M and P embed in the standard lattice on $\mathbb{Z}^{n+1}$ and satisfy some additional requirements derived by Owens and presented in Proposition 3.9.

Finding a lattice embedding satisfying Proposition 3.9 implies that the lens space $L(p,q)$ is DO-unobstructed from embedding in $\mathbb{C}P^2$. In general, we must work with the intersection lattices of both the plumbing bounded by $L(p,q)$ and that bounded by $-L(p,q)$. If it is not possible to find an embedding as in Proposition 3.9 for either lattice, then we conclude that $L(p,q)$ does not embed in $\mathbb{C}P^2$.

This analysis was carefully carried out for all lens spaces of type (2) or (3) of Theorem 3.2. It yielded a complete classification of all such lens spaces that are DO-unobstructed from embedding in $\mathbb{C}P^2$. The precise statement is presented in Theorem 1. The result is then refined in Theorem 2 for lens spaces of type (2) or (3) with p even, using an obstruction by Lidman–Moore–Vazquez [47] presented in Theorem 5.2. The latter concerns d-invariants and restrictions of Spin structures from appropriate 4-manifolds.

Finally, we remark that the techniques used to obtain Theorem 1 underpin many of the results mentioned in this introduction, showcasing the importance of Donaldson's Diagonalisation Theorem. More recent work employing these techniques includes [39], in which

Jo–Park–Park obtain infinite families of lens spaces bounding smooth 4-manifolds with $b_2 = 1$ together with different constraints, and [4], where Aceto–McCoy–Park address the problem of determining which smooth negative definite filling of a connected sum of lens spaces has minimal second Betti number.

Overview. This first part of the thesis is divided into four chapters: in Chapter 3 we introduce the required terminology, carefully set up the problem, and state the main result; in Chapter 4 we first discuss in greater detail the method of proof of Theorem 1 and then proceed to analyse each case; in Chapter 5 we discuss the obstruction due to Lidman–Moore–Vazquez and prove Theorem 2; finally, in Chapter 6 we discuss future directions.

Chapter 3

Deriving a Lattice Obstruction

§ 3.1 | Properties of Lens Spaces in $\mathbb{C}P^2$

As the simplest closed 3-manifolds after S^3, lens spaces are the focus of the first part of this thesis. There are several equivalent definitions of this class of manifolds, out of which we shall provide two. We remark that we are interested in 3-dimensional lens spaces, but this class of manifolds exists in higher-dimensional versions as well.

Let $p > q > 0$ be coprime integers. Visualise the 3-sphere as sitting in $\mathbb{C}^2$, that is $S^3 = \{(z_1, z_2) \in \mathbb{C}^2 \mid |z_1|^2 + |z_2|^2 = 1\}$. The lens space $L(p, q)$ is defined as the orbit space of the free action of $\mathbb{Z}/p\mathbb{Z}$ on S^3 generated by the rotation homeomorphism of S^3, defined as $r(z_1, z_2) = (e^{\frac{2\pi i}{p}} \cdot z_1, e^{\frac{2\pi qi}{p}} \cdot z_2)$. In particular observe that when $p = 2$, r is the antipodal map and $L(2, 1) \cong \mathbb{R}P^3$. From this definition we directly deduce that $\pi_1(L(p, q)) \cong \mathbb{Z}/p\mathbb{Z}$.

Alternatively, we may define $L(p, q)$ as the $-\frac{p}{q}$-surgery on the unknot in S^3. The complement of a tubular neighbourhood of the unknot is a solid torus $D^2 \times S^1$, so in particular lens spaces are obtained via the gluing of solid tori along their boundaries, hence they are oriented manifolds with genus 1 Heegaard splittings. Further details on the definition of lens spaces can be found in [11, 30].

Note that some definitions in the literature yield $L(1, 0) \cong S^3$ and $L(0, 1) \cong S^1 \times S^2$. We shall always exclude these cases from consideration and work under the assumption that $p > q > 0$; note that $p \geq 2$.

From the discussion above, it is possible to directly derive the integer homology groups of a lens space $L(p,q)$:

$$H_n(L(p,q);\mathbb{Z}) = \begin{cases} \mathbb{Z} & \text{if } n = 0,3; \\ \mathbb{Z}/p\mathbb{Z} & \text{if } n = 1; \\ 0 & \text{otherwise.} \end{cases}$$

A straightforward application of the Universal Coefficient Theorem reveals that lens spaces are rational homology 3-spheres, i. e. $H_n(L(p,q);\mathbb{Q}) = H_n(S^3;\mathbb{Q})$. This is an important observation that will be of use.

Finally, 3-dimensional lens spaces were classified up to diffeomorphism by Reidemeister in [70]. Let $L(p,q)$ and $L(p',q')$ be two lens spaces. Then they are diffeomorphic if and only if $p = p'$ and $q' \equiv \pm q^{\pm 1} \mod p$, where q^{-1} is the multiplicative inverse modulo p. Observe that a lens space inherits an orientation coming from the standard orientation of the 3-sphere. We remark that a given $L(p,q)$ is orientation-preserving diffeomorphic to $L(p,q^{-1})$, while it is orientation-reversing diffeomorphic to its dual lens space $L(p,p-q)$. In turn, the latter is orientation-preserving diffeomorphic to $L(p,p-q^{-1})$.

As discussed in the introduction, we are interested in embeddings of $L(p,q)$ in $\mathbb{C}P^2$, the space of complex lines through the origin in $\mathbb{C}^3$. The first important observation is that if $L(p,q)$ embeds in $\mathbb{C}P^2$, it separates it into two components. This can be seen using Mayer-Vietoris. Let $\nu L(p,q) \cong L(p,q) \times I$ be a tubular neighbourhood of $L(p,q)$ in $\mathbb{C}P^2$. Let $A := \overline{\mathbb{C}P^2 \backslash \nu L(p,q)}$ and note that $A \cup \nu L(p,q) = \mathbb{C}P^2$ and $A \cap \nu L(p,q) = L(p,q) \times \{0,1\}$. The reduced Mayer-Vietoris sequence with integer coefficients

$$\begin{array}{ccccccc} & & & & 0 & & \mathbb{Z} \\ & & & & \rotatebox{90}{$=$} & & \rotatebox{90}{$=$} \\ \cdots & \longrightarrow & & & \tilde{H}_1(\mathbb{C}P^2) & \longrightarrow & \tilde{H}_0(L(p,q) \times \{0,1\}) \\ & & & \swarrow & & & \\ & & 0 & & 0 & & \\ & & \rotatebox{90}{$=$} & & \rotatebox{90}{$=$} & & \\ \tilde{H}_0(A) \oplus \tilde{H}_0(\nu L(p,q)) & \longrightarrow & \tilde{H}_0(\mathbb{C}P^2) & \longrightarrow & 0 & & \end{array}$$

immediately tells us $\tilde{H}_0(A) \cong \mathbb{Z}$, hence $H_0(A) \cong \mathbb{Z} \oplus \mathbb{Z}$.

We now know that if $L(p,q)$ smoothly embeds in $\mathbb{C}P^2$, it separates it into two submanifolds, say M and B. The next step is to try to understand these manifolds. We

begin by proving a standard fact.

Proposition 3.1. *If a lens space $L(p,q)$ smoothly embeds in $\mathbb{C}P^2$, it splits off a rational homology 4-ball.*

Proof. Recall that lens spaces are rational homology spheres. Given a ring R, we remark that the homology groups of $\mathbb{C}P^2$ are the following:

$$H_n(\mathbb{C}P^2;R) = \begin{cases} R & \text{if } n = 0,2,4 \\ 0 & \text{otherwise.} \end{cases}$$

Let $\mathbb{C}P^2 = M \underset{L(p,q)}{\cup} B$. We have the following Mayer-Vietoris sequence with rational coefficients:

$$\begin{array}{ccccccccc}
 & & & & \mathbb{Q} & & \mathbb{Q} & & \\
 & & & & \rotatebox{90}{$\cong$} & & \rotatebox{90}{$\cong$} & & \\
\cdots & \longrightarrow & H_4(M)\oplus H_4(B) & \longrightarrow & H_4(\mathbb{C}P^2) & \xrightarrow{f} & H_3(L(p,q)) & & \\
 & & & & & \overset{g}{\searrow} & \downarrow & & \\
 & & & & 0 & & 0 & & \\
 & & & & \rotatebox{90}{$\cong$} & & \rotatebox{90}{$\cong$} & & \\
H_3(M)\oplus H_3(B) & \longrightarrow & H_3(\mathbb{C}P^2) & \longrightarrow & H_2(L(p,q)) & \longrightarrow & H_2(M)\oplus H_2(B) & & \\
 & & & & & \searrow & \downarrow & & \\
 & & \mathbb{Q} & & 0 & & 0 & & \\
 & & \rotatebox{90}{$\cong$} & & \rotatebox{90}{$\cong$} & & \rotatebox{90}{$\cong$} & & \\
H_2(\mathbb{C}P^2) & \longrightarrow & H_1(L(p,q)) & \longrightarrow & H_1(M)\oplus H_1(B) & \longrightarrow & H_1(\mathbb{C}P^2) & & \\
 & & & & & \searrow & \downarrow & & \\
 & & \mathbb{Q} & & & & \mathbb{Q} & & \\
 & & \rotatebox{90}{$\cong$} & & & & \rotatebox{90}{$\cong$} & & \\
H_0(L(p,q)) & \longrightarrow & H_0(M)\oplus H_0(B) & \longrightarrow & H_0(\mathbb{C}P^2) & \longrightarrow & 0. & &
\end{array}$$

Observe that both M and B are connected compact 4-manifolds with boundary, hence $H_4(M) = H_4(B) = 0$. Moreover, it is straightforward that $H_0(M) \cong H_0(B) \cong \mathbb{Q}$. Since $H_1(M)\oplus H_1(B)$ injects into the trivial group, we have $H_1(M) = H_1(B) = 0$. Now observe that $H_2(M)\oplus H_2(B) \cong \mathbb{Q}$, so one of the summands must be trivial and the other one must be $\mathbb{Q}$. Without loss of generality, assume that $H_2(M) \cong \mathbb{Q}$ and $H_2(B) = 0$. Finally, note that the map f is an isomorphism and thus $im(f) = ker(g) \cong \mathbb{Q}$. Since g is a surjection, $H_3(M)\oplus H_3(B) \cong H_3(L(p,q))/ker(g) = 0$. Thus both $H_3(M)$ and $H_3(B)$ are trivial and we have determined that B is a rational homology 4-ball. □

The above proposition implies that if a lens space embeds in $\mathbb{C}P^2$ it must bound a rational homology ball. The ones which do not share this property are immediately excluded from our consideration. In [49], Lisca proved the slice-ribbon conjecture holds for 2-bridge knots. Keeping in mind that the double branched cover of such a knot is always a lens space (a proof of which can be found in [11], Chapter 12), Lisca obtained a characterisation of which lens spaces bound a rational homology 4-ball. The original slice-ribbon statement for 2-bridge knots and subsequent lens space classification can be found in [49, Definition 1.1, Theorem 1.2, Corollary 1.3]. Below we present a readapted version focusing only on the characterisation of lens spaces.

Theorem 3.2 (Lisca [49])**.** *Let $p > q > 0$ be coprime natural numbers. Up to diffeomorphism, both orientation-preserving and orientation-reversing, a lens space $L(p,q)$ bounds a rational homology 4-ball if and only if $p = m^2$ and q equals one of the following:*

(1) *$mk \pm 1$ with $m > k > 0$ and $\gcd(m,k) \in \{1,2\}$;*

(2) *$d(m \pm 1)$, where $d > 1$ divides $2m \mp 1$;*

(3) *$d(m \pm 1)$, where $d > 1$ is odd and divides $m \pm 1$.*

Remark 3.3. In this thesis we shall often refer to the lens spaces above as of Lisca type or family (i), where $i \in \{1,2,3\}$.

This thesis addresses lens spaces belonging to families (2) and (3). In [28], Golla–Owens focus on lens spaces from family (1) and study disjoint embeddings of triples of rational homology balls in $\mathbb{C}P^2$. Corollary 3 of their paper also gives a sufficient condition for lens spaces of type (1) to admit an embedding in $\mathbb{C}P^2$.

The next lemma gives us some information about the manifold M that is bounded by a lens space if the latter embeds in $\mathbb{C}P^2$. The result and proof are readapted from Owens in [59], where he provided an infinite family of rational homology balls that embed smoothly in $\mathbb{C}P^2$. We remark that the lens spaces bounding said rational homology balls are of Lisca type (1).

Lemma 3.4 (Owens [59])**.** *Let B be the rational homology ball bounded by the lens space $L(m^2,q)$ and suppose that B embeds smoothly in $\mathbb{C}P^2$. Then the complement $M = \mathbb{C}P^2 \backslash B$ has $H_1(M;\mathbb{Z}) = 0$ and $H_2(M;\mathbb{Z}) \cong \mathbb{Z}$.*

Proof. Consider the following part of the Mayer-Vietoris sequence with integer coeffi-

cients:

$$\begin{array}{ccccccc}
 & & 0 & & 0 & & \\
 & & \wr\| & & \wr\| & & \\
\cdots & \longrightarrow & H_3(\mathbb{C}P^2) & \longrightarrow & H_2(L(m^2,q)) & \longrightarrow & H_2(M)\oplus H_2(B) \\
 & & & & & & \downarrow \\
 & & \mathbb{Z} & & \mathbb{Z}/m^2\mathbb{Z} & & 0 \\
 & & \wr\| & & \wr\| & & \wr\| \\
H_2(\mathbb{C}P^2) & \longrightarrow & H_1(L(m^2,q)) & \longrightarrow & H_1(M)\oplus H_1(B) & \longrightarrow & H_1(\mathbb{C}P^2) \\
 & & & & & & \downarrow \\
 & & \mathbb{Z} & & & & \mathbb{Z} \\
 & & \wr\| & & & & \wr\| \\
H_0(L(m^2,q)) & \longrightarrow & H_0(M)\oplus H_0(B) & & \longrightarrow & H_0(\mathbb{C}P^2) & \longrightarrow 0.
\end{array}$$

We use the Universal Coefficient Theorem to compute $H_2(B;\mathbb{Z})$. Consider the following short exact sequence:

$$0 \longrightarrow H_2(B;\mathbb{Z})\otimes\mathbb{Q} \longrightarrow H_2(B;\mathbb{Q}) \longrightarrow \mathrm{Tor}(H_1(B;\mathbb{Z}),\mathbb{Q}) \longrightarrow 0.$$

Since B is a rational homology ball, $H_2(B;\mathbb{Q}) = 0$, which implies $\mathrm{Tor}(H_1(B;\mathbb{Z}),\mathbb{Q}) = 0$ and $H_2(B;\mathbb{Z})\otimes\mathbb{Q} = 0$. The latter implies that $H_2(B;\mathbb{Z})$ is torsion only and, from the Mayer-Vietoris sequence, we see that $H_2(B;\mathbb{Z})$ is a subgroup of $\mathbb{Z}$, hence $H_2(B;\mathbb{Z}) = 0$. Next, look at the long exact sequence of the pair $(B, L(m^2,q))$ with coefficients in $\mathbb{Z}$:

$$\begin{array}{ccccccc}
 & & 0 & & 0 & & \\
 & & \wr\| & & \wr\| & & \\
\cdots & \longrightarrow & H_2(L(m^2,q)) & \longrightarrow & H_2(B) & \longrightarrow & H_2(B,L(m^2,q)) \\
 & & & & & & \downarrow \\
 & & \mathbb{Z}/m^2\mathbb{Z} & & & & \mathbb{Z} \\
 & & \wr\| & & & & \wr\| \\
H_1(L(m^2,q)) & \longrightarrow & H_1(B) & \longrightarrow & H_1(B,L(m^2,q)) & \longrightarrow & H_0(L(m^2,q)) \\
 & & & & & & \downarrow \\
 & & \mathbb{Z} & & & & \\
 & & \wr\| & & & & \\
H_0(B) & \longrightarrow & H_0(B,L(m^2,q)) & & \longrightarrow & 0. &
\end{array}$$

Using Poincaré-Lefschetz duality we have $H_2(B,L(m^2,q)) \cong H^2(B) \cong H_2(B)/T_2 \oplus T_1 \cong T_1$, where T_i is the torsion of $H_i(B)$. Moreover, by using the Universal Coefficient Theorem again, we see that $H_1(B)$ consists of torsion only. Going back to the exact sequence of the pair $(B, L(m^2,q))$ above, we immediately see that $T_1 = 0$ implies $\mathbb{Z}/m^2\mathbb{Z}$ injects into $T_1 = 0$, which is a contradiction. Similarly, if $T_1 \cong \mathbb{Z}/m^2\mathbb{Z}$, then we have an

isomorphism between $H_1(L(m^2,q))$ and $H_2(B, L(m^2,q))$, resulting in the contradiction $H_1(B) = 0 = T_1$. Now let $T_1 \cong \mathbb{Z}/k\mathbb{Z}$, where $1 < k < m^2$ divides m^2, so there exists n such that $m^2 = nk$. We remark that $H_1(B, L(m^2,q)) = 0$, therefore $H_1(B)$ must be isomorphic to the quotient of $\mathbb{Z}/m^2\mathbb{Z}$ by $\mathbb{Z}/k\mathbb{Z}$, that is $\mathbb{Z}/n\mathbb{Z}$. This forces $n = k = m$, therefore $H_1(B) \cong T_1 = \mathbb{Z}/m\mathbb{Z}$.

Piecing everything together in the Mayer-Vietoris sequence, we see that $H_2(M)$ must now be a finite index subgroup of $H_2(\mathbb{C}P^2) \cong \mathbb{Z}$, hence $H_2(M) \cong \mathbb{Z}$. Next, note that we have a surjective map from $H_1(L(m^2,q)) \cong \mathbb{Z}/m^2\mathbb{Z}$ to $H_1(M) \oplus \mathbb{Z}/m\mathbb{Z}$. Hence the direct sum is finite cyclic, and cyclic summands of $H_1(M)$ have order dividing m, thus there cannot be any non-trivial direct summands. Therefore $H_1(M) = 0$. □

The discussion presented in this section can be summarised as follows.

Suppose $L(p,q)$ smoothly embeds in $\mathbb{C}P^2$. Then:

- $\mathbb{C}P^2$ splits as $M \underset{L(p,q)}{\cup} B$;
- B is a rational homology 4-ball bounded by $-L(p,q)$;
- M is a manifold bounded by $L(p,q)$ such that $H_1(M;\mathbb{Z}) = 0$ and $H_2(M;\mathbb{Z}) \cong \mathbb{Z}$.

§ 3.2 | Lattices and Intersection Forms

In this section we provide the machinery that will allow us to state and prove the main result of this thesis.

Definition 3.5. *A* lattice Λ *is a pair consisting of a free R-module and a symmetric bilinear pairing taking values in the ring R. We say two lattices are* equivalent *(or* isomorphic*) if there exists an isomorphism of the underlying modules which preserves the symmetric bilinear pairing.*

Remark 3.6. In this thesis, we will be working with integer lattices ($R = \mathbb{Z}$). Hence, unless specified, by lattice we shall always mean a free abelian group together with a bilinear pairing taking values in $\mathbb{Z}$.

Quite often in the literature, authors refer to lattices via their group or via their bilinear pairing only. This is imprecise notation, but its meaning is clear in context. Whenever this terminology appears in the present thesis, it is understood to follow the same convention.

We now discuss some examples of lattices. Consider the free abelian group $\mathbb{Z}^n$ generated by the standard orthonormal basis $e_1, \ldots, e_n$. The standard scalar product $e_i \cdot e_j = \delta_{ij}$, where δ_{ij} is the Kronecker delta, defines a symmetric bilinear pairing. Then $\Lambda := (\mathbb{Z}^n, e_i \cdot e_j = \delta_{ij})$ is a lattice, known as the standard lattice on $\mathbb{Z}^n$.

A lattice can also be defined starting from integers $a_1, \ldots, a_n$. Once again, take the free abelian group $\mathbb{Z}^n$, this time with generators $v_1, \ldots, v_n$ (which may for instance be linear combinations of the standard orthonormal basis vectors above). Define the symmetric bilinear pairing as follows:

$$v_i \cdot v_j := \begin{cases} a_i & \text{if } i = j; \\ -1 & \text{if } |i - j| = 1; \\ 0 & \text{if } |i - j| > 1. \end{cases}$$

Thus, $\mathbb{Z}^n$ with the pairing above defines a lattice Λ associated to the integers $a_1, \ldots, a_n$ (often simply denoted by $\Lambda(a_1, \ldots, a_n)$). This lattice is also called a *linear lattice* and the generators $v_1, \ldots, v_n$ are referred to as its vertices. The reason behind this nomenclature is that the symmetric bilinear pairing can be recovered as the adjacency matrix of a weighted linear graph. This is a finite graph with vertices $v_1, \ldots, v_n$ where each v_i, $2 \leq i \leq n-1$, is connected only to v_{i-1} and v_{i+1}, while v_1 is only connected to v_2 and v_n is only connected to v_{n-1}. For instance, the following graph

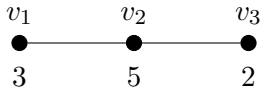

Figure 3.1: Example of linear graph.

is linear and represents the lattice $\Lambda(3, 5, 2)$, which is $\mathbb{Z}^3$ with pairing given by the matrix

$$\begin{pmatrix} 3 & -1 & 0 \\ -1 & 5 & -1 \\ 0 & -1 & 2 \end{pmatrix}.$$

Definition 3.7. *Given a compact, oriented, topological 4-manifold X, it is always possible to associate to it a symmetric bilinear form*

$$Q_X : H^2(X, \partial X; \mathbb{Z}) \times H^2(X, \partial X; \mathbb{Z}) \to \mathbb{Z}$$

defined by $Q_X(a, b) := \langle a \cup b, [X] \rangle = a \cdot b \in \mathbb{Z}$, called the intersection form *of X. By*

Poincaré-Lefschetz duality this form is also defined on $H_2(X;\mathbb{Z}) \times H_2(X;\mathbb{Z})$.

Notice that Q_X vanishes on torsion elements, so it descends to a pairing on homology modulo torsion. The pair $\Lambda_X \coloneqq (H_2(X;\mathbb{Z})/\text{torsion}, Q_X)$ is called the *intersection lattice* of X. Intuitively speaking, the intersection form counts the signed number of intersections of two surfaces in X, hence the name. This thesis will only cover what is essential to our work, so it should not be taken as an introduction to this topic. A thorough discussion about the intersection form can be found in [30], while [66] presents a more intuitive introduction. Observe that although we are working with smooth manifolds, this definition only required X to be a topological manifold. Given an intersection form Q_X on the finitely generated free abelian group $\mathbb{Z}^n$, we call n the *rank* of Q_X (equivalently, the rank is the second Betti number $b_2(X)$). After extending and diagonalising Q_X as a matrix over $\mathbb{R}$, we can consider the difference between the number of positive eigenvalues and that of negative ones, which is called the *signature* σ_X of Q_X. If $Q_X(a,a) > 0$ (< 0) for any non-zero class a then we say that the form is *positive* (*negative*) definite. Finally, we observe that changing the orientation of X changes the sign of its intersection form, that is $Q_{-X} = -Q_X$.

A trivial example of an intersection form is given by S^4. Recall that $H_2(S^4;\mathbb{Z}) = 0$, therefore it immediately follows that Q_{S^4} is trivial.
Now consider $\mathbb{C}P^2$. We will sketch the idea behind the computation of the intersection form of this manifold, following [30, 66]. Recall that $H_2(\mathbb{C}P^2;\mathbb{Z}) \cong \mathbb{Z}$: this group is generated by the fundamental class of $L = \{[x : y : z] \in \mathbb{C}P^2 \,|\, z = 0\}$. Note that L is the complex projective line $\mathbb{C}P^1$. Now take another such line $L_1 = \{[x : y : z] \in \mathbb{C}P^2 \,|\, y = 0\}$ and observe that it intersects L transversally at $[1 : 0 : 0]$ (two projective lines always intersect in a point). Thus $Q_{\mathbb{C}P^2}([L],[L_1]) = \pm 1$. Since $\mathbb{C}P^2$ is a complex manifold, it has a canonical orientation in which transverse holomorphic subsurfaces intersect positively, and we conclude that $Q_{\mathbb{C}P^2} = (1)$.

We say that an intersection form is *unimodular* if it has determinant ± 1. Since $\det(Q_{\mathbb{C}P^2}) = 1$, we observe that $Q_{\mathbb{C}P^2}$ is unimodular. This is actually always the case for closed manifolds (i.e. compact and without boundary) and follows from Poincaré duality.

Up to now it is not clear why intersection forms are of interest to us, since we are specifically working with smooth manifolds. The next celebrated result, known as Donaldson's Diagonalisation Theorem, will shed light on this discussion.

Theorem 3.8 (Donaldson [16])**.** *If X is a closed, oriented smooth 4-manifold whose intersection form is positive (resp. negative) definite, then the form is equivalent over the integers to the standard form $\bigoplus_{b_2(X)} (1)$ (resp. $\bigoplus_{b_2(X)} (-1)$).*

Together with Freedman's Theorem ([30]) this implies that if a closed, smooth, simply connected manifold X has a definite intersection form, then it is homeomorphic to either $\#_{b_2(X)}\mathbb{C}P^2$ or $\#_{b_2(X)}\overline{\mathbb{C}P^2}$ [66]. Since the intersection form is an integer lattice, we can read this theorem as telling us that every positive definite intersection lattice of a closed, smooth, oriented 4-manifold is equivalent to the standard lattice on $\mathbb{Z}^n$ previously discussed. Finally, we shall not provide a proof of this result in this thesis, but aside from the original proof, a sketch of it can be found in [66].

Let us now introduce the notion of a plumbing. Suppose S is a closed, possibly disconnected, orientable surface and let $\pi : X \to S$ be a D^2-bundle over S. Given disjoint discs D_i in S, for $i = 1, 2$, each $\pi^{-1}(D_i)$ is a trivial bundle. We may *plumb* X at D_1 and D_2 by identifying $D_1 \times D^2$ and $D_2 \times D^2$ using a map that preserves product structures but swaps the factors. Note that this gluing introduces self-intersections in S. A *plumbing* is a manifold obtained after applying this procedure finitely many times. A thorough discussion of this construction in greater generality can be found in [30]. Each plumbing comes with a graph associated with it, known as a *plumbing diagram*: each vertex represents a connected component of the surface S and is labelled by a pair of numbers representing the genus and Euler number of that component, and each edge corresponds to a plumbing (with an associated sign corresponding to the sign of the intersection introduced). At the same time, any such graph determines a plumbing.

Let us focus on a plumbing P of D^2-bundles over 2-spheres associated to a linear graph; we remark that since spheres have genus 0, each vertex may only be decorated by the relevant Euler number. It is possible to represent the corresponding 4-manifold using Kirby calculus. Each vertex will correspond to a 2-handle, attached along an unknot, linked with other 2-handles via a clasp, according to the edges of the graph. The framing on each handle corresponds to the Euler number of the related D^2-bundle. The linking matrix corresponding to this Kirby diagram, which is also the adjacency matrix associated to the graph, is precisely the intersection form of P (see [30, Proposition 4.5.11]). For instance, take the linear graph in Figure 3.1 as a plumbing graph. The corresponding Kirby diagram is shown in Figure 3.2.

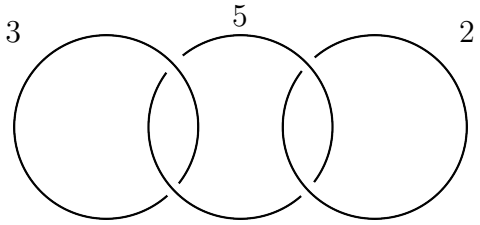

Figure 3.2: Kirby diagram of plumbing of D^2-bundles over S^2 arising from Figure 3.1.

Finally, if we perform iterated slam-dunk moves on such a Kirby diagram, we obtain an unknot with rational surgery coefficient $-\frac{p}{q}$ derived from the individual integer framings of the 2-handles (depending on where we start, we might also get $-\frac{p}{q^*}$, where q^* is the multiplicative inverse of $q \mod p$). This tells us that the boundary of a plumbing associated with a linear graph is actually a lens space. For instance, performing slam dunks on Figure 3.2 yields an unknot with rational surgery coefficient $\frac{25}{9}$. More interestingly, any lens space can be expressed as the boundary of a linear plumbing. Consider the lens space $L(p,q)$. It is always possible to associate the Hirzebruch-Jung continued fraction expansion to a rational number as follows:

$$\frac{p}{p-q} = [a_1, a_2, \ldots, a_n]^- := a_1 - \cfrac{1}{a_2 - \cfrac{1}{a_3 - \cfrac{1}{\ddots - \cfrac{1}{a_n}}}},$$

where the integers $a_1, \ldots, a_n$ are called weights and each $a_i \geq 2$. We note that $p - q \equiv -q \mod p$. One can construct a plumbing P corresponding to the linear graph with n vertices of weight a_i for $i = 1, \ldots, n$. The boundary of such plumbing is the lens space $L(p,q)$, and its intersection form is a linear lattice associated to the integers $a_1, \ldots, a_n$, as discussed in the previous section. In particular, there is no torsion in $H_2(P;\mathbb{Z})$. We call such a manifold the canonical positive definite plumbing bounded by a lens space $L(p,q)$.

§ 3.3 | Obstruction

The discussion so far has presented some properties that lens spaces embedding in $\mathbb{C}P^2$ must satisfy and has introduced important tools for the understanding of 4-manifolds. In this section, everything comes together.

We have seen that a lens space smoothly embedding in $\mathbb{C}P^2$ splits off a rational homology

4-ball B and a manifold M such that $H_1(M;\mathbb{Z}) = 0$ and $H_2(M;\mathbb{Z}) \cong \mathbb{Z}$. Therefore, $\mathbb{C}P^2$ can be obtained by gluing of these two manifolds along their common boundary $L(p,q)$. Note that the gluing map must be an orientation-reversing diffeomorphism, thus $L(p,q)$ as a boundary must have opposite orientations on B and M. In the discussion that follows, we assume $\partial M = L(p,q)$ and $\partial B = -L(p,q)$.

In the current set-up, it can be deduced that M is a positive-definite manifold. In fact, we may use Mayer-Vietoris with rational coefficients to see that since B is a rational homology 4-ball, there is an isomorphism $H_2(M;\mathbb{Q}) \cong H_2(\mathbb{C}P^2;\mathbb{Q}) \cong \mathbb{Q}$. The second Betti number of M is therefore $b_2(M) = 1$, which equals the rank of the intersection form Q_M. From Novikov additivity we know that $\sigma_{\mathbb{C}P^2} = \sigma_M + \sigma_B$. Since $b_2(B) = 0$, we deduce $\sigma_M = 1$ and hence M is positive definite. In an intuitive sense, we can picture this to mean that M retains some of the information from $\mathbb{C}P^2$. Furthermore, from the integer long exact sequence of the pair $(M, L(p,q))$

$$\cdots \longrightarrow 0 \longrightarrow \underset{\wr\!|\!|}{\mathbb{Z}} H_2(M) \longrightarrow \underset{\wr\!|\!|}{\mathbb{Z}} H_2(M, L(p,q)) \longrightarrow \underset{\wr\!|\!|}{\mathbb{Z}/p\mathbb{Z}} H_1(L(p,q)) \longrightarrow 0 \longrightarrow \cdots$$

it can be seen that the map $H_2(M) \to H_2(M, L(p,q)) \cong H^2(M)$ is multiplication by $\pm p$. This map also represents the intersection form of M, which is positive definite, hence $Q_M = (p)$.

We now aim to construct a new 4-manifold X, which will be obtained by gluing M to another appropriately chosen manifold. Based on previous assumptions, note that M must be bounded by $L(p,q)$. In the previous section we discussed about how any lens space $L(p,p-q) \cong -L(p,q)$ can be viewed as the boundary of the canonical positive definite plumbing of spheres P, associated to the continued fraction expansion of $\frac{p}{q}$ with weights $a_1, \ldots, a_n$ for some $n \in \mathbb{N}$. Note that $b_2(P) = n$. Let $X = M \underset{L(p,q)}{\cup} P$. This manifold is often called a rational "blow-up" of $\mathbb{C}P^2$, and it is a closed, oriented, smooth 4-manifold with positive definite intersection form. Hence, Donaldson's Theorem 3.8 applies, and we know that Q_X is equivalent to the standard lattice on $\mathbb{Z}^{n+1}$.

At this point it is important to understand the relations of Q_M and Q_P with Q_X. From the Mayer-Vietoris sequence with integer coefficients

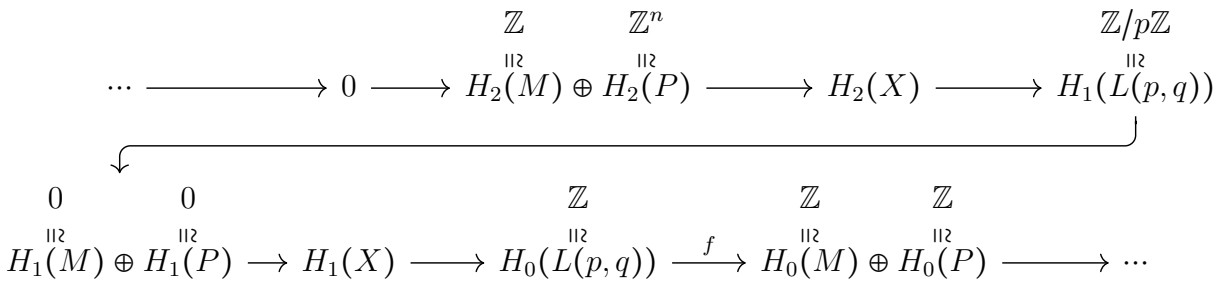

we see that since $L(p,q)$ is connected, the map f is injective, hence $H_1(X) = 0$. Since $H_1(X) \cong H^3(X) \cong (H_3(X)/T_3) \bigoplus T_2$, where T_i is the torsion subgroup of $H_i(X)$, we see that $H_2(X)$ is free, and in particular $H_2(X) \cong \mathbb{Z}^{n+1}$, since $b_2(X) = n+1$. Moreover, observe that $H_2(M) \oplus H_2(P) \cong \mathbb{Z} \oplus \mathbb{Z}^n$ injects into $H_2(X)$. Since the cokernel of this map is finite, we conclude that it is a finite-index embedding. Moreover, this embedding preserves the bilinear pairing, hence in terms of intersection lattices we also have that $Q_M \oplus Q_P$ admits a finite-index embedding in Q_X, and thus in the standard lattice on $\mathbb{Z}^{n+1}$.

It is now possible to derive some additional constraints on this lattice embedding: these precisely constitute the result revealing which lens spaces are obstructed from embedding in $\mathbb{C}P^2$. This result was derived by Owens in [59, Proposition 3.2], and a readapted version is presented below, together with its proof.

Proposition 3.9 (Owens [59])**.** *Let B be a rational homology ball bounded by a lens space $-L(p,q)$ and suppose it embeds smoothly in $\mathbb{C}P^2$. Let $X = M \underset{L(p,q)}{\cup} P$ be the resulting positive definite rational blow-up of $\mathbb{C}P^2$. Then there exists a finite-index intersection lattice embedding*

$$\Lambda_M \oplus \Lambda_P \hookrightarrow \mathbb{Z}^{n+1}$$

such that each unit vector $e \in \mathbb{Z}^{n+1}$ has non-zero pairing with each of Λ_M and Λ_P. Moreover, the image of the generator of Λ_M is a primitive vector in $\mathbb{Z}^{n+1}$.

Remark 3.10. To better understand this proposition, consider the generators $v_1, \dots, v_{n+1}$ of $\Lambda_M \oplus \Lambda_P$, where $v_1 \in \Lambda_M$ and $v_2, \dots, v_{n+1} \in \Lambda_P$. Let $\mathbb{Z}^{n+1}$ be generated by the standard orthonormal basis vectors $e_1, \dots, e_{n+1}$. The lattice embedding is obtained by specifying a linear combination of vectors $e_1, \dots, e_{n+1}$ to which the generators of Λ_M and Λ_P are mapped. By a unit vector $e \in \mathbb{Z}^{n+1}$ having non-zero pairing with Λ_M and Λ_P we mean that the generator of Λ_M is mapped to a linear combination which includes e, and that there is at least a generator of Λ_P which is mapped to a linear combination which includes e. It is possible to visualise this condition in terms of a matrix A representing the lattice embedding above in terms of the aforementioned bases. The proposition tells us that

each unit vector of $\mathbb{Z}^{n+1}$ is employed in the embedding description. In particular, each row of A has at least two non-zero entries, one of which is always in the first column, which represents the vector generating Λ_M. This vector is primitive, which means that the entries of the first column of A have no common divisor.

Proof. Recall from our previous discussion that since $H_1(X) = 0$, all homology groups of X are free, and in particular $H_2(X) \cong \mathbb{Z}^{n+1}$. Consider the Mayer-Vietoris sequence for cohomology with integer coefficients:

$$\cdots \longrightarrow \overset{0}{\overset{\shortparallel}{H^1(L(p,q))}} \longrightarrow H^2(X) \longrightarrow H^2(M) \oplus H^2(P) \longrightarrow H^2(L(p,q)) \longrightarrow \cdots$$

and observe that $H^2(X)$ injects into $H^2(M) \oplus H^2(P) \cong H_2(M, L(p,q)) \oplus H_2(P, L(p,q))$, where we have used Poincaré–Lefschetz duality. Thus, any class in $H^2(X) \cong H_2(X)$ can be represented using classes in $H_2(M, L(p,q))$ and $H_2(P, L(p,q))$. Let e be a unit vector in $H_2(X)$ which we write as

$$e = e_M + e_P,$$

where $e_M \in H_2(M, L(p,q))$ and $e_P \in H_2(P, L(p,q))$. Note that if $e_P = 0$, this implies that e_M is a unit vector and an element in the image of $H_2(M) \hookrightarrow H_2(M, L(p,q)) \cong H^2(M)$. But we have seen that this map is described by $Q_M = (p)$, so this is impossible (recall that we are working under the assumption that $p \geq 2$).
Similarly, if $e_M = 0$, then e_P is a unit vector in the image of $H_2(P) \hookrightarrow H_2(P, L(p,q)) \cong H^2(P)$. Since we assumed that each weight in the plumbing P is at least 2, this yields a contradiction. Hence we must have $e_M \neq 0$ and $e_P \neq 0$.

Recall that the free abelian group $H_2(M) \cong \mathbb{Z}$ is the underlying group of the integer lattice $\Lambda_M = (H_2(M), Q_M)$. Using the Universal Coefficient Theorem

$$0 \longrightarrow \overset{0}{\overset{\shortparallel}{\mathrm{Ext}(H_1(M), \mathbb{Z})}} \longrightarrow H^2(M) \longrightarrow \mathrm{Hom}(H_2(M), \mathbb{Z}) \longrightarrow 0$$

we have the isomorphism $H^2(M) \cong \mathrm{Hom}(H_2(M), \mathbb{Z})$. Then $H_2(M, L(p,q)) \cong H^2(M)$ is the group underlying the lattice $\Lambda_M^* = (H^2(M), Q_M^*)$, the dual lattice to Λ_M. Note that the dual lattice to an integer lattice is not necessarily an integer lattice as well, and that $\Lambda_M \subset \Lambda_M^*$. Now observe that an element of $H_2(M, L(p,q)) \cong H^2(M)$ is a non-zero class if and only if its pairing with some element of $H_2(M)$ is non-zero (since Q_M is positive

definite). Hence, e_M, and therefore e, must have non-zero intersection with some element of $H_2(M)$.
Apply the same argument to $H^2(P) \cong H_2(P, L(p,q)) \cong \mathrm{Hom}(H_2(P), \mathbb{Z})$, to show that e_P (and thus e) also has non-zero intersection with some element of $H_2(P) \cong \mathbb{Z}^n$, the underlying group of $\Lambda_P = (H_2(P), Q_P)$. Moreover, note that Λ_M is the orthogonal complement of Λ_P.
We have now proved the first part of the proposition.

Now suppose v is the image in $H_2(X)$ of the generator of Λ_M and that $v = kw$ for some $k \in \mathbb{N}$ and $w \in H_2(X)$. From the discussion above, we can write $w = w_M + w_P$ with $w_M \in H_2(M, L(p,q))$ and $w_P \in H_2(P, L(p,q))$. Since v is the image of a generator of Λ_M, it has zero intersection pairing with $H_2(P)$. This implies that w has zero intersection pairing with $H_2(P)$ as well, therefore we must have $w_P = 0$ and $w = w_M$. Now we know that $w_M \in \Lambda_M$ and is the image of a generator, hence $k = 1$.
This proves the second part of the proposition. □

Using the result above, it is possible to determine when a lens space is DO-unobstructed from embedding in $\mathbb{C}P^2$. Given a lens space $L(p,q)$, consider the continued fraction expansion $p/q = [a_1, \ldots, a_n]^-$, with each $a_i \geq 2$. The linear graph with vertices $a_1, \ldots, a_n$ corresponds to the plumbing graph of the 4-manifold P bounded by $-L(p,q)$. We know it is possible to find an embedding of Q_P in the standard lattice on $\mathbb{Z}^{n+1}$, with orthonormal basis $e_1, \ldots, e_{n+1}$. If the embedding found respects the conditions of Proposition 3.9 – all the orthonormal basis vectors $e_1, \ldots, e_{n+1}$ are hit, and the orthogonal complement is generated by a primitive vector with no zero entries and square p – then we deduce that $-L(p,q)$, and thus $L(p,q)$, is DO-unobstructed from embedding in $\mathbb{C}P^2$.

This thesis focuses on lens spaces of Lisca type (2) and (3). It does not simply provide a list of infinite families of such spaces that are DO-unobstructed from embedding in $\mathbb{C}P^2$, using the obstruction from Prop. 3.9, but it provides a complete classification. This is stated in Theorem 1 below.

Theorem 1. *Any lens space $L(m^2, q)$, up to diffeomorphism, that embeds in $\mathbb{C}P^2$ and is of Lisca type (2) or (3) must have m and q of one of the following forms:*

(1) $m = (2s+3)k^2 + 1$ *and* $q = m^2 - (2s+3)(m-1)$, *with* $s \geq 0$ *and* $k \neq 0, \pm 1$;

(2) $m = 24k^2 + 12k + 2$ *and* $q = (m+1)(8k^2 + 4k + 1)$, *with* $k \neq 0$;

(3) $m = 81k^2 - 72k + 17$ *and* $q = 9(m+1)$, *with* $k \in \mathbb{Z}$;

(4) $m = 3k^2 - 1$ *and* $q = 6k^4 - 3k^2$, *with* $k \neq 0, \pm 1$;

(5) $m = 18k + 23$ *and* $q = (m+1)(4k+5)$, *with* $k \geq 0$;

(6) $m = 81k^2 + 36k + 5$ *and* $q = 9(m+1)$, *with* $k \neq 0$;

(7) $m = (2t+5)k^2 - 1$ *and* $q = (2m-1)k^2$, *with* $t \geq 0$ *and* $k \neq 0, \pm 1$;

(8) $m = 18k + 17$ *and* $q = (2m-1)(2k+2)$, *with* $k \geq 0$;

(9) $m = 18k + 31$ *and* $q = (4k+7)(m-1)$, *with* $k \geq 1$;

(10) $m = 128k^2 + 48k + 5$ *and* $q = 4(32k^2 + 12k + 1)^2$, *with* $k \neq 0$;

(11) $m = 128k^2 - 80k + 13$ *and* $q = 4(32k^2 - 20k + 3)^2$, *with* $k \in \mathbb{Z}$;

(12) $m = 18k + 19$ *and* $q = 162(k+1)$, *with* $k \geq 0$;

(13) *either of* $L(7^2, 31)$, $L(9^2, 50)$, $L(31^2, 270)$ *or* $L(11^2, 50)$.

The proof of this result is presented in the next chapter. We conclude this chapter by remarking that all the arguments involved in the derivation of Proposition 3.9 are homological. Therefore, the classification derived in Theorem 1 is valid for any homology $\mathbb{C}P^2$.

Chapter 4

Proof of Theorem 1

This chapter presents a careful proof of Theorem 1. The classification presented in the theorem relies on Donaldson's Diagonalisation Theorem and on Proposition 3.9 by Owens. Lens spaces satisfying the conditions of Proposition 3.9 are said to be DO-unobstructed from embedding in $\mathbb{C}P^2$. In this chapter, the term unobstructed should always be understood to mean DO-unobstructed. In order to proceed with the proof of Theorem 1, some further understanding of Lisca's paper [49], in which he characterized lens spaces bounding rational homology balls, is needed.

The core idea behind the classification from Theorem 3.2 is essentially the same as that presented in the previous chapter. If a lens space $L(p,q)$ bounds a rational homology ball B, it is possible to form a manifold $W = B \underset{L(p,q)}{\cup} P$ where P is a positive definite plumbing bounded by $-L(p,q)$. Similarly, we can construct $W' = B' \underset{-L(p,q)}{\cup} P'$, where P' is the plumbing bounded by $L(p,q)$ and B' is the rational homology ball bounded by $-L(p,q)$. Since W and W' are closed, smooth, oriented, positive definite manifolds, Donaldson's Diagonalisation Theorem applies, and we know that the intersection lattice Λ_W is isomorphic to the standard lattice on $\mathbb{Z}^{b_2(W)}$, while $\Lambda_{W'}$ is isomorphic to $\mathbb{Z}^{b_2(W')}$. This enables us to find lattice embeddings $\Lambda_P \hookrightarrow \mathbb{Z}^{b_2(W)}$ and $\Lambda_{P'} \hookrightarrow \mathbb{Z}^{b_2(W')}$. The existence of both embeddings yields the constraints on (p,q) presented in Theorem 3.2.

The process leading to such constraints also leads to an explicit description of all the continued fraction expansions arising from the families in Theorem 3.2. These expansions are called "strings" and we shall adopt the same terminology. We shall also refer to them as infinite families, referring to the infinite number of lens spaces associated with each string type. In order to prove Theorem 1, we shall work with the strings associated with

the lens spaces of Lisca type (2) and (3). The string classification presented by Lisca has been recast in [2] by Aceto–Golla–Larson–Lecuona with some slight modifications in order to get rid of redundancies and symmetries, and we shall adopt it in this thesis while highlighting some missing details as well. We use the notation $2^{[s]}$ (or $2^{[t]}$) to indicate s (or t) consecutive vertices of weight 2. The strings of interest are the following:

- $B^1_{s,t} = [2^{[t]}, 3, s+2, t+2, 3, 2^{[s]}]^-$ with $s \geq t > 0$, of type (2);
- $B^2_{s,t} = [2^{[t]}, s+3, 2, t+2, 3, 2^{[s]}]^-$ with $s \geq 0$, $t > 0$, of type (3);
- $C^1_{s,t} = [t+2, s+2, 3, 2^{[t]}, 4, 2^{[s]}]^-$ with $s > 0$, $t \geq 0$, of type (3);
- $C^2_{s,t} = [t+2, 2, s+3, 2^{[t]}, 4, 2^{[s]}]^-$ with $s, t \geq 0$, of type (2);
- $C^3_{s,t} = [t+3, 2, s+3, 3, 2^{[t]}, 3, 2^{[s]}]^-$ with $s, t \geq 0$, of type (3);
- $D^1_{s,t} = [t+3, 3, 2^{[s]}, 3, 2^{[t]}, 3, s+3]^-$ where $s \geq t \geq 0$, of type (2);
- $D^2_{s,t} = [t+3, 2^{[s]}, 4, 2^{[t]}, 3, s+2]^-$ with s, $t \geq 0$, of type (3).

In addition to these strings, we must also consider the reverse strings. These are the strings associated to the continued fraction with weights in the reversed order. It is important to note that given a string associated to $\frac{p}{q}$, the reverse string is associated to $\frac{p}{q^*}$, where q^* is the multiplicative inverse of $q \mod p$. In particular, note that $L(p,q) \cong L(p,q^*)$, therefore we are working with a diffeomorphic lens space. In the proof of Theorem 1 we will only consider the strings as presented above, ignoring the issue of the reverse strings. This is because the plumbing diagram associated to a string represents a manifold with boundary $-L(p,q) \cong -L(p,q^*)$. However, it is important to keep reverse strings in mind to properly understand the relations between the lens spaces considered. For each string we denote its reverse by adding an r: for example, $rB^1_{s,t}$ is the reverse of $B^1_{s,t}$ and so on. We also remark that the differences between the classifications in [49] and [2] relevant to this thesis are due to the following relations (also refined in this thesis): $B^1_{s,0} = rB^2_{0,s}$, $B^1_{s,t} = rB^1_{t,s}$, $C^1_{0,t} = C^2_{0,t}$.

Recall that for a given lens space $L(p,q)$ we have the orientation-preserving diffeomorphism $L(p,q) \cong -L(p,p-q)$. The lens space $L(p,p-q)$ is called the *dual* to $L(p,q)$. This notion of duality also translates to strings, and we say that a string $[\mathbf{b}]^- = \frac{p}{q}$ is dual or *complementary* to $[\mathbf{c}]^- = \frac{p}{p-q}$ [2].

Dualities between the strings presented above are as follows: $B^1_{s+1,t+1}$ is dual to $D^1_{s,t}$;

$rB^1_{s+1,t+1}$ is dual to $rD^1_{s,t}$; $B^2_{s,t+1}$ is dual to $D^2_{s,t}$; $rB^2_{s,t+1}$ is dual to $rD^2_{s,t}$; $C^1_{s,t}$ is dual to $rC^3_{t,s-1}$; $rC^1_{s,t}$ is dual to $C^3_{t,s-1}$; $C^2_{s,t}$ is dual to $rC^2_{t,s}$.

Let us now outline the strategy employed to prove Theorem 1. For each string $[a_1, \dots, a_n]^-$, we consider the related linear graph and map each vertex to a linear combination of orthogonal basis vectors for $\mathbb{Z}^{n+1}$ so that the pairing is preserved. This corresponds to finding a lattice embedding of Λ_P, where P is the plumbing corresponding to the diagram, into $\mathbb{Z}^{n+1}$. Note that by Lisca's work, this lattice embedding is guaranteed to exist (in particular, the one in [49] is unique up to automorphism [6, Lemma 5.2]). However, finding such an embedding does not show that the lens space bounding P is unobstructed from embedding in $\mathbb{C}P^2$. We need an embedding satisfying all the conditions of Proposition 3.9; this translates to making sure that each basis vector of $\mathbb{Z}^{n+1}$ appears in at least one of the linear combinations that the vertices of the linear graph are mapped to, and that the orthogonal complement of Λ_P in $\mathbb{Z}^{n+1}$ — which corresponds to the embedding $\Lambda_M \hookrightarrow \mathbb{Z}^{n+1}$ from the proposition — is generated by a primitive vector with no zero entries. Moreover, we require the square of this vector to equal p, the numerator of $p/q = [a_1, \dots, a_n]^-$.

We now make an important observation. Suppose we are working with a given string $\frac{p}{q} = [a_1, \dots, a_n]^-$ and that an embedding satisfying the conditions of Proposition 3.9 is found. This implies that the lens space $-L(p,q) \cong L(p, p-q)$ associated to the string is unobstructed from embedding in $\mathbb{C}P^2$. Naturally, this conclusion holds for $L(p,q)$ – the lens space with opposite orientation – as well. However, if for a given string it is not possible to construct such an embedding, no conclusions can be drawn yet. In order to deduce that the corresponding lens space cannot embed in $\mathbb{C}P^2$, we must work with its dual string as well and verify that it is not possible to construct the required lattice embedding either. In this chapter, we will analyse each string individually and consider all possible lattice embeddings up to lattice automorphism of $\mathbb{Z}^{n+1}$: if we find one satisfying Proposition 3.9, we conclude that the relevant lens space is unobstructed from embedding in $\mathbb{C}P^2$; if it is not possible to find the required lattice embedding, we consider the dual string (and hence lens space) and proceed to look for an embedding satisfying Proposition 3.9. If such an embedding is found, we conclude that the lens space considered is unobstructed from embedding in $\mathbb{C}P^2$. If no such embedding is found, we conclude the lens space is obstructed from embedding in $\mathbb{C}P^2$. Recall that the duality relations between the strings have been explicitly stated, and thus we know that given $L(p,q)$ we will analyse both the graph corresponding to $\frac{p}{q} = [a_1, \dots, a_n]^-$ and its dual, corresponding

to $\frac{p}{p-q} = [b_1, \ldots, b_m]^-$. Therefore, after going through all of the strings mentioned above, we will also be able to conclude which lens spaces cannot embed in $\mathbb{C}P^2$, obtaining the complete classification of Theorem 1.

The argument for each string is divided in two subsections; in the first one we provide a general argument under the condition that the parameters s and t are "big enough", the precise meaning of which will be defined in each case. In the second subsection, we go over all the strings excluded from consideration in the previous case: first by considering infinite families of strings where only one of the parameters is "big enough", and then by considering the finite number of cases remaining. These cases, also referred to as sporadic cases, were analysed using GAP [25] and its `OrthogonalEmbeddings` command. There will be one fully worked example to explain how the required information is extracted, but afterwards only strings with an embedding satisfying Proposition 3.9 will be presented.

Throughout the whole proof we will be implicitly making use of some considerations in order to construct a lattice embedding. We shall say that two embeddings into $\mathbb{Z}^n$ are equivalent if they differ by a lattice automorphism of $\mathbb{Z}^n$. Whenever we say that there is only a finite number of ways to construct an embedding, it is always to be understood as meaning up to equivalent embeddings. This will be the case any time we say a certain mapping is "forced". When looking at linear graphs, we always start by looking for 2-chains, which are subchains made of vertices of weight 2.

Suppose we have a graph with n vertices which contains as a sub-graph a 2-chain of length l linked to a vertex of weight w. Recall that we are looking for lattice embeddings in $\mathbb{Z}^{n+1}$, which has orthonormal basis $e_1, \ldots, e_{l+1}, \ldots, e_{n+1}$. First, observe that up to lattice automorphism of $\mathbb{Z}^{n+1}$, there is only one way to map each vertex of weight 2 to a combination of basis vectors of $\mathbb{Z}^{n+1}$, shown in Figure 4.1.

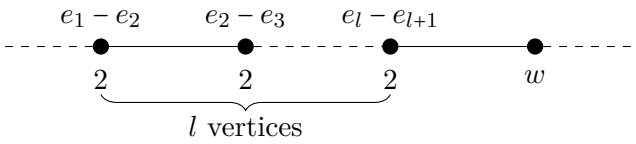

Figure 4.1: A 2-chain contained in a linear graph.

Now we need to determine where to map the vertex with weight w. In general, this vertex is mapped to a linear combination of the form $c_1e_1 + \cdots + c_{l+1}e_{l+1} + \cdots + c_{n+1}e_{n+1}$, with the integer coefficients c_i to be determined. Moreover, observe that it needs to be

orthogonal to all vertices in the 2-chain, except for the last one, with which the pairing must evaluate to -1. This immediately tells us that $c_1 = \cdots = c_l = c$, for some $c \in \mathbb{Z}$, and $c_{l+1} = c + 1$. We now distinguish three cases:

- $w < l$: this forces $c = 0$ and $c_{l+1} = 1$, thus the vertex is mapped to $e_{l+1} + c_{l+2}e_{l+2} \cdots + c_{n+1}e_{n+1}$;
- $w = l$: in this case, either $c = -1$ or $c = 0$. The first maps the vertex to $-(e_1 + \cdots + e_l)$ (note that the remaining c_i are forced to be 0), while the second maps it to $e_{l+1} + c_{l+2}e_{l+2} \cdots + c_{n+1}e_{n+1}$, as in the previous case;
- $w > l$: in this case, for $c \in \mathbb{Z}$, we map the vertex to $c(e_1 + \cdots + e_l) + (1 + c)e_{l+1} + c_{l+2}e_{l+2} + \cdots + c_{n+1}e_{n+1}$.

These ideas have been presented in the simplest case possible, but concatenation with vertices on either side of a 2-chain gives rise to additional constraints. Moreover, this same logic can be applied to vertices that are not immediately linked to a 2-chain to deduce something about the linear combination of vectors they should map to. These types of arguments underlie all the upcoming discussion.

§ 4.1 | String $B^1_{s,t}$

We start by analysing the string $B^1_{s,t} = [2^{[t]}, 3, s+2, t+2, 3, 2^{[s]}]^-$ with $s \geq t > 0$, according to the classification in [2]. It can be found in [49] that $B^1_{s,t}$ corresponds to the continued fraction expansion of

$$\frac{p}{q} = \frac{(2st + 3s + 3t + 4)^2}{(2st + 3s + 3t + 4)^2 - (2s + 3)(2st + 3s + 3t + 3)}.$$

Note that $B^1_{s+1,t+1}$ is dual to $D^1_{s,t}$, and from this duality relation we deduce that $B^1_{s,t}$ is obtained from lens spaces of Lisca type (2) with $q = d(m-1)$ (see Theorem 3.2). Since the string contains $s + t + 4$ weights, we seek lattice embeddings in $\mathbb{Z}^{s+t+5}$. Throughout this section, let $e_1, \ldots, e_{s+1}, f_1, \ldots, f_{t+1}, a, b, c$ be an orthonormal basis for $\mathbb{Z}^{s+t+5}$.

§ 4.1.1 | General Argument

The general argument presented in this subsection holds for $s, t \geq 3$. The remaining cases will be analysed in the next subsection.

We need to map each vertex of the diagram associated to $B^1_{s,t}$ to a linear combination of $e_1, \ldots, e_{s+1}, f_1, \ldots, f_{t+1}, a, b, c$. Figure 4.2 below shows one such way to do it. Note that

this mapping is forced in the sense previously discussed, that is, up to lattice automorphism of $\mathbb{Z}^{s+t+5}$ (sign-swapping and reindexing of basis vectors).

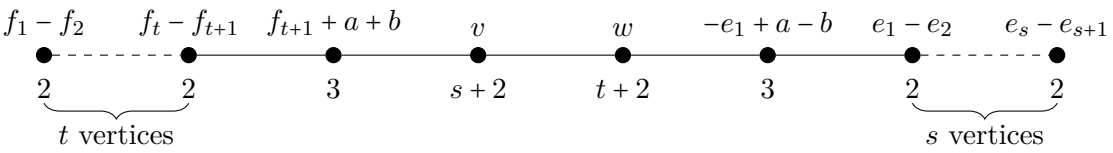

Figure 4.2: Potential embedding of $B^1_{s,t}$ in $\mathbb{Z}^{s+t+5}$ for $s \geq t \geq 3$.

It remains to determine what the images v and w should be. From the discussion of the general strategy, we know that v and w must be of the form $v := \rho_v(e_1 + \cdots + e_{s+1}) + \eta_v(f_1 + \cdots + f_{t+1}) + \alpha_v a + \beta_v b + \gamma_v c$ and $w := \rho_w(e_1 + \cdots + e_{s+1}) + \eta_w(f_1 + \cdots + f_{t+1}) + \alpha_w a + \beta_w b + \gamma_w c$. The additional parameters represent the integer coefficients of the required linear combinations. We need to consider all possible options which preserve the bilinear pairing, therefore we set up the following system of equations:

$$v \cdot v = (s+1)\rho_v^2 + (t+1)\eta_v^2 + \alpha_v^2 + \beta_v^2 + \gamma_v^2 = s+2 \implies |\rho_v| \leq 1 \tag{1}$$

$$w \cdot w = (s+1)\rho_w^2 + (t+1)\eta_w^2 + \alpha_w^2 + \beta_w^2 + \gamma_w^2 = t+2 \implies |\eta_w| \leq 1 \tag{2}$$

$$v \cdot (f_{t+1} + a + b) = \eta_v + \alpha_v + \beta_v = -1 \tag{3}$$

$$v \cdot (-e_1 + a - b) = -\rho_v + \alpha_v - \beta_v = 0 \tag{4}$$

$$w \cdot (f_{t+1} + a + b) = \eta_w + \alpha_w + \beta_w = 0 \tag{5}$$

$$w \cdot (-e_1 + a - b) = -\rho_w + \alpha_w - \beta_w = -1 \tag{6}$$

$$v \cdot w = (s+1)\rho_v\rho_w + (t+1)\eta_w\eta_v + \alpha_v\alpha_w + \beta_v\beta_w + \gamma_w\gamma_v = -1. \tag{7}$$

From the system above we see there are three cases to consider for equation (1): $\rho_v = -1$, $\rho_v = 0$, $\rho_v = 1$. Similarly for equation (2). The solution to this system, together with Figure 4.2, will yield a lattice embedding in $\mathbb{Z}^{s+t+5}$.

- **Case $\rho_v = -1$:**

After substituting for ρ_v and simplifying, the system becomes:

$$\eta_v = 0, \quad \gamma_v = 0 \tag{1}$$
$$(s+1)\rho_w^2 + (t+1)\eta_w^2 + \alpha_w^2 + \beta_w^2 + \gamma_w^2 = t+2 \implies |\eta_w| \leq 1 \tag{2}$$
$$\beta_v = 0 \tag{3}$$
$$\alpha_v = -1 \tag{4}$$
$$\eta_w + \rho_w + 2\beta_w = 1 \tag{5}$$
$$\alpha_w = \rho_w + \beta_w - 1 \tag{6}$$
$$(s+1)\rho_w + \alpha_w = 1. \tag{7}$$

– Case $\eta_w = -1$:
We focus on a subset of equations to see that this case leads to a contradiction:

$$(s+1)\rho_w^2 + \alpha_w^2 + \beta_w^2 + \gamma_w^2 = 1 \implies \rho_w = 0, \quad \alpha_w^2 + \beta_w^2 + \gamma_w^2 = 1 \tag{2}$$
$$\beta_w = 1 \tag{5}$$
$$\alpha_w = 0 \tag{6}$$
$$\alpha_w = 1. \tag{7}$$

Hence, we cannot find the required embedding when $\rho_v = -1$ and $\eta_w = -1$.

– Case $\eta_w = 0$:
We focus on a subset of equations to see that this case leads to a contradiction:

$$(s+1)\rho_w^2 + \alpha_w^2 + \beta_w^2 + \gamma_w^2 = t+2 \tag{2}$$
$$\rho_w = 1 - 2\beta_w \tag{5}$$
$$\alpha_w = -\beta_w \tag{6}$$
$$\beta_w = \frac{s}{2s+3}. \tag{7}$$

We know that $s \geq 3$ is an integer, so from equation (7) we see that it is not possible for β_w to be an integer as well. Hence, we cannot find the required embedding when $\rho_v = -1$ and $\eta_w = 0$.

– Case $\eta_w = 1$:

We focus on a subset of equations to see that this case leads to a contradiction:

$$(s+1)\rho_w^2 + \alpha_w^2 + \beta_w^2 + \gamma_w^2 = 1 \implies \rho_w = 0, \quad \alpha_w^2 + \beta_w^2 + \gamma_w^2 = 1 \tag{2}$$
$$\beta_w = 0 \tag{5}$$
$$\alpha_w = -1 \tag{6}$$
$$\alpha_w = 1. \tag{7}$$

Hence, we cannot find the required embedding when $\rho_v = -1$ and $\eta_w = 1$.

- **Case $\rho_v = 0$:**
  After substituting for ρ_v and simplifying, the system becomes:

$$(t+1)\eta_v^2 + \alpha_v^2 + \beta_v^2 + \gamma_v^2 = s + 2 \tag{1}$$
$$(s+1)\rho_w^2 + (t+1)\eta_w^2 + \alpha_w^2 + \beta_w^2 + \gamma_w^2 = t + 2 \implies |\eta_w| \le 1 \tag{2}$$
$$\eta_v = -2\beta_v - 1 \tag{3}$$
$$\alpha_v = \beta_v \tag{4}$$
$$\eta_w + \rho_w + 2\beta_w = 1 \tag{5}$$
$$\alpha_w = \rho_w + \beta_w - 1 \tag{6}$$
$$-\eta_w(t+1)(2\beta_v + 1) + \beta_v(\rho_w + 2\beta_w - 1) + \gamma_w\gamma_v = -1. \tag{7}$$

  - Case $\eta_w = -1$:
    We focus on a subset of equations to see that this case leads to a contradiction:

$$(s+1)\rho_w^2 + \alpha_w^2 + \beta_w^2 + \gamma_w^2 = 1 \implies \rho_w = 0, \quad \alpha_w^2 + \beta_w^2 + \gamma_w^2 = 1 \tag{2}$$
$$\beta_w = 1 \implies \gamma_w = 0 \tag{5}$$
$$\alpha_w = 0 \tag{6}$$
$$\beta_v = -\frac{t+2}{2t+3}. \tag{7}$$

    We know that $t \ge 3$ is an integer, so from equation (7) we see that it is not possible for β_v to be an integer as well. Hence, we cannot find the required embedding when $\rho_v = 0$ and $\eta_w = -1$.

  - Case $\eta_w = 0$:

The full system of equations is now the following:

$$(t+1)\eta_v^2 + \alpha_v^2 + \beta_v^2 + \gamma_v^2 = s+2 \tag{1}$$
$$(s+1)\rho_w^2 + \alpha_w^2 + \beta_w^2 + \gamma_w^2 = t+2 \tag{2}$$
$$\eta_v = -2\beta_v - 1 \tag{3}$$
$$\alpha_v = \beta_v \tag{4}$$
$$\rho_w = 1 - 2\beta_w \tag{5}$$
$$\alpha_w = -\beta_w \tag{6}$$
$$\gamma_w\gamma_v = -1. \tag{7}$$

At this point we observe that equation (7) implies that either $\gamma_w = 1$ and $\gamma_v = -1$, or $\gamma_w = -1$ and $\gamma_v = 1$.

* Case $\gamma_w = 1$, $\gamma_v = -1$:

$$(t+1)\eta_v^2 + 2\beta_v^2 = s+1 \tag{1}$$
$$(s+1)\rho_w^2 + 2\beta_w^2 = t+1 \tag{2}$$
$$\eta_v = -2\beta_v - 1 \tag{3}$$
$$\alpha_v = \beta_v \tag{4}$$
$$\rho_w = 1 - 2\beta_w \tag{5}$$
$$\alpha_w = -\beta_w. \tag{6}$$

Combining equations (1) and (2) we obtain $(t+1)\eta_v^2\rho_w^2 + 2\beta_v^2\rho_w^2 + 2\beta_w^2 = t+1$, which implies $|\eta_v^2\rho_w^2| \leq 1$. Note that $|\eta_v^2\rho_w^2| = -1$ is impossible. It is straightforward to verify that $|\eta_v^2\rho_w^2| = 0$ leads to a contradiction in any case. Finally, we consider $\eta_v^2\rho_w^2 = 1$, which happens whenever $\eta_v^2 = 1$ and $\rho_w^2 = 1$, leading to four possible cases. The only time we are not led to a contradiction is when $\eta_v = -1$ and $\rho_w = 1$. The equations become the

following:

$$s = t \tag{1}$$
$$s = t \tag{2}$$
$$\beta_v = 0 \tag{3}$$
$$\alpha_v = 0 \tag{4}$$
$$\beta_w = 0 \tag{5}$$
$$\alpha_w = 0. \tag{6}$$

The system has a consistent solution when the condition $s = t$ is satisfied. We have determined that $v = -(f_1 + \cdots + f_{t+1}) - c$ and $w = e_1 + \cdots + e_{s+1} + c$, thus completing the embedding of the lattice generated by $B^1_{s,t}$ in $\mathbb{Z}^{s+t+5}$. However, the orthogonal complement of this embedding is generated by the vector

$$(\underbrace{1, \ldots, 1}_{s+1 \text{ times}}, \underbrace{1, \ldots, 1}_{t+1 \text{ times}}, 0, -1, -(s+1)),$$

hence does not satisfy the conditions of Proposition 3.9.

∗ Case $\gamma_w = -1$, $\gamma_v = 1$:

$$(t+1)\eta_v^2 + \alpha_v^2 + \beta_v^2 = s + 1 \tag{1}$$
$$(s+1)\rho_w^2 + \alpha_w^2 + \beta_w^2 = t + 1 \tag{2}$$
$$\eta_v = -2\beta_v - 1 \tag{3}$$
$$\alpha_v = \beta_v \tag{4}$$
$$\rho_w = 1 - 2\beta_w \tag{5}$$
$$\alpha_w = -\beta_w. \tag{6}$$

Analogously to the previous case, we combine equations (1) and (2) to obtain $(t+1)\eta_v^2\rho_w^2 + 2\beta_v^2\rho_w^2 + 2\beta_w^2 = t + 1$. This implies $|\eta_v^2\rho_w^2| \leq 1$. Again, both the cases $\eta_v^2\rho_w^2 = -1$ and $\eta_v^2\rho_w^2 = 0$ are impossible, so the only one left is $\eta_v^2\rho_w^2 = 1$, which breaks into four possible cases. The only one not

leading to a contradiction is when $\eta_v = -1, \rho_w = 1$. We have:

$$s = t \tag{1}$$
$$s = t \tag{2}$$
$$\beta_v = 0 \tag{3}$$
$$\alpha_v = 0 \tag{4}$$
$$\beta_w = 0 \tag{5}$$
$$\alpha_w = 0. \tag{6}$$

Once again the system has a consistent solution when $s = t$. We have determined that $v = -(f_1 + \cdots + f_{t+1}) + c$ and $w = e_1 + \cdots + e_{s+1} - c$. Note that the embedding determined in this case is the same as in the previous case except for the switching of the signs of c. The orthogonal complement is generated by the vector

$$(\underbrace{1, \ldots, 1}_{s+1 \text{ times}}, \underbrace{1, \ldots, 1}_{t+1 \text{ times}}, 0, -1, (s+1)),$$

hence does not satisfy the conditions of Proposition 3.9.

– Case $\eta_w = 1$:

We focus on a subset of equations to see that this case leads to a contradiction:

$$(s+1)\rho_w^2 + \alpha_w^2 + \beta_w^2 + \gamma_w^2 = 1 \implies \rho_w = 0, \quad \alpha_w^2 + \beta_w^2 + \gamma_w^2 = 1 \tag{2}$$
$$\beta_w = 0 \tag{5}$$
$$\alpha_w = -1 \implies \gamma_w = 0 \tag{6}$$
$$\beta_v = -\frac{t}{2t+3}. \tag{7}$$

We know that $t \geq 3$ is an integer, so from equation (7) we see that it is not possible for β_v to be an integer as well. Hence, we cannot find the required embedding when $\rho_v = 0$ and $\eta_w = 1$.

- **Case $\rho_v = 1$:**

After substituting for ρ_v and simplifying, the system becomes:

$$(t+1)\eta_v^2 + \alpha_v^2 + \beta_v^2 + \gamma_v^2 = 1 \implies \eta_v = 0, \quad \alpha_v^2 + \beta_v^2 + \gamma_v^2 = 1 \tag{1}$$

$$(s+1)\rho_w^2 + (t+1)\eta_w^2 + \alpha_w^2 + \beta_w^2 + \gamma_w^2 = t+2 \implies |\eta_w| \leq 1 \tag{2}$$

$$\alpha_v = 0 \tag{3}$$

$$\beta_v = -1 \implies \gamma_v = 0 \tag{4}$$

$$\eta_w + \rho_w + 2\beta_w = 1 \tag{5}$$

$$\alpha_w = \rho_w + \beta_w - 1 \tag{6}$$

$$\rho_w = \frac{\beta_w - 1}{s+1}. \tag{7}$$

– Case $\eta_w = -1$:
We focus on a subset of equations:

$$(s+1)\rho_w^2 + \alpha_w^2 + \beta_w^2 + \gamma_w^2 = 1 \implies \rho_w = 0, \quad \alpha_w^2 + \beta_w^2 + \gamma_w^2 = 1 \tag{2}$$

$$\beta_w = 1 \implies \gamma_w = 0 \tag{5}$$

$$\alpha_w = 0 \tag{6}$$

$$\rho_w = 0. \tag{7}$$

The system above determines the mapping $v = e_1 + \cdots + e_{s+1} - b$ and $w = -(f_1 + \cdots + f_{t+1}) + b$. The resulting embedding is into $\mathbb{Z}^{s+t+4}$, and corresponds to the one provided by Lisca in [49]. Each of the strings we are examining always presents such an embedding, however it does not satisfy the conditions of Proposition 3.9.

– Case $\eta_w = 0$:
We focus on a subset of equations to see that this case leads to a contradiction:

$$\rho_w = 1 - 2\beta_w \tag{5}$$

$$\alpha_w = -\beta_w \tag{6}$$

$$\beta_w = \frac{s+2}{2s+3}. \tag{7}$$

We know that $s \geq 3$ is an integer, so from equation (7) we see that it is not possible for β_w to be an integer as well. Hence, we cannot find the required embedding when $\rho_v = 0$ and $\eta_w = 0$.

– Case $\eta_w = 1$:

We focus on a subset of equations to see that this case leads to a contradiction:

$$(s+1)\rho_w^2 + \alpha_w^2 + \beta_w^2 + \gamma_w^2 = 1 \implies \rho_w = 0, \quad \alpha_w^2 + \beta_w^2 + \gamma_w^2 = 1 \tag{2}$$

$$\beta_w = 0 \tag{5}$$

$$\alpha_w = -1 \tag{6}$$

$$\beta_w = 1. \tag{7}$$

Hence, we cannot find the required embedding when $\rho_v = 1$ and $\eta_w = 1$.

We conclude that in the general case, when $s, t \geq 3$, the only possible embedding into $\mathbb{Z}^{s+t+5}$ corresponds to Lisca's embedding from [49].

§ 4.1.2 | Remaining Cases

The previous section argued that there are no lattice embeddings satisfying Proposition 3.9 for any $s \geq 3$ and $t \geq 3$. In this section we discuss the cases where at least one of the parameters s, t is less than 3. This is done in two steps: first, we analyse the infinite families arising under such conditions, and then we go through the remaining cases individually.

The first infinite family that we analyse is $B^1_{s,1} = [2, 3, s+2, 3, 3, 2^{[s]}]^-$ when $s \geq 3$. When looking at the plumbing diagram, one can check that the only way to construct a lattice embedding is via the pattern discussed for the general case, substituting $t = 1$. This will result in a single embedding, which is the one determined by [49], and which does not satisfy Proposition 3.9.

The next infinite family is $B^1_{s,2} = [2, 2, 3, s+2, 4, 3, 2^{[s]}]^-$ with $s \geq 3$. This time, the embedding can be constructed in potentially two ways. The first one is via the pattern discussed in the general case with $t = 2$, resulting again in Lisca's embedding. The second way is presented below (we are using the same notation as for the general case).

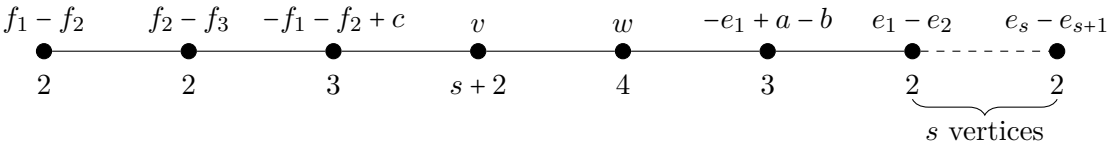

Figure 4.3: Potential embedding of $B^1_{s,2}$ in $\mathbb{Z}^{s+7}$ for $s \geq 3$.

Once again, let $v := \rho_v(e_1 + \cdots + e_{s+1}) + \eta_v(f_1 + f_2 + f_3) + \alpha_v a + \beta_v b + \gamma_v c$ and $w := \rho_w(e_1 + \cdots + e_{s+1}) + \eta_w(f_1 + f_2 + f_3) + \alpha_w a + \beta_w b + \gamma_w c$. In order to determine what v and w should

be, we need to solve the following simplified system of equations:

$$(s+1)\rho_v^2 + 3\eta_v^2 + \alpha_v^2 + \beta_v^2 + \gamma_v^2 = s+2 \implies |\rho_v| \leq 1 \quad (1)$$
$$\rho_w^2(s+1) + 7\eta_w^2 + \alpha_w^2 + \beta_w^2 = 4 \implies \eta_w = 0 \quad (2)$$
$$\gamma_v = 2\eta_v - 1 \quad (3)$$
$$\alpha_v = \beta_v + \rho_v \quad (4)$$
$$\gamma_w = 2\eta_w \quad (5)$$
$$\alpha_w = \rho_w + \beta_w - 1 \quad (6)$$
$$(s+1)\rho_v\rho_w + \alpha_v\alpha_w + \beta_v\beta_w + \gamma_w\gamma_v = -1. \quad (7)$$

A direct computation as in the previous cases shows that when $\rho_v = -1$ or $\rho_v = 1$ the system is inconsistent (this results from equations (1), (3) and (4)). It remains to examine the case $\rho_v = 0$. The system simplifies to:

$$3\eta_v^2 + 2\alpha_v^2 + \gamma_v^2 = s+2 \quad (1)$$
$$\rho_w^2(s+1) + \alpha_w^2 + \beta_w^2 = 4 \quad (2)$$
$$\gamma_v = 2\eta_v - 1 \quad (3)$$
$$\alpha_v = \beta_v \quad (4)$$
$$\gamma_w = 0 \quad (5)$$
$$\alpha_w = \rho_w + \beta_w - 1 \quad (6)$$
$$\alpha_v(\alpha_w + \beta_w) = -1. \quad (7)$$

We focus on equation (2) and start by considering what happens when $\rho_w = 0$. This implies $\alpha_w = \beta_w - 1$ and thus $\alpha_v = -\frac{1}{2\beta_w - 1}$. There are two possibilities: $\beta_w = 0$ and $\alpha_w = -1$, or $\beta_w = 1$ and $\alpha_w = 0$. Both give rise to a contradiction in equation (2).
Now consider the case $\rho_w \neq 0$. By equation (2) this forces $s = 3$ and $\alpha_w = \beta_w = 0$. This gives rise to a contradiction in equation (7).
Hence, we cannot find the required embedding for the lattice on $B^1_{s,2}$ in $\mathbb{Z}^{s+7}$.

We have thus examined all possible infinite families that may arise from the string $B^1_{s,t}$, taking into account the symmetry with respect to s and t. It remains to check sporadic cases for $s < 3$ and $t < 3$. These were all analysed via GAP and produced no embeddings

satisfying Proposition 3.9. Table 4.1 presents a summary of the outcome of the analysis of these cases using GAP.

$B^1_{s,t}$	s	t	Result
	1	1	Obstructed by zero entries in vector generating orthogonal complement
	2	1	Obstructed since Lisca's embedding is the only possibility
	2	2	Obstructed by zero entries in vector generating orthogonal complement

Table 4.1: Summary of GAP analysis for $B^1_{s,t}$ when $s < 3$ and $t < 3$.

§ 4.2 | String $B^2_{s,t}$

In this section, we consider the string $B^2_{s,t} = [2^{[t]}, s+3, 2, t+2, 3, 2^{[s]}]^-$ with $s \geq 0$, $t > 0$. In [49] it is determined that $B^2_{s,t}$ corresponds to the continued fraction expansion of

$$\frac{p}{q} = \frac{(2st+2s+3t+4)^2}{(2st+2s+3t+4)^2 - (2s+3)(2st+2s+3t+3)}.$$

Note that $B^2_{s,t+1}$ is dual to $D^2_{s,t}$ and hence $B^2_{s,t}$ is associated to a lens space of Lisca type (3) with $q = d(m-1)$ (see Theorem 3.2). As $B^2_{s,t}$ contains $s+t+4$ weights, we seek lattice embeddings in $\mathbb{Z}^{s+t+5}$. Throughout this section let $e_1, \ldots, e_{s+1}, f_1, \ldots, f_{t+1}, a, b, c$ be an orthonormal basis for $\mathbb{Z}^{s+t+5}$.

§ 4.2.1 | General Argument

The general argument presented in this subsection holds for $s, t \geq 3$. The remaining cases will be discussed in the next subsection.

In order to obtain a lattice embedding, we need to map each vertex of the diagram associated to $B^2_{s,t}$ to a linear combination of basis vectors for $\mathbb{Z}^{s+t+5}$ in a way that respects the bilinear pairing. Figure 4.4 below shows the only way to do it up to automorphism.

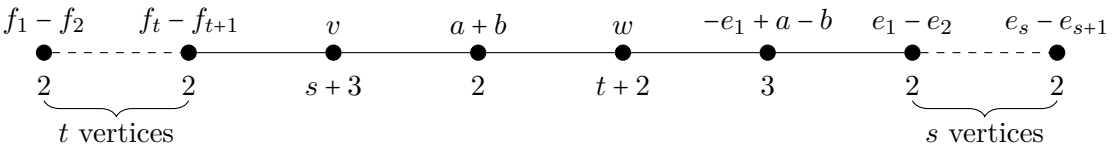

Figure 4.4: Potential embedding of $B^2_{s,t}$ in $\mathbb{Z}^{s+t+5}$ for $s \geq 3$, $t \geq 3$.

It remains to determine what the images v and w should be. Observe that we must have $v := \rho_v(e_1 + \cdots + e_{s+1}) + \eta_v(f_1 + \cdots + f_t) + (\eta_v + 1)f_{t+1} + \alpha_v a - (1+\alpha_v)b + \gamma_v c$ and $w := \rho_w(e_1 + \cdots + e_{s+1}) + \eta_w(f_1 + \cdots + f_{t+1}) + \alpha_w a - (1+\alpha_w)b + \gamma_w c$. Like in the previous

section, the additional parameters represent integer coefficients of the required linear combinations. We need to consider all possible options that preserve the bilinear pairing, therefore we set up the following system of equations:

$$v \cdot v = (s+1)\rho_v^2 + \eta_v^2 t + (\eta_v + 1)^2 + \alpha_v^2 + (1+\alpha_v)^2 + \gamma_v^2 = s+3 \implies |\rho_v| \leq 1 \tag{1}$$

$$w \cdot w = (s+1)\rho_w^2 + (t+1)\eta_w^2 + \alpha_w^2 + (1+\alpha_w)^2 + \gamma_w^2 = t+2 \implies |\eta_w| \leq 1 \tag{2}$$

$$v \cdot (-e_1 + a - b) = -\rho_v + 2\alpha_v + 1 = 0 \implies \alpha_v = \frac{\rho_v - 1}{2} \tag{3}$$

$$w \cdot (-e_1 + a - b) = 2\alpha_w - \rho_w = -2 \implies \alpha_w = \frac{\rho_w - 2}{2} \tag{4}$$

$$v \cdot w = (s+1)\rho_v\rho_w + t\eta_w\eta_v + (\eta_v+1)\eta_w + \alpha_v\alpha_w + (1+\alpha_v)(1+\alpha_w) + \gamma_w\gamma_v = 0. \tag{5}$$

Note that equation (3) implies $\rho_v = \pm 1$, and equation (4) implies ρ_w is even.

- **Case $\rho_v = -1$:**
  After substituting for ρ_v and simplifying, the system becomes:

$$\eta_v^2 t + (\eta_v+1)^2 + \gamma_v^2 = 1 \implies \eta_v = \gamma_v = 0 \tag{1}$$

$$(s+1)\rho_w^2 + (t+1)\eta_w^2 + \alpha_w^2 + (1+\alpha_w)^2 + \gamma_w^2 = t+2 \implies |\eta_w| \leq 1 \tag{2}$$

$$\alpha_v = -1 \tag{3}$$

$$\alpha_w = \frac{\rho_w - 2}{2} \tag{4}$$

$$(s+1)\rho_w + \alpha_w = \eta_w \implies \rho_w = \frac{2(\eta_w+1)}{2s+3}. \tag{5}$$

  We are working under the assumption that $t \geq 3$. This implies that in equation (1) $\eta_v = 0$, and thus $\gamma_v = 0$. A direct calculation shows that whenever η_w equals 0 or 1 the system is inconsistent. This can be seen in equation (5) where we obtain that ρ_w is not an integer. This leaves us with the case $\eta_w = -1$. It immediately follows that $v = -(e_1 + \cdots + e_{s+1}) + f_{t+1} - a$ and $w = -(f_1 + \cdots + f_{t+1}) - a$. The resulting lattice embedding is that of [49], which does not satisfy the conditions of Proposition 3.9.

- **Case $\rho_v = 1$:**
  After substituting for ρ_v and simplifying, the system becomes:

$$\eta_v^2 t + (\eta_v + 1)^2 + \gamma_v^2 = 1 \implies \eta_v = \gamma_v = 0 \tag{1}$$

$$(s+1)\rho_w^2 + (t+1)\eta_w^2 + \alpha_w^2 + (1+\alpha_w)^2 + \gamma_w^2 = t+2 \implies |\eta_w| \leq 1 \tag{2}$$

$$\alpha_v = 0 \tag{3}$$

$$\alpha_w = \frac{\rho_w - 2}{2} \tag{4}$$

$$(s+1)\rho_w + \alpha_w + \eta_w + 1 = 0 \implies \rho_w = -\frac{2\eta_w}{2s+3}. \tag{5}$$

As in the previous case, $t \geq 3$ implies that both η_v and γ_v are equal to 0. From equation (5) we see that $\eta_w = \pm 1$ leads to an inconsistent system, since ρ_w would not be an integer. The case $\eta_w = 0$ directly leads to the mapping $v = e_1 + \cdots + e_{s+1} + f_{t+1} - b$ and $w = -a + \gamma_w c$, whenever $t = \gamma_w^2 - 1$. This gives rise to a lattice embedding that employs each basis vector for $\mathbb{Z}^{s+t+5}$. The orthogonal complement vector is generated by

$$(\underbrace{\gamma_w, \ldots, \gamma_w}_{s+1 \text{ times}}, \underbrace{-\gamma_w(2s+3), \ldots, -\gamma_w(2s+3)}_{t+1 \text{ times}}, \gamma_w, -\gamma_w, 1),$$

Note that $t \geq 3$ and $t = \gamma_w^2 - 1$ imply that $\gamma_w \leq -2$ or $\gamma_w \geq 2$. In particular, this means that the orthogonal vector presented has no zero entries. The square of this vector is $\gamma_w^4(2s+3)^2 + 2\gamma_w^2(2s+3) + 1$, which is equal to p with the condition $t = \gamma_w^2 - 1$. Thus, by Proposition 3.9, lens spaces satisfying the aforementioned conditions for p and q, are unobstructed from embedding in $\mathbb{C}P^2$.

The analysis of the general case shows that it is always possible to find an embedding satisfying Proposition 3.9 whenever $t = \gamma_w^2 - 1$, $t \geq 3$.

§ 4.2.2 | Remaining Cases

In this section we analyse the possible lattice embeddings of $B^2_{s,t}$ in $\mathbb{Z}^{s+t+5}$ whenever either $s < 3$ or $t < 3$.

We begin with the infinite family $B^2_{s,1}$, for $s \geq 3$. We follow the same approach as for the general case for $s \geq 3$. Additional care is required because of $t = 1$. This will result in two embeddings in $\mathbb{Z}^{s+6}$, both equivalent to the one in [49]. As expected, no embedding will satisfy the conditions of Proposition 3.9.

Next, we look for embeddings of $B^2_{s,2}$ in $\mathbb{Z}^{s+7}$, for $s \geq 3$. The only way to construct an

embedding is that of the general case, thus there is no embedding satisfying the conditions of Proposition 3.9.

Now we focus on the string $B^2_{0,t}$, assuming $t \geq 3$. If we try to map each vertex of the corresponding plumbing diagram to a linear combination of the basis vectors of $\mathbb{Z}^{t+5}$, then the only possible pattern is the one discussed for the general case. Some additional care must be taken when solving the resulting system of equations, particularly when $t = 3$. These calculations will give the same result as the general case (also in the case $t = 3$). Whenever $t = \gamma_w^2 - 1$, we may embed $B^2_{0,t}$ in $\mathbb{Z}^{t+5}$ as discussed in the previous subsection. The embedding in question satisfies the conditions of Proposition 3.9, hence any lens space with $p = (3t+4)^2$ and $q = (3t+4)^2 - 3(3t+3)$ for $t = \gamma_w^2 - 1 > 0$ is unobstructed from embedding in $\mathbb{C}P^2$.

Next, we consider the infinite family $B^2_{1,t}$ with $t \geq 3$ and try to find a lattice embedding in $\mathbb{Z}^{t+6}$. Even in this case, the only possible way to map each vertex of the plumbing diagram to a linear combination of the basis vectors of $\mathbb{Z}^{t+6}$ is via the pattern of the general case, resulting in embeddings satisfying Proposition 3.9 whenever $t = \gamma_w^2 - 1$.

Now consider the embedding of the lattice on $B^2_{2,t}$ in $\mathbb{Z}^{t+7}$, with $t \geq 3$. One possible lattice embedding follows the pattern of the general case and, as expected, leads to embeddings of interest whenever $t = \gamma_w^2 - 1$. In this case, however, there is also another potential lattice embedding we may consider, which is presented in Figure 4.5 below.

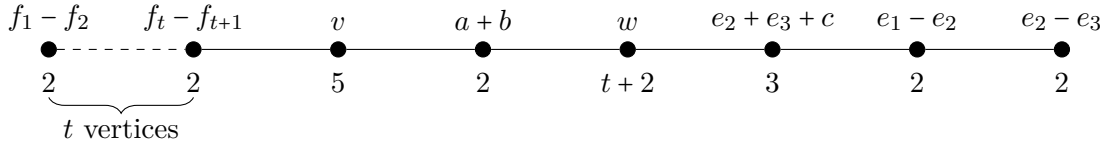

Figure 4.5: Potential embedding of $B^2_{2,t}$ in $\mathbb{Z}^{t+7}$ for $t \geq 3$.

Let $v := \rho_v(e_1 + e_2 + e_3) + \eta_v(f_1 + \cdots + f_t) + (\eta_v + 1)f_{t+1} + \alpha_v a - (1 + \alpha_v)b + \gamma_v c$ and $w := \rho_w(e_1 + e_2 + e_3) + \eta_w(f_1 + \cdots + f_{t+1}) + \alpha_w a - (1 + \alpha_w)b + \gamma_w c$. In order to explicitly determine the coefficients of the linear combinations described, we set up the following system of equations:

$$3\rho_v^2 + \eta_v^2 t + (\eta_v + 1)^2 + \alpha_v^2 + (1 + \alpha_v)^2 + \gamma_v^2 = 5 \tag{1}$$
$$3\rho_w^2 + (t+1)\eta_w^2 + \alpha_w^2 + (1 + \alpha_w)^2 + \gamma_w^2 = t + 2 \implies |\eta_w| \leq 1 \tag{2}$$
$$\gamma_v = -2\rho_v \tag{3}$$
$$\gamma_w = -1 - 2\rho_w \tag{4}$$
$$3\rho_v\rho_w + \eta_w\eta_v t + (\eta_v + 1)\eta_w + \alpha_v\alpha_w + (1 + \alpha_v)(1 + \alpha_w) + \gamma_v\gamma_w = 0. \tag{5}$$

Note that after substituting $\gamma_v = -2\rho_v$ into equation (1), we are forced to have $\rho_v = 0$. The system thus simplifies to the following:

$$\eta_v^2 t + (\eta_v + 1)^2 + \alpha_v^2 + (1 + \alpha_v)^2 = 5 \tag{1}$$
$$3\rho_w^2 + (t+1)\eta_w^2 + \alpha_w^2 + (1 + \alpha_w)^2 + \gamma_w^2 = t + 2 \implies |\eta_w| \leq 1 \tag{2}$$
$$\gamma_v = 0 \tag{3}$$
$$\gamma_w = -1 - 2\rho_w \tag{4}$$
$$\eta_w\eta_v t + (\eta_v + 1)\eta_w + \alpha_v\alpha_w + (1 + \alpha_v)(1 + \alpha_w) = 0. \tag{5}$$

Note that whenever $\eta_w = \pm 1$, equation (2) simplifies to $3\rho_w^2 + \alpha_w^2 + (1+\alpha_w)^2 + \gamma_w^2 = 1$. Then we must have $\rho_w = 0$ and equation (2) becomes $2\alpha_w^2 + 2\alpha_w + \gamma_w^2 = 0$, forcing $\gamma_w = 0$ (and $\alpha_w = 0$ or $\alpha_w = -1$). But this contradicts equation (4), by which $\gamma_w = -1$. Thus, it is not possible to find a lattice embedding of $B_{2,t}^2$ in $\mathbb{Z}^{t+7}$ when $\rho_v = 0$ and $\eta_w = \pm 1$. We now analyse the case $\eta_w = 0$. The system of equations becomes:

$$\eta_v^2 t + (\eta_v + 1)^2 + \alpha_v^2 + (1 + \alpha_v)^2 + \gamma_v^2 = 5 \tag{1}$$
$$3\rho_w^2 + \alpha_w^2 + (1 + \alpha_w)^2 + \gamma_w^2 = t + 2 \tag{2}$$
$$\gamma_v = 0 \tag{3}$$
$$\gamma_w = -1 - 2\rho_w \tag{4}$$
$$\alpha_v\alpha_w + (1 + \alpha_v)(1 + \alpha_w) = 0 \implies \alpha_v = -\frac{1 + \alpha_w}{1 + 2\alpha_w}. \tag{5}$$

Equation (5) leads to two cases to consider:

- Case $\alpha_w = 0$:

The system can be simplified as follows:

$$\eta_v^2(7\rho_w^2 + 4\rho_w + 1) + 2\eta_v - 3 = 0 \tag{1}$$
$$t = 7\rho_w^2 + 4\rho_w \tag{2}$$
$$\gamma_v = 0 \tag{3}$$
$$\gamma_w = -1 - 2\rho_w \tag{4}$$
$$\alpha_v = -1. \tag{5}$$

We try to solve equation (1) for η_v. The reduced discriminant is $21\rho_w^2 + 12\rho_w + 4$. Since we are looking for integer solutions, we want this to equal a square number, so set $21\rho_w^2 + 12\rho_w + 4 = k^2$, for some $k \in \mathbb{Z}$. The two solutions for η_v are then $-\frac{3}{k-1}$ and $\frac{3}{k+1}$. Suppose $\eta_v = -\frac{3}{k-1}$: since we want it to be an integer, the only possible values of k are 0, ± 2, 4. The only case in which $21\rho_w^2 + 12\rho_w + 4 = k^2$ has an integer solution is when $k = \pm 2$ and we obtain $\rho_w = 0$. However, using equation (2) this implies that $t = 0$, contradicting our initial assumption. Next, consider $\eta_v = \frac{3}{k+1}$. As for the other solution, this implies that k must be either 0, ± 2 or -4. The only option we can consider is when $k = \pm 2$ and $\rho_w = 0$, which again leads to a contradiction. Hence, for $t \geq 3$ there is no embedding of $B_{2,t}^2$ in $\mathbb{Z}^{t+7}$ for the specified parameters.

- Case $\alpha_w = -1$:
  The system can be simplified as follows:

$$\eta_v^2(7\rho_w^2 + 4\rho_w + 1) + 2\eta_v - 3 = 0 \tag{1}$$
$$t = 7\rho_w^2 + 4\rho_w \tag{2}$$
$$\gamma_v = 0 \tag{3}$$
$$\gamma_w = -1 - 2\rho_w \tag{4}$$
$$\alpha_v = 0. \tag{5}$$

  The system follows the same pattern as for $\alpha_w = 0$ for equations (1) and (2), hence the same conclusions apply.

We have proved that for $t \geq 3$ there is no way to embed the lattice on $B_{2,t}^2$ in $\mathbb{Z}^{t+7}$, according to the mapping in Figure 4.5.

We have concluded our analysis of the infinite families $B_{s,t}^2$ when either $s < 3$ or $t < 3$, so it only remains to check the individual cases excluded up to now. This was done via GAP's `OrthogonalEmbeddings` command [25], and we will present an example of how such code was used.

Consider $B^2_{0,1} = [2,3,2,3,3]^-$ and its lattice embeddings in $\mathbb{Z}^6$. To obtain the information wanted, we input the adjacency matrix corresponding to $B^2_{0,1}$ into the `OrthogonalEmbeddings` command, together with the dimension of $\mathbb{Z}^n$ we want to embed in:

```
OrthogonalEmbeddings([[2,-1,0,0,0],
                      [-1,3,-1,0,0],
                      [0,-1,2,-1,0],
                      [0,0,-1,3,-1],
                      [0,0,0,-1,3]], 6);
```

This will output:

```
rec( norms := [ 1, 1, 1, 1, 1, 48/49, 48/49, 47/49, 47/49, 45/49, 41/49,
40/49, 40/49, 38/49, 34/49, 34/49, 31/49, 31/49, 27/49, 26/49, 24/49, 19/49 ],
    solutions := [ [ 1, 2, 3, 4, 5 ], [ 6, 7, 10, 12, 13, 21 ] ],
    vectors := [ [ 1, -1, 0, 1, 0 ], [ -1, 0, 0, 1, 0 ], [ 0, -1, 1, -1, 1 ],
            [ 0, 1, 0, 0, 1 ], [ 0, 0, -1, 0, 1 ], [ 1, -1, 0, 0, 1 ],
            [ -1, 0, 0, 0, 1 ], [ 0, 1, -1, 0, 1 ], [ 0, 0, 1, -1, 1 ],
            [ 0, 1, 0, -1, 1 ], [ 0, -1, 0, 0, 1 ], [ 0, 1, -1, 1, 0 ],
            [ 0, 0, 1, 0, 0 ], [ 0, -1, 0, 1, 0 ], [ 0, -1, 1, 0, 0 ],
            [ 0, 0, -1, 1, 0 ], [ -1, 1, 0, 0, 0 ], [ 1, 0, 0, 0, 0 ],
            [ 0, 0, 0, -1, 1 ], [ 0, 1, 0, 0, 0 ], [ 0, 0, 0, 1, 0 ],
            [ 0, 0, 0, 0, 1 ] ] ).
```

The list named `solutions` contains two sublists, which correspond to two possible lattice embeddings in $\mathbb{Z}^6$. The elements of each sublist specify which elements should be taken from `vectors` as the rows of a matrix describing the embedding. Note that the first embedding in `solutions` employs five vectors: this is the embedding found in [49]. The second list contains six vectors and specifies the embedding below. The orthogonal

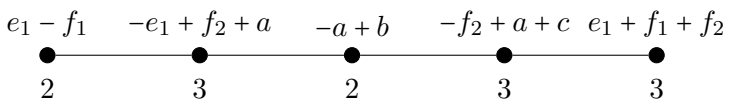

Figure 4.6: Lattice embedding of $B^2_{0,1}$ in $\mathbb{Z}^6$.

complement is generated by the vector

$$(1,1,-2,3,3,-5),$$

which has square equal to $49 = p$. Thus, the lens space $L(49, 31)$ is unobstructed from embedding into $\mathbb{C}P^2$.

The remaining cases were analysed via GAP in the same fashion, but did not produce any embeddings satisfying Proposition 3.9. Table 4.2 presents a summary of the outcome of the analysis of these cases using GAP.

$B^2_{s,t}$	s	t	Result
	0	1	Unobstructed
	0	2	Obstructed since Lisca's embedding is the only possibility
	1	1	Obstructed since Lisca's embedding is the only possibility
	1	2	Obstructed since Lisca's embedding is the only possibility
	2	1	Obstructed since Lisca's embedding is the only possibility
	2	2	Obstructed since Lisca's embedding is the only possibility

Table 4.2: Summary of GAP analysis for $B^2_{s,t}$ when $s < 3$ and $t < 3$.

§ 4.3 | String $C^1_{s,t}$

In this section we discuss the string $C^1_{s,t} = [t+2, s+2, 3, 2^{[t]}, 4, 2^{[s]}]^-$ with $s > 0$, $t \geq 0$, according to the classification in [2]. From [49] it is known that the string $C^1_{s,t}$ corresponds to the continued fraction expansion of:

$$\frac{p}{q} = \frac{(2st + 4s + 3t + 5)^2}{(2s+3)^2(t+2)}.$$

Note that q can be rewritten as $q = (2s+3)(2st + 4s + 3t + 6)$ and hence we deduce that $C^1_{s,t}$ is obtained from lens spaces of Lisca type (3) with $q = d(m+1)$ (from Theorem 3.2). Recall that $C^1_{s,t}$ is dual to $rC^3_{t,s-1}$. As the string $C^1_{s,t}$ has $s+t = 4$ vertices, we are interested in lattice embeddings in $\mathbb{Z}^{s+t+5}$. Throughout this section, let $e_1, \ldots, e_{s+1}, f_1, \ldots, f_{t+1}, a, b, c$ be an orthonormal basis for $\mathbb{Z}^{s+t+5}$.

§ 4.3.1 | General Argument

The general argument presented in this subsection holds for $s \geq 4$ and $t \geq 3$. The remaining possibilities will be analysed in the next subsection.

As usual, we need to map each vertex of the diagram associated to $C^1_{s,t}$ to a linear combination of basis vectors of $\mathbb{Z}^{s+t+5}$. Under the conditions specified above, there is only one way to do it, shown in Figure 4.7.

Let $v := \rho_v(e_1 + \cdots + e_{s+1}) + \eta_v(f_1 + \cdots + f_{t+1}) + \alpha_v a + \beta_v b + \gamma_v c$ and $w := \rho_w(e_1 + \cdots + e_{s+1}) + \eta_w(f_1 + \cdots + f_{t+1}) + \alpha_w a + \beta_w b + \gamma_w c$. In order to determine the integer coefficients, set up

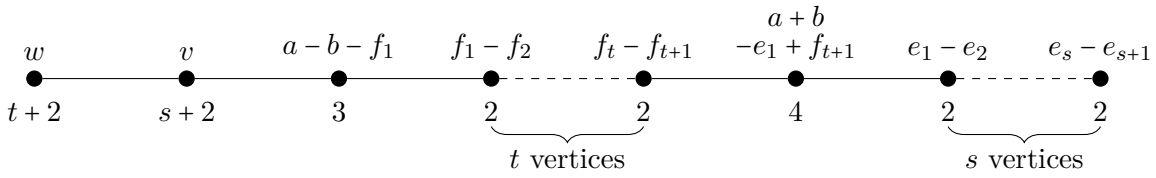

Figure 4.7: Potential embedding of $C^1_{s,t}$ in $\mathbb{Z}^{s+t+5}$ for $s \geq 4$ and $t \geq 3$.

the following system:

$$v \cdot v = (s+1)\rho_v^2 + (t+1)\eta_v^2 + \alpha_v^2 + \beta_v^2 + \gamma_v^2 = s+2 \implies |\rho_v| \leq 1 \tag{1}$$
$$w \cdot w = (s+1)\rho_w^2 + (t+1)\eta_w^2 + \alpha_w^2 + \beta_w^2 + \gamma_w^2 = t+2 \implies |\eta_w| \leq 1 \tag{2}$$
$$v \cdot (a - b - f_1) = \alpha_v - \beta_v - \eta_v = -1 \tag{3}$$
$$v \cdot (a + b - e_1 + f_{t+1}) = \alpha_v + \beta_v - \rho_v + \eta_v = 0 \tag{4}$$
$$w \cdot (a - b - f_1) = \alpha_w - \beta_w - \eta_w = 0 \tag{5}$$
$$w \cdot (a + b - e_1 + f_{t+1}) = \alpha_w + \beta_w - \rho_w + \eta_w = 0 \tag{6}$$
$$v \cdot w = (s+1)\rho_v\rho_w + (t+1)\eta_v\eta_w + \alpha_v\alpha_w + \beta_v\beta_w + \gamma_v\gamma_w = -1. \tag{7}$$

We need to consider the cases $\rho_v = -1$, $\rho_v = 0$, $\rho_v = 1$, and do the same for η_w.

- **Case $\rho_v = -1$:**
  The system can be reduced to:

$$(t+1)\eta_v^2 + \alpha_v^2 + \beta_v^2 + \gamma_v^2 = 1 \implies \eta_v = 0 \tag{1}$$
$$(s+1)\rho_w^2 + (t+1)\eta_w^2 + \alpha_w^2 + \beta_w^2 + \gamma_w^2 = t+2 \implies |\eta_w| \leq 1 \tag{2}$$
$$\alpha_v = -1 \implies \gamma_v = 0 \tag{3}$$
$$\beta_v = 0 \tag{4}$$
$$\alpha_w - \beta_w - \eta_w = 0 \tag{5}$$
$$\alpha_w + \beta_w - \rho_w + \eta_w = 0 \tag{6}$$
$$(s+1)\rho_w + \alpha_w = 1. \tag{7}$$

  - Case $\eta_w = \pm 1$:

Focus on the following subset of equations:

$$(s+1)\rho_w^2 + \alpha_w^2 + \beta_w^2 + \gamma_w^2 = 1 \implies \rho_w = 0 \tag{2}$$
$$\alpha_w = 0 \tag{5}$$
$$\beta_w = \mp 1 \tag{6}$$
$$0 = 1. \tag{7}$$

The system is inconsistent, hence there is no lattice embedding of $C^1_{s,t}$ in $\mathbb{Z}^{s+t+5}$ when $\rho_v = -1$ and $\eta_w = \pm 1$.

– Case $\eta_w = 0$:
Once again, focus on the following subset of equations:

$$(s+1)\rho_w^2 + \alpha_w^2 + \beta_w^2 + \gamma_w^2 = t+2 \tag{2}$$
$$\alpha_w = \beta_w \tag{5}$$
$$\rho_w = 2\alpha_w \tag{6}$$
$$\alpha_w = \frac{1}{2s+3}. \tag{7}$$

The variable s is defined so that $s > 0$ (and in this case $s \geq 4$), so it is not possible to obtain an integer solution for α_w. Hence, there is no lattice embedding of $C^1_{s,t}$ in $\mathbb{Z}^{s+t+5}$ when $\rho_v = -1$ and $\eta_w = 0$.

- **Case** $\rho_v = 0$**:**
After substituting $\rho_v = 0$, we may focus on a subset of equations:

$$(t+1)\eta_v^2 + \alpha_v^2 + \beta_v^2 + \gamma_v^2 = s+2 \tag{1}$$
$$(s+1)\rho_w^2 + (t+1)\eta_w^2 + \alpha_w^2 + \beta_w^2 + \gamma_w^2 = t+2 \implies |\eta_w| \leq 1 \tag{2}$$
$$\eta_v = \alpha_v - \beta_v + 1 \tag{3}$$
$$\alpha_v = -\frac{1}{2}. \tag{4}$$

As α_v does not admit any integer solutions, there is no lattice embedding of $C^1_{s,t}$ in $\mathbb{Z}^{s+t+5}$ when $\rho_v = 0$.

- **Case** $\rho_v = 1$**:**

The system can be simplified as follows:

$$(t+1)\eta_v^2 + \alpha_v^2 + \beta_v^2 + \gamma_v^2 = 1 \implies \eta_v = 0 \tag{1}$$
$$(s+1)\rho_w^2 + (t+1)\eta_w^2 + \alpha_w^2 + \beta_w^2 + \gamma_w^2 = t+2 \implies |\eta_w| \leq 1 \tag{2}$$
$$\alpha_v = 0 \tag{3}$$
$$\beta_v = 1 \implies \gamma_v = 0 \tag{4}$$
$$\alpha_w - \beta_w - \eta_w = 0 \tag{5}$$
$$\alpha_w + \beta_w - \rho_w + \eta_w = 0 \tag{6}$$
$$(s+1)\rho_w + \beta_w = -1. \tag{7}$$

– Case $\eta_w = -1$:
The system is inconsistent, as can be seen from the following equations:

$$(s+1)\rho_w^2 + \alpha_w^2 + \beta_w^2 + \gamma_w^2 = 1 \implies \rho_w = 0 \tag{2}$$
$$\alpha_w = 0 \tag{5}$$
$$\beta_w = 1 \tag{6}$$
$$1 = -1. \tag{7}$$

Hence there is no lattice embedding of $C^1_{s,t}$ in $\mathbb{Z}^{s+t+5}$ when $\rho_v = 1$ and $\eta_w = -1$.

– Case $\eta_w = 0$:
Focus on the following equations:

$$(s+1)\rho_w^2 + \alpha_w^2 + \beta_w^2 + \gamma_w^2 = t+2 \tag{2}$$
$$\alpha_w = \beta_w \tag{5}$$
$$\rho_w = 2\alpha_w \tag{6}$$
$$\alpha_w = -\frac{1}{2s+3}. \tag{7}$$

As there are no integer solutions for α_w when $s \geq 4$, there is no lattice embedding of $C^1_{s,t}$ in $\mathbb{Z}^{s+t+5}$ when $\rho_v = 1$ and $\eta_w = 0$.

– Case $\eta_w = 1$:

The system has the following solution:

$$\eta_v = 0,\ \gamma_v = 0 \tag{1}$$
$$\gamma_w = 0 \tag{2}$$
$$\alpha_v = 0 \tag{3}$$
$$\beta_v = 1 \tag{4}$$
$$\alpha_w = 0 \tag{5}$$
$$\beta_w = -1 \tag{6}$$
$$\rho_w = 0. \tag{7}$$

Together with Figure 4.7, $v = e_1 + \cdots + e_{s+1} + b$ and $w = f_1 + \cdots + f_{t+1} - b$ define an embedding of $C^1_{s,t}$ in $\mathbb{Z}^{s+t+5}$. This corresponds to Lisca's embedding from [49], so it does not satisfy the conditions of Proposition 3.9.

The complete analysis of $C^1_{s,t}$ showed that for $s \geq 4$ and $t \geq 3$ there are no lattice embeddings into $\mathbb{Z}^{s+t+5}$ satisfying Proposition 3.9.

§ 4.3.2 | Remaining Cases

In this section we analyse possible embeddings of $C^1_{s,t}$ in $\mathbb{Z}^{s+t+5}$ when either $s < 4$ or $t < 3$. We start by considering infinite families and then focus on the remaining cases.

The first infinite family we consider is the one associated to the string $C^1_{s,0}$, where $s \geq 4$. It can be seen that the only way to map each vertex to a combination of basis elements of $\mathbb{Z}^{s+5}$ is by following the same pattern as in the general case. Some additional care is required in the calculations, since in this case $t \leq 3$, but we will obtain two equivalent embeddings, corresponding to the one in [49].

Next, we consider the string $C^1_{s,1}$ and look for lattice embeddings in $\mathbb{Z}^{s+6}$ where $s \geq 4$. One way to obtain such an embedding is by following the general case, hence the same conclusions will apply. The second way to potentially obtain a lattice embedding is shown in Figure 4.8.

Again, let $v := \rho_v(e_1 + \cdots + e_{s+1}) + \eta_v(f_1 + f_2) + \alpha_v a + \beta_v b + \gamma_v c$ and $w := \eta_w(f_1 + f_2) + \alpha_w a + \beta_w b + \gamma_w c$. Set up the following system of equations to determine the coefficients of v and w:

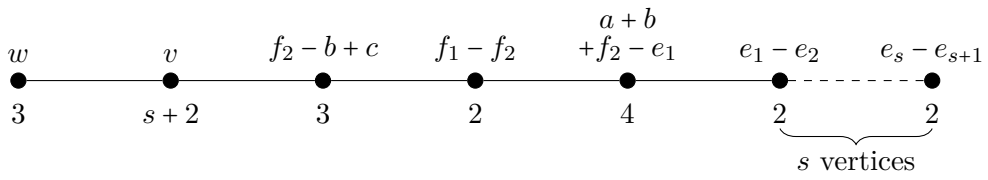

Figure 4.8: Second potential embedding of $C^1_{s,1}$ in $\mathbb{Z}^{s+6}$ for $s \geq 4$.

$$(s+1)\rho_v^2 + 2\eta_v^2 + \alpha_v^2 + \beta_v^2 + \gamma_v^2 = s+2 \implies |\rho_v| \leq 1 \tag{1}$$
$$2\eta_w^2 + \alpha_w^2 + \beta_w^2 + \gamma_w^2 = 3 \tag{2}$$
$$\eta_v - \beta_v + \gamma_v = -1 \tag{3}$$
$$\eta_v - \rho_v + \alpha_v + \beta_v = 0 \tag{4}$$
$$\eta_w - \beta_w + \gamma_w = 0 \tag{5}$$
$$\eta_w + \alpha_w + \beta_w = 0 \tag{6}$$
$$2\eta_v\eta_w + \alpha_v\alpha_w + \beta_v\beta_w + \gamma_v\gamma_w = -1. \tag{7}$$

We consider three different cases.

- **Case $\rho_v = -1$:**
  After performing the required substitution, we focus on a subset of equations to show that the system is inconsistent:

  $$2\eta_v^2 + \alpha_v^2 + \beta_v^2 + \gamma_v^2 = 1 \implies \eta_v = 0 \tag{1}$$
  $$\gamma_v = \beta_v - 1 \tag{3}$$
  $$\alpha_v = -1 - \beta_v. \tag{4}$$

  Combining everything in equation (1) we obtain $\beta_v^2 = -\frac{1}{3}$. Hence, there is no lattice embedding in $\mathbb{Z}^{s+6}$ when $\rho_v = -1$.

- **Case $\rho_v = 0$:**
  After performing the appropriate substitution, the system can be simplified as follows:

$$2\eta_v^2 + \alpha_v^2 + \beta_v^2 + \gamma_v^2 = s + 2 \tag{1}$$
$$2\eta_w^2 + \alpha_w^2 + \beta_w^2 + \gamma_w^2 = 3 \tag{2}$$
$$\eta_v - \beta_v + \gamma_v = -1 \tag{3}$$
$$\eta_v + \alpha_v + \beta_v = 0 \tag{4}$$
$$\eta_w - \beta_w + \gamma_w = 0 \tag{5}$$
$$\eta_w + \alpha_w + \beta_w = 0 \tag{6}$$
$$2\eta_v\eta_w + \alpha_v\alpha_w + \beta_v\beta_w + \gamma_v\gamma_w = -1. \tag{7}$$

From equation (2) we see that in order to have integer solutions for the parameters, we need to consider two main cases: $\eta_w = \pm 1$ and $\eta_w = 0$.

– Case $\eta_w = \pm 1$:
Focus on the following subset of equations:

$$\alpha_w^2 + 2\gamma_w^2 \pm 2\gamma_w = 0 \implies \alpha_w = 0 \text{ and } \gamma_w \in \{0, \mp 1\} \tag{2}$$
$$\beta_w = \gamma_w \pm 1 \tag{5}$$
$$\beta_w = -\eta_w = \mp 1. \tag{6}$$

Observe that γ_w can either be 0 or ∓ 1, but both these values make the system inconsistent, as equation (5) and (6) would contradict each other. Hence, there is no lattice embedding of $C^1_{s,1}$ in $\mathbb{Z}^{s+6}$ when $\rho_v = 0$ and $\eta_w = \pm 1$.

– Case $\eta_w = 0$:
Perform the substitution and simplify the system as follows:

$$2\eta_v^2 + \alpha_v^2 + \beta_v^2 + \gamma_v^2 = s + 2 \tag{1}$$
$$\alpha_w^2 + \beta_w^2 + \gamma_w^2 = 3 \implies \alpha_w^2 = 1 \tag{2}$$
$$\eta_v - \beta_v + \gamma_v = -1 \tag{3}$$
$$\eta_v + \alpha_v + \beta_v = 0 \tag{4}$$
$$\beta_w = \gamma_w \tag{5}$$
$$\alpha_w = -\beta_w \tag{6}$$
$$\alpha_v\alpha_w + \beta_v\beta_w + \gamma_v\gamma_w = -1. \tag{7}$$

From equation (2) we see that $\alpha_w = \pm 1$. When $\alpha_w = 1$ we immediately see from equation (7) that $\beta_v = \frac{2}{3}$, which is not an integer solution. When $\alpha_w = -1$, the system has the following solution:

$$s = 4\eta_v^2 + 2\eta_v - 1 \tag{1}$$
$$\alpha_w^2 + \beta_w^2 + \gamma_w^2 = 3 \implies \alpha_w^2 = 1 \tag{2}$$
$$\gamma_v = -1 - \eta_v \tag{3}$$
$$\alpha_v = -\eta_v \tag{4}$$
$$\gamma_w = 1 \tag{5}$$
$$\beta_w = 1 \tag{6}$$
$$\beta_v = 0. \tag{7}$$

Hence $v = \eta_v(f_1 + f_2) - \eta_v a - (1+\eta_v)c$ and $w = -a + b + c$ together with Figure 4.8 describe a lattice embedding in $\mathbb{Z}^{s+6}$, when $s = 4\eta_v^2 + 2\eta_v - 1$. The orthogonal complement is generated by the vector

$$(\underbrace{12\eta_v + 3, \ldots, 12\eta_v + 3}_{s+1 \text{ times}}, 3\eta_v + 1, 3\eta_v + 1, 5\eta_v + 1, 4\eta_v + 1, \eta_v),$$

which has square $576\eta_v^4 + 576\eta_v^3 + 240\eta_v^2 + 48\eta_v + 4 = p$. Since $s \geq 4$, we have $\eta_v \leq -2$ or $\eta_v \geq 1$; in particular, $\eta_v \neq 0$. Hence, the embedding satisfies the conditions of Proposition 3.9. Therefore, any lens space with $\frac{p}{q} = C^1_{s,1}$, with $s = 4\eta_v^2 + 2\eta_v - 1 \geq 4$, is unobstructed from embedding in $\mathbb{C}P^2$.

– **Case** $\rho_v = 1$**:**
After performing the substitution, the system simplifies to:

$$2\eta_v^2 + \alpha_v^2 + \beta_v^2 + \gamma_v^2 = 1 \implies \eta_v = 0 \tag{1}$$
$$2\eta_w^2 + \alpha_w^2 + \beta_w^2 + \gamma_w^2 = 3 \tag{2}$$
$$\gamma_v = \beta_v - 1 \tag{3}$$
$$\alpha_v = 1 - \beta_v \tag{4}$$
$$\beta_w = \eta_w + \gamma_w \tag{5}$$
$$2\eta_w + \alpha_w + \gamma_w = 0 \tag{6}$$
$$\alpha_v\alpha_w + \beta_v\beta_w + \gamma_v\gamma_w = -1. \tag{7}$$

Substituting equations (3) and (4) in (1), we obtain $3\beta_v^2 - 4\beta_v + 1 = 0$. The only

integer solution to this equation is therefore $\beta_v = 1$ and the system is solved as follows:

$$\beta_v = 1 \tag{1}$$
$$4\eta_w^2 = 0 \implies \eta_w = 0 \tag{2}$$
$$\gamma_v = 0 \tag{3}$$
$$\alpha_v = 0 \tag{4}$$
$$\gamma_w = -1 - \eta_w = -1 \tag{5}$$
$$\alpha_w = 1 - \eta_w = 1 \tag{6}$$
$$\beta_w = -1. \tag{7}$$

Hence $v = e_1 + \cdots + e_{s+1} + b$ and $w = a - b - c$ together with Figure 4.8 provide a lattice embedding in $\mathbb{Z}^{s+6}$. The orthogonal complement is generated by the vector

$$(\underbrace{0, \ldots, 0}_{s+1 \text{ times}}, -1, -1, 1, 0, 1).$$

As it is evident from the 0 entries, this embedding does not satisfy the conditions of Proposition 3.9.

This concludes the analysis of $C^1_{s,1}$ when $s \geq 4$.

We now turn to the string $C^1_{s,2}$ and look for lattice embeddings in $\mathbb{Z}^{s+7}$, $s \geq 4$. One way to find such embeddings is by following the pattern of the general case, which will result in Lisca's embedding. Figure 4.9 shows another potential way to obtain lattice embeddings in $\mathbb{Z}^{s+7}$, with $v := \rho_v(e_1 + \cdots + e_{s+1}) + \eta_v(f_1 + f_2 + f_3) + \alpha_v a + \beta_v b + \gamma_v c$ and $w := \eta_w(f_1 + f_2 + f_3) + \alpha_w a + \beta_w b + \gamma_w c$.

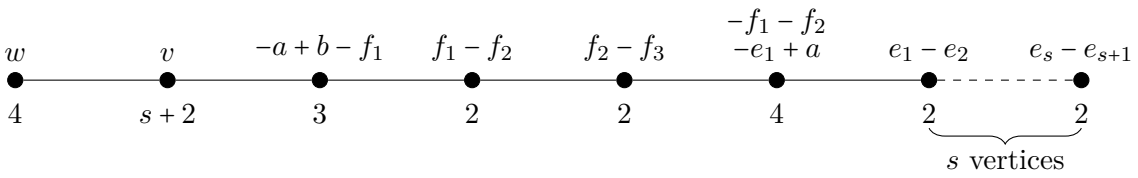

Figure 4.9: Potential embedding of $C^1_{s,2}$ in $\mathbb{Z}^{s+7}$ for $s \geq 4$.

Set up the following system of equations:

$$(s+1)\rho_v^2 + 3\eta_v^2 + \alpha_v^2 + \beta_v^2 + \gamma_v^2 = s+2 \implies |\rho_v| \leq 1 \tag{1}$$
$$3\eta_w^2 + \alpha_w^2 + \beta_w^2 + \gamma_w^2 = 4 \tag{2}$$
$$\beta_v - \alpha_v - \eta_v = -1 \tag{3}$$
$$\alpha_v - 2\eta_v - \rho_v = 0 \tag{4}$$
$$\beta_w - \eta_w - \alpha_w = 0 \tag{5}$$
$$\alpha_w - 2\eta_w = 0 \tag{6}$$
$$3\eta_v\eta_w + \alpha_v\alpha_w + \beta_v\beta_w + \gamma_v\gamma_w = -1. \tag{7}$$

Equation (2) can be rewritten as $7\eta_w^2 + \beta_w^2 + \gamma_w^2 = 4$, which implies $\eta_w = \alpha_w = \beta_w = 0$ and $\gamma_w = \pm 2$. Substituting these values into equation (7), we obtain $\pm 2\gamma_v = -1$, which does not give rise to integer solutions for γ_v. Hence, the only lattice embedding of $C_{s,2}^1$ in $\mathbb{Z}^{s+7}$ is Lisca's.

For the string $C_{1,t}^1$ we are interested in embeddings in $\mathbb{Z}^{t+6}$, when $t \geq 3$. It can be directly verified that the only way to produce such an embedding is by following the pattern from the general case, hence the same conclusions apply.

Next, we consider $C_{2,t}^1$ when $t \geq 3$. Aside from the pattern provided in the general case, which gives rise to the embedding in [49], we may also try to find an embedding in $\mathbb{Z}^{t+7}$ as shown in Figure 4.10. Here $v \coloneqq \rho_v(e_1+e_2+e_3) + \alpha_v a + \beta_v b + \gamma_v c$ and $w \coloneqq \rho_w(e_1+e_2+e_3) + \eta_w(f_1+\cdots+f_{t+1}) + \alpha_w a + \beta_w b + \gamma_w c$. Set up the following system of

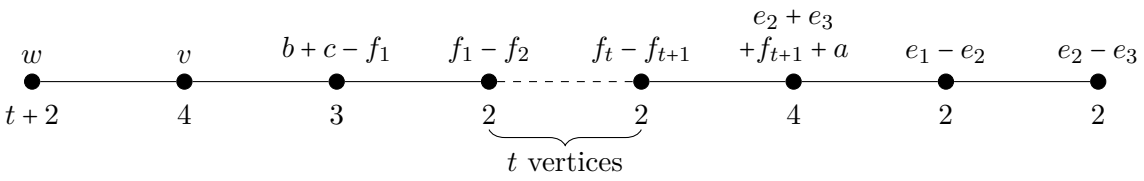

Figure 4.10: Potential embedding of $C_{2,t}^1$ in $\mathbb{Z}^{t+7}$ for $t \geq 3$.

equations:

$$3\rho_v^2 + \alpha_v^2 + \beta_v^2 + \gamma_v^2 = 4 \tag{1}$$
$$3\rho_w^2 + (t+1)\eta_w^2 + \alpha_w^2 + \beta_w^2 + \gamma_w^2 = t+2 \tag{2}$$
$$\beta_v + \gamma_v = -1 \tag{3}$$
$$2\rho_v + \alpha_v = 0 \tag{4}$$
$$\beta_w + \gamma_w - \eta_w = 0 \tag{5}$$
$$\eta_w + 2\rho_w + \alpha_w = 0 \tag{6}$$
$$3\rho_v\rho_w + \alpha_v\alpha_w + \beta_v\beta_w + \gamma_v\gamma_w = -1. \tag{7}$$

Combining equations (3) and (4) in (1), we obtain $2\beta_v^2 + 2\beta_v - 3 = 0$, which has no integer solutions. Therefore it is not possible to obtain a lattice embedding via the mapping in Figure 4.10.

Finally, we analyse lattice embeddings of $C^1_{3,t}$ in $\mathbb{Z}^{t+8}$ when $t \geq 3$. As usual, one embedding can be obtained following the pattern discussed in the general case. We now discuss an alternative way to potentially obtain a lattice embedding, shown in Figure 4.11 with $v := \rho_v(e_1 + \cdots + e_4) + \eta_v(f_1 + \cdots + f_{t+1}) + \alpha_v a + \beta_v b + \gamma_v c$ and $w := \rho_w(e_1 + \cdots + e_4) + \eta_w(f_1 + \cdots + f_{t+1}) + \alpha_w a + \beta_w b + \gamma_w c$.

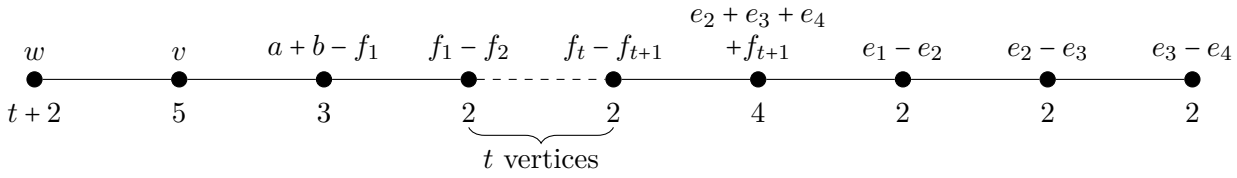

Figure 4.11: Potential embedding of $C^1_{3,t}$ in $\mathbb{Z}^{t+8}$ for $t \geq 3$.

Set up the following system of equations in order to determine the integer coefficients of

v and w:

$$4\rho_v^2 + (t+1)\eta_v^2 + \alpha_v^2 + \beta_v^2 + \gamma_v^2 = 5 \tag{1}$$
$$4\rho_w^2 + (t+1)\eta_w^2 + \alpha_w^2 + \beta_w^2 + \gamma_w^2 = t+2 \implies |\eta_w| \leq 1 \tag{2}$$
$$\alpha_v + \beta_v - \eta_v = -1 \tag{3}$$
$$\eta_v + 3\rho_v = 0 \tag{4}$$
$$\alpha_w + \beta_w - \eta_w = 0 \tag{5}$$
$$\eta_w + 3\rho_w = 0 \tag{6}$$
$$4\rho_v\rho_w + (t+1)\eta_v\eta_w + \alpha_v\alpha_w + \beta_v\beta_w + \gamma_v\gamma_w = -1. \tag{7}$$

Substituting $\eta_v = -3\rho_v$ in equation (1), we obtain $(9t+13)\rho_v^2+\alpha_v^2+\beta_v^2+\gamma_v^2 = 5$, which implies $\rho_v = 0$. Similarly, substituting $\eta_w = -3\rho_w$ in equation (2) gives $(9t+13)\rho_w^2+\alpha_w^2+\beta_w^2+\gamma_w^2 = t+2$, which implies $\rho_w = 0$. The system can be further simplified as follows:

$$2\alpha_v^2 + 2\alpha_v + \gamma_v^2 = 4 \implies -2 \leq \alpha_v \leq 1 \tag{1}$$
$$\alpha_w^2 + \beta_w^2 + \gamma_w^2 = t+2 \tag{2}$$
$$\beta_v = -1 - \alpha_v \tag{3}$$
$$\eta_v = \rho_v = 0 \tag{4}$$
$$\beta_w = -\alpha_w \tag{5}$$
$$\eta_w = \rho_w = 0 \tag{6}$$
$$\alpha_w(2\alpha_v + 1) + \gamma_v\gamma_w = -1. \tag{7}$$

As can be seen from equation (1), α_v can take four different integer values, which need to be considered separately. We remark that when $\alpha_v = -2$, we have $\beta_v = 1$ and $\gamma_v = 0$, which lead to $\alpha_w = \frac{1}{3}$ in equation (7), thus excluding this possibility. Similarly, when $\alpha_v = 1$, we have $\beta_v = -2$ and $\gamma_v = 0$, and thus $\alpha_w = -\frac{1}{3}$, excluding this case as well. Hence we only need to focus on the cases when $\alpha_v = -1$ and $\alpha_v = 0$.

Let $\alpha_v = -1$. Then $\beta_v = 0$ and $\gamma_v = \pm 2$.

- When $\gamma_v = -2$ we have $\alpha_w = 1 - 2\gamma_w$ and $t = 9\gamma_w^2 - 8\gamma_w$. Hence $v = -a - 2c$ and $w = (1-2\gamma_w)a-(1-2\gamma_w)b+\gamma_w c$ together with Figure 4.11 provide a lattice embedding

in $\mathbb{Z}^{t+8}$ when $t = 9\gamma_w^2 - 8\gamma_w$. The orthogonal complement is generated by

$$(\underbrace{-(9\gamma_w-4),\ldots,-(9\gamma_w-4)}_{4\text{ times}},\underbrace{3(9\gamma_w-4),\ldots,3(9\gamma_w-4)}_{t+1\text{ times}},12\gamma_w-6,15\gamma_w-6,6\gamma_w-3),$$

which has square $6561\gamma_w^4 - 11664\gamma_w^3 + 7938\gamma_w^2 - 2448\gamma_w + 289 = p$. Note that since $t \geq 3$, we have $\gamma_w \leq -1$ or $\gamma_w \geq 2$, thus the embedding satisfies the conditions of Proposition 3.9. Therefore, lens spaces with $\frac{p}{q} = C^1_{3,t}$, where $t = 9\gamma_w^2 - 8\gamma_w$, are unobstructed from embedding in $\mathbb{C}P^2$.

- When $\gamma_v = 2$ we immediately obtain $\alpha_w = 1+2\gamma_w$ and $t = 9\gamma_w^2+8\gamma_w$. Hence $v = -a+2c$ and $w = (1+2\gamma_w)a - (1+2\gamma_w)b + \gamma_w c$ together with Figure 4.11 provide a lattice embedding in $\mathbb{Z}^{t+8}$ when $t = 9\gamma_w^2+8\gamma_w \geq 3$. The orthogonal complement is generated by

$$(\underbrace{-(9\gamma_w+4),\ldots,-(9\gamma_w+4)}_{4\text{ times}},\underbrace{3(9\gamma_w+4),\ldots,3(9\gamma_w+4)}_{t+1\text{ times}},12\gamma_w+6,15\gamma_w+6,6\gamma_w+3),$$

which has square $6561\gamma_w^4 + 11664\gamma_w^3 + 7938\gamma_w^2 + 2448\gamma_w + 289 = p$. Note that $\gamma_w \leq -2$ or $\gamma_w \geq 1$, thus the embedding satisfies the conditions of Proposition 3.9. Hence, lens spaces with $\frac{p}{q} = C^1_{3,t}$ and $t = 2\gamma_w^2 + 8\gamma_w \geq 3$ are unobstructed from embedding in $\mathbb{C}P^2$.

Let $\alpha_v = 0$. Then $\beta_v = -1$ and $\gamma_v = \pm 2$.

- When $\gamma_v = -2$ we obtain $v = -b - 2c$ and $w = (2\gamma_w - 1)a + (1 - 2\gamma_w)b + \gamma_w c$. Thus together with Figure 4.11, we have a lattice embedding equivalent to the one found when $\gamma_w = -1$ and $\gamma_v = -2$ and the same conclusions apply.

- When $\gamma_v = 2$ the solution to the system determines that $v = -b + 2c$ and $w = -(1+2\gamma_w)a + (1+2\gamma_w)b + \gamma_w c$, which together with Figure 4.11 determine a lattice embedding equivalent to the one found in the case $\gamma_w = -1$, $\gamma_v = 2$. Therefore the same conclusions apply.

This concludes our analysis of $C^1_{3,t}$, and more generally of the infinite families of lens spaces associated with $C^1_{s,t}$. All that remains is to analyse the individual cases where both $s < 4$ and $t < 3$. Table 4.3 presents a summary of the outcome of the analysis of these cases using GAP.

Let us explicitly present the lattice embeddings that satisfy Proposition 3.9, found using GAP. The string $C^1_{1,0} = [2,3,3,4,2]^-$ presents an unobstructed embedding in $\mathbb{Z}^6$, shown in Figure 4.12. The orthogonal complement is generated by the vector

$C^1_{s,t}$	s	t	Result
	1	0	Unobstructed
	1	1	Unobstructed
	1	2	Obstructed since Lisca's embedding is the only possibility
	2	0	Obstructed since Lisca's embedding is the only possibility
	2	1	Obstructed by zero entries in vector generating orthogonal complement
	2	2	Obstructed since Lisca's embedding is the only possibility
	3	0	Unobstructed
	3	1	Unobstructed
	3	2	Obstructed since Lisca's embedding is the only possibility

Table 4.3: Summary of GAP analysis for $C^1_{s,t}$ when $s < 4$ and $t < 3$.

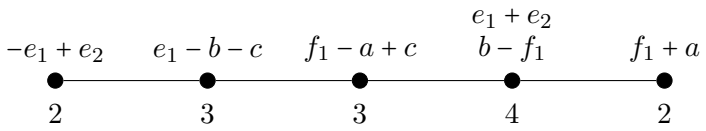

Figure 4.12: Lattice embedding of $C^1_{1,0}$ in $\mathbb{Z}^6$.

$$(1, 1, -3, 3, -5, 6),$$

which has square $81 = 9^2 = p$. Hence the embedding satisfies the conditions of Proposition 3.9 and the lens space $L(81, 50)$ is unobstructed from embedding in $\mathbb{C}P^2$.

The string $C^1_{1,1}$ presents an unobstructed lattice embedding, shown in Figure 4.13. This

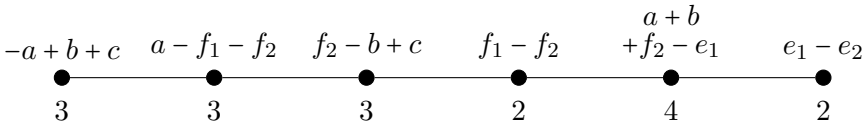

Figure 4.13: Lattice embedding of $C^1_{1,1}$ in $\mathbb{Z}^7$.

embedding follows the pattern discussed more generally for $C^1_{s,1}$ when $s = 4\eta_v^2 + 2\eta_v - 1$, and in fact has orthogonal embedding generated by

$$(9, 9, 2, 2, 4, 3, 1),$$

which has square $196 = 13^2 = p$. Hence, the lens space $L(196, 75)$ is unobstructed from embedding in $\mathbb{C}P^2$.

The string $C^1_{3,0}$ also presents an unobstructed lattice embedding in $\mathbb{Z}^8$, presented in Figure 4.14. Note that this embedding follows the same pattern as $C^1_{3,t}$. The orthogonal

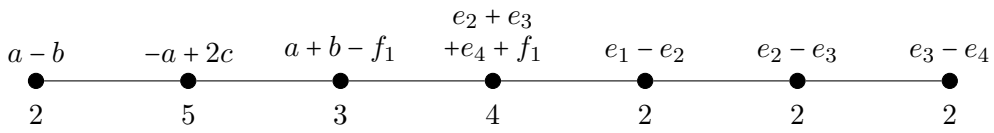

Figure 4.14: Lattice embedding of $C^1_{3,0}$ in $\mathbb{Z}^8$.

complement is generated by the vector

$$(-4,-4,-4,-4,12,6,6,3),$$

which has square $289 = 17^2 = p$. Hence the lens space $L(289,162)$ is unobstructed from embedding in $\mathbb{C}P^2$.

Finally, the string $C^1_{3,1}$ also presents an unobstructed embedding in $\mathbb{Z}^9$, which follows the same pattern for $C^1_{3,t}$ with $t = 9\gamma_w^2 + 8\gamma_w$. This is shown in Figure 4.15. The orthogonal

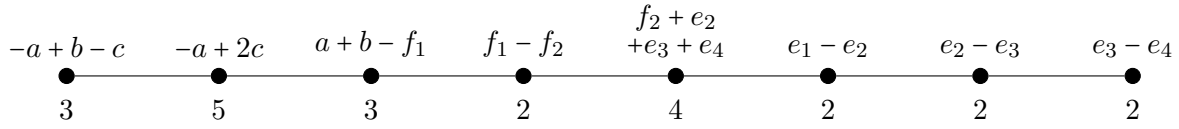

Figure 4.15: Lattice embedding of $C^1_{3,1}$ in $\mathbb{Z}^9$.

embedding is generated by the vector

$$(5,5,5,5,-15,-15,-6,-9,-3),$$

which has square $676 = 26^2 = p$. Hence, the lens space $L(676,243)$ is unobstructed from embedding in $\mathbb{C}P^2$.

§ 4.4 | String $C^2_{s,t}$

In this section, we study the string $C^2_{s,t} = [t+2,2,s+3,2^{[t]},4,2^{[s]}]^-$ with $s,t \geq 0$. From [49], we know that $C^2_{s,t}$ results as the continued fraction expansion of

$$\frac{p}{q} = \frac{(2st+3s+3t+5)^2}{(2s+3)(2st+3s+3t+6)},$$

so we observe that $C^2_{s,t}$ is obtained from lens spaces of Lisca type (2) with $q = d(m+1)$ (see Theorem 3.2). Note that this string is dual to itself, more precisely $C^2_{s,t}$ is dual to $rC^2_{t,s}$. The string presents $s+t+4$ vertices, thus we are interested in lattice embeddings in $\mathbb{Z}^{s+t+5}$. Throughout this section, let $e_1,\dots,e_{s+1},f_1,\dots,f_{t+1},a,b,c$ be an orthonormal basis for $\mathbb{Z}^{s+t+5}$.

§ 4.4.1 | General Argument

The general argument we now present holds for $s, t \geq 4$. The remaining cases will be analysed in the next subsection.

We need to map each vertex of the plumbing diagram of $C^2_{s,t}$ to a linear combination of $e_1, \ldots, e_{s+1}, f_1, \ldots, f_{t+1}, a, b, c$. The only way to do it is shown in Figure 4.16, where $v := \rho_v(e_1 + \ldots e_{s+1}) + \eta_v(f_1 + \cdots + f_{t+1}) - f_1 + \alpha_v a + \beta_v b + \gamma_v c$ and $w := \rho_w(e_1 + \cdots + e_{s+1}) + \eta_w(f_1 + \cdots + f_{t+1}) + \alpha_w a + \beta_w b + \gamma_w c$.

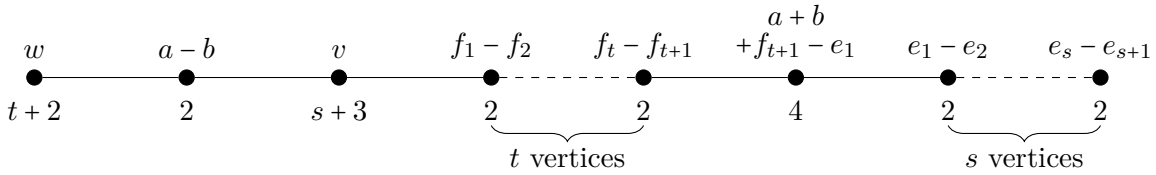

Figure 4.16: Potential embedding of $C^2_{s,t}$ in $\mathbb{Z}^{s+t+5}$ for $s \geq 4$ and $t \geq 4$.

In order to determine the integer coefficients of v and w, set up the following system of equations:

$$v \cdot v = (s+1)\rho_v^2 + (\eta_v - 1)^2 + \eta_v^2 t + \alpha_v^2 + \beta_v^2 + \gamma_v^2 = s + 3 \implies |\rho_v| \leq 1 \tag{1}$$

$$w \cdot w = (s+1)\rho_w^2 + (t+1)\eta_w^2 + \alpha_w^2 + \beta_w^2 + \gamma_w^2 = t + 2 \implies |\eta_w| \leq 1 \tag{2}$$

$$v \cdot (a - b) = \alpha_v - \beta_v = -1 \tag{3}$$

$$v \cdot (a + b + f_{t+1} - e_1) = \eta_v - \rho_v + \alpha_v + \beta_v = 0 \tag{4}$$

$$w \cdot (a - b) = \alpha_w - \beta_w = -1 \tag{5}$$

$$w \cdot (a + b + f_{t+1} - e_1) = \eta_w - \rho_w + \alpha_w + \beta_w = 0 \tag{6}$$

$$v \cdot w = (s+1)\rho_v\rho_w + (t+1)\eta_v\eta_w - \eta_w + \alpha_v\alpha_w + \beta_v\beta_w + \gamma_v\gamma_w = 0. \tag{7}$$

We begin a case-by-case analysis for ρ_v, followed by η_w.

- **Case $\rho_v = -1$:**

After substituting for ρ_v and simplifying, we obtain:

$$(\eta_v - 1)^2 + \eta_v^2 t + \alpha_v^2 + \beta_v^2 + \gamma_v^2 = 2 \implies \eta_v = 0 \tag{1}$$
$$(s+1)\rho_w^2 + (t+1)\eta_w^2 + \alpha_w^2 + \beta_w^2 + \gamma_w^2 = t + 2 \implies |\eta_w| \leq 1 \tag{2}$$
$$\beta_v = 1 + \alpha_v = 0 \tag{3}$$
$$\alpha_v = -1 \implies \gamma_v = 0 \tag{4}$$
$$\beta_w = 1 + \alpha_w \tag{5}$$
$$\rho_w = \eta_w + 2\alpha_w + 1 \tag{6}$$
$$\eta_w = -(s+1)\rho_w - \alpha_w. \tag{7}$$

– Case $\eta_w = -1$:
Focus on the following subset of equations:

$$(s+1)\rho_w^2 + \alpha_w^2 + \beta_w^2 + \gamma_w^2 = 1 \implies \rho_w = 0 \tag{2}$$
$$\beta_w = 1 \tag{5}$$
$$\alpha_w = 0 \tag{6}$$
$$-1 = 0. \tag{7}$$

The system is inconsistent; therefore, there is no lattice embedding of $C_{s,t}^2$ in $\mathbb{Z}^{s+t+5}$ when $\rho_v = -1$ and $\eta_w = -1$.

– Case $\eta_w = 0$:
We focus on a subset of equations:

$$(s+1)\rho_w^2 + \alpha_w^2 + \beta_w^2 + \gamma_w^2 = t + 2 \tag{2}$$
$$\beta_w = 1 + \alpha_w \tag{5}$$
$$\rho_w = \frac{1}{2s+3} \tag{6}$$
$$\alpha_w = -(s+1)\rho_w. \tag{7}$$

Since $s \geq 4$ (and $s \geq 0$ in general), ρ_w cannot be an integer. Hence, there is no lattice embedding of $C_{s,t}^2$ in $\mathbb{Z}^{s+t+5}$ when $\rho_v = -1$ and $\eta_w = 0$.

– Case $\eta_w = 1$:

The system simplifies as follows:

$$\eta_v = 0,\ \alpha_v^2 + \beta_v^2 + \gamma_v^2 = 1 \tag{1}$$
$$(s+1)\rho_w^2 + \alpha_w^2 + \beta_w^2 + \gamma_w^2 = 1 \implies \rho_w = 0 \tag{2}$$
$$\beta_v = 0 \tag{3}$$
$$\alpha_v = -1 \implies \gamma_v = 0 \tag{4}$$
$$\beta_w = 0 \tag{5}$$
$$\alpha_w = -1 \implies \gamma_w = 0 \tag{6}$$
$$1 = 1. \tag{7}$$

Thus, we determine that $v = -(e_1 + \cdots + e_{s+1}) - f_1 - a$ and $w = f_1 + \cdots + f_{t+1} - a$, which together with Figure 4.16 provide a lattice embedding in $\mathbb{Z}^{s+t+5}$. This corresponds to Lisca's embedding from [49], hence it does not satisfy Proposition 3.9.

- **Case $\rho_v = 0$:**
  The system can now be rearranged as follows:

$$(\eta_v - 1)^2 + \eta_v^2 t + \alpha_v^2 + \beta_v^2 + \gamma_v^2 = s + 3 \tag{1}$$
$$(s+1)\rho_w^2 + (t+1)\eta_w^2 + \alpha_w^2 + \beta_w^2 + \gamma_w^2 = t + 2 \implies |\eta_w| \leq 1 \tag{2}$$
$$\beta_v = 1 + \alpha_v \tag{3}$$
$$\eta_v + 2\alpha_v + 1 = 0 \tag{4}$$
$$\beta_w = 1 + \alpha_w \tag{5}$$
$$\rho_w = \eta_w + 2\alpha_w + 1 \tag{6}$$
$$\eta_w = (t+1)\eta_v\eta_w + \alpha_v\alpha_w + \beta_v\beta_w + \gamma_v\gamma_w. \tag{7}$$

  - Case $\eta_w = -1$:

After simplifying, focus on the following equations:

$$(s+1)\rho_w^2 + \alpha_w^2 + \beta_w^2 + \gamma_w^2 = 1 \implies \rho_w = 0 \tag{2}$$
$$\alpha_v = (t+1)\eta_v - 2 \tag{3}$$
$$\eta_v = \frac{3}{3+2t} \tag{4}$$
$$\beta_w = 1 \implies \gamma_w = 0 \tag{5}$$
$$\alpha_w = 0 \tag{6}$$
$$\beta_v = (t+1)\eta_v - 1. \tag{7}$$

Observe that there is no value of $t \geq 4 > 0$ such that η_v is an integer. Therefore, no lattice embedding can be found when $\rho_v = 0$ and $\eta_w = -1$.

– Case $\eta_w = 0$:
After substituting and simplifying, the system is as follows:

$$(\eta_v - 1)^2 + \eta_v^2 t + \alpha_v^2 + \beta_v^2 + \gamma_v^2 = s + 3 \tag{1}$$
$$(s+1)\rho_w^2 + \alpha_w^2 + \beta_w^2 + \gamma_w^2 = t + 2 \tag{2}$$
$$\beta_v = 1 + \alpha_v \tag{3}$$
$$\eta_v + 2\alpha_v + 1 = 0 \tag{4}$$
$$\beta_w = 1 + \alpha_w \tag{5}$$
$$\rho_w = 2\alpha_w + 1 \tag{6}$$
$$\alpha_v\alpha_w + \beta_v\beta_w + \gamma_v\gamma_w = 0. \tag{7}$$

Combine equations (1) and (2) to obtain

$$\rho_w^2\eta_v^2 t + \rho_w^2(\eta_v - 1)^2 + \rho_w^2(\alpha_v^2 + \beta_v^2 + \gamma_v^2 - 2) + \alpha_w^2 + \beta_w^2 + \gamma_w^2 = t + 2,$$

which implies $\rho_w^2\eta_v^2 \leq 1$. Note that $\rho_w = 0$ and $\eta_v = 0$ lead to non-integer solutions for α_w and α_v respectively, hence such cases must be excluded. We analyse the remaining cases.

* $\rho_w = -1$, $\eta_v = -1$: We have the following solution

$$s = \gamma_v^2 + t + 2 \tag{1}$$
$$t = \gamma_w^2 + s \tag{2}$$
$$\beta_v = 1 \tag{3}$$
$$\alpha_v = 0 \tag{4}$$
$$\beta_w = 0 \tag{5}$$
$$\alpha_w = -1 \tag{6}$$
$$\gamma_v\gamma_w = 0. \tag{7}$$

Note that equations (1) and (2) combine to give $\gamma_v^2 + \gamma_w^2 = -2$, making the system inconsistent. No lattice embedding can be found in this case.

* $\rho_w = -1$, $\eta_v = 1$: We have the following solution

$$s = \gamma_v^2 + t - 2 \tag{1}$$
$$t = \gamma_w^2 + s \tag{2}$$
$$\beta_v = 0 \tag{3}$$
$$\alpha_v = -1 \tag{4}$$
$$\beta_w = 0 \tag{5}$$
$$\alpha_w = -1 \tag{6}$$
$$\gamma_v\gamma_w = -1. \tag{7}$$

Equations (1) and (2) now combine to give $\gamma_v^2 + \gamma_w^2 = 2$, which has two possible solutions. Note that in either case $t = s + 1$. Suppose $\gamma_v = -1$ and $\gamma_w = 1$. Then $v = f_2 + \cdots + f_{t+1} - a - c$ and $w = -(e_1 + \cdots + e_{s+1}) - a + c$, together with Figure 4.16 provide a lattice embedding of $C^2_{s,s+1}$ in $\mathbb{Z}^{2s+6}$. However, the orthogonal complement of this embedding is generated by

$$(\underbrace{1, \ldots, 1}_{2s+3 \text{ times}}, 0, 0, 1),$$

and so does not satisfy the conditions of Proposition 3.9. Suppose instead that $\gamma_v = 1$ and $\gamma_w = -1$. We then have $v = f_2 + \cdots + f_{t+1} - a + c$ and $w = -(e_1 + \cdots + e_{s+1}) - a - c$, which together with Figure 4.16 provide a lattice embedding equivalent to the one just discussed. Hence, the same

conclusions apply.

* $\rho_w = 1$, $\eta_v = -1$: Similarly to the first case examined, equations (1) and (2) eventually combine to give $\gamma_v^2 + \gamma_w^2 = -2$, making the system inconsistent.

* $\rho_w = 1$, $\eta_v = 1$: We have the following solution:

$$s = \gamma_v^2 + t - 2 \tag{1}$$
$$t = \gamma_w^2 + s \tag{2}$$
$$\beta_v = 0 \tag{3}$$
$$\alpha_v = -1 \tag{4}$$
$$\beta_w = 1 \tag{5}$$
$$\alpha_w = 0 \tag{6}$$
$$\gamma_v \gamma_w = 0. \tag{7}$$

Note that equations (1) and (2) combine to give $\gamma_v^2 + \gamma_w^2 = 2$. However, note that there are no integer values of γ_v and γ_w simultaneously satisfying this equation and equation (7). Hence, the system has no solution.

– Case $\eta_w = 1$:
Simplify the system and focus on the following equations:

$$(s+1)\rho_w^2 + \alpha_w^2 + \beta_w^2 + \gamma_w^2 = 1 \implies \rho_w = 0 \tag{2}$$
$$\eta_v = \frac{1}{2t+3} \tag{4}$$
$$\beta_w = 0 \tag{5}$$
$$\alpha_w = -1 \implies \gamma_w = 0 \tag{6}$$
$$\alpha_v = (t+1)\eta_v - 1. \tag{7}$$

Once again, we note that it is not possible to achieve an integer value for η_v. Therefore, no lattice embedding can be found when $\rho_v = 0$ and $\eta_w = 1$.

- **Case $\rho_v = 1$:**

After substituting $\rho_v = 1$ and simplifying, we obtain:

$$(\eta_v - 1)^2 + \eta_v^2 t + \alpha_v^2 + \beta_v^2 + \gamma_v^2 = 2 \implies \eta_v = 0 \tag{1}$$
$$(s+1)\rho_w^2 + (t+1)\eta_w^2 + \alpha_w^2 + \beta_w^2 + \gamma_w^2 = t + 2 \implies |\eta_w| \leq 1 \tag{2}$$
$$\alpha_v = 0 \tag{3}$$
$$\beta_v = 1 \implies \gamma_v = 0 \tag{4}$$
$$\beta_w = 1 + \alpha_w \tag{5}$$
$$\rho_w = \eta_w + \alpha_w + \beta_w \tag{6}$$
$$\eta_w = (s+1)\rho_w + \alpha_v\alpha_w + \beta_v\beta_w + \gamma_v\gamma_w. \tag{7}$$

– Case $\eta_w = -1$:
Focus on the following equations:

$$(s+1)\rho_w^2 + \alpha_w^2 + \beta_w^2 + \gamma_w^2 = 1 \implies \rho_w = 0 \tag{2}$$
$$\beta_w = 1 \implies \gamma_w = 0 \tag{5}$$
$$\alpha_w = 0 \tag{6}$$
$$-1 = 1. \tag{7}$$

The system is inconsistent; therefore, there is no lattice embedding of $C_{s,t}^2$ in $\mathbb{Z}^{s+t+5}$ when $\rho_v = 1$ and $\eta_w = -1$.

– Case $\eta_w = 0$:
Focus on the following subset of equations:

$$(s+1)\rho_w^2 + \alpha_w^2 + \beta_w^2 + \gamma_w^2 = t + 2 \tag{2}$$
$$\beta_w = \frac{\rho_w + 1}{2} \tag{5}$$
$$\alpha_w = \frac{\rho_w - 1}{2} \tag{6}$$
$$\rho_w = -\frac{1}{2s+3}. \tag{7}$$

Observe that ρ_w cannot be an integer value, since $s \geq 4 > 0$. Hence, there is no lattice embedding of $C_{s,t}^2$ in $\mathbb{Z}^{s+t+5}$ when $\rho_v = 1$ and $\eta_w = 0$.

– Case $\eta_w = 1$:

Consider the following equations:

$$(s+1)\rho_w^2 + \alpha_w^2 + \beta_w^2 + \gamma_w^2 = 1 \implies \rho_w = 0 \tag{2}$$
$$\beta_w = 0 \tag{5}$$
$$\alpha_w = -1 \implies \gamma_w = 0 \tag{6}$$
$$1 = 0. \tag{7}$$

The system is inconsistent; therefore, there is no lattice embedding of $C^2_{s,t}$ in $\mathbb{Z}^{s+t+5}$ when $\rho_v = 1$ and $\eta_w = 1$.

This concludes the analysis of lattice embeddings of $C^2_{s,t}$ in $\mathbb{Z}^{s+t+5}$ when both $s \geq 4$ and $t \geq 4$. We have shown that the only embedding possible is Lisca's.

§ 4.4.2 | Remaining Cases

In the previous section, we showed that there are no lattice embeddings of $C^2_{s,t}$ in $\mathbb{Z}^{s+t+5}$ satisfying Proposition 3.9 whenever $s \geq 4$ and $t \geq 4$. We will now analyse the cases where one of the parameters s or t is strictly smaller than 4. Finally, we discuss the remaining cases.

We start by discussing the lattice embeddings of $C^2_{s,0}$ in $\mathbb{Z}^{s+5}$, when $s \geq 4$. The potential embedding from Figure 4.16 can be equipped with the further restriction $\rho_w = 0$. We may then repeat the same argument from the previous section to determine the integer coefficients of $v := \rho_v(e_1 + \cdots + e_{s+1}) + \eta_v f_1 + \alpha_v a + \beta_v b + \gamma_v c$ and $w := \eta_w f_1 + \alpha_w a + \beta_w b + \gamma_w c$; this will not be presented fully again, but we observe that when $\rho_v = -1$ we obtain Lisca's embedding, and when $\rho_v = 1$ we cannot find integer solutions for α_w. Let us analyse the system of equations when $\rho_v = 0$:

$$\eta_v^2 + \alpha_v^2 + \beta_v^2 + \gamma_v^2 = s + 3 \tag{1}$$
$$\eta_w^2 + \alpha_w^2 + \beta_w^2 + \gamma_w^2 = 2 \tag{2}$$
$$\alpha_v - \beta_v = -1 \tag{3}$$
$$\alpha_v + \beta_v + \eta_v = -1 \tag{4}$$
$$\alpha_w - \beta_w = -1 \tag{5}$$
$$\alpha_w + \beta_w + \eta_w = 0 \tag{6}$$
$$\eta_v\eta_w + \alpha_v\alpha_w + \beta_w\beta_v + \gamma_v\gamma_w = 0. \tag{7}$$

Equation (2) may be written as $6\alpha_w^2 + 6\alpha_w + \gamma_w^2 = 0$, which yields $\gamma_w = 0$ and $\alpha_w \in \{-1, 0\}$. When $\epsilon = -1$, we have $\beta_w = 0$ and $\eta_w = 1$, and from equation (7) we have $\eta_v = \alpha_v$. Combining equations (3) and (4), we obtain $\alpha_v = -\frac{2}{3}$, which is not an integer solution. Hence, we cannot find the required lattice embedding in this case. Now suppose $\alpha_w = \gamma_w = 0$, implying that $\beta_w = 1$, $\eta_w = -1$. Substituting the values found in (7) yields $\eta_v = \beta_v$, which in turn implies $\eta_v = \beta_v = 0$, $\alpha_v = -1$ and $s = \gamma_v^2 - 2$. Hence $v = -a + \gamma_v c$ and $w = -f_1 + b$ together with Figure 4.16 provides a lattice embedding in $\mathbb{Z}^{s+5}$, when $s = \gamma_v^2 - 2$, with orthogonal complement generated by

$$(\underbrace{\gamma_v, \ldots, 3\gamma_v}_{s+1 \text{ times}}\gamma_v, \gamma_v, \gamma_v, 1).$$

The vector has square $9\gamma_v^4 - 6\gamma_v^2 + 1 = (3\gamma_v^2 - 1)^2 = p$, thus it satisfies the conditions of Proposition 3.9 (note that γ_v cannot be 0). Hence, lens spaces with $\frac{p}{q} = C_{s,0}^2$ and $s = \gamma_v^2 - 2$ are unobstructed from embedding in $\mathbb{C}P^2$.

Next, consider lattice embeddings of $C_{s,1}^2$ in $\mathbb{Z}^{s+6}$, when $s \geq 4$. The only way to map each vertex of $C_{s,1}^2$ to a combination of vectors in $\mathbb{Z}^{s+6}$ is by following the same pattern as in the general case, which yields the same result.

For the string $C_{s,2}^2$ with $s \geq 4$, there is another way to potentially obtain a lattice embedding in $\mathbb{Z}^{s+7}$, aside from the one presented in the general argument (which yields the same results). This is shown in Figure 4.17 with $v := \rho_v(e_1 + \cdots + e_{s+1}) + \eta_v(f_1 + f_2 + f_3) - f_1 + \alpha_v a + \beta_v b + \gamma_v c$ and $w := \eta_w(f_1 + f_2 + f_3) + \alpha_w a + \beta_w b + \gamma_w c$. Set up the following system

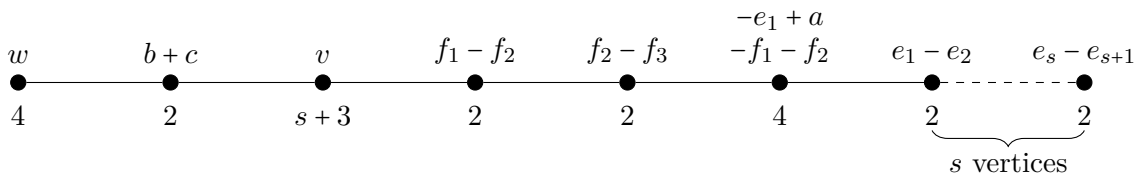

Figure 4.17: Potential embedding of $C_{s,2}^2$ in $\mathbb{Z}^{s+7}$ for $s \geq 4$.

of equations:

$$(s+1)\rho_v^2 + 2\eta_v^2 + (\eta_v - 1)^2 + \alpha_v^2 + \beta_v^2 + \gamma_v^2 = s+3 \implies |\rho_v| \leq 1 \quad (1)$$

$$3\eta_w^2 + \alpha_w^2 + \beta_w^2 + \gamma_w^2 = 4 \quad (2)$$

$$\beta_v + \gamma_v = -1 \quad (3)$$

$$1 - 2\eta_v - \rho_v + \alpha_v = 0 \quad (4)$$

$$\beta_w + \gamma_w = -1 \quad (5)$$

$$\alpha_w - 2\eta_w = 0 \quad (6)$$

$$(\eta_v - 1)\eta_w + 2\eta_v\eta_w + \alpha_v\alpha_w + \beta_v\beta_w + \gamma_v\gamma_w = 0. \quad (7)$$

Note that substituting $\alpha_w = 2\eta_w$ in equation (2), we obtain $7\eta_w^2 + \beta_w^2 + \gamma_w^2 = 4$, which implies $\eta_w = \alpha_w = 0$. Moreover, after substituting in $\gamma_w = -1 - \beta_w$, equation (2) further simplifies to $2\beta_w^2 + 2\beta_w = 3$, which has no integer solution. Hence, no alternative lattice embedding of $C_{s,2}^2$ in $\mathbb{Z}^{s+7}$ is possible for $s \geq 4$.

Now consider lattice embeddings of $C_{s,3}^2$ in $\mathbb{Z}^{s+8}$, when $s \geq 4$. One embedding is obtained via the mapping presented in the general case, while a potentially alternative one is presented in Figure 4.18 with $v \coloneqq \rho_v(e_1 + \cdots + e_{s+1}) + \eta_v(f_1 + \cdots + f_4) - f_1 + \alpha_v a + \beta_v b + \gamma_v c$ and $w \coloneqq \eta_w(f_1 + \cdots + f_4) + \alpha_w a + \beta_w b + \gamma_w c$. Set up the following system of equations to

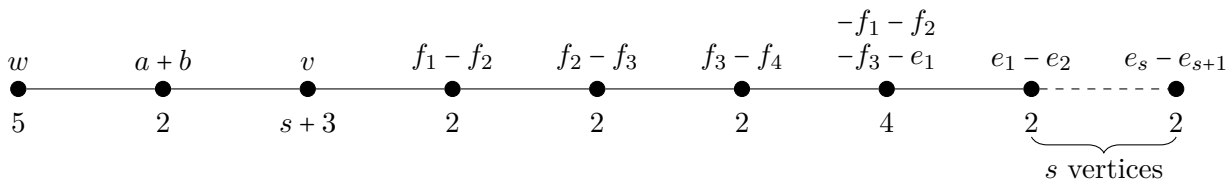

Figure 4.18: Potential embedding of $C_{s,3}^2$ in $\mathbb{Z}^{s+8}$ for $s \geq 4$.

determine the coefficients of v and w:

$$(s+1)\rho_v^2 + 3\eta_v^2 + (\eta_v - 1)^2 + \alpha_v^2 + \beta_v^2 + \gamma_v^2 = s+3 \implies |\rho_v| \leq 1 \quad (1)$$

$$4\eta_w^2 + \alpha_w^2 + \beta_w^2 + \gamma_w^2 = 5 \quad (2)$$

$$\alpha_v + \beta_v = -1 \quad (3)$$

$$1 - 3\eta_v - \rho_v = 0 \quad (4)$$

$$\alpha_w + \beta_w = -1 \quad (5)$$

$$-3\eta_w = 0 \quad (6)$$

$$4\eta_v\eta_w - \eta_w + \alpha_v\alpha_w + \beta_v\beta_w + \gamma_v\gamma_w = 0. \quad (7)$$

We can immediately observe that equation (4) can be written as $\eta_v = \frac{1-\rho_v}{3}$, which forces $\rho_v = 1$, since we need η_v to be an integer. The system can be further simplified as follows:

$$\alpha_v^2 + \beta_v^2 + \gamma_v^2 = 1 \tag{1}$$
$$2\alpha_w^2 + 2\alpha_w + \gamma_w^2 = 4 \tag{2}$$
$$\alpha_v + \beta_v = -1 \tag{3}$$
$$\eta_v = 0 \tag{4}$$
$$\beta_w = -1 - \alpha_w \tag{5}$$
$$\eta_w = 0 \tag{6}$$
$$4\eta_v\eta_w - \eta_w + \alpha_v\alpha_w + \beta_v\beta_w + \gamma_v\gamma_w = 0. \tag{7}$$

Looking at (2), note that $2\alpha_w^2 + 2\alpha_w \leq 4$ happens whenever $\alpha_w \in \{-2, -1, 0, 1\}$, therefore we need to examine what happens in each case.

- $\alpha_w = -2$: We have $\beta_w = 1$ and $\gamma_w = 0$. Equation (7) gives $\beta_v = 2\alpha_v$, which then implies $\alpha_v = -\frac{1}{3}$ in (3). Hence, there is no lattice embedding in this case.

- $\alpha_w = -1$: We have $\beta_w = 0$ and $\gamma_w = \pm 2$. Equation (7) then gives $\alpha_v = \pm 2\gamma_v$ and (3) gives $\beta_v = -1 \mp 2\gamma_v$. Combining everything in (1) we obtain $9\gamma_v^2 \pm 4\gamma_v = 0$, which implies $\gamma_v = 0$, since it is the only integer solution. Thus we have determined that $v = e_1 + \cdots + e_{s+1} - f_1 - b$ and $w = -a \pm 2c$, which together with Figure 4.18 constitute a lattice embedding of $C^2_{s,t}$ in $\mathbb{Z}^{s+8}$. When s is odd, the orthogonal complement is generated by the vector

  $$(\underbrace{6, \ldots, 6}_{s+1 \text{ times}}, -2, -2, -2, -2, -2(3s+4), 2(3s+4), \mp(3s+4)),$$

  which has square $81s^2 + 252s + 196 = (9s+14)^2 = p$. Therefore, the embedding satisfies the conditions of Proposition 3.9 and lens spaces with $\frac{p}{q} = C^2_{s,3}$ with s odd are unobstructed from embedding in $\mathbb{C}P^2$. Note that this does not happen when s is even, as the square of the primitive vector generating the orthogonal complement is not equal to p in this case.

- $\alpha_w = 0$: We have $\beta_w = -1$ and $\gamma_w = \pm 2$. Following the same reasoning as in the previous case, we obtain $v = e_1 + \cdots + e_{s+1} - f_1 - a$ and $w = -b \pm 2c$, which together with Figure 4.18 provide a lattice embedding of $C^2_{s,3}$ in $\mathbb{Z}^{s+8}$. This embedding is equivalent to the one found in the case $\alpha_w = -1$, hence the same conclusions apply.

- $\alpha_w = 1$: We have $\beta_w = -2$ and $\gamma_w = 0$. Equation (7) gives $\alpha_v = 2\beta_v$, which then implies $\beta_v = -\frac{1}{3}$ in (3). Hence, there is no lattice embedding in this case.

This concludes our analysis of $C^2_{s,3}$.

We now move on to $C^2_{0,t}$, when $t \geq 4$, and look for lattice embeddings in $\mathbb{Z}^{t+5}$. When $t \geq 5$, the only way to obtain a lattice embedding is via the mapping provided during the general argument. For the case $t = 4$, additional care must be taken to show that no other embedding is possible, which can also be verified via GAP [25]. Similarly, the string $C^2_{1,t}$, for $t \geq 4$, only admits an embedding in $\mathbb{Z}^{t+6}$ via the mapping from the general argument.

Next, we examine lattice embeddings of $C^2_{2,t}$ in $\mathbb{Z}^{t+7}$, when $t \geq 4$. Apart from the mapping presented in the general case, there is potentially another way to obtain a lattice embedding, shown in Figure 4.19.

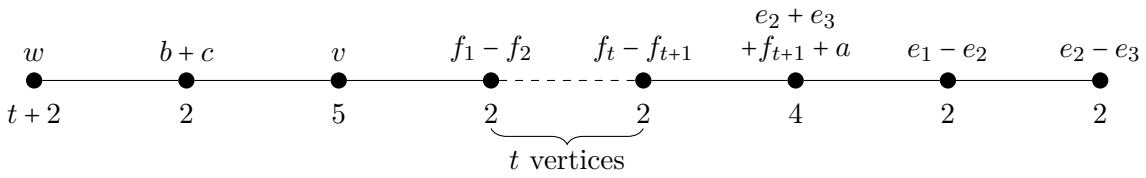

Figure 4.19: Potential embedding of $C^2_{2,t}$ in $\mathbb{Z}^{t+7}$ for $t \geq 4$.

Let $v := \rho_v(e_1 + e_2 + e_3) - f_1 + \alpha_v a + \beta_v b + \gamma_v c$ and $w := \rho_w(e_1 + e_2 + e_3) + \eta_w(f_1 + \cdots + f_{t+1}) + \alpha_w a + \beta_w b + \gamma_w c$. Set up the following system of equations:

$$3\rho_v^2 + \alpha_v^2 + \beta_v^2 + \gamma_v^2 + 1 = 5 \tag{1}$$

$$3\rho_w^2 + (t+1)\eta_w^2 + \alpha_w^2 + \beta_w^2 + \gamma_w^2 = t + 2 \implies |\eta_w| \leq 1 \tag{2}$$

$$\beta_v + \gamma_v = -1 \tag{3}$$

$$2\rho_v + \alpha_v = 0 \tag{4}$$

$$\beta_w + \gamma_w = -1 \tag{5}$$

$$2\rho_w + \alpha_w + \eta_w = 0 \tag{6}$$

$$3\rho_w\rho_v - \eta_w + \alpha_v\alpha_w + \beta_w\beta_v + \gamma_v\gamma_w = 0. \tag{7}$$

Equation (1) can be written as $7\rho_v^2 + 2\beta_v^2 + 2\beta_v - 3 = 0$, which implies $\rho_v = 0 = \alpha_v$. Moreover, observe that there is no integer solution for β_v in (1), hence no alternative lattice embedding is possible for $C^2_{2,t}$.

Finally, we focus on lattice embeddings of $C^2_{3,t}$ in $\mathbb{Z}^{t+8}$ when $t \geq 4$. Aside from the mapping discussed in the general case, the one provided in Figure 4.20 potentially provides an alternative embedding. Let $v := \rho_v(e_1 + \cdots + e_4) - f_1 + \alpha_v a + \beta_v b + \gamma_v c$ and $w := \rho_w(e_1 + \cdots +$

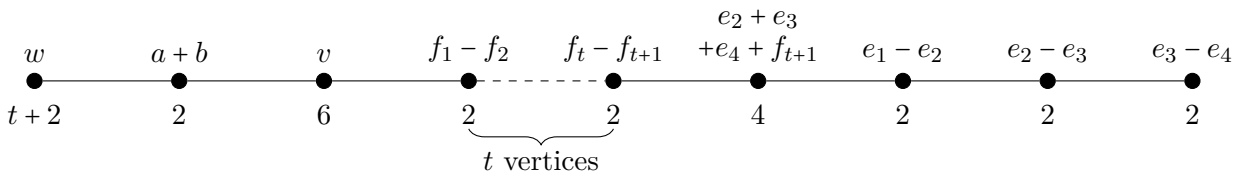

Figure 4.20: Potential embedding of $C^2_{3,t}$ in $\mathbb{Z}^{t+8}$ for $t \geq 4$.

$e_4) + \eta_w(f_1 + \cdots + f_{t+1}) + \alpha_w a + \beta_w b + \gamma_w c$. Set up the following system of equations:

$$4\rho_v^2 + \alpha_v^2 + \beta_v^2 + \gamma_v^2 + 1 = 6 \tag{1}$$
$$4\rho_w^2 + (t+1)\eta_w^2 + \alpha_w^2 + \beta_w^2 + \gamma_w^2 = t + 2 \implies |\eta_w| \leq 1 \tag{2}$$
$$\alpha_v + \beta_v = -1 \tag{3}$$
$$3\rho_v = 0 \tag{4}$$
$$\alpha_w + \beta_w = -1 \tag{5}$$
$$3\rho_w + \eta_w = 0 \tag{6}$$
$$4\rho_v\rho_w - \eta_w + \alpha_v\alpha_w + \beta_v\beta_w + \gamma_v\gamma_w = 0. \tag{7}$$

Note that equation (2) can be written as $(9t+13)\rho_w^2 + \alpha_w^2 + \beta_w^2 + \gamma_w^2 = t + 2$, which implies $\rho_w = 0 = \eta_w$. The system can be further simplified as follows:

$$2\alpha_v^2 + 2\alpha_v + \gamma_v^2 = 4 \tag{1}$$
$$\alpha_w^2 + \beta_w^2 + \gamma_w^2 = t + 2 \tag{2}$$
$$\beta_v = -1 - \alpha_v \tag{3}$$
$$\rho_v = 0 \tag{4}$$
$$\beta_w = -1 - \alpha_w \tag{5}$$
$$3\rho_w = \eta_w = 0 \tag{6}$$
$$\alpha_v\alpha_w + \beta_v\beta_w + \gamma_v\gamma_w = 0. \tag{7}$$

Equation (1) implies that $\alpha_v \in \{-2, -1, 0, 1\}$. We examine each scenario.

- $\alpha_v = -2$: We obtain $\beta_v = 1$ and $\gamma_v = 0$. Then equation (7) reduces to $\beta_w = 2\alpha_w$, which when substituted in (5) gives $\alpha_w = -\frac{1}{3}$. Hence no lattice embedding is possible in this case.

- $\alpha_v = -1$:The system yields the following solution

$$\gamma_v = \pm 2 \tag{1}$$
$$t = 9\gamma_w^2 \pm 4\gamma_w - 1 \tag{2}$$
$$\beta_v = 0 \tag{3}$$
$$\rho_v = 0 \tag{4}$$
$$\beta_w = -1 \mp 2\gamma_w \tag{5}$$
$$3\rho_w = \eta_w = 0 \tag{6}$$
$$\alpha_w = \pm 2\gamma_w. \tag{7}$$

Therefore, $v = -f_1 - a \pm 2c$ and $w = \pm 2\gamma_w a + (-1 \mp 2\gamma_w)b + \gamma_w c$ together with Figure 4.20 provide a lattice embedding in $\mathbb{Z}^{t+8}$ when $t = 9\gamma_w^2 \pm 4\gamma_w - 1 \geq 4$. The orthogonal complement is generated by

$$(\underbrace{-(9\gamma_w \pm 2), \ldots, -(9\gamma_w \pm 2)}_{4 \text{ times}}, \underbrace{3(9\gamma_w \pm 2), \ldots, 3(9\gamma_w \pm 2)}_{t+1 \text{ times}}, -3\gamma_w, 3\gamma_w, -3(4\gamma_w \pm 1)),$$

which has square $6561\gamma_w^4 \pm 5832\gamma_w^3 + 2106\gamma_w^2 \pm 360\gamma_w + 25 = (81\gamma_w^2 \pm 36\gamma_w + 5)^2 = p$. Therefore, any lens space with $\frac{p}{q} = C^2_{3,t}$ and $t = 9\gamma_w^2 \pm 4\gamma_w - 1 \geq 4$ is unobstructed from embedding in $\mathbb{C}P^2$.

- $\alpha_v = 0$: The system yields the following solution

$$\gamma_v = \pm 2 \tag{1}$$
$$t = 9\gamma_w^2 \pm 4\gamma_w - 1 \tag{2}$$
$$\beta_v = -1 \tag{3}$$
$$\rho_v = 0 \tag{4}$$
$$\beta_w = \pm 2\gamma_w \tag{5}$$
$$3\rho_w = \eta_w = 0 \tag{6}$$
$$\alpha_w = -1 - \mp 2\gamma_w. \tag{7}$$

Hence $v = -f_1 - b \pm 2c$ and $w = (-1 \mp 2\gamma_w)a \pm 2\gamma_w b + \gamma_w c$ together with Figure 4.20 provide a lattice embedding in $\mathbb{Z}^{t+8}$. Note that this embedding is equivalent to the one found in the previous case, thus the same conclusions apply.

- $\alpha_v = 1$: We obtain $\beta_v = -2$ and $\gamma_v = 0$. Equation (7) gives $\alpha_w = 2\beta_w$, thus (5) gives $\beta_w = -\frac{1}{3}$. Therefore, no lattice embedding is possible in this case.

This concludes the analysis of each infinite family of $C^2_{s,t}$ where one of s and t is strictly

less than 4. It remains to analyse all the strings arising when both parameters are strictly less than 4; this was done via GAP [25]. Table 4.4 presents a summary of the outcome of the analysis of these cases using GAP.

$C^2_{s,t}$	s	t	Result
	0	0	Obstructed since Lisca's embedding is the only possibility
	0	1	Obstructed by zero entries in vector generating orthogonal complement
	0	2	Obstructed since Lisca's embedding is the only possibility
	0	3	Obstructed since the image of Λ_M is not a primitive vector
	1	0	Obstructed since Lisca's embedding is the only possibility
	1	1	Obstructed since Lisca's embedding is the only possibility
	1	2	Two embeddings that are not Lisca's: obstructed by zero entries in vector generating orthogonal complement, and since the image of Λ_M is not a primitive vector, respectively
	1	3	Unobstructed
	2	0	Unobstructed
	2	1	Obstructed since Lisca's embedding is the only possibility
	2	2	Obstructed since Lisca's embedding is the only possibility
	2	3	Two embeddings that are not Lisca's: obstructed by zero entries in vector generating orthogonal complement, and since the image of Λ_M is not a primitive vector, respectively
	3	0	Obstructed since Lisca's embedding is the only possibility
	3	1	Obstructed since Lisca's embedding is the only possibility
	3	2	Obstructed since Lisca's embedding is the only possibility
	3	3	Unobstructed

Table 4.4: Summary of GAP analysis for $C^2_{s,t}$ when $s < 4$ and $t < 3$.

Let us explicitly present the lattice embeddings that satisfy Proposition 3.9, found using GAP. Figure 4.21 presents an embedding of $C^2_{1,3}$ in $\mathbb{Z}^9$.

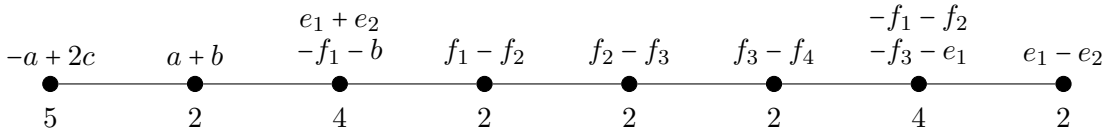

Figure 4.21: Lattice embedding of $C^2_{1,3}$ in $\mathbb{Z}^9$.

The orthogonal complement is generated by

$$(6, 6, -2, -2, -2, -2, -14, 14, -7),$$

which has square $529 = 23^2 = p$, hence the lens space $L(529, 120)$ is unobstructed from embedding $\mathbb{C}P^2$. Note that this embedding exactly follows the mapping discussed for $C^2_{s,3}$ with s odd.

The string $C^2_{2,0}$ presents the lattice embedding in $\mathbb{Z}^7$ shown in Figure 4.22. The orthogonal

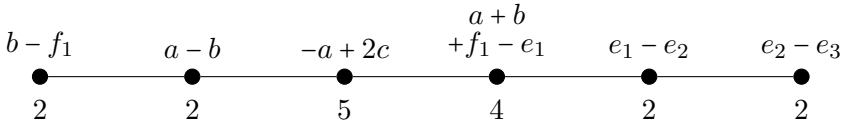

Figure 4.22: Lattice embedding of $C^2_{2,0}$ in $\mathbb{Z}^7$.

complement is generated by

$$(6, 6, 6, 2, 2, 2, 1),$$

which has square $121 = 11^2 = p$, hence the lens space $L(121, 84)$ is unobstructed from embedding in $\mathbb{C}P^2$. Note that this embedding exactly follows the mapping discussed for $C^2_{s,0}$ with $s = \gamma_w^2 - 2$, $\gamma_w = 2$.

Finally, we present a lattice embedding of $C^2_{3,3}$ in $\mathbb{Z}^{11}$ in Figure 4.23. The orthogonal

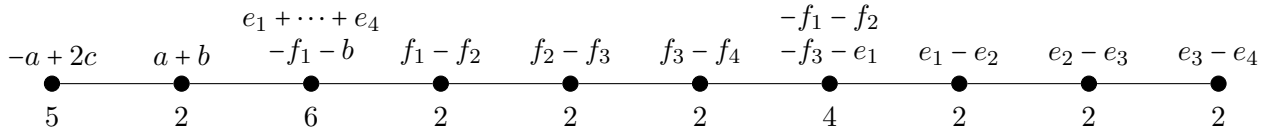

Figure 4.23: Lattice embedding of $C^2_{3,3}$ in $\mathbb{Z}^{11}$.

embedding is generated by

$$(6, 6, 6, 6, -2, -2, -2, -2, -26, 26, -13),$$

which has square $1681 = 41^2 = p$, hence the lens space $L(1681, 378)$ is unobstructed from embedding in $\mathbb{C}P^2$. Once again, we remark that this embedding exactly follows the mapping discussed for $C^2_{s,3}$ with s odd.

§ 4.5 | String $C^3_{s,t}$

In this section we address the string $C^3_{s,t} = [t+3, 2, s+3, 3, 2^{[t]}, 3, 2^{[s]}]^-$ with $s, t \geq 0$. From [49] we know this string is associated to the continued fraction expansion of

$$\frac{p}{q} = \frac{(2st + 5s + 4t + 9)^2}{(s+2)(4st + 10s + 8t + 17)},$$

and it is related to lens spaces of Lisca type (3) with $q = d(m+1)$ (see Theorem 3.2). Recall that $C^3_{s,t}$ is dual to $rC^1_{t+1,s}$. As the string presents $s+t+5$ weights, we are looking for lattice embeddings in $\mathbb{Z}^{s+t+6}$. Throughout this section, let $e_1, \ldots, e_{s+1}, f_1, \ldots f_{t+1}, a, b, c, d$ be an orthonormal basis for $\mathbb{Z}^{s+t+6}$.

§ 4.5.1 | General Argument

The general argument presented in this subsection holds for $s, t \geq 3$. As usual, all cases not covered by this argument will be analysed in the next subsection.

We need to map each vertex of the plumbing diagram of $C^3_{s,t}$ to a linear combination of $e_1, \ldots, e_{s+1}, f_1, \ldots f_{t+1}, a, b, c, d$. Figure 4.24 shows the only way to do it up to sign swapping and relabelling (i.e. automorphism).

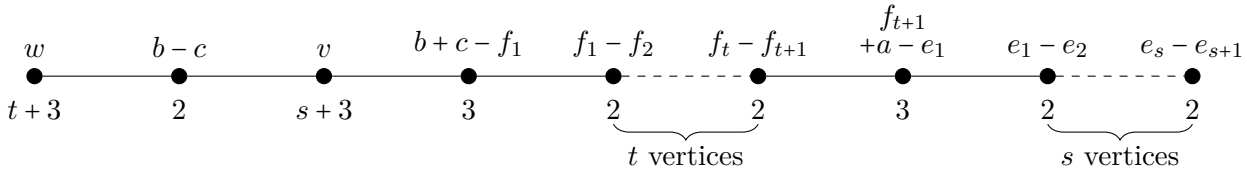

Figure 4.24: Potential embedding of $C^3_{s,t}$ in $\mathbb{Z}^{s+t+6}$ for $s, t \geq 3$.

Let $v \coloneqq \rho_v(e_1 + \cdots + e_{s+1}) + \eta_v(f_1 + \cdots + f_{t+1}) + \alpha_v a + \beta_v b + \gamma_v c + \psi d$ and $w \coloneqq \rho_w(e_1 + \cdots + e_{s+1}) + \eta_w(f_1 + \cdots + f_{t+1}) + \alpha_w a + \beta_w b + \gamma_w c + \tau d$. In order to determine the value of the integer coefficients of v and w, set up the following system of equations:

$$v \cdot v = (s+1)\rho_v^2 + (t+1)\eta_v^2 + \alpha_v^2 + \beta_v^2 + \gamma_v^2 + \psi^2 = s + 3 \implies |\rho_v| \leq 1 \tag{1}$$

$$w \cdot w = (s+1)\rho_w^2 + (t+1)\eta_w^2 + \alpha_w^2 + \beta_w^2 + \gamma_w^2 + \tau^2 = t + 3 \implies |\eta_w| \leq 1 \tag{2}$$

$$v \cdot (b - c) = \beta_v - \gamma_v = -1 \tag{3}$$

$$v \cdot (b + c - f_1) = \beta_v + \gamma_v - \eta_v = -1 \tag{4}$$

$$v \cdot (f_{t+1} + a - e_1) = \eta_v - \rho_v + \alpha_v = 0 \tag{5}$$

$$w \cdot (b - c) = \beta_w - \gamma_w = -1 \tag{6}$$

$$w \cdot (b + c - f_1) = \beta_w + \gamma_w - \eta_w = 0 \tag{7}$$

$$w \cdot (f_{t+1} + a - e_1) = \eta_w - \rho_w + \alpha_w = 0 \tag{8}$$

$$v \cdot w = (s+1)\rho_v\rho_w + (t+1)\eta_v\eta_w + \alpha_v\alpha_w + \beta_v\beta_w + \gamma_v\gamma_w + \psi\tau = 0. \tag{9}$$

There are three possible values for either ρ_v or η_w: -1, 0, 1. We discuss what happens in each case.

- **Case $\rho_v = -1$:**

Substitute for $\rho_v = -1$ and simplify the system as follows:

$$(t+1)\eta_v^2 + \alpha_v^2 + \beta_v^2 + \gamma_v^2 + \psi^2 = 2 \implies \eta_v = 0 \tag{1}$$
$$(s+1)\rho_w^2 + (t+1)\eta_w^2 + \alpha_w^+\beta_w^2 + \gamma_w^2 + \tau^2 = t+3 \implies |\eta_w| \leq 1 \tag{2}$$
$$\gamma_v = 0 \tag{3}$$
$$\beta_v = -1 \tag{4}$$
$$\alpha_v = -1 \implies \psi = 0 \tag{5}$$
$$\beta_w - \gamma_w = -1 \tag{6}$$
$$\beta_w + \gamma_w = \eta_w \tag{7}$$
$$\eta_w - \rho_w + \alpha_w = 0 \tag{8}$$
$$(s+1)\rho_w + \alpha_w + \beta_w = 0. \tag{9}$$

– Case $\eta_w = -1$:
We obtain the following solution:

$$\eta_v = 0,\ \psi = 0 \tag{1}$$
$$(s+1)\rho_w^2 + \alpha_w^2 + \beta_w^2 + \gamma_w^2 + \tau^2 = 2 \implies \rho_w = 0 \tag{2}$$
$$\gamma_v = 0 \tag{3}$$
$$\beta_v = -1 \tag{4}$$
$$\alpha_v = -1 \tag{5}$$
$$\beta_w = -1 \tag{6}$$
$$\gamma_w = 0 \tag{7}$$
$$\alpha_w = 1 \implies \tau = 0 \tag{8}$$
$$1 - 1 = 0. \tag{9}$$

Therefore, $v = -(e_1 + \cdots + e_{s+1}) - a - b$ and $w = -(f_1 + \cdots + f_{t+1}) + a - b$ together with Figure 4.24 determine a lattice embedding of $C^3_{s,t}$ in $\mathbb{Z}^{s+t+6}$, when $s,t \geq 3$. This embedding corresponds to the one in [49], hence does not satisfy the conditions of Proposition 3.9.

– Case $\eta_w = 0$: It is enough to focus on equations (6) and (7) to see that we obtain $\beta_w = -\frac{1}{2}$. Since β_w is not an integer, there is no lattice embedding possible in this case.

– Case $\eta_w = 1$:

Focus on the following subset of equations:

$$(s+1)\rho_w^2 + \alpha_w^2 + \beta_w^2 + \gamma_w^2 + \tau^2 = t+3 \implies \rho_w = 0 \tag{2}$$
$$\beta_w = 0 \tag{6}$$
$$\gamma_w = 1 \tag{7}$$
$$\alpha_w = -1 \tag{8}$$
$$-1 = 0. \tag{9}$$

The system is inconsistent, therefore there is no lattice embedding when $\rho_v = -1$ and $\eta_w = 1$.

- **Case $\rho_v = 0$:**
  We may rewrite the system as follows:

$$(t+1)\eta_v^2 + \alpha_v^2 + \beta_v^2 + \gamma_v^2 + \psi^2 = s+3 \tag{1}$$
$$(s+1)\rho_w^2 + (t+1)\eta_w^2 + \alpha_w^2 + \beta_w^2 + \gamma_w^2 + \tau^2 = t+3 \implies |\eta_w| \leq 1 \tag{2}$$
$$\gamma_v = 1 + \beta_v \tag{3}$$
$$\beta_v = \frac{\eta_v - 2}{2} \tag{4}$$
$$\alpha_v = -\eta_v \tag{5}$$
$$\beta_w - \gamma_w = -1 \tag{6}$$
$$\beta_w + \gamma_w = \eta_w \tag{7}$$
$$\eta_w - \rho_w + \alpha_w = 0 \tag{8}$$
$$(t+1)\eta_v\eta_w + \alpha_v\alpha_w + \beta_v\beta_w + \gamma_v\gamma_w + \psi\tau = 0. \tag{9}$$

  – Case $\eta_w = -1$:
    Focus on the following subset of equations:

$$(s+1)\rho_w^2 + \alpha_w^2 + \beta_w^2 + \gamma_w^2 + \tau^2 = 2 \implies \rho_w = 0 \tag{2}$$
$$\beta_v = \frac{\eta_v - 2}{2} \tag{4}$$
$$\alpha_v = -\eta_v \tag{5}$$
$$\beta_w = -1 \tag{6}$$
$$\gamma_w = 0 \tag{7}$$
$$\alpha_w = 1 \implies \tau = 0 \tag{8}$$
$$-(t+1)\eta_v + \alpha_v - \beta_v = 0 \implies \eta_v = \frac{2}{2t+5}. \tag{9}$$

    Note that in equation (9) there is no non-negative value of t that would make

η_v an integer. Hence, no lattice embedding is possible when $\rho_v = 0$ and $\eta_w = -1$.

– Case $\eta_w = 0$: Focus on equations (6) and (7) to see that they yield $\beta_w = -\frac{1}{2}$, which is not an integer. Hence, no lattice embedding is possible in this case.

– Case $\eta_w = 1$:
The system yields the following solution:

$$(t+1)\eta_v^2 + \alpha_v^2 + \beta_v^2 + \gamma_v^2 + \psi^2 = s + 3 \tag{1}$$
$$(s+1)\rho_w^2 + \alpha_w^2 + \beta_w^2 + \gamma_w^2 + \tau^2 = 2 \implies \rho_w = 0 \tag{2}$$
$$\gamma_v = 1 + \beta_v \tag{3}$$
$$\beta_v = \frac{\eta_v - 2}{2} \tag{4}$$
$$\alpha_v = -\eta_v \tag{5}$$
$$\beta_w = 0 \tag{6}$$
$$\gamma_w = 1 \tag{7}$$
$$\alpha_w = -1 \implies \tau = 0 \tag{8}$$
$$(t+1)\eta_v - \alpha_v + \gamma_v = 0 \implies \eta_v(2t+5) = 0 \implies \eta_v = 0. \tag{9}$$

Hence, we have determined that $v = -b + \psi d$ and $w = f_1 + \cdots + f_{t+1} - a + c$, whenever $s = \psi^2 - 2 \geq 3$ (this can be seen after simplifying equation (1)). Together with Figure 4.24, we now have a lattice embedding in $\mathbb{Z}^{s+t+6}$. The orthogonal complement is generated by

$$(\underbrace{\psi(2t+5), \ldots, \psi(2t+5)}_{s+1 \text{ times}}, \underbrace{2\psi, \ldots, 2\psi}_{t+1 \text{ times}}, \psi(2t+3), \psi, \psi, 1),$$

which has square $\psi^4(2t+5)^2 - 2\psi^2(2t+5) + 1 = (\psi^2(2t+5) - 1)^2 = p$. Hence, lens spaces with $\frac{p}{q} = C^3_{s,t}$ and $s = \psi^2 - 2 \geq 3$ are unobstructed from embedding in $\mathbb{C}P^2$.

- **Case $\rho_v = 1$:**

Substitute $\rho_v = 1$ and rewrite the system as follows:

$$(t+1)\eta_v^2 + \alpha_v^2 + \beta_v^2 + \gamma_v^2 + \psi^2 = 2 \implies \eta_v = 0 \tag{1}$$
$$(s+1)\rho_w^2 + (t+1)\eta_w^2 + \alpha_w^2 + \beta_w^2 + \gamma_w^2 + \tau^2 = t+3 \implies |\eta_w| \leq 1 \tag{2}$$
$$\beta_v = -1 \tag{3}$$
$$\gamma_v = 0 \tag{4}$$
$$\alpha_v = 1 \implies \psi = 0 \tag{5}$$
$$\beta_w - \gamma_w = -1 \tag{6}$$
$$\beta_w + \gamma_w = \eta_w \tag{7}$$
$$\eta_w - \rho_w + \alpha_w = 0 \tag{8}$$
$$(s+1)\rho_w + \alpha_w - \beta_w = 0. \tag{9}$$

– Case $\eta_w = -1$:
Focus on the following subset of equations:

$$(s+1)\rho_w^2 + \alpha_w^2 + \beta_w^2 + \gamma_w^2 + \tau^2 = 2 \implies \rho_w = 0 \tag{2}$$
$$\beta_w = -1 \tag{6}$$
$$\gamma_w = 0 \tag{7}$$
$$\alpha_w = 1 \tag{8}$$
$$1 + 1 = 0. \tag{9}$$

The system is inconsistent, hence there is no lattice embedding in $\mathbb{Z}^{s+t+6}$ when $\rho_v = 1$ and $\eta_w = -1$.

– Case $\eta_w = 0$: Focus on equations (6) and (7) and note that this results in $\beta_w = -\frac{1}{2}$. As it is not an integer value, no embedding is possible in this case.

– Case $\eta_w = 1$:
Consider the following subset of equations:

$$(s+1)\rho_w^2 + \alpha_w^2 + \beta_w^2 + \gamma_w^2 + \tau^2 = 2 \implies \rho_w = 0 \tag{2}$$
$$\beta_w = 0 \tag{6}$$
$$\gamma_w = 1 \tag{7}$$
$$\alpha_w = -1 \tag{8}$$
$$-1 = 0. \tag{9}$$

The system is inconsistent, thus there is no lattice embedding in $\mathbb{Z}^{s+t+6}$ when

$\rho_v = 1$ and $\eta_w = 1$.

We have concluded the analysis of $C^3_{s,t}$ when $s,\ t \geq 3$, and found out that whenever $s = \psi^2 - 2$ we can define an embedding satisfying Proposition 3.9.

§ 4.5.2 | Remaining Cases

We now analyse all the possible lattice embeddings of $C^3_{s,t}$ in $\mathbb{Z}^{s+t+6}$ which were excluded in the general argument. We start by considering all the strings $C^3_{s,t}$ where one of s and t is strictly smaller than 3, then move on to the remaining cases.

The first string we consider is $C^3_{s,0}$ with $s \geq 3$. Up to relabelling and sign swapping, the only way to obtain a lattice embedding in $\mathbb{Z}^{s+6}$ is via the mapping presented in the general case. It is possible to repeat the calculations with some additional care since $t = 0$ and verify that the same conclusions apply.

Next, we consider $C^3_{s,1}$ with $s \geq 3$. It is possible to find lattice embeddings in $\mathbb{Z}^{s+7}$ via the mapping discussed in the general case; this will lead to the same conclusions. However, there is another potential mapping that should be considered, shown in Figure 4.25. Let

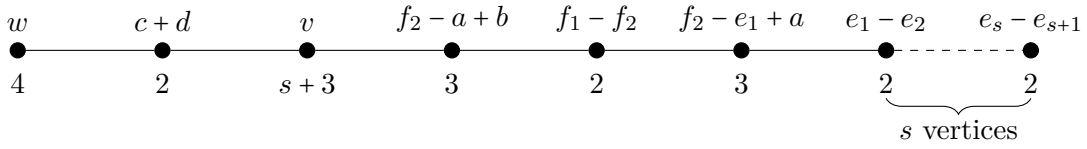

Figure 4.25: Potential embedding of $C^3_{s,1}$ in $\mathbb{Z}^{s+7}$ for $s \geq 3$.

$v := \rho_v(e_1+\cdots+e_{s+1})+\eta_v(f_1+f_2)+\alpha_v a+\beta_v b+\gamma_v c+\psi d$ and $w := \eta_w(f_1+f_2)+\alpha_w a+\beta_w b+\gamma_w c+\tau d$. Set up the following system of equations:

$$(s+1)\rho_v^2 + 2\eta_v^2 + \alpha_v^2 + \beta_v^2 + \gamma_v^2 + \psi^2 = s+3 \implies |\rho_v| \leq 1 \tag{1}$$
$$2\eta_w^2 + \alpha_w^2 + \beta_w^2 + \gamma_w^2 + \tau^2 = 4 \tag{2}$$
$$\gamma_v + \psi = -1 \tag{3}$$
$$\eta_v - \alpha_v + \beta_v = -1 \tag{4}$$
$$\eta_v - \rho_v + \alpha_v = 0 \tag{5}$$
$$\gamma_w + \tau = -1 \tag{6}$$
$$\eta_w - \alpha_w + \beta_w = 0 \tag{7}$$
$$\eta_w + \alpha_w = 0 \tag{8}$$
$$2\eta_v\eta_w + \alpha_v\alpha_w + \beta_v\beta_w + \gamma_v\gamma_w + \tau\psi = 0. \tag{9}$$

We may combine equations (2), (7), (8) to obtain $7\alpha_w^2 + \gamma_w^2 + \tau^2 = 4$, which immediately implies $\alpha_w = 0$. Moreover, after substituting $\gamma_w = -1-\tau$ from (6), we obtain $2\tau^2+2\tau-3 = 0$, which has no integer solutions. Hence, the system does not have a solution, and no alternative mapping is possible to construct lattice embeddings of $C^3_{s,1}$ in $\mathbb{Z}^{s+7}$.

Now consider lattice embeddings of $C^3_{s,2}$ in $\mathbb{Z}^{s+8}$, when $s \geq 3$. If we use the mapping discussed in the general argument, we find that whenever $s = \psi^2 - 2$ we can define an embedding satisfying Proposition 3.9. However, it might still be possible to find more such embeddings under different conditions. Figure 4.26 presents a potential alternative lattice embedding of $C^3_{s,2}$ in $\mathbb{Z}^{s+8}$. Let $v := \rho_v(e_1 + \cdots + e_{s+1}) + \eta_v(f_1 + f_2 + f_3) + \alpha_v a + \beta_v b + \gamma_v c + \psi d$

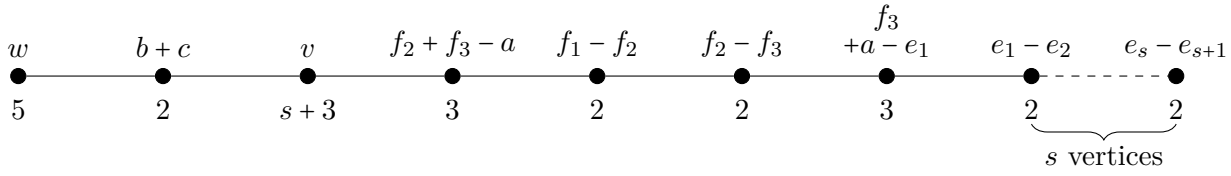

Figure 4.26: Potential embedding of $C^3_{s,2}$ in $\mathbb{Z}^{s+8}$ for $s \geq 3$.

and $w := \eta_w(f_1+f_2+f_3)+\alpha_w a+\beta_w b+\gamma_w c+\tau d$, and set up the following system of equations:

$$(s+1)\rho_v^2 + 3\eta_v^2 + \alpha_v^2 + \beta_v^2 + \gamma_v^2 + \psi^2 = s+3 \implies |\rho_v| \leq 1 \tag{1}$$
$$3\eta_w^2 + \alpha_w^2 + \beta_w^2 + \gamma_w^2 + \tau^2 = 5 \tag{2}$$
$$\beta_v + \gamma_v = -1 \tag{3}$$
$$2\eta_v - \alpha_v = -1 \tag{4}$$
$$\eta_v - \rho_v + \alpha_v = 0 \tag{5}$$
$$\beta_w + \gamma_w = -1 \tag{6}$$
$$2\eta_w - \alpha_w = 0 \tag{7}$$
$$\eta_w + \alpha_w = 0 \tag{8}$$
$$3\eta_v\eta_w + \alpha_v\alpha_w + \beta_v\beta_w + \gamma_v\gamma_w + \psi\tau = 0. \tag{9}$$

Note that equations (4) and (5) can be combined to obtain $\eta_v = \frac{\rho_v - 1}{3}$, which implies $\rho_v = 1$. Similarly, (7) and (8) imply $\eta_w = \alpha_w = 0$. Now the system can be simplified as

follows:

$$2\beta_v^2 + 2\beta_v + \psi^2 = 0 \implies \psi = 0 \text{ and } \beta_v \in \{-1, 0\} \tag{1}$$
$$\beta_w^2 + \gamma_w^2 + \tau^2 = 5 \tag{2}$$
$$\gamma_v = -1 - \beta_v \tag{3}$$
$$2\eta_v = 0 \tag{4}$$
$$\alpha_v = 1 \tag{5}$$
$$\gamma_w = -1 - \beta_w \tag{6}$$
$$\eta_w = 0 \tag{7}$$
$$\alpha_w = 0 \tag{8}$$
$$\beta_v\beta_w + \gamma_v\gamma_w = 0. \tag{9}$$

When $\beta_v = -1$ we have $\gamma_v = 0$, $\beta_w = 0$ and $\tau = \pm 2$. Thus $v = e_1 + \cdots + e_{s+1} + a - b$ and $w = -c \pm 2d$ together with Figure 4.26 provide an alternative lattice embedding of $C^3_{s,2}$ in $\mathbb{Z}^{s+8}$. When s is even, the orthogonal complement is generated by

$$(\underbrace{6, \ldots, 6}_{s+1 \text{ times}}, 2, 2, 2, 4, 2(3s+5), -2(3s+5), \mp(3s+5)),$$

which has square $81s^2 + 306s + 289 = (9s + 17)^2 = p$. The embedding satisfies Proposition 3.9, thus lens spaces with $\frac{p}{q} = C^2_{s,2}$ with $s \geq 3$ even are unobstructed from embedding in $\mathbb{C}P^2$. Note that this does not happen when s is odd.
When $\beta_v = 0$ instead we have $\gamma_v = -1$, $\gamma_w = 0$, $\beta_w = -1$ and $\tau = \pm 2$, thus $v = e_1 + \cdots + e_{s+1} + a - c$ and $w = -b \pm 2d$. Together with Figure 4.26 they provide a lattice embedding equivalent to the one in the previous case, hence the same conclusions apply.

Up to relabelling and sign-swapping, the mapping presented in Figure 4.24 is the only one possible for the string $C^2_{0,t}$ with $t \geq 3$. Interestingly, this will produce two lattice embeddings in $\mathbb{Z}^{t+6}$, both equivalent to the one in [49], and thus not relevant to Proposition 3.9. The same applies for the string $C^3_{1,t}$, $t \geq 3$, but the general argument gives rise to a single lattice embedding in $\mathbb{Z}^{t+7}$, corresponding to the one in [49].

Finally, note that any lens space with $\frac{p}{q} = C^3_{2,t}$, $t \geq 3$, is unobstructed from embedding in $\mathbb{C}P^2$. This is because we can find a lattice embedding in $\mathbb{Z}^{t+8}$ satisfying Proposition 3.9 by just applying the pattern for the general case with $\psi = 2$, hence $s = \psi^2 - 2 = 2$.

It remains to discuss strings where both s and t are strictly smaller than 3. Possible lattice embeddings were analysed using GAP [25]. The outcome of this analysis is summarised in Table 4.5.

$C^3_{s,t}$	s	t	Result
	0	0	Obstructed since Lisca's embedding is the only possibility
	0	1	Obstructed since Lisca's embedding is the only possibility
	0	2	Unobstructed
	1	0	Obstructed since Lisca's embedding is the only possibility
	1	1	Obstructed since Lisca's embedding is the only possibility
	1	2	Obstructed since the image of Λ_M is not a primitive vector
	2	0	Unobstructed
	2	1	Unobstructed
	2	2	Unobstructed

Table 4.5: Summary of GAP analysis for $C^3_{s,t}$ when $s < 3$ and $t < 3$.

Let us explicitly present the lattice embeddings that satisfy Proposition 3.9, found using GAP. The string $C^3_{0,2}$ presents the lattice embedding in $\mathbb{Z}^8$ shown in Figure 4.27; note that it follows the pattern discussed for $C^3_{s,2}$ with s even. The orthogonal embedding is

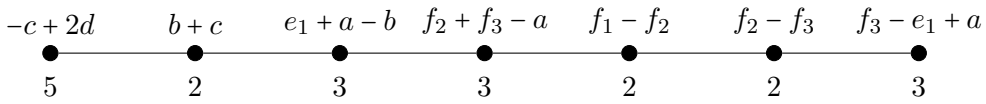

Figure 4.27: Lattice embedding of $C^3_{0,2}$ in $\mathbb{Z}^8$.

generated by

$$(6, 2, 2, 2, 4, 10, -10, -5),$$

which has square $289 = 17^2 = p$. Hence, the lens space $L(289, 66)$ is unobstructed from embedding in $\mathbb{C}P^2$.

Figure 4.28 shows a lattice embedding of $C^3_{2,0}$ in $\mathbb{Z}^8$; note that this embedding respects the pattern discussed in the general case with $\psi = 2$. The orthogonal complement is

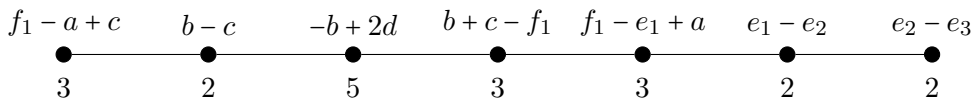

Figure 4.28: Lattice embedding of $C^3_{2,0}$ in $\mathbb{Z}^8$.

generated by

$$(10, 10, 10, 4, 6, 2, 2, 1),$$

which has square $361 = 19^2 = p$. Hence, the lens space $L(361, 148)$ is unobstructed from embedding in $\mathbb{C}P^2$.

Following the pattern from the general argument with $\psi = 2$, we also obtain the lattice embedding of $C^3_{2,1}$ in $\mathbb{Z}^9$ shown in Figure 4.29.

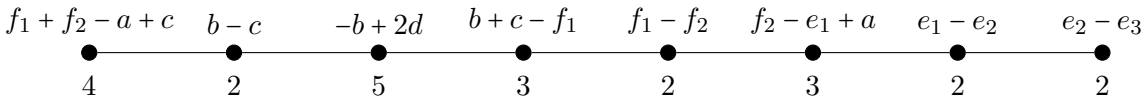

Figure 4.29: Lattice embedding of $C^3_{2,1}$ in $\mathbb{Z}^9$.

The orthogonal complement is generated by

$$(14, 14, 14, 4, 4, 10, 2, 2, 1),$$

which has square $729 = 27^2 = p$. Hence, the lens space $L(729, 212)$ is unobstructed from embedding in $\mathbb{C}P^2$.

Finally, the string $C^3_{2,2}$ presents two lattice embeddings in $\mathbb{Z}^{10}$ satisfying Proposition 3.9: one follows the pattern from the general argument, the other the pattern from the case $C^3_{s,2}$ with s even. Figure 4.30 presents the latter embedding. The orthogonal embedding

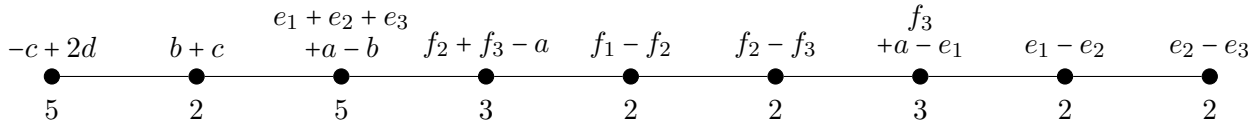

Figure 4.30: Lattice embedding of $C^3_{2,2}$ in $\mathbb{Z}^{10}$.

is generated by

$$(6, 6, 6, 2, 2, 2, 4, 22, -22, -11),$$

which has square $1225 = 35^2 = p$. Hence, the lens space $L(1225, 276)$ is unobstructed from embedding in $\mathbb{C}P^2$.

§ 4.6 | String $D^1_{s,t}$

We now analyse the string $D^1_{s,t} = [t+3, 3, 2^{[s]}, 3, 2^{[t]}, 3, s+3]^-$ where $s \geq t \geq 0$, according to the classification in [2]. From [49] we know that it corresponds to the continued fraction expansion of

$$\frac{p}{q} = \frac{(2st + 5t + 5s + 12)^2}{(2s + 5)(2st + 5t + 5s + 11)},$$

and it is associated with lens spaces of Lisca type (2) with $q = d(m-1)$ (as in Theorem 3.2). Recall that $D^1_{s,t}$ is dual to $B^1_{s+1,t+1}$. The string $D^1_{s,t}$ contains $s+t+5$ vertices, so we seek lattice embeddings in $\mathbb{Z}^{s+t+6}$. Throughout this section, let $e_1, \ldots, e_{s+1}$, $f_1, \ldots, f_{t+1}$, a, b, c, d be an orthonormal basis for $\mathbb{Z}^{s+t+6}$.

§ 4.6.1 | General Argument

In this section, we present a general argument for $s, t \geq 3$. As usual, the remaining cases will be addressed in the next section.

We need to map each vertex of the diagram associated to $D^1_{s,t}$ to a linear combination of the orthonormal basis vectors for $\mathbb{Z}^{s+t+6}$. Figure 4.31 below shows the way to do it.

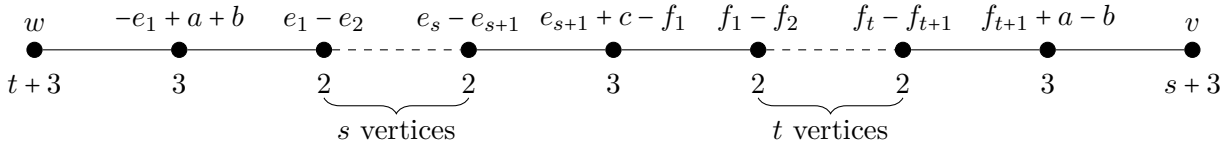

Figure 4.31: Potential embedding of $D^1_{s,t}$ in $\mathbb{Z}^{s+t+6}$ for $s \geq t \geq 3$.

It remains to determine what the images v and w should be. Let $v := \rho_v(e_1 + \cdots + e_{s+1}) + \eta_v(f_1 + \cdots + f_{t+1}) + \alpha_v a + \beta_v b + \gamma_v c + \psi d$ and $w := \rho_w(e_1 + \cdots + e_{s+1}) + \eta_w(f_1 + \cdots + f_{t+1}) + \alpha_w a + \beta_w b + \gamma_w c + \tau d$. The additional parameters represent the integer coefficients of the required linear combinations. We want to determine all possible solutions for such parameters, hence we set up the following system of equations:

$$v \cdot v = (s+1)\rho_v^2 + (t+1)\eta_v^2 + \alpha_v^2 + \beta_v^2 + \gamma_v^2 + \psi^2 = s+3 \implies |\rho_v| \leq 1 \tag{1}$$

$$w \cdot w = (s+1)\rho_w^2 + (t+1)\eta_w^2 + \alpha_w^2 + \beta_w^2 + \gamma_w^2 + \tau^2 = t+3 \implies |\eta_w| \leq 1 \tag{2}$$

$$v \cdot (-e_1 + a + b) = -\rho_v + \alpha_v + \beta_v = 0 \tag{3}$$

$$v \cdot (e_{s+1} + c - f_1) = \rho_v - \eta_v + \gamma_v = 0 \tag{4}$$

$$v \cdot (f_{t+1} + a - b) = \eta_v + \alpha_v - \beta_v = -1 \tag{5}$$

$$w \cdot (-e_1 + a + b) = -\rho_w + \alpha_w + \beta_w = -1 \tag{6}$$

$$w \cdot (e_{s+1} + c - f_1) = \rho_w - \eta_w + \gamma_w = 0 \tag{7}$$

$$w \cdot (f_{t+1} + a - b) = \eta_w + \alpha_w - \beta_w = 0 \tag{8}$$

$$v \cdot w = (s+1)\rho_v\rho_w + (t+1)\eta_w\eta_v + \alpha_v\alpha_w + \beta_v\beta_w + \gamma_w\gamma_v + \psi\tau = 0. \tag{9}$$

We see there are three cases to consider for equation (1): $\rho_v = -1$, $\rho_v = 0$, $\rho_v = 1$. Similarly

for equation (2).

- **Case $\rho_v = -1$:**
  After substituting $\rho_v = -1$ and simplifying, the system of equations becomes the following:

$$(t+1)\eta_v^2 + \alpha_v^2 + \beta_v^2 + \gamma_v^2 + \psi^2 = 2 \implies \eta_v = 0 \tag{1}$$
$$(s+1)\rho_w^2 + (t+1)\eta_w^2 + \alpha_w^2 + \beta_w^2 + \gamma_w^2 + \tau^2 = t+3 \implies |\eta_w| \leq 1 \tag{2}$$
$$\alpha_v = -1 \tag{3}$$
$$\gamma_v = 1 \implies \tau = 0 \tag{4}$$
$$\beta_v = 0 \tag{5}$$
$$\alpha_w + \beta_w = \rho_w - 1 \tag{6}$$
$$\rho_w - \eta_w + \gamma_w = 0 \tag{7}$$
$$\eta_w + \alpha_w - \beta_w = 0 \tag{8}$$
$$-(s+1)\rho_w - \alpha_w + \gamma_w = 0. \tag{9}$$

  Note that equation (1) implies that $\eta_v = 0$. Once it is determined that $\alpha_v = 1$ and $\gamma_v = 1$, it also follows that $\tau = \beta_v = 0$.

  - Case $\eta_w = -1$:
    We focus on a subset of equations and see that we are led to a contradiction:

$$(s+1)\rho_w^2 + \alpha_w^2 + \beta_w^2 + \gamma_w^2 + \tau^2 = 2 \implies \rho_w = 0 \tag{2}$$
$$\alpha_w = 0 \tag{6}$$
$$\gamma_w = -1 \tag{7}$$
$$\beta_w = -1 \tag{8}$$
$$\gamma_w = \alpha_w \implies -1 = 0. \tag{9}$$

    Hence, we cannot find the required lattice embedding when $\rho_v = -1$ and $\eta_w = -1$.

  - Case $\eta_w = 0$:
    After simplifying the system, we focus on a subset of equations and see that

we are led to a contradiction:

$$(s+1)\rho_w^2 + \alpha_w^2 + \beta_w^2 + \gamma_w^2 + \tau^2 = t+3 \tag{2}$$

$$\alpha_w = \frac{\rho_w - 1}{2} \tag{6}$$

$$\gamma_w = -\rho_w \tag{7}$$

$$\beta_w = \alpha_w \tag{8}$$

$$(s+1)\rho_w + \frac{\rho_w - 1}{2} + \rho_w = 0 \implies \rho_w = \frac{1}{2s+5}. \tag{9}$$

Any non-negative value of s will lead to an invalid solution in equation (9), as ρ_w would not be an integer. Hence, we cannot find the required lattice embedding when $\rho_v = -1$ and $\eta_w = 0$.

– Case $\eta_w = 1$:
After simplifying the system, we focus on a subset of equations and see that we are led to a contradiction:

$$(s+1)\rho_w^2 + \alpha_w^2 + \beta_w^2 + \gamma_w^2 + \tau^2 = 2 \implies \rho_w = 0 \tag{2}$$

$$\alpha_w = -1 \tag{6}$$

$$\gamma_w = 1 \tag{7}$$

$$\beta_w = 0 \tag{8}$$

$$\gamma_w = \alpha_w \implies 1 = 0. \tag{9}$$

Hence, we cannot find the required lattice embedding when $\rho_v = -1$ and $\eta_w = 1$.

- **Case $\rho_v = 0$:**
After substituting $\rho_v = 0$ and simplifying, the system of equations becomes the following:

$$(t+2)\eta_v^2 + 2\alpha_v^2 + \psi^2 = s+3 \tag{1}$$

$$(s+1)\rho_w^2 + (t+1)\eta_w^2 + \alpha_w^2 + \beta_w^2 + \gamma_w^2 + \tau^2 = t+3 \implies |\eta_w| \leq 1 \tag{2}$$

$$\beta_v = -\alpha_v \tag{3}$$

$$\gamma_v = \eta_v \tag{4}$$

$$\alpha_v = -\frac{1+\eta_v}{2} \tag{5}$$

$$-\rho_w + \alpha_w + \beta_w = -1 \tag{6}$$

$$\rho_w - \eta_w + \gamma_w = 0 \tag{7}$$

$$\eta_w + \alpha_w - \beta_w = 0 \tag{8}$$

$$(t+1)\eta_w\eta_v + \alpha_v(\alpha_w - \beta_w) + \gamma_w\gamma_v + \psi\tau = 0. \tag{9}$$

– Case $\eta_w = -1$:

We focus on a subset of equations and see that we are led to a contradiction:

$$(s+1)\rho_w^2 + \alpha_w^2 + \beta_w^2 + \gamma_w^2 + \tau^2 = 2 \implies \rho_w = 0 \tag{2}$$

$$\gamma_v = \eta_v \tag{4}$$

$$\alpha_v = -\frac{1+\eta_v}{2} \tag{5}$$

$$\alpha_w = 0 \tag{6}$$

$$\gamma_w = -1 \tag{7}$$

$$\beta_w = -1 \implies \tau = 0 \tag{8}$$

$$(t+1)\eta_v + \frac{1+\eta_v}{2} + \eta_v = 0 \implies \eta_v = -\frac{1}{2t+5}. \tag{9}$$

Note that substituting $\alpha_w = 0$, $\gamma_w = \beta_w = -1$ in equation (1) implies that $\tau = 0$. In equation (9), observe that any non-negative value of t makes the system inconsistent, as η_v would not be an integer. Hence, we cannot find the required lattice embedding when $\rho_v = 0$ and $\eta_w = -1$.

– Case $\eta_w = 0$:

The simplified system of equations is now the following:

$$(2t+5)\eta_v^2 + 2\eta_v + 2\psi^2 = 2s+5 \tag{1}$$
$$(2s+5)\rho_w^2 - 2\rho_w + 2\tau^2 = 2t+5 \tag{2}$$
$$\beta_v = -\alpha_v \tag{3}$$
$$\gamma_v = \eta_v \tag{4}$$
$$\alpha_v = -\frac{1+\eta_v}{2} \tag{5}$$
$$\alpha_w = \frac{\rho_w - 1}{2} \tag{6}$$
$$\gamma_w = -\rho_w \tag{7}$$
$$\alpha_w = \beta_w \tag{8}$$
$$\rho_w\eta_v = \psi\tau. \tag{9}$$

Combining equations (1) and (2) we obtain $\eta_v^2\rho_w^2(2s+5) - 2\rho_w\eta_v^2 + 2\eta_v^2\tau^2 + 2\eta_v + 2\psi^2 = 2s+5$, which implies $|\eta_v^2\rho_w^2| \leq 1$. We cannot have $\eta_v^2\rho_w^2 = -1$. When $|\eta_v^2\rho_w^2| = 0$, we must have either $\eta_v = 0$ or $\rho_w = 0$, and it is straightforward to verify that in each case the system is inconsistent. When $|\eta_v^2\rho_w^2| = 1$, there are four possible options. The only one that does not lead to a contradiction is when $\eta_v = -1$ and $\rho_w = 1$. The equations become the following:

$$(2t+5)\eta_v^2 + 2\eta_v + 2\psi^2 = 2s+5 \tag{1}$$
$$(2s+5)\rho_w^2 - 2\rho_w + 2\tau^2 = 2t+5 \tag{2}$$
$$\beta_v = 0 \tag{3}$$
$$\gamma_v = -1 \tag{4}$$
$$\alpha_v = 0 \tag{5}$$
$$\alpha_w = 0 \tag{6}$$
$$\gamma_w = -\rho_w \tag{7}$$
$$\beta_w = 0 \tag{8}$$
$$\psi\tau = -1. \tag{9}$$

Moreover, combining (1) and (2) now results in $\tau^2 + \psi^2 = 2$. Considering equation (9), we have the following two cases:

* Case $\psi = 1$, $\tau = -1$:
  Performing the appropriate substitutions in equations (1) and (2), we deduce that $s = t$. Thus, we determine that $v = -(f_1+\cdots+f_{t+1})-c+d$ and $w =$

$e_1+\cdots+e_{s+1}-c-d$. Figure 4.31 now determines a lattice embedding of $D^1_{s,t}$ in the standard lattice on $\mathbb{Z}^{s+t+6}$. However, the orthogonal complement is generated by the vector

$$(\underbrace{1,\ldots,1}_{2s+2 \text{ times}},0,1,0,(s+1)),$$

hence it does not satisfy the conditions of Proposition 3.9.

∗ Case $\psi=-1$, $\tau=1$:

As in the previous case, we perform the appropriate substitutions and deduce that $s=t$. We determine that $v=-(f_1+\cdots+f_{t+1})-c-d$ and $w=e_1+\cdots+e_{s+1}-c+d$ and have thus provided another lattice embedding (note that it is actually equivalent to the embedding found in the previous case). However, the orthogonal complement is generated by the vector

$$(\underbrace{1,\ldots,1}_{2s+2 \text{ times}},0,1,0,-(s+1)),$$

hence it does not satisfy the conditions of Proposition 3.9.

– Case $\eta_w=1$:

Focus on the following subset of simplified equations:

$$(s+1)\rho_w^2+\alpha_w^2+\beta_w^2+\gamma_w^2+\tau^2=2 \implies \rho_w=0 \tag{2}$$

$$\gamma_v=\eta_v \tag{4}$$

$$\alpha_v=-\frac{1+\eta_v}{2} \tag{5}$$

$$\alpha_w=-1 \tag{6}$$

$$\gamma_w=1 \implies \tau=0 \tag{7}$$

$$\beta_w=0 \tag{8}$$

$$(t+1)\eta_v+\frac{1+\eta_v}{2}+\eta_v=0 \implies \eta_v=-\frac{1}{2t+5}. \tag{9}$$

As in previous cases, we see that by performing the appropriate substitutions in equation (2), we deduce that $\tau=0$. In equation (9), we see that η_v can never be an integer for any non-negative t. Hence, we cannot find the required lattice embedding when $\rho_v=0$ and $\eta_w=1$.

- **Case $\rho_v=1$:**

After substituting $\rho_v=1$ and simplifying, the system of equations becomes the

following:

$$(t+1)\eta_v^2 + \alpha_v^2 + \beta_v^2 + \gamma_v^2 + \psi^2 = 2 \implies \eta_v = 0 \tag{1}$$
$$(s+1)\rho_w^2 + (t+1)\eta_w^2 + \alpha_w^2 + \beta_w^2 + \gamma_w^2 + \tau^2 = t+3 \implies |\eta_w| \leq 1 \tag{2}$$
$$\alpha_v = 0 \tag{3}$$
$$\gamma_v = -1 \tag{4}$$
$$\beta_v = 1 \implies \psi = 0 \tag{5}$$
$$-\rho_w + \alpha_w + \beta_w = -1 \tag{6}$$
$$\rho_w - \eta_w + \gamma_w = 0 \tag{7}$$
$$\eta_w + \alpha_w - \beta_w = 0 \tag{8}$$
$$(s+1)\rho_w + \beta_w - \gamma_w + \psi\tau = 0. \tag{9}$$

– Case $\eta_w = -1$:
Focus on the following subset of equations:

$$(s+1)\rho_w^2 + \alpha_w^2 + \beta_w^2 + \gamma_w^2 + \tau^2 = 2 \implies \rho_w = 0 \tag{2}$$
$$\alpha_w = 0 \tag{6}$$
$$\gamma_w = -1 \tag{7}$$
$$\beta_w = -1 \implies \tau = 0 \tag{8}$$
$$0 = 0. \tag{9}$$

The system of equations has a unique solution in this case, hence $v = (e_1 + \cdots + e_{s+1}) + b - c$ and $w = -(f_1 + \cdots + f_{t+1}) - b - c$. Now Figure 4.31 explicitly describes an embedding of the lattice on $D^1_{s,t}$ in the standard diagonal lattice on $\mathbb{Z}^{s+t+6}$. This embedding corresponds to Lisca's in [49], hence does not satisfy Proposition 3.9.

– Case $\eta_w = 0$:
Focus on the following subset of equations:

$$(s+1)\rho_w^2 + \alpha_w^2 + \beta_w^2 + \gamma_w^2 + \tau^2 = t+3 \tag{2}$$
$$\beta_w = \frac{\rho_w - 1}{2} \tag{6}$$
$$\gamma_w = -\rho_w \tag{7}$$
$$\alpha_w = \beta_w \tag{8}$$
$$(s+1)\rho_w + \frac{\rho_w - 1}{2} + \rho_w = 0 \implies \rho_w = \frac{1}{2s+5}. \tag{9}$$

Equation (9) directly implies that for any non-negative value of s, ρ_w is never an integer. Hence, we cannot find the required lattice embedding when $\rho_v = 1$ and $\eta_w = 0$.

– Case $\eta_w = 1$:
Focus on the following subset of equations:

$$(s+1)\rho_w^2 + \alpha_w^2 + \beta_w^2 + \gamma_w^2 + \tau^2 = 2 \implies \rho_w = 0 \tag{2}$$
$$\alpha_w = -1 \tag{6}$$
$$\gamma_w = 1 \tag{7}$$
$$\beta_w = 0 \implies \tau = 0 \tag{8}$$
$$-1 = 0. \tag{9}$$

Hence, we cannot find the required lattice embedding when $\rho_v = 1$ and $\eta_w = 1$.

We have concluded our analysis of $D^1_{s,t}$ when $s, t \geq 3$ and have shown it is not possible to construct an embedding satisfying the conditions of Proposition 3.9.

§ 4.6.2 | Remaining Cases

We now analyse the possible lattice embeddings of $D^1_{s,t}$ in $\mathbb{Z}^{s+t+6}$ whenever one of s or t is strictly less than 3. We will then go over the remaining sporadic cases.

We begin with the infinite family $D^1_{s,0}$, where $s \geq 3$. The only way to map each vertex of the corresponding string to a linear combination of basis vectors of $\mathbb{Z}^{s+6}$ is that of the general case, and the same conclusions apply.

Consider $D^1_{s,1}$ with $s \geq 3$. One lattice embedding into $\mathbb{Z}^{s+7}$ can be obtained following the pattern for the general case, hence the same conclusions apply. Another potential embedding is shown in Figure 4.32, with $v := \rho_v(e_1+\cdots+e_{s+1})+\eta_v(f_1+f_2)+\alpha_v a+\beta_v b+\gamma_v c+\psi d$ and $w := \eta_w(f_1+f_2)\alpha_w a + \beta_w b + \gamma_w c + \tau d$.

In order to determine the integer coefficients of v and w, set up the following system of

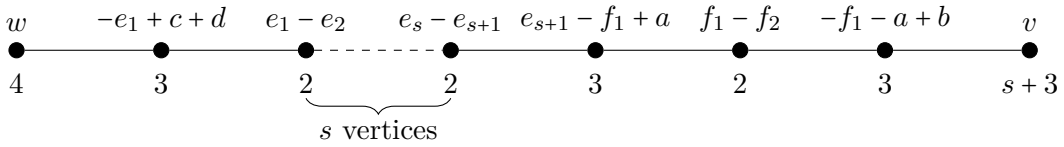

Figure 4.32: Potential embedding of $D^1_{s,1}$ in $\mathbb{Z}^{s+7}$ for $s \geq 3$.

equations:

$$(s+1)\rho_v^2 + 2\eta_v^2 + \alpha_v^2 + \beta_v^2 + \gamma_v^2 + \psi^2 = s+3 \implies |\rho_v| \leq 1 \tag{1}$$

$$2\eta_w^2 + \alpha_w^2 + \beta_w^2 + \gamma_w^2 + \tau^2 = 4 \tag{2}$$

$$\gamma_v + \psi = \rho_v \tag{3}$$

$$\eta_v = \alpha_v + \rho_v \tag{4}$$

$$\beta_v - \alpha_v - \eta_v = -1 \tag{5}$$

$$\gamma_w + \tau = -1 \tag{6}$$

$$\alpha_w - \eta_w = 0 \tag{7}$$

$$\beta_w - \alpha_w - \eta_w = 0 \tag{8}$$

$$2\eta_v\eta_w + \alpha_v\alpha_w + \beta_v\beta_w + \gamma_v\gamma_w + \psi\tau = 0. \tag{9}$$

Observe that from equations (7) and (8) we obtain $\alpha_w = \eta_w$ and $\beta_w = 2\eta_w$, which when substituted in equation (2) imply $\eta_w = \alpha_w = \beta_w = 0$. Using equation (6), we may write (2) as $2\tau^2 + 2\tau - 3 = 0$, which has no integer solutions. Hence, no alternative embedding of $D^1_{s,1}$ in $\mathbb{Z}^{s+7}$ is possible.

Now consider $D^1_{s,2}$ with $s \geq 3$. We are interested in lattice embeddings in $\mathbb{Z}^{s+8}$. We may attempt to construct the embedding as in the general case, but this will not yield any outcome of interest. However, there is another potential embedding to consider, shown in Figure 4.33 below. Let $v := \rho_v(e_1 + \cdots + e_{s+1}) + \eta_v(f_1 + f_2 + f_3) + \alpha_v a + \beta_v b + \gamma_v c + \psi d$

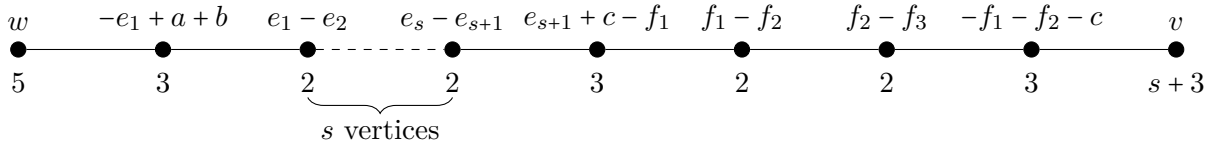

Figure 4.33: Potential embedding of $D^1_{s,2}$ in $\mathbb{Z}^{s+8}$ for $s \geq 3$.

and $w := \rho_w(e_1 + \cdots + e_{s+1}) + \eta_w(f_1 + f_2 + f_3) + \alpha_w a + \beta_w b + \gamma_w c + \tau d$. Set up the following system of equations to determine the coefficients for v and w:

$$(s+1)\rho_v^2 + 3\eta_v^2 + \alpha_v^2 + \beta_v^2 + \gamma_v^2 + \psi^2 = s+3 \implies |\rho_v| \leq 1 \quad (1)$$
$$(s+1)\rho_w^2 + 3\eta_w^2 + \alpha_w^2 + \beta_w^2 + \gamma_w^2 + \tau^2 = 5 \quad (2)$$
$$\alpha_v + \beta_v = \rho_v \quad (3)$$
$$\eta_v = \gamma_v + \rho_v \quad (4)$$
$$2\eta_v + \gamma_v = 1 \quad (5)$$
$$-\rho_w + \alpha_w + \beta_w = -1 \quad (6)$$
$$\rho_w - \eta_w + \gamma_w = 0 \quad (7)$$
$$\gamma_w = -2\eta_w \quad (8)$$
$$(s+1)\rho_w\rho_v + 3\eta_v\eta_w + \alpha_v\alpha_w + \beta_v\beta_w + \gamma_v\gamma_w + \psi\tau = 0. \quad (9)$$

When $\rho_v \in \{0, 1\}$ the system can immediately be seen to be inconsistent. Thus, we only need to consider the case $\rho_v = -1$. After simplifying, the system becomes:

$$3\eta_v^2 + \alpha_v^2 + \beta_v^2 + \gamma_v^2 + \psi^2 = 2 \implies \eta_v = 0 \quad (1)$$
$$(s+1)\rho_w^2 + 3\eta_w^2 + \alpha_w^2 + \beta_w^2 + \gamma_w^2 + \tau^2 = 5 \quad (2)$$
$$\alpha_v + \beta_v = -1 \quad (3)$$
$$\gamma_v = 1 \quad (4)$$
$$1 = 1 \quad (5)$$
$$\alpha_w + \beta_w = \rho_w - 1 \quad (6)$$
$$\rho_w - \eta_w + \gamma_w = 0 \quad (7)$$
$$\gamma_w = -2\eta_w \quad (8)$$
$$-(s+1)\rho_w + \alpha_v\alpha_w + \beta_v\beta_w + \gamma_w + \psi\tau = 0. \quad (9)$$

Note that equation (1) may be written as $2\alpha_v^2 + 2\alpha_v + \psi^2 = 0$. This implies either $\alpha_v = -1$ or $\alpha_v = 0$.

- Case $\alpha_v = -1$:

The system reduces to:

$$\psi = 0 \tag{1}$$
$$(s+1)\rho_w^2 + 3\eta_w^2 + \alpha_w^2 + \beta_w^2 + \gamma_w^2 + \tau^2 = 5 \tag{2}$$
$$\beta_v = 0 \tag{3}$$
$$\gamma_v = 1 \tag{4}$$
$$\alpha_w + \beta_w = \rho_w - 1 \tag{6}$$
$$\rho_w - \eta_w + \gamma_w = 0 \tag{7}$$
$$\gamma_w = -2\eta_w \tag{8}$$
$$-(s+1)\rho_w - \alpha_w + \gamma_w = 0. \tag{9}$$

We now need to consider the possible values of η_w: for $\eta_w = \pm 1$ the system is inconsistent; when $\eta_w = 0$ we have a lattice embedding with $v = -(e_1 + \dots e_{s+1}) - a + c$ and $w = -b \pm 2d$. When s is odd, the orthogonal complement is generated by the vector

$$(\underbrace{6, \dots, 6}_{s+1 \text{ times}}, 2, 2, 2, -2(3s+5), 2(3s+8), -4, \pm(3s+8)),$$

which has square $(9s+22)^2 = p$, thus satisfying Proposition 3.9. Hence, lens spaces belonging to $D^1_{s,2}$ with s odd are unobstructed from embedding in $\mathbb{C}P^2$.

- Case $\alpha_v = 0$:
  The system reduces to:

$$\psi = 0 \tag{1}$$
$$(s+1)\rho_w^2 + 3\eta_w^2 + \alpha_w^2 + \beta_w^2 + \gamma_w^2 + \tau^2 = 5 \tag{2}$$
$$\beta_v = -1 \tag{3}$$
$$\gamma_v = 1 \tag{4}$$
$$\alpha_w + \beta_w = \rho_w - 1 \tag{6}$$
$$\rho_w - \eta_w + \gamma_w = 0 \tag{7}$$
$$\gamma_w = -2\eta_w \tag{8}$$
$$-(s+1)\rho_w - \beta_w + \gamma_w = 0. \tag{9}$$

When $\eta_w = \pm 1$ the system is inconsistent. When $\eta_w = 0$, $v = -(e_1 + \dots e_{s+1}) - b + c$ and $w = -a \pm 2d$ determine a lattice embedding. Note that it is equivalent to the

embedding found when $\alpha_v = -1$. Hence, the same conclusions apply.

We have thus examined all possible infinite families that may arise from the string $D^1_{s,t}$, taking into account the symmetry with respect to s and t. Finally, we analyse the individual cases remaining when $s, t < 3$. Table 4.6 presents a summary of the outcome of the analysis of these cases using GAP.

$D^1_{s,t}$	s	t	Result
	0	0	Three embeddings that are not Lisca's: all obstructed by zero entries in vector generating orthogonal complement
	1	0	Obstructed since Lisca's embedding is the only possibility
	1	1	Obstructed by zero entries in vector generating orthogonal complement
	2	0	Obstructed since the image of Λ_M is not a primitive vector
	2	1	Unobstructed
	2	2	Three embeddings that are not Lisca's: one obstructed by zero entries in vector generating orthogonal complement, the remaining ones since the image of Λ_M is not a primitive vector

Table 4.6: Summary of GAP analysis for $D^1_{s,t}$ when $s < 3$ and $t < 3$.

The case $D^1_{2,1}$ was the only one that gave rise to an unobstructed lattice embedding, shown below.

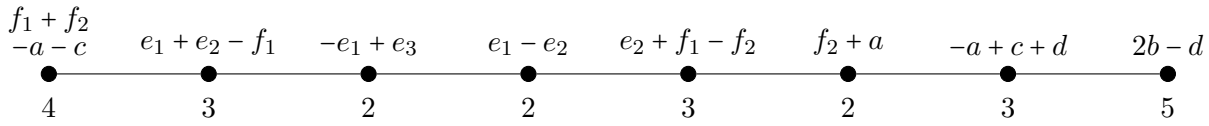

Figure 4.34: Lattice embedding of $D^1_{2,1}$ in $\mathbb{Z}^9$.

The orthogonal complement of this embedding is generated by the vector

$$(2, 2, 2, 4, 6, -6, -11, 16, -22),$$

which has square $961 = 31^2 = p$. Therefore, the lens space $L(961, 270)$ is unobstructed from embedding in $\mathbb{C}P^2$.

§ 4.7 | String $D^2_{s,t}$

The last string we address is $D^2_{s,t} = [t + 3, 2^{[s]}, 4, 2^{[t]}, 3, s + 2]^-$ with $s, t \geq 0$. It results as the continued fraction expansion of

$$\frac{p}{q} = \frac{(2st + 4s + 3t + 7)^2}{(2s + 3)(2st + 4s + 3t + 6)},$$

thus it is obtained from lens spaces of Lisca type (3) with $q = d(m-1)$ (see Theorem 3.2). Recall that $D^2_{s,t}$ is dual to $B^2_{s,t+1}$. The string $D^2_{s,t}$ has $s+t+4$ weights, so we look for lattice embeddings in $\mathbb{Z}^{s+t+5}$. Throughout this section let $e_1, \dots, e_{s+1}$, $f_1, \dots, f_{t+1}$, a, b, c be an orthonormal basis for $\mathbb{Z}^{s+t+5}$.

§ 4.7.1 | General Argument

The argument presented in this subsection holds for $s \geq 4$ and $t \geq 3$. The remaining cases will be analysed in the next subsection. The aim is to embed the linear lattice on $D^2_{s,t}$ in the standard lattice on $\mathbb{Z}^{s+t+5}$.

Each vertex of the plumbing diagram associated to $D^2_{s,t}$ is mapped to $\mathbb{Z}^{s+t+5}$ as shown in Figure 4.35 below. Under the specified conditions for s and t, this is the only possible mapping up to automorphism.

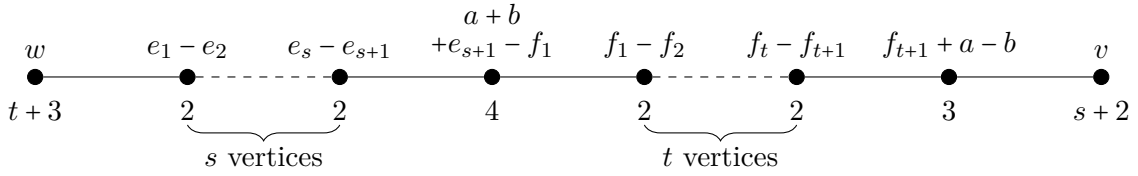

Figure 4.35: Embedding of $D^2_{s,t}$ in $\mathbb{Z}^{s+t+5}$ for $s \geq 4$, $t \geq 3$.

In order to determine what v and w should be, let $v := \rho_v(e_1 + \cdots + e_{s+1}) + \eta_v(f_1 + \cdots + f_{t+1}) + \alpha_v a + \beta_v b + \gamma_v c$ and $w := (\rho_w - 1)e_1 + \rho_w(e_2 + \cdots + e_{s+1}) + \eta_w(f_1 + \cdots + f_{t+1}) + \alpha_w a + \beta_w b + \gamma_w c$. Set up the following system of equations to determine the integer coefficients:

$$v \cdot v = (s+1)\rho_v^2 + (t+1)\eta_v^2 + \alpha_v^2 + \beta_v^2 + \gamma_v^2 = s+2 \implies |\rho_v| \leq 1 \tag{1}$$

$$w \cdot w = (\rho_w - 1)^2 + s\rho_w^2 + (t+1)\eta_w^2 + \alpha_w^2 + \beta_w^2 + \gamma_w^2 = t+3 \implies |\eta_w| \leq 1 \tag{2}$$

$$v \cdot (a + b + e_{s+1} - f_1) = \alpha_v + \beta_v + \rho_v - \eta_v = 0 \tag{3}$$

$$v \cdot (f_{t+1} + a - b) = \alpha_v - \beta_v + \eta_v = -1 \tag{4}$$

$$w \cdot (a + b + e_{s+1} - f_1) = \alpha_w + \beta_w + \rho_w - \eta_w = 0 \tag{5}$$

$$w \cdot (f_{t+1} + a - b) = \alpha_w - \beta_w + \eta_w = 0 \tag{6}$$

$$v \cdot w = (s+1)\rho_v\rho_w - \rho_v + (t+1)\eta_v\eta_w + \alpha_v\alpha_w + \beta_v\beta_w + \gamma_v\gamma_w = 0. \tag{7}$$

- **Case $\rho_v = -1$:**
  After performing the appropriate substitution, the system simplifies as follows:

$$(t+1)\eta_v^2 + \alpha_v^2 + \beta_v^2 + \gamma_v^2 = 1 \implies \eta_v = 0 \tag{1}$$
$$(\rho_w - 1)^2 + s\rho_w^2 + (t+1)\eta_w^2 + \alpha_w^2 + \beta_w^2 + \gamma_w^2 = t+3 \implies |\eta_w| \leq 1 \tag{2}$$
$$\alpha_v = 0 \tag{3}$$
$$\beta_v = 1 \implies \gamma_v = 0 \tag{4}$$
$$\alpha_w + \beta_w = \eta_w - \rho_w \tag{5}$$
$$\alpha_w - \beta_w = -\eta_w \tag{6}$$
$$-(s+1)\rho_w + 1 + \beta_w = 0. \tag{7}$$

When $\eta_w \in \{0, 1\}$, the system is inconsistent: this can be verified by carrying out the appropriate substitutions in equation (7). Therefore, we consider the case $\eta_w = -1$:

$$\alpha_v^2 + \beta_v^2 + \gamma_v^2 = 1 \tag{1}$$
$$(\rho_w - 1)^2 + s\rho_w^2 + \alpha_w^2 + \beta_w^2 + \gamma_w^2 = 2 \implies \rho_w = 0 \tag{2}$$
$$\alpha_v = 0 \tag{3}$$
$$\beta_v = 1 \implies \gamma_v = 0 \tag{4}$$
$$\alpha_w = 0 \tag{5}$$
$$\beta_w = -1 \implies \gamma_w = 0 \tag{6}$$
$$\beta_w = -1. \tag{7}$$

Thus $v = -(e_1 + \cdots + e_{s+1}) + b$ and $w = -e_1 - (f_1 + \cdots + f_{t+1}) - b$. Figure 4.35 now provides a lattice embedding in $\mathbb{Z}^{s+t+5}$. However, this embedding corresponds to the one in [49], and thus is not of interest for us, as it does not satisfy the conditions of Proposition 3.9.

- **Case $\rho_v = 0$:**
  We focus on a subset of equations to show that the system is inconsistent:

$$(t+1)\eta_v^2 + \alpha_v^2 + \beta_v^2 + \gamma_v^2 = s+2 \tag{1}$$
$$(\rho_w - 1)^2 + s\rho_w^2 + (t+1)\eta_w^2 + \alpha_w^2 + \beta_w^2 + \gamma_w^2 = t+3 \implies |\eta_w| \leq 1 \tag{2}$$
$$\alpha_v + \beta_v = \eta_v \tag{3}$$
$$\alpha_v - \beta_v = -1 - \eta_v \implies \alpha_v = -\frac{1}{2}. \tag{4}$$

Hence, there is no lattice embedding when $\rho_v = 0$.

- **Case $\rho_v = 1$:**
  After performing the appropriate substitution, the system simplifies as follows:

$$(t+1)\eta_v^2 + \alpha_v^2 + \beta_v^2 + \gamma_v^2 = 1 \implies \eta_v = 0 \tag{1}$$
$$(\rho_w - 1)^2 + s\rho_w^2 + (t+1)\eta_w^2 + \alpha_w^2 + \beta_w^2 + \gamma_w^2 = t+3 \implies |\eta_w| \leq 1 \tag{2}$$
$$\alpha_v = -1 \implies \gamma_v = 0 \tag{3}$$
$$\beta_v = 0 \tag{4}$$
$$\alpha_w + \beta_w = \eta_w - \rho_w \tag{5}$$
$$\alpha_w - \beta_w = -\eta_w \tag{6}$$
$$(s+1)\rho_w - 1 - \alpha_w = 0. \tag{7}$$

  - Case $\eta_w = -1$:
    Focus on the following subset of equations:

$$(\rho_w - 1)^2 + s\rho_w^2 + \alpha_w^2 + \beta_w^2 + \gamma_w^2 = 2 \implies \rho_w = 0 \tag{2}$$
$$\alpha_w = 0 \tag{5}$$
$$\beta_w = -1 \tag{6}$$
$$\alpha_w = -1. \tag{7}$$

    The system is inconsistent, hence there is no lattice embedding when $\rho_v = 1$ and $\eta_w = -1$.

  - Case $\eta_w = 0$:

Focus on the following subset of equations:

$$(\rho_w - 1)^2 + s\rho_w^2 + \alpha_w^2 + \beta_w^2 + \gamma_w^2 = t + 3 \tag{2}$$
$$\alpha_w = -\frac{\rho_w}{2} \tag{5}$$
$$\beta_w = \alpha_w \tag{6}$$
$$\rho_w = \frac{2}{2s+3}. \tag{7}$$

For any $s \geq 4$, ρ_w is not an integer, thus the system is inconsistent. There is no lattice embedding when $\rho_v = 1$ and $\eta_w = 0$.

– Case $\eta_w = 1$:
Focus on the following subset of equations:

$$(\rho_w - 1)^2 + s\rho_w^2 + \alpha_w^2 + \beta_w^2 + \gamma_w^2 = 2 \implies \rho_w = 0 \tag{2}$$
$$\alpha_w = 0 \tag{5}$$
$$\beta_w = 1 \tag{6}$$
$$\alpha_w = -1. \tag{7}$$

The system is inconsistent, hence there is no lattice embedding when $\rho_v = 1$ and $\eta_w = 1$.

We summarise our analysis by observing that it is not possible to construct an embedding satisfying Proposition 3.9 when $s \geq 4$ and $t \geq 3$.

§ 4.7.2 | Remaining Cases

In this section, we analyse the possible lattice embeddings of $D^2_{s,t}$ in $\mathbb{Z}^{s+t+5}$ whenever either $s < 4$ or $t < 3$.

Start with $D^2_{s,0}$ when $s \geq 4$. We require a lattice embedding in $\mathbb{Z}^{s+5}$, and Figure 4.36 shows the only option (notice the similarity to the general case). We only need to determine the coefficients of $v := \rho_v(e_1 + \cdots + e_{s+1}) + \eta_v f_1 + \alpha_v a + \beta_v b + \gamma_v c$.

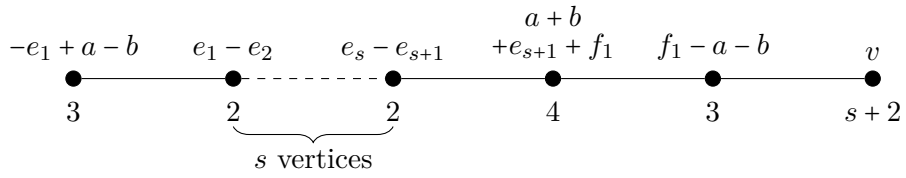

Figure 4.36: Potential embedding of $D^2_{s,0}$ in $\mathbb{Z}^{s+5}$ for $s \geq 4$.

In order to do so, set up the following system of equations:

$$(s+1)\rho_v^2 + \eta_v^2 + \alpha_v^2 + \beta_v^2 + \gamma_v^2 = s + 2 \implies |\rho_v| \leq 1 \tag{1}$$
$$\alpha_v - \beta_v = \rho_v \tag{2}$$
$$\rho_v + \eta_v + \alpha_v + \beta_v = 0 \tag{3}$$
$$\eta_v - \alpha_v - \beta_v = -1. \tag{4}$$

- **Case** $\rho_v = -1$**:**
  The system simplifies as follows:

$$\eta_v^2 + \alpha_v^2 + \beta_v^2 + \gamma_v^2 = 1 \tag{1}$$
$$\alpha_v = \beta_v - 1 \tag{2}$$
$$\eta_v = 2 - 2\beta_v \tag{3}$$
$$\beta_v = 1 \implies \alpha_v = \eta_v = \gamma_v = 0. \tag{4}$$

  Substituting $v = -(e_1 + \cdots + e_{s+1}) + b$ in Figure 4.36 provides a lattice embedding in $\mathbb{Z}^{s+5}$. This is the embedding found in [49], hence not relevant for our purposes.

- **Case** $\rho_v = 0$**:**
  The system becomes as follows:

$$\eta_v^2 + \alpha_v^2 + \beta_v^2 + \gamma_v^2 = s + 2 \tag{1}$$
$$\alpha_v = \beta_v \tag{2}$$
$$\eta_v = -2\alpha_v \tag{3}$$
$$\alpha_v = \frac{1}{4}. \tag{4}$$

There is no integer solution for α_v, hence we cannot find the required lattice embedding when $\rho_v = 0$.

- **Case $\rho_v = 1$:**
  The system simplifies as follows:

$$\eta_v^2 + \alpha_v^2 + \beta_v^2 + \gamma_v^2 = 1 \tag{1}$$
$$\alpha_v = \beta_v + 1 \tag{2}$$
$$\eta_v = -2 - 2\beta_v \tag{3}$$
$$\beta_v = -\frac{1}{2}. \tag{4}$$

There is no integer solution for β_v, hence we cannot find the required lattice embedding when $\rho_v = 1$.

We next analyse lattice embeddings of $D_{s,1}^2$ in $\mathbb{Z}^{s+6}$ when $s \geq 4$. When mapping each vertex of $D_{s,1}^2$ to linear combinations of basis vectors for $\mathbb{Z}^{s+6}$, we have two possibilities. The first possibility is given by the mapping discussed in the general case and presented in Figure 4.35 and the same conclusions apply. We now study another potential embedding, presented in Figure 4.37.

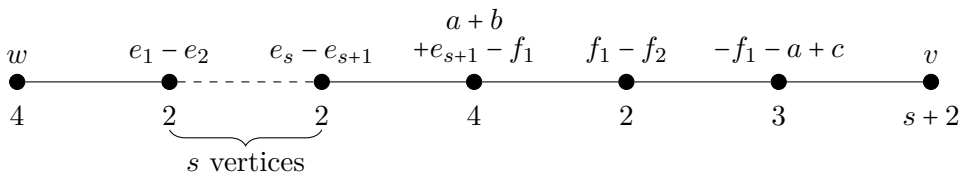

Figure 4.37: Second potential embedding of $D_{s,1}^2$ in $\mathbb{Z}^{s+6}$ for $s \geq 4$.

Once again, let $v := \rho_v(e_1 + \cdots + e_{s+1}) + \eta_v(f_1 + f_2) + \alpha_v a + \beta_v b + \gamma_v c$ and $w := -e_1 + \eta_w(f_1 +$

$f_2) + \alpha_w a + \beta_w b + \gamma_w c$. We set up the following system of equations:

$$(s+1)\rho_v^2 + 2\eta_v^2 + \alpha_v^2 + \beta_v^2 + \gamma_v^2 = s+2 \implies |\rho_v| \leq 1 \tag{1}$$
$$2\eta_w^2 + \alpha_w^2 + \beta_w^2 + \gamma_w^2 = 3 \tag{2}$$
$$\rho_v - \eta_v + \alpha_v + \beta_v = 0 \tag{3}$$
$$\gamma_v - \eta_v - \alpha_v = -1 \tag{4}$$
$$\alpha_w + \beta_w = \eta_w \tag{5}$$
$$\gamma_w - \alpha_w - \eta_w = 0 \tag{6}$$
$$2\eta_w\eta_v + \alpha_v\alpha_w + \beta_v\beta_w + \gamma_v\gamma_w = \rho_v. \tag{7}$$

- **Case $\rho_v = -1$:**

$$2\eta_v^2 + \alpha_v^2 + \beta_v^2 + \gamma_v^2 = 1 \implies \eta_v = 0 \tag{1}$$
$$2\eta_w^2 + \alpha_w^2 + \beta_w^2 + \gamma_w^2 = 3 \tag{2}$$
$$\beta_v = 1 - \alpha_v \tag{3}$$
$$\gamma_v = \alpha_v - 1 \tag{4}$$
$$\beta_w = \eta_w - \alpha_w \tag{5}$$
$$\gamma_w = \eta_w + \alpha_w \tag{6}$$
$$\alpha_w = -\frac{1}{3\alpha_v - 2}. \tag{7}$$

  Observe that combining equations (1), (3) and (4) yields $3\alpha_v^2 - 4\alpha_v + 1 = 0$ for which the only integer solution is $\alpha_v = 1$. This implies $\beta_v = \gamma_v = 0$. Similarly, combining the remaining equations yields $\eta_w = 0$. Thus, $v = -(e_1 + \cdots + e_{s+1}) + a$ and $w = -e_1 - a + b - c$, and Figure 4.37 now determines a lattice embedding in $\mathbb{Z}^{s+6}$. The orthogonal complement is generated by the vector

$$(\underbrace{0, \ldots, 0}_{s+1 \text{ times}}, 1, 1, 0, 1, 1),$$

  hence it does not satisfy the conditions of Proposition 3.9.

- **Case $\rho_v = 0$:**
  After substituting $\rho_v = 0$ the system simplifies to:

$$2\eta_v^2 + \alpha_v^2 + \beta_v^2 + \gamma_v^2 = s + 2 \tag{1}$$
$$2\eta_w^2 + \alpha_w^2 + \beta_w^2 + \gamma_w^2 = 3 \tag{2}$$
$$\eta_v = \alpha_v + \beta_v \tag{3}$$
$$\gamma_v = 2\alpha_v + \beta_v - 1 \tag{4}$$
$$\alpha_w + \beta_w = \eta_w \tag{5}$$
$$\gamma_w = 2\alpha_w + \beta_w \tag{6}$$
$$2\eta_w\eta_v + \alpha_v\alpha_w + \beta_v\beta_w + \gamma_v\gamma_w = 0. \tag{7}$$

– Case $\eta_w = -1$:
Focus on the following subset of equations:

$$\alpha_w^2 + \beta_w^2 + \gamma_w^2 = 1 \tag{2}$$
$$\beta_w = -1 - \alpha_w \tag{5}$$
$$\gamma_w = \alpha_w - 1. \tag{6}$$

Performing the required substitutions in equation (2) yields $\alpha_w^2 = -\frac{1}{3}$. Hence, there is no embedding with $\rho_v = 0$ and $\eta_w = -1$.

– Case $\eta_w = 0$:
Focus on the following subset of equations:

$$\alpha_w^2 = 1 \tag{2}$$
$$\gamma_v = 2\alpha_v + \beta_v - 1 \tag{4}$$
$$\beta_w = -\alpha_w \tag{5}$$
$$\gamma_w = \alpha_w \tag{6}$$
$$\alpha_w(\alpha_v - \beta_v + \gamma_v) = 0 \implies \alpha_w(3\alpha_v - 1) = 0. \tag{7}$$

In order for the system to be consistent, we must have $3\alpha_v - 1 = 0$ in the last equation, but this implies there is no integer solution for α_v. Hence, there is no embedding with $\rho_v = 0$ and $\eta_w = 0$.

– Case $\eta_w = 1$:
Focus on the following subset of equations:

$$\alpha_w^2 + \beta_w^2 + \gamma_w^2 = 1 \tag{2}$$
$$\beta_w = 1 - \alpha_w \tag{5}$$
$$\gamma_w = 1 + \alpha_w. \tag{6}$$

Performing the required substitutions in equation (2) yields $\alpha_w^2 = -\frac{1}{3}$. Hence, there is no embedding with $\rho_v = 0$ and $\eta_w = 1$.

This concludes the analysis of possible embeddings of $D_{s,1}^2$ in $\mathbb{Z}^{s+6}$.
Next, we consider lattice embeddings of $D_{s,2}^2$ in $\mathbb{Z}^{s+7}$ with $s \geq 4$. There are two main ways to map vertices of $D_{s,2}^2$ to linear combinations of basis vectors of $\mathbb{Z}^{s+7}$. The first possibility is shown in Figure 4.38.

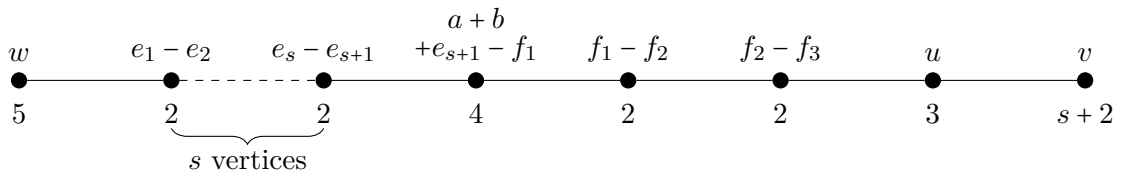

Figure 4.38: First potential embedding of $D_{s,2}^2$ in $\mathbb{Z}^{s+7}$ for $s \geq 4$.

We need to determine the integer coefficients of $u := \eta_u(f_1+f_2+f_3)+f_3+\alpha_u a+\beta_u b+\gamma_u c$, $v := \rho_v(e_1+\cdots+e_{s+1})+\eta_v(f_1+f_2+f_3)+\alpha_v a+\beta_v b+\gamma_v c$, and $w := -e_1+\eta_w(f_1+f_2+f_3)+\alpha_w a+\beta_w b+\gamma_w c$. We set up the following system of equations:

$$2\eta_u^2 + (\eta_u + 1)^2 + \alpha_u^2 + \beta_u^2 + \gamma_u^2 = 3 \implies \eta_u \in \{-1, 0\} \tag{1}$$
$$(s+1)\rho_v^2 + 3\eta_v^2 + \alpha_v^2 + \beta_v^2 + \gamma_v^2 = s + 2 \implies |\rho_v| \leq 1 \tag{2}$$
$$3\eta_w^2 + \alpha_w^2 + \beta_w^2 + \gamma_w^2 = 4 \tag{3}$$
$$\eta_u = \alpha_u + \beta_u \tag{4}$$
$$\rho_v - \eta_v + \alpha_v + \beta_v = 0 \tag{5}$$
$$\alpha_w + \beta_w - \eta_w = 0 \tag{6}$$
$$\eta_v(3\eta_u + 1) + \alpha_v\alpha_u + \beta_v\beta_u + \gamma_v\gamma_u = -1 \tag{7}$$
$$3\eta_v\eta_w + \alpha_v\alpha_w + \beta_v\beta_w + \gamma_v\gamma_w = \rho_v \tag{8}$$
$$\eta_w(3\eta_u + 1) + \alpha_w\alpha_u + \beta_w\beta_u + \gamma_w\gamma_u = 0. \tag{9}$$

- **Case $\rho_v = -1$, $\eta_u = -1$:**
  After performing the appropriate substitutions and simplifying, the system is the following:

$$2\alpha_u^2 + 2\alpha_u + \gamma_u^2 = 0 \implies \gamma_u = 0 \text{ and } \alpha_u \in \{-1, 0\} \tag{1}$$
$$3\eta_v^2 + \alpha_v^2 + \beta_v^2 + \gamma_v^2 = 1 \implies \eta_v = 0 \tag{2}$$
$$3\eta_w^2 + \alpha_w^2 + \beta_w^2 + \gamma_w^2 = 4 \tag{3}$$
$$\beta_u = -1 - \alpha_u \tag{4}$$
$$\beta_v = 1 - \alpha_v \tag{5}$$
$$\alpha_w + \beta_w - \eta_w = 0 \tag{6}$$
$$\alpha_v\alpha_u + \beta_v\beta_u = -1 \tag{7}$$
$$\alpha_v\alpha_w + \beta_v\beta_w + \gamma_v\gamma_w = -1 \tag{8}$$
$$\alpha_w\alpha_u + \beta_w\beta_u = 2\eta_w. \tag{9}$$

  - Case $\alpha_u = -1$:

Focus on the following subset of equations:

$$\beta_u = 0 \tag{4}$$
$$\alpha_v = 1 \implies \beta_v = \gamma_v = 0 \tag{7}$$
$$\alpha_w = -1 \tag{8}$$
$$\eta_w = \frac{1}{2}. \tag{9}$$

There is no integer solution for η_w, hence no embedding is possible when $\rho_v = \eta_u = \alpha_u = -1$.

– Case $\alpha_u = 0$:
Focus on the following subset of equations:

$$\beta_u = -1 \tag{4}$$
$$\beta_v = 1 \implies \alpha_v = \gamma_v = 0 \tag{7}$$
$$\beta_w = -1 \tag{8}$$
$$\eta_w = \frac{1}{2}. \tag{9}$$

There is no integer solution for η_w, hence no embedding is possible when $\rho_v = \eta_u = \alpha_u = -1$.

- **Case $\rho_v = -1$, $\eta_u = 0$:**
After performing the required substitutions, the system simplifies as follows:

$$2\alpha_u^2 + \gamma_u^2 = 2 \implies \gamma_u = 0 \text{ and } \alpha_u = \pm 1 \tag{1}$$
$$3\eta_v^2 + \alpha_v^2 + \beta_v^2 + \gamma_v^2 = 1 \implies \eta_v = 0 \tag{2}$$
$$3\eta_w^2 + \alpha_w^2 + \beta_w^2 + \gamma_w^2 = 4 \tag{3}$$
$$\beta_u = -\alpha_u \tag{4}$$
$$\beta_v = 1 - \alpha_v \tag{5}$$
$$\alpha_w + \beta_w - \eta_w = 0 \tag{6}$$
$$\alpha_u(2\alpha_v - 1) = -1 \tag{7}$$
$$\alpha_v\alpha_w + \beta_v\beta_w + \gamma_v\gamma_w = -1 \tag{8}$$
$$\eta_w + \alpha_u(2\alpha_w - \eta_w) = 0. \tag{9}$$

– Case $\alpha_u = -1$:

The system can be simplified as follows:

$$2\alpha_v^2 - 2\alpha_v + \gamma_v^2 = 0 \implies \gamma_v = 0 \tag{2}$$
$$3\eta_w^2 + \alpha_w^2 + \beta_w^2 + \gamma_w^2 = 4 \tag{3}$$
$$\beta_u = 1 \tag{4}$$
$$\beta_v = 1 - \alpha_v = 0 \tag{5}$$
$$\alpha_w + \beta_w - \eta_w = 0 \tag{6}$$
$$\alpha_v = 1 \tag{7}$$
$$\alpha_w = -1 \tag{8}$$
$$\eta_w = -1 \implies \gamma_w = 0. \tag{9}$$

This determines that $u = f_3 - a + b$, $v = -(e_1 + \cdots + e_{s+1}) + a$, and $w = -e_1 - (f_1 + f_2 + f_3) - a$. Together with Figure 4.38, this determines a lattice embedding in $\mathbb{Z}^{s+7}$ which corresponds to the one in [49], and hence is not the one we require.

– Case $\alpha_u = 1$:

The system can be simplified as follows:

$$2\alpha_v^2 - 2\alpha_v + \gamma_v^2 = 0 \implies \gamma_v = 0 \tag{2}$$
$$3\eta_w^2 + \alpha_w^2 + \beta_w^2 + \gamma_w^2 = 4 \tag{3}$$
$$\beta_u = -1 \tag{4}$$
$$\beta_v = 1 - \alpha_v = 1 \tag{5}$$
$$\alpha_w + \beta_w - \eta_w = 0 \tag{6}$$
$$\alpha_v = 0 \tag{7}$$
$$\beta_w = -1 \tag{8}$$
$$\alpha_w = 0 \implies \eta_w = -1 \text{ and } \gamma_w = 0. \tag{9}$$

This determines that $u = f_3 + a - b$, $v = -(e_1 + \cdots + e_{s+1}) + b$, and $w = -e_1 - (f_1 + f_2 + f_3) - b$. Together with Figure 4.38, this determines a lattice embedding in $\mathbb{Z}^{s+7}$, equivalent to the one found in the case $\alpha_u = 1$, hence it is not the one we require.

- **Case $\rho_v = 0$, $\eta_u = -1$:**

Perform the required substitutions and simplify the system as follows:

$$2\alpha_u^2 + 2\alpha_u + \gamma_u^2 = 0 \implies \gamma_u = 0 \text{ and } \alpha_u \in \{-1, 0\} \tag{1}$$
$$3\eta_v^2 + \alpha_v^2 + \beta_v^2 + \gamma_v^2 = s + 2 \tag{2}$$
$$3\eta_w^2 + \alpha_w^2 + \beta_w^2 + \gamma_w^2 = 4 \tag{3}$$
$$\beta_u = -1 - \alpha_u \tag{4}$$
$$\eta_v = \alpha_v + \beta_v \tag{5}$$
$$\alpha_w + \beta_w - \eta_w = 0 \tag{6}$$
$$\alpha_v\alpha_u + \beta_v\beta_u = 2\eta_v - 1 \tag{7}$$
$$3\eta_v\eta_w + \alpha_v\alpha_w + \beta_v\beta_w + \gamma_v\gamma_w = 0 \tag{8}$$
$$2\eta_w = \alpha_w\alpha_u + \beta_w\beta_u. \tag{9}$$

– Case $\alpha_u = -1$:
  The system becomes the following:

$$3\eta_v^2 + \alpha_v^2 + \beta_v^2 + \gamma_v^2 = s + 2 \tag{2}$$
$$7\eta_w^2 + \beta_w^2 + \gamma_w^2 = 4 \implies \eta_w = 0 \tag{3}$$
$$\beta_u = 0 \tag{4}$$
$$\beta_v = 3\eta_v - 1 \tag{5}$$
$$\beta_w = \eta_w - \alpha_w = 0 \tag{6}$$
$$\alpha_v = 1 - 2\eta_v \tag{7}$$
$$\beta_v\beta_w + \gamma_v\gamma_w = 0 \tag{8}$$
$$\alpha_w = -2\eta_w. \tag{9}$$

  Observe that equation (2) implies $\gamma_w = \pm 2$, and so in (8) we must have $\gamma_v = 0$. We have thus determined that for $s = 16\eta_v^2 - 10\eta_v \geq 4$ we have $u = -f_1 - f_2 - a$, $v = \eta_v(f_1+f_2+f_3)+(1-2\eta_v)a+(3\eta_v-1)b$, and $w = -e_1 \pm 2c$. Together with Figure 4.38 this provides a lattice embedding in $\mathbb{Z}^{s+7}$. The orthogonal complement vector is generated by

$$(\underbrace{2(16\eta_v-5),\ldots,2(16\eta_v-5)}_{s+1 \text{ times}},\underbrace{2(3\eta_v-1),\ldots,2(3\eta_v-1)}_{3 \text{ times}},-2(6\eta_v-2),-2(7\eta_v-2),\pm(16\eta_v-5)),$$

and has square $16384\eta_v^4 - 20480\eta_v^3 + 9728\eta_v^2 - 2080\eta_v + 169 = p$. This embedding satisfies the conditions of Proposition 3.9, hence any lens space with $\frac{p}{q} = D^2_{s,2}$ with $s = 16\eta_v^2 - 10\eta_v \geq 4$ is unobstructed from embedding in $\mathbb{C}P^2$.

– Case $\alpha_u = 0$:
The system becomes the following:

$$3\eta_v^2 + \alpha_v^2 + \beta_v^2 + \gamma_v^2 = s + 2 \tag{2}$$
$$7\eta_w^2 + \alpha_w^2 + \gamma_w^2 = 4 \implies \eta_w = 0 \tag{3}$$
$$\beta_u = -1 \tag{4}$$
$$\alpha_v = 3\eta_v - 1 \tag{5}$$
$$\alpha_w = \eta_w - \beta_w = 0 \tag{6}$$
$$\beta_v = 1 - 2\eta_v \tag{7}$$
$$\beta_v\beta_w + \gamma_v\gamma_w = 0 \tag{8}$$
$$\beta_w = -2\eta_w. \tag{9}$$

Once again, observe that equation (2) implies $\gamma_w = \pm 2$, and so in (8) we must have $\gamma_v = 0$. We have thus determined that for $s = 16\eta_v^2 - 10\eta_v$ we have $u = -f_1 - f_2 - b$, $v = \eta_v(f_1 + f_2 + f_3) + (3\eta_v - 1)a + (1 - 2\eta_v)b$, and $w = -e_1 \pm 2c$. Together with Figure 4.38 this provides a lattice embedding in $\mathbb{Z}^{s+7}$, equivalent to the one found in the case $\alpha_u = -1$. Hence, the same conclusions apply.

- **Case $\rho_v = 0$, $\eta_u = 0$:**
After the substitutions, the system simplifies as follows:

$$\alpha_u^2 + \beta_u^2 + \gamma_u^2 = 2 \tag{1}$$
$$3\eta_v^2 + \alpha_v^2 + \beta_v^2 + \gamma_v^2 = s + 2 \tag{2}$$
$$3\eta_w^2 + \alpha_w^2 + \beta_w^2 + \gamma_w^2 = 4 \tag{3}$$
$$\beta_u = -\alpha_u \tag{4}$$
$$\eta_v = \alpha_v + \beta_v \tag{5}$$
$$\alpha_w + \beta_w - \eta_w = 0 \tag{6}$$
$$\eta_v + \alpha_u(\alpha_v - \beta_v) + \gamma_v\gamma_u = -1 \tag{7}$$
$$3\eta_v\eta_w + \alpha_v\alpha_w + \beta_v\beta_w + \gamma_v\gamma_w = 0 \tag{8}$$
$$\eta_w + \alpha_u(\alpha_w - \beta_w) + \gamma_w\gamma_u = 0. \tag{9}$$

Substituting equation (4) in (1) we obtain $2\alpha_u^2 + \gamma_u^2 = 2$. Since we are interested in integer solutions only, we deduce that $\gamma_u = 0$ and $\alpha_u = \pm 1$.

- Case $\alpha_u = -1$:
  Focus on the following two equations:

$$\eta_v = \alpha_v + \beta_v \tag{5}$$
$$\beta_v = -\frac{1}{2}. \tag{7}$$

  As we cannot find an integer value for β_v, there is no lattice embedding in $\mathbb{Z}^{s+7}$ when $\rho_v = \eta_u = 0$ and $\alpha_u = -1$.

- Case $\alpha_u = 1$:
  Focus on the following two equations:

$$\eta_v = \alpha_v + \beta_v \tag{5}$$
$$\alpha_v = -\frac{1}{2}. \tag{7}$$

  As we cannot find an integer value for α_v, there is no lattice embedding in $\mathbb{Z}^{s+7}$ when $\rho_v = \eta_u = 0$ and $\alpha_u = -1$.

- **Case $\rho_v = 1$, $\eta_u = -1$:**

After the substitutions, the system becomes the following:

$$\alpha_u^2 + \beta_u^2 + \gamma_u^2 = 1 \tag{1}$$
$$3\eta_v^2 + \alpha_v^2 + \beta_v^2 + \gamma_v^2 = 1 \implies \eta_v = 0 \tag{2}$$
$$3\eta_w^2 + \alpha_w^2 + \beta_w^2 + \gamma_w^2 = 4 \tag{3}$$
$$\beta_u = -1 - \alpha_u \tag{4}$$
$$\alpha_v + \beta_v = -1 \tag{5}$$
$$\alpha_w + \beta_w - \eta_w = 0 \tag{6}$$
$$\alpha_v\alpha_u + \beta_v\beta_u + \gamma_v\gamma_u = -1 \tag{7}$$
$$\alpha_v\alpha_w + \beta_v\beta_w + \gamma_v\gamma_w = 1 \tag{8}$$
$$\alpha_w\alpha_u + \beta_w\beta_u + \gamma_w\gamma_u = 2\eta_w. \tag{9}$$

If we substitute equation (4) into (1) we obtain $2\alpha_u^2 + 2\alpha_u + \gamma_u^2 = 0$. Since we are looking for integer solutions, we must have $\gamma_u = 0$ and $\alpha_u \in \{-1, 0\}$.

– Case $\alpha_u = -1$:
  Focus on the following subset of equations:

$$\alpha_v^2 + \beta_v^2 + \gamma_v^2 = 1 \tag{2}$$
$$\beta_u = 0 \tag{4}$$
$$\beta_v = -1 - \alpha_v \tag{5}$$
$$\alpha_v = 1. \tag{7}$$

  Substituting $\alpha_v = 1$ and $\beta_v = -2$ in equation (2) results in $\gamma_v^2 = -4$, making the system inconsistent. Hence, there is no lattice embedding in $\mathbb{Z}^{s+7}$ when $\rho_v = 1$ and $\eta_u = \alpha_u = -1$.

– Case $\alpha_u = 0$:
  Focus on the following subset of equations:

$$\alpha_v^2 + \beta_v^2 + \gamma_v^2 = 1 \tag{2}$$
$$\beta_u = -1 \tag{4}$$
$$\beta_v = -1 - \alpha_v \tag{5}$$
$$\beta_v = 1. \tag{7}$$

  Substituting $\beta_v = 1$ and $\alpha_v = -2$ in equation (2) results in $\gamma_v^2 = -4$, making the

system inconsistent. Hence, there is no lattice embedding in $\mathbb{Z}^{s+7}$ when $\rho_v = 1$, $\eta_u = -1$, and $\alpha_u = 0$.

- **Case $\rho_v = 1$, $\eta_u = 0$:**
  After the substitutions, the system becomes the following:

$$2\alpha_u^2 + \gamma_u^2 = 2 \implies \gamma_u = 0 \text{ and } \alpha_u = \pm 1 \tag{1}$$
$$3\eta_v^2 + \alpha_v^2 + \beta_v^2 + \gamma_v^2 = 1 \implies \eta_v = 0 \tag{2}$$
$$3\eta_w^2 + \alpha_w^2 + \beta_w^2 + \gamma_w^2 = 4 \tag{3}$$
$$\beta_u = -\alpha_u \tag{4}$$
$$\alpha_v + \beta_v = -1 \tag{5}$$
$$\alpha_w + \beta_w - \eta_w = 0 \tag{6}$$
$$\alpha_v\alpha_u + \beta_v\beta_u = -1 \tag{7}$$
$$\alpha_v\alpha_w + \beta_v\beta_w + \gamma_v\gamma_w = 1 \tag{8}$$
$$\eta_w + \alpha_w\alpha_u + \beta_w\beta_u = 0. \tag{9}$$

  - Case $\alpha_u = -1$:
    Focus on the following subset of equations:

$$\alpha_v^2 + \beta_v^2 + \gamma_v^2 = 1 \tag{2}$$
$$\beta_u = 1 \tag{4}$$
$$\alpha_v = 0 \tag{5}$$
$$\eta_w = \alpha_w + \beta_w \tag{6}$$
$$\beta_v = -1 \implies \gamma_v = 0 \tag{7}$$
$$\beta_w = -1 \tag{8}$$
$$\beta_w = 0. \tag{9}$$

    The system is inconsistent, hence there is no lattice embedding in $\mathbb{Z}^{s+7}$ when $\rho_v = 1$, $\eta_u = 0$, and $\alpha_u = -1$.

  - Case $\alpha_u = 1$:

Focus on the following subset of equations:

$$\alpha_v^2 + \beta_v^2 + \gamma_v^2 = 1 \tag{2}$$
$$\beta_u = -1 \tag{4}$$
$$\beta_v = 0 \tag{5}$$
$$\eta_w = \alpha_w + \beta_w \tag{6}$$
$$\alpha_v = -1 \implies \gamma_v = 0 \tag{7}$$
$$\alpha_w = -1 \tag{8}$$
$$\alpha_w = 0. \tag{9}$$

The system is inconsistent, hence there is no lattice embedding in $\mathbb{Z}^{s+7}$ when $\rho_v = \alpha_u = 1$ and $\eta_u = 0$.

This concludes the analysis of all possible lattice embeddings of $D_{s,2}^2$ in $\mathbb{Z}^{s+7}$ arising from Figure 4.38. We previously mentioned there is also another way to map the vertices of $D_{s,2}^2$ to linear combinations of basis vectors of $\mathbb{Z}^{s+7}$ in order to hopefully construct a lattice embedding. This second option is shown in Figure 4.39. Once again, let $u :=$

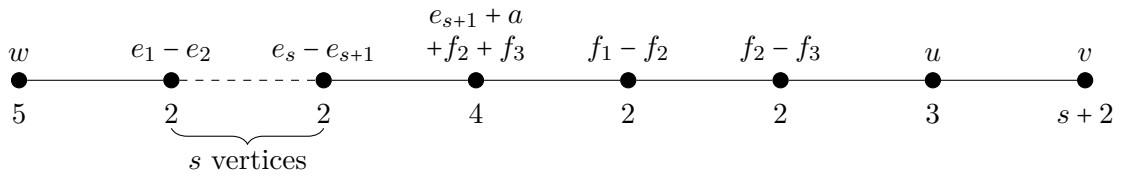

Figure 4.39: Second potential embedding of $D_{s,2}^2$ in $\mathbb{Z}^{s+7}$ for $s \geq 4$.

$\eta_u(f_1 + f_2 + f_3) + f_3 + \alpha_u a + \beta_u b + \gamma_u c$, $v := \rho_v(e_1 + \cdots + e_{s+1}) + \eta_v(f_1 + f_2 + f_3) + \alpha_v a + \beta_v b + \gamma_v c$, and $w := -e_1 + \eta_w(f_1 + f_2 + f_3) + \alpha_w a + \beta_w b + \gamma_w c$. We set up the following system of equations:

$$2\eta_u^2 + (\eta_u + 1)^2 + \alpha_u^2 + \beta_u^2 + \gamma_u^2 = 3 \implies \eta_u \in \{-1, 0\} \tag{1}$$
$$(s+1)\rho_v^2 + 3\eta_v^2 + \alpha_v^2 + \beta_v^2 + \gamma_v^2 = s + 2 \implies |\rho_v| \leq 1 \tag{2}$$
$$3\eta_w^2 + \alpha_w^2 + \beta_w^2 + \gamma_w^2 = 4 \tag{3}$$
$$2\eta_u + \alpha_u + 1 = 0 \tag{4}$$
$$\rho_v + \alpha_v + 2\eta_v = 0 \tag{5}$$
$$\alpha_w + 2\eta_w = 0 \tag{6}$$
$$\eta_v(3\eta_u + 1) + \alpha_v\alpha_u + \beta_v\beta_u + \gamma_v\gamma_u = -1 \tag{7}$$
$$3\eta_v\eta_w + \alpha_v\alpha_w + \beta_v\beta_w + \gamma_v\gamma_w = \rho_v \tag{8}$$
$$\eta_w(3\eta_u + 1) + \alpha_w\alpha_u + \beta_w\beta_u + \gamma_w\gamma_u = 0. \tag{9}$$

- **Case $\rho_v = -1$, $\eta_u = -1$:**
  We perform the appropriate substitutions and focus on the following subset of equations:

$$\beta_u^2 + \gamma_u^2 = 0 \implies \beta_u = \gamma_u = 0 \tag{1}$$
$$3\eta_v^2 + \alpha_v^2 + \beta_v^2 + \gamma_v^2 = 1 \implies \eta_v = 0 \tag{2}$$
$$\alpha_u = 1 \tag{4}$$
$$\alpha_v = 1 - 2\eta_v = 1 \implies \beta_v = \gamma_v = 0 \tag{5}$$
$$\alpha_v = -1 \tag{7}$$

  The system is inconsistent, hence there is no lattice embedding of $D_{s,2}^2$ in $\mathbb{Z}^{s+7}$ when $\rho_v = \eta_u = -1$.

- **Case $\rho_v = -1$, $\eta_u = 0$:**
  Focus on the following subset of equations:

$$3\eta_v^2 + \alpha_v^2 + \beta_v^2 + \gamma_v^2 = 1 \implies \eta_v = 0 \tag{2}$$
$$3\eta_w^2 + \alpha_w^2 + \beta_w^2 + \gamma_w^2 = 4 \tag{3}$$
$$\alpha_v = 1 - 2\eta_v = 1 \implies \beta_v = \gamma_v = 0 \tag{5}$$
$$\alpha_w = -2\eta_w = 0 \tag{6}$$
$$0 = -1. \tag{8}$$

The system is inconsistent, hence there is no lattice embedding of $D_{s,2}^2$ in $\mathbb{Z}^{s+7}$ when $\rho_v = -1$ and $\eta_u = 0$.

- **Case $\rho_v = 0$, $\eta_u = -1$:**
  Focus on the following subset of equations:

$$\beta_u^2 + \gamma_u^2 = 0 \implies \beta_u = \gamma_u = 0 \tag{1}$$
$$\alpha_u = 1 \tag{4}$$
$$\alpha_v = -2\eta_v \tag{5}$$
$$\alpha_v = -1 \implies \eta_v = \frac{1}{2}. \tag{7}$$

  Thus $\eta_v = \frac{1}{2}$, which is not an integer solution. Hence there is no lattice embedding of $D_{s,2}^2$ in $\mathbb{Z}^{s+7}$ when $\rho_v = 0$ and $\eta_u = -1$.

- **Case $\rho_v = 0$, $\eta_u = 0$:**
  The system is now the following:

$$\beta_u^2 + \gamma_u^2 = 1 \tag{1}$$
$$3\eta_v^2 + \alpha_v^2 + \beta_v^2 + \gamma_v^2 = s + 2 \tag{2}$$
$$3\eta_w^2 + \alpha_w^2 + \beta_w^2 + \gamma_w^2 = 4 \tag{3}$$
$$\alpha_u = -1 \tag{4}$$
$$\alpha_v = -2\eta_v \tag{5}$$
$$\alpha_w = -2\eta_w \tag{6}$$
$$\eta_v - \alpha_v + \beta_v\beta_u + \gamma_v\gamma_u = -1 \tag{7}$$
$$3\eta_v\eta_w + \alpha_v\alpha_w + \beta_v\beta_w + \gamma_v\gamma_w = 0 \tag{8}$$
$$\eta_w - \alpha_w + \beta_w\beta_u + \gamma_w\gamma_u = 0. \tag{9}$$

  Observe that substituting $\alpha_w = -2\eta_w$ in equation (3), we obtain $7\eta_w^2 + \beta_w^2 + \gamma_w^2 = 4$, which implies $\eta_w = 0 = \alpha_w$. We now focus on equation (1) and note that it gives rise to four possibilities. The first one is presented in detail below. The remaining ones give rise to equivalent embeddings, therefore we will only present the final result.

  – Case $\beta_u = -1$, $\gamma_u = 0$: We perform the appropriate substitutions and solve as follows:

$$s = 16\eta_v^2 + 6\eta_v - 1 \tag{2}$$
$$\beta_w^2 + \gamma_w^2 = 4 \tag{3}$$
$$\alpha_u = -1 \tag{4}$$
$$\alpha_v = -2\eta_v \tag{5}$$
$$\alpha_w = \eta_w = 0 \tag{6}$$
$$\beta_v = 1 + 3\eta_v \tag{7}$$
$$\beta_v\beta_w + \gamma_v\gamma_w = 0 \implies \gamma_v\gamma_w = 0 \tag{8}$$
$$\beta_w = 0. \tag{9}$$

Equation (9) tells us that $\beta_w = 0$, thus $\gamma_w = \pm 2$ and $\gamma_v = 0$. We have found that $u = f_3 - a - b$, $v = \eta_v(f_1 + f_2 + f_3) - 2\eta_v a + (1 + 3\eta_v)b$, and $w = -e_1 \pm 2c$. Together with Figure 4.39 this determines a lattice embedding of $D_{s,2}^2$ in $\mathbb{Z}^{s+7}$. The orthogonal complement vector is generated by

$$(\underbrace{2(16\eta_v + 3), \ldots, 2(16\eta_v + 5)}_{s+1 \text{ times}}, \underbrace{-2(5\eta_v + 1), \ldots, -2(5\eta_v + 1)}_{3 \text{ times}}, -2(6\eta_v+1), 2\eta_v, \pm(16\eta_v+3)),$$

and its square is $16384\eta_v^4 + 12288\eta_v^3 + 3584\eta_v^2 + 480\eta_v + 25 = p$. This embedding satisfies the conditions of Proposition 3.9, hence any lens space with $\frac{p}{q} = D_{s,2}^2$ with $s = 16\eta_v^2 + 6\eta_v - 1 \geq 4$ is unobstructed from embedding in $\mathbb{C}P^2$.

- Case $\beta_u = 1$, $\gamma_u = 0$: we obtain $u = f_3 - a + b$, $v = \eta_v(f_1 + f_2 + f_3) - 2\eta_v a - (1 + 3\eta_v)b$, and $w = -e_1 \pm 2c$.
- Case $\beta_u = 0$, $\gamma_u = -1$: we obtain $u = f_3 - a - c$, $v = \eta_v(f_1 + f_2 + f_3) - 2\eta_v a + (1 + 3\eta_v)c$, and $w = -e_1 \pm 2b$.
- Case $\beta_u = 0$, $\gamma_u = 1$: we obtain $u = f_3 - a + c$, $v = \eta_v(f_1 + f_2 + f_3) - 2\eta_v a - (1 + 3\eta_v)c$, and $w = -e_1 \pm 2b$.

- **Case $\rho_v = 1$, $\eta_u = -1$:**
  Focus on the following subset of equations:

$$\beta_u^2 + \gamma_u^2 = 0 \implies \beta_u = \gamma_u = 0 \tag{1}$$
$$3\eta_v^2 + \alpha_v^2 + \beta_v^2 + \gamma_v^2 = 1 \implies \eta_v = 0 \tag{2}$$
$$\alpha_u = 1 \tag{4}$$
$$\alpha_v = -1 \implies \beta_v = \gamma_v = 0 \tag{5}$$
$$\alpha_w = -2\eta_w \tag{6}$$
$$\alpha_w = -1. \tag{8}$$

Thus $\eta_w = \frac{1}{2}$, which is not an integer solution. Hence there is no lattice embedding of $D_{s,2}^2$ in $\mathbb{Z}^{s+7}$ when $\rho_v = 1$ and $\eta_u = -1$.

- **Case $\rho_v = 1$, $\eta_u = 0$:**
  Focus on the following subset of equations:

$$3\eta_v^2 + \alpha_v^2 + \beta_v^2 + \gamma_v^2 = 1 \implies \eta_v = 0 \tag{2}$$
$$\alpha_u = -1 \tag{4}$$
$$\alpha_v = -1 \implies \beta_v = \gamma_v = 0 \tag{5}$$
$$1 = -1. \tag{7}$$

The system is inconsistent, hence there is no lattice embedding of $D_{s,2}^2$ in $\mathbb{Z}^{s+7}$ when $\rho_v = 1$ and $\eta_u = 0$.

This concludes the analysis of $D_{s,2}^2$ when $s \geq 4$.

Next we look for lattice embeddings of $D_{0,t}^2$ in $\mathbb{Z}^{t+5}$, when $t \geq 3$. It can be directly observed that the only possible embedding follows the pattern from the general case, hence the same conclusions apply. The same holds when looking for embeddings of $D_{1,t}^2$ in $\mathbb{Z}^{t+6}$ when $t \geq 3$.

When working with the family $D_{2,t}^2$ with $t \geq 3$, we are interested in lattice embeddings in $\mathbb{Z}^{t+7}$. One way to obtain an embedding is by following the general case, which will lead to Lisca's from [49]. Figure 4.40 shows another way to potentially find more lattice embeddings.

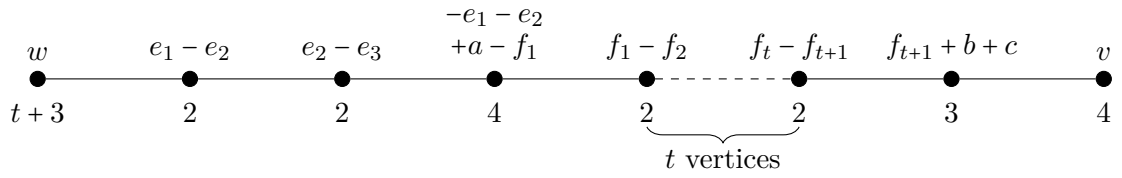

Figure 4.40: Potential embedding of $D_{2,t}^2$ in $\mathbb{Z}^{t+7}$ for $t \geq 3$.

Let $v := \rho_v(e_1+e_2+e_3) + \eta_v(f_1+\cdots+f_{t+1}) + \alpha_v a + \beta_v b + \gamma_v c$ and $w := \rho_w(e_1+e_2+e_3) - e_1 + \eta_w(f_1+\cdots+f_{t+1}) + \alpha_w a + \beta_w b + \gamma_w c$. Set up the following system of equations:

$$3\rho_v^2 + (t+1)\eta_v^2 + \alpha_v^2 + \beta_v^2 + \gamma_v^2 = 4 \tag{1}$$

$$(\rho_w - 1)^2 + 2\rho_w^2 + (t+1)\eta_w^2 + \alpha_w^2 + \beta_w^2 + \gamma_w^2 = t+3 \implies |\eta_w| \leq 1 \tag{2}$$

$$-2\rho_v - \eta_v + \alpha_v = 0 \tag{3}$$

$$\eta_v + \beta_v + \gamma_v = -1 \tag{4}$$

$$-2\rho_w - \eta_w + \alpha_w + 1 = 0 \tag{5}$$

$$\eta_w + \beta_w + \gamma_w = 0 \tag{6}$$

$$(3\rho_w - 1)\rho_v + (t+1)\eta_v\eta_w + \alpha_v\alpha_w + \beta_v\beta_w + \gamma_v\gamma_w = 0. \tag{7}$$

As usual, we will consider different cases.

- **Case $\rho_v = -1$:**
  Focus on the following two equations to verify that the system is inconsistent:

  $$(t+1)\eta_v^2 + \alpha_v^2 + \beta_v^2 + \gamma_v^2 = 1 \implies \eta_v = 0,\ \alpha_v^2 + \beta_v^2 + \gamma_v^2 = 1 \tag{1}$$

  $$\alpha_v = -2. \tag{3}$$

  Hence there is no lattice embedding of $D_{2,t}^2$ in $\mathbb{Z}^{t+7}$ when $\rho_v = -1$.

- **Case $\rho_v = 0$:**
  Focus on the following subset of equations:

  $$(t+1)\eta_v^2 + \alpha_v^2 + \beta_v^2 + \gamma_v^2 = 4 \tag{1}$$

  $$\alpha_v = \eta_v \implies \eta_v = 0 \tag{3}$$

  $$\gamma_v = -1 - \beta_v. \tag{4}$$

  Observe that now equation (1) becomes $2\beta_v^2 + 2\beta_v - 3 = 0$ and it presents no integer solutions. Hence there is no lattice embedding of $D_{2,t}^2$ in $\mathbb{Z}^{t+7}$ when $\rho_v = 0$.

- **Case $\rho_v = 1$:**
  Focus on the following two equations to verify that the system is inconsistent:

$$(t+1)\eta_v^2 + \alpha_v^2 + \beta_v^2 + \gamma_v^2 = 1 \implies \eta_v = 0 \tag{1}$$

$$\alpha_v = 2 \tag{3}$$

  Hence there is no lattice embedding of $D_{2,t}^2$ in $\mathbb{Z}^{t+7}$ when $\rho_v = 1$.

Finally, we consider lattice embeddings of $D_{3,t}^2$ in $\mathbb{Z}^{t+8}$ when $t \geq 3$. As well as the general case, there is an additional way to find more lattice embeddings, shown in Figure 4.41. Let $v := \rho_v(e_1 + \cdots + e_4) + \alpha_v a + \beta_v b + \gamma_v c$ and $w := \rho_w(e_1 + \cdots + e_4) - e_1 + \eta_w(f_1 + \cdots + f_{t+1}) +$

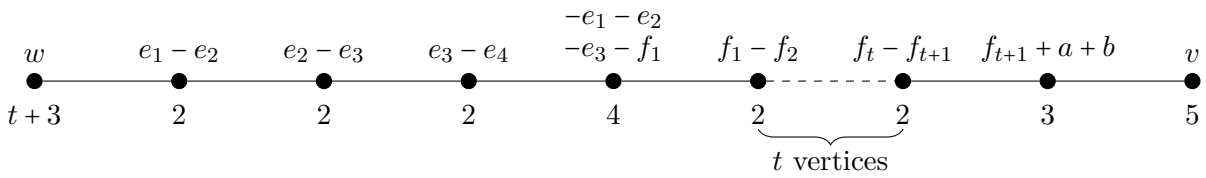

Figure 4.41: Potential embedding of $D_{3,t}^2$ in $\mathbb{Z}^{t+8}$ for $t \geq 3$.

$\alpha_w a + \beta_w b + \gamma_w c$. We set up the following system of equations:

$$4\rho_v^2 + \alpha_v^2 + \beta_v^2 + \gamma_v^2 = 5 \tag{1}$$

$$(\rho_w - 1)^2 + 3\rho_w^2 + (t+1)\eta_w^2 + \alpha_w^2 + \beta_w^2 + \gamma_w^2 = t + 3 \implies |\eta_w| \leq 1 \tag{2}$$

$$-3\rho_v = 0 \tag{3}$$

$$\alpha_v + \beta_v = -1 \tag{4}$$

$$\eta_w + 3\rho_w - 1 = 0 \implies \rho_w = \frac{1 - \eta_w}{3} \tag{5}$$

$$\eta_w + \alpha_w + \beta_w = 0 \tag{6}$$

$$\rho_v(4\rho_w - 1) + \alpha_v\alpha_w + \beta_v\beta_w + \gamma_v\gamma_w = 0. \tag{7}$$

We observe that equation (5) forces $\eta_w = 1$. Therefore, the system simplifies as follows:

$$2\alpha_v^2 + 2\alpha_v + \gamma_v^2 = 4 \implies -2 \leq \alpha_v \leq 1 \tag{1}$$

$$2\alpha_w^2 + 2\alpha_w + \gamma_w^2 = 0 \implies \gamma_w = 0 \text{ and } \alpha_w \in \{-1, 0\} \tag{2}$$

$$\rho_v = 0 \tag{3}$$

$$\beta_v = -1 - \alpha_v \tag{4}$$

$$\rho_w = 0 \tag{5}$$

$$\beta_w = -1 - \alpha_w \tag{6}$$

$$\alpha_v\alpha_w + \beta_v\beta_w = 0. \tag{7}$$

A direct computation shows that for $\alpha_v \in \{-2, 1\}$ we cannot find any embedding, as we would have non-integer solutions for α_w and β_w, respectively. We consider the remaining cases:

- Case $\alpha_v = -1$: The system gives rise to the solution $v = -a \pm 2c$ and $w = -e_1 + f_1 + \cdots + f_{t+1} - b$, which together with Figure 4.41 realises a lattice embedding in $\mathbb{Z}^{t+8}$. When t is even, the orthogonal complement is generated by the vector

$$(-2, -2, -2, -2, \underbrace{6, \ldots, 6}_{t+1 \text{ times}}, -2(3t+7), 2(3t+4), \mp(3t+7)),$$

  and has square $(9t + 19)^2 = p$. Hence, lens spaces belonging to $D^2_{3,t}$, with t even, are unobstructed from embedding in $\mathbb{C}P^2$. Note that when t is odd, the embedding does not satisfy the conditions of Proposition 3.9.

- Case $\alpha_v = 0$: The system gives rise to the solution $v = -b \pm 2c$ and $w = -e_1 + f_1 + \cdots + f_{t+1} - a$, which together with Figure 4.41 realises a lattice embedding in $\mathbb{Z}^{t+8}$. This embedding is equivalent to the one found in the previous case, thus the same conclusions apply.

This ends the analysis of the infinite families of lens spaces associated to the strings of $D^2_{s,t}$ for $s < 4$ or $t < 3$. It remains to check the cases when we have $s < 4$ and $t < 3$. Table 4.7 presents a summary of the outcome of the analysis of these cases using GAP.

Let us explicitly present the lattice embeddings that satisfy Proposition 3.9, found using GAP.

$D^2_{s,t}$	s	t	Result
	0	0	Obstructed since Lisca's embedding is the only possibility
	0	1	Obstructed by zero entries in vector generating orthogonal complement
	0	2	Unobstructed
	1	0	Unobstructed
	1	1	Obstructed by zero entries in vector generating orthogonal complement
	1	2	Obstructed since Lisca's embedding is the only possibility
	2	0	Obstructed by zero entries in vector generating orthogonal complement
	2	1	Obstructed by zero entries in vector generating orthogonal complement
	2	2	Obstructed since Lisca's embedding is the only possibility
	3	0	Unobstructed
	3	1	Two embeddings that are not Lisca's: one obstructed by zero entries in vector generating orthogonal complement, the other since the image of Λ_M is not a primitive vector
	3	2	Unobstructed

Table 4.7: Summary of GAP analysis for $D^2_{s,t}$ when $s < 4$ and $t < 3$.

Figure 4.42 presents a lattice embedding of $D^2_{0,2}$ in $\mathbb{Z}^7$.

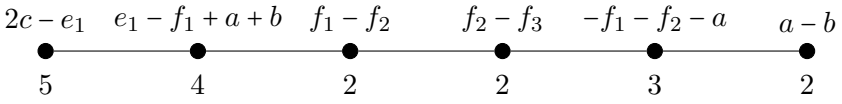

Figure 4.42: Lattice embedding of $D^2_{0,2}$ in $\mathbb{Z}^7$.

The orthogonal complement is generated by

$$(10, 2, 2, 2, -4, -4, 5),$$

which has square $169 = 13^2 = p$. Hence, the lens space with $\frac{p}{q} = D^2_{0,2}$ is unobstructed from embedding in $\mathbb{C}P^2$. Note that this embedding follows the first pattern discussed for $D^2_{s,2}$ when $s = 16\eta_v^2 - 10\eta_v$, and is indeed equivalent to the one found in that case.

The string $D^2_{1,0} = [3, 2, 4, 3, 3]^-$ presents an unobstructed lattice embedding in $\mathbb{Z}^6$, shown in Figure 4.43. The orthogonal complement is generated by the vector

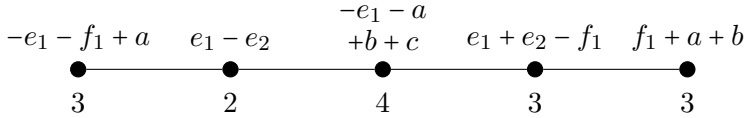

Figure 4.43: Lattice embedding of $D^2_{1,0}$ in $\mathbb{Z}^6$.

$$(1, 1, 2, 3, -5, 9),$$

which has square $121 = 11^2 = p$. Hence, the lens space $L(11^2, 50)$ is unobstructed from embedding in $\mathbb{C}P^2$.

Next, we consider the string $D^2_{3,0}$ and look for embeddings in $\mathbb{Z}^8$. One embedding is provided in Figure 4.44. The orthogonal complement is generated by

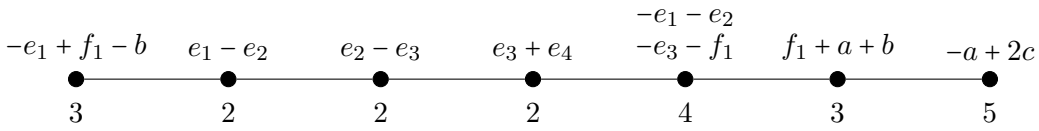

Figure 4.44: Lattice embedding of $D^2_{3,0}$ in $\mathbb{Z}^8$.

$$(-2, -2, -2, -2, 6, -14, 8, -7),$$

which has square $361 = 19^2 = p$. Therefore, the lens space with $\frac{p}{q} = D^2_{3,0}$ is unobstructed from embedding in $\mathbb{C}P^2$. Note that this embedding follows the pattern discussed more generally for $D^2_{3,t}$ with t even.

Finally, there is a lattice embedding of $D^2_{3,2}$ in $\mathbb{Z}^8$, shown in Figure 4.45.

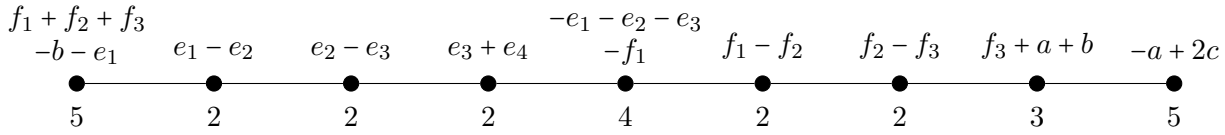

Figure 4.45: Lattice embedding of $D^2_{3,2}$ in $\mathbb{Z}^{10}$.

The orthogonal complement is generated by

$$(-2, -2, -2, -2, 6, 6, 6, -26, 20, -13),$$

and has square $1369 = 37^2 = p$. Hence, the lens space $L(1369, 324)$ is unobstructed from embedding in $\mathbb{C}P^2$. Note that this embedding follows the pattern discussed for the case $D^2_{3,t}$ with t even.

§ 4.8 | Conclusion

The previous sections showed how to construct appropriate lattice embeddings in order to show that a lens space of Lisca type (2) or (3) is unobstructed from embedding in

$\mathbb{C}P^2$. However, what is even more important is that we presented careful arguments to show that the embeddings found are the only ones possible up to automorphism, thus excluding any other options. This enabled us to present the complete classification of lens spaces that are unobstructed from embedding in $\mathbb{C}P^2$ from Theorem 1. We may now restate this classification in a way that explicitly references the strings and parameters we worked with. Note that sporadic cases have been incorporated in infinite families whenever it was possible.

Theorem 1 *Any lens space $L(m^2, q)$, up to diffeomorphism and orientation reversal, that embeds in $\mathbb{C}P^2$ and is of Lisca type* (2) *or* (3) *must belong to the table below.*

String	s	t	m	q	Comments
$B^2_{s,t}$	0	1	7	31	
$B^2_{s,t}$	s	k^2-1	$(2s+3)k^2+1$	$m^2-k^2(2s+3)^2$	$k\neq\pm1,0,\ s\geq 0$
$C^1_{s,t}$	1	0	9	50	
$C^1_{s,t}$	$4k^2+2k-1$	1	$24k^2+12k+2$	$3(8k^2+4k+1)^2$	$k\neq 0$
$C^1_{s,t}$	3	$9k^2-8k$	$81k^2-72k+17$	$81(9k^2-8k+2)$	$\forall k$
$C^2_{s,t}$	k^2-2	0	$3k^2-1$	$6k^4-3k^2$	$k\neq\pm1,0$
$C^2_{s,t}$	$2k+1$	3	$18k+23$	$6(4k+5)(3k+4)$	$k\geq 0$
$C^2_{s,t}$	3	$9k^2+4k-1$	$81k^2+36k+5$	$27(27k^2+12k+2)$	$k\neq 0$
$C^3_{s,t}$	k^2-2	t	$(5+2t)k^2-1$	$2k^4(5+2t)-3k^2$	$k\neq\pm1,0,\ t\geq 0$
$C^3_{s,t}$	$2k$	2	$18k+17$	$6(k+1)(12k+11)$	$k\geq 0$
$D^1_{s,t}$	2	1	31	270	
$D^1_{s,t}$	$2k+1$	2	$18k+31$	$(4k+7)(18k+30)$	$k\geq 1$
$D^2_{s,t}$	1	0	11	50	
$D^2_{s,t}$	$16k^2+6k-1$	2	$128k^2+48k+5$	$4(32k^2+12k+1)^2$	$k\neq 0$
$D^2_{s,t}$	$16k^2-10k$	2	$128k^2-80k+13$	$4(32k^2-20k+3)^2$	$\forall k$
$D^2_{s,t}$	3	$2k$	$18k+19$	$162(k+1)$	$k\geq 0$

Chapter 5

A Further Obstruction

§ 5.1 | Set-up

In this chapter, we refine the result presented in Theorem 1 via an additional obstruction, due to Lidman–Moore–Vazquez [47], after work by Lin [48]. Let W be a smooth 4-manifold admitting a cellular decomposition, and let T_W be its tangent bundle. The k-skeleton of W is the union of all its cells of dimension $\leq k$. A *spin structure* on W is a choice of trivialisation of T_W over the 1-skeleton that can be extended over the 2-skeleton, considered up to homotopies. A manifold endowed with a spin structure is called a spin manifold [66]. Interestingly, any 3-manifold admits a spin structure, while any 4-manifold without 2-torsion in its first homology admits a spin structure if and only if its intersection form is even. There also exists a complex generalisation of a spin structure, called a spin$^{\mathbb{C}}$ structure. It turns out that every smooth 4-manifold admits a spin$^{\mathbb{C}}$ structure. Moreover, we remark that any spin structure induces a spin$^{\mathbb{C}}$ structure. In this chapter, we shall limit ourselves to basic intuitions following [66], and shall not provide any technical definitions, although an introduction to this vast topic can be found in [30].

In the context of developing Floer homology in [60], Ozsváth–Szabó introduced a "correction term", called the d-invariant $d(Y, \mathfrak{s})$, associated to a rational homology sphere Y with a spin$^{\mathbb{C}}$ structure $\mathfrak{s}$. Roughly speaking, the d-invariant is closely related to the intersection form of any smooth, definite 4-manifold bounded by Y, and can be seen as a refinement of the torsion linking form on homology [47]. Indeed, the d-invariant is the minimal degree of any non-torsion class in $HF^+(Y, \mathfrak{s})$ [60], and it is a rational number. An important property of d-invariants for us is that given $(Y, \mathfrak{s})$ as above, we have that

$$d(-Y, \mathfrak{s}) = -d(Y, \mathfrak{s}),$$

where $-Y$ has opposite orientation to Y [60].

Let us now introduce some definitions and results essential to continuing the discussion. A compact, orientable, smooth 4-manifold W is a *Kollár manifold* if $H_1(W;\mathbb{Z}) = 0$, $H_2(W;\mathbb{Z}) \cong \mathbb{Z}$, and ∂W is a union of rational homology 3-spheres [29].

Proposition 5.1 (Golla–Owens [29])**.** *Let B be a rational homology 4-ball embedded in X, a homology $\mathbb{C}P^2$, and such that $H_1(\partial B;\mathbb{Z})$ is cyclic of even order. Then $M = X\backslash \mathring{B}$ is a spin Kollár manifold. Moreover, the restriction of the unique spin structure on M to ∂M does not extend to B.*

We highlight that not only a Kollár manifold as above admits a spin structure, but indeed it admits a unique one. This is because there is a one-to-one correspondence between the spin structures on a manifold M as above and $H^1(M;\mathbb{Z}/2\mathbb{Z})$[43]. The latter can be seen to be the trivial group by noting that $H_1(M;\mathbb{Z}) = 0$ and applying the Universal Coefficient Theorem. Let us now introduce the notion of an L-space, needed to state the next result. An L-space Y is a 3-manifold with $b_1(Y) = 0$ for which $|H^2(Y;\mathbb{Z})| = \operatorname{rk}\widehat{HF}(Y)$. This special class of manifolds includes all lens spaces [61]. The next result is presented in [40, Corollary 2.18] and in [29, Theorem 4.4], but it actually comes from the work of Lidman-Moore-Vazquez [47, Lemma 2.7] and Lin [48].

Theorem 5.2 (Jo–Park–Park [40], Golla–Owens [29])**.** *Let M be a positive-definite, spin Kollár manifold, and let $Y = \partial M$, with induced spin structure $\mathfrak{s}$. If Y is an L-space then $d(Y,\mathfrak{s}) = -\frac{1}{4}$.*

Let us now combine the two theorems above and observe how they relate to our current work.

Corollary 5.3. *Let M be a positive-definite, manifold, with $H_1(M;\mathbb{Z}) = 0$, $H_2(M;\mathbb{Z}) \cong \mathbb{Z}$, bounded by $L(m^2,q)$, with m even and induced spin structure $\mathfrak{s}$. Then $d(L(m^2,q),\mathfrak{s}) = -\frac{1}{4}$.*

We are interested in any lens space $L(p,q)$ which embeds in $\mathbb{C}P^2$, and have observed that when this is the case $L(p,q)$ bounds a positive definite manifold M, which is actually a Kollár manifold. In order to make use of the obstruction from Corollary 5.3, we restrict ourselves to lens spaces from Theorem 1 with $p = m^2$ even. We now want to compute $d(L(p,q),\mathfrak{s})$ for any spin structure $\mathfrak{s}$ on $L(p,q)$. If we find a spin structure such that $d(L(p,q),\mathfrak{s}) = -\frac{1}{4}$, then the conditions of Corollary 5.3 are satisfied, and we conclude that $L(p,q)$ is LMV-unobstructed from embedding in $\mathbb{C}P^2$. Failure to satisfy the conditions of Corollary 5.3 for every spin structure implies that $L(p,q)$ does not bound the

aforementioned 4-manifold M, and thus cannot embed in $\mathbb{C}P^2$. Throughout this chapter, whenever a lens space is LMV-unobstructed from embedding in $\mathbb{C}P^2$, we shall simply use the term unobstructed.

Let us now discuss how to carry out the required computation. Recall that a lens space $L(p,q)$ can be described as the double branched cover $\Sigma_2(S^3, L)$ of S^3 branched over a 2-bridge knot or link L. As we require p to be even, in this chapter L will always indicate a link. In order to compute the correction term $d(L(p,q), \mathfrak{s})$ of a lens space, we rely on [69], in which Turaev establishes a bijection between the quasi-orientations of a link $L \subset S^3$ and the spin structures on $\Sigma_2(S^3, L)$. A quasi-orientation of a link is an orientation up to overall reversal; thus, any link with n components admits 2^{n-1} quasi-orientations. We shall make use of [15, Lemma 3.4], stated below.

Lemma 5.4 (Donald–Owens [15])**.** *Let L be a non-split alternating link with a quasi-orientation o, and let $\mathfrak{s}_o$ be the corresponding spin structure on $\Sigma_2(S^3, L)$. Then*

$$d(\Sigma_2(S^3, L), \mathfrak{s}_o) = -\frac{\sigma(L, o)}{4}.$$

Here, $\sigma(L, o)$ denotes the signature of the link L, an algebraic invariant of an appropriate quadratic form defined in terms of an orientable surface spanning the link. In [32], Gordon–Litherland show how to define such a quadratic form using a spanning surface, and how to use it to compute the signature of a link.

Consider a diagram of an oriented link L: choose a chessboard colouring of the diagram, that is, colour each region either black or white, so that any two adjacent regions have different colours. Let $R_0, \dots, R_n$ denote the white regions, and assign an incidence number $\eta(D) = \pm 1$ to each double point D in the diagram as in Figure 5.1. For $0 \leq i$ and $j \leq n$ define

$$g_{ij} := \begin{cases} -\sum \eta(D) & \text{summed over double points incident to } R_i,\ R_j, \text{ with } i \neq j \\ -\sum_{k=0,\dots,n,\, k \neq i} g_{ik} & \text{if } i = j. \end{cases}$$

The *Goeritz matrix* associated to L is the $n \times n$ symmetric matrix $G(L) = (g_{ij})$, with $i, j = 1, \dots, n$. Then the signature of the link L, with quasi-orientation o, is given by $\sigma(L, o) = \sigma(G(L)) - \mu$, where $\mu = \sum \eta(D)$ summed over all double points of type II, shown in Figure 5.2. In the calculations that follow, μ will always equal the number

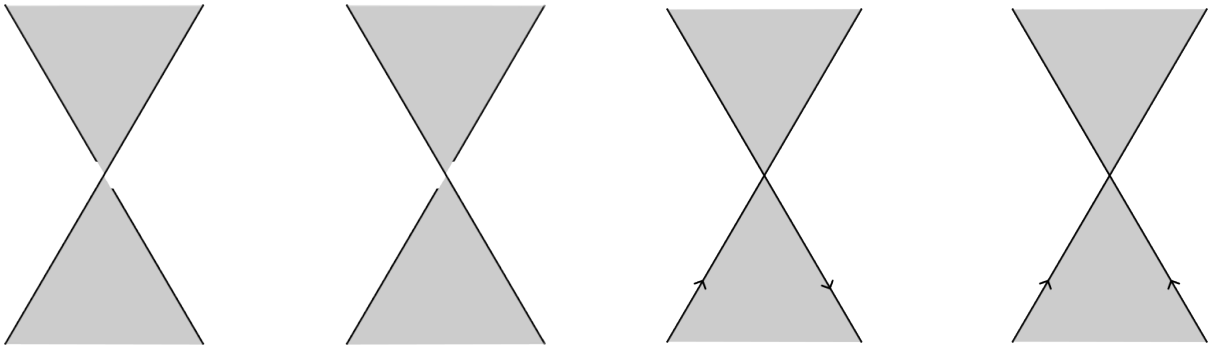

Figure 5.1: Signed crossings.

Figure 5.2: Type I and II crossings.

of double points of type II, because our choice of alternating diagrams and chessboard colourings will always yield $\eta(D) = +1$ for any double point D.

We are now able to compute $d(L(p,q), \mathfrak{s}_o)$ for any lens space with $p = m^2$ even and any choice of quasi-orientation o. Note that we are working with a 2-bridge link of two components, hence we need to consider two possible quasi-orientations, which in turn correspond to two different spin structures $\mathfrak{s}_o$ on $L(p,q)$. The computation was carried out for all lens spaces from the table of Theorem 1 which admit even p. It produced the next result.

Theorem 2. *Any lens space $L(m^2,q)$ that embeds into $\mathbb{C}P^2$, and is of Lisca type* (2) *or* (3) *with m even, must be, up to diffeomorphism and orientation reversal, either $L(26^2, 243)$, or $L((24k^2+12k+2)^2, 3(8k^2+4k+1)^2)$ with $k \neq 0$.*

We highlight that the results presented in this chapter are valid for any integer homology $\mathbb{C}P^2$, including the aforementioned one. In the following section, we present the computations carried out for the relevant lens spaces, thus proving Theorem 2. Before proceeding with such proof, we discuss the strategy employed and some subtleties due to the orientation of the lens spaces considered. The table of Theorem 1 lists all lens spaces up to diffeomorphism (either orientation-preserving or reversing) that are unobstructed from embedding in $\mathbb{C}P^2$; among these lens spaces, we shall only consider those with p even, in order to verify the obstruction from Corollary 5.3. Recall that for a given lens space $Y = L(p,q)$, we have assumed up to now that $\partial M = Y$ and $\partial B = -Y$. When computing the d-invariant, we will be interested in both the cases when $d(Y, \mathfrak{s}_o) = \pm\frac{1}{4}$. This is to account for the assumption $\partial M = -Y$ and $\partial B = Y$ as well. Therefore, in order to prove Theorem 2, we combine the approach employed to prove Theorem 1 with the current one.

In particular, we need to consider two cases. For the first case, suppose that for a given lens space $L(p,q)$, with corresponding 2-bridge link L and quasi-orientations o_1 and o_2, we have $d(L(p,q),\mathfrak{s}_{o_1}) = \frac{1}{4}$ and $d(L(p,q),\mathfrak{s}_{o_2}) \neq -\frac{1}{4}$: in this case we want to consider the lattice on $\frac{p}{p-q}$ and verify whether it is possible to find an embedding satisfying Proposition 3.9. The second case to consider is when $d(L(p,q),\mathfrak{s}_{o_1}) = -\frac{1}{4}$ and $d(L(p,q),\mathfrak{s}_{o_2}) \neq \frac{1}{4}$: in this case we want to consider the lattice on $\frac{p}{q}$ and verify whether it is possible to find an embedding satisfying Proposition 3.9. In either case, failure to find such an embedding implies that $L(p,q)$ does not embed in $\mathbb{C}P^2$.

§ 5.2 | Proof of Theorem 2

§ 5.2.1 | String $B^2_{s,t}$

Let us now compute the d-invariant of lens spaces $L(p,p-q) \cong -L(p,q)$ such that $\frac{p}{q} = B^2_{s,k^2-1} = [2^{[k^2-1]}, s+3, 2, k^2+1, 3, 2^{[s]}]$, with $k \neq \pm 1, 0$. Recall that we are interested in lens spaces with p even: from the table of Theorem 1, note that this is the case only when k is odd. Lens spaces $L(p,p-q)$ with $\frac{p}{q} = B^2_{s,k^2-1}$ are double covers of S^3 branched over the 2-bridge link shown in Figure 5.3 (a) when s is even, and (b) when s is odd. See [58] for orientation conventions. Observe that the total number of crossings of such a link is $2s+2k^2+5$ and that the signature of the associated Goeritz matrix G is $\sigma(G(L)) = s+k^2+3$.

Suppose s is even. We now need to compute the d-invariant for each spin structure associated to a possible choice of quasi-orientation of the link. Figure 5.3 (a) fixes an orientation for one of the link components, so we need to consider the two orientations available for the second component. One choice of quasi-orientation o_1 yields $s+2k^2+3$ crossings of type II, hence

$$d(L(p,p-q),\mathfrak{s}_{o_1}) = \frac{k^2}{4},$$

which is never equal to $\pm\frac{1}{4}$, since $k \neq \pm 1$. The second choice of quasi-orientation, o_2, yields $s+5$ crossings of type II, and thus

$$d(L(p,p-q),\mathfrak{s}_{o_2}) = \frac{2-k^2}{4},$$

which once again never equals $\pm\frac{1}{4}$, since $k \neq \pm 1$ is an integer. We conclude that when s is even, lens spaces with $\frac{p}{q} = B^2_{s,k^2-1}$ with $k \neq \pm 1$ odd are obstructed from embedding in $\mathbb{C}P^2$.

Let us now suppose that s is odd and compute the d-invariants associated to the link in Figure 5.3 (b). One choice of quasi-orientation, o_1, yields $s+2k^2+3$ crossings of type II,

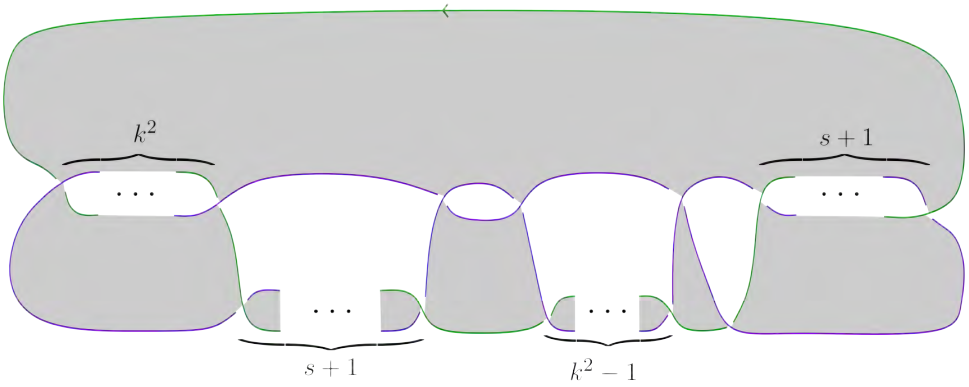

(a)

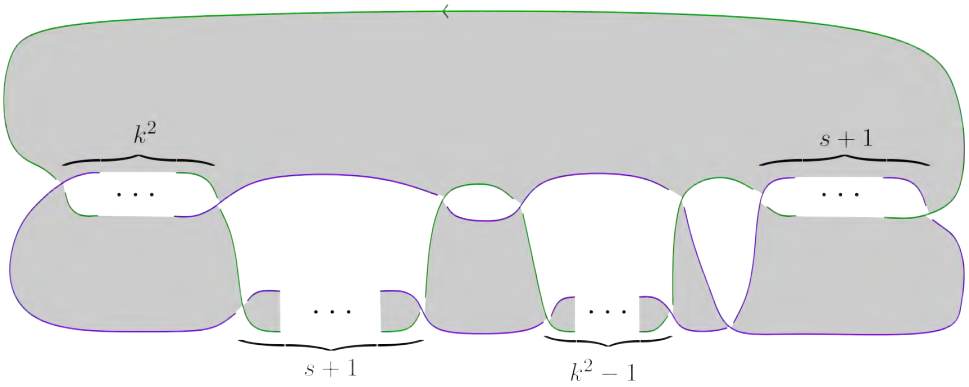

(b)

Figure 5.3: The 2-bridge link associated with $\frac{p}{p-q}$ such that $\frac{p}{q} = B^2_{s,k^2-1}$ when s is even (a) and when s is odd (b).

and consequently

$$d(L(p,p-q),\mathfrak{s}_{o_1}) = \frac{k^2}{4},$$

which cannot equal $\pm\frac{1}{4}$. The second choice of quasi-orientation, o_2, yields $s+1$ type II crossings, and thus

$$d(L(p,p-q),\mathfrak{s}_{o_2}) = -\frac{k^2+2}{4}.$$

Therefore, lens spaces with $\frac{p}{q} = B^2_{s,k^2-1}$ with $k \neq \pm 1$ odd are obstructed from embedding in $\mathbb{C}P^2$ for any value of s. This concludes our analysis of $B^2_{s,t}$.

§ 5.2.2 | String $C^1_{s,t}$

For the string $C^1_{s,t}$ we need to consider two infinite families of lens spaces. The first family we shall discuss is that of lens spaces with $\frac{p}{q} = C^1_{4k^2+2k-1,1} = [3, 4k^2+2k+1, 3, 2, 4, 2^{[4k^2+2k-1]}]$, with $k \neq 0$. The relevant 2-bridge link is shown in Figure 5.4. Note that the total number

of crossings is $8k^2 + 4k + 8$ and that the signature of the associated Goeritz matrix G is $\sigma(G(L)) = 4k^2 + 2k + 4$.

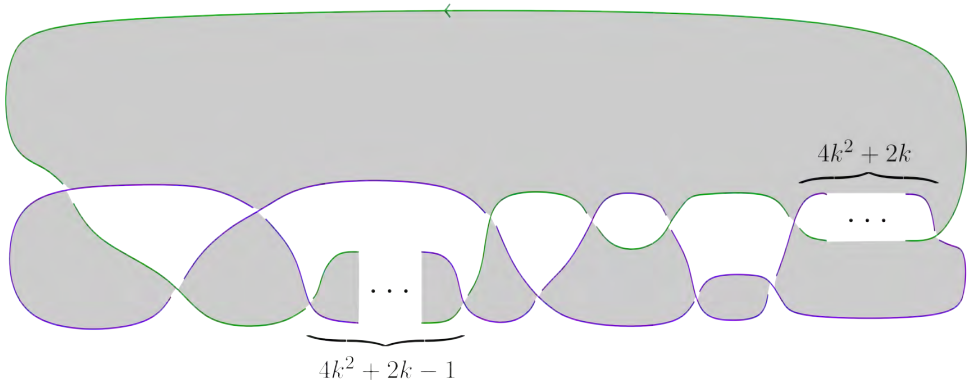

Figure 5.4: The 2-bridge link associated with $\frac{p}{p-q}$ such that $\frac{p}{q} = C^1_{4k^2+2k-1,1}$.

Let us compute the d-invariants for both choices of quasi-orientations of the aforementioned link. One choice, o_1, yields $4k^2 + 2k + 1$ type II crossings, and hence

$$d(L(p, p-q), \mathfrak{s}_{o_1}) = -\frac{3}{4}.$$

The second choice of quasi-orientation, o_2, yields $4k^2 + 2k + 5$ type II crossings, and thus

$$d(L(p, p-q), \mathfrak{s}_{o_2}) = \frac{1}{4}.$$

In light of our earlier discussion, we need to consider the lattice on $\frac{p}{q} = C^1_{4k^2+2k-1,1}$ and verify whether it is possible to find an embedding satisfying Proposition 3.9. The required embedding was found in Chapter 4, hence lens spaces $L((24k^2+12k+2)^2, 3(8k^2+4k+1)^2)$ with $k \neq 0$ are unobstructed from embedding in $\mathbb{C}P^2$.

Next, we discuss lens spaces with $\frac{p}{q} = C^1_{3,9k^2-8k} = [9k^2 - 8k + 2, 5, 3, 2^{[9k^2-8k]}, 4, 2, 2, 2]$, with k odd. Figure 5.5 shows the associated 2-bridge link. The total number of crossings is $18k^2 - 16k + 14$, and the signature of the Goeritz matrix is $9k^2 - 8k + 7$.

One choice of quasi-orientation, o_1, for said link yields $18k^2 - 9k$ type II crossings, and consequently

$$d(L(p, p-q), \mathfrak{s}_{o_1}) = \frac{9k^2 - 8k}{4}.$$

which equals $\frac{1}{4}$ only when $k = 1$ and can never equal $-\frac{1}{4}$ with an integer k. The second

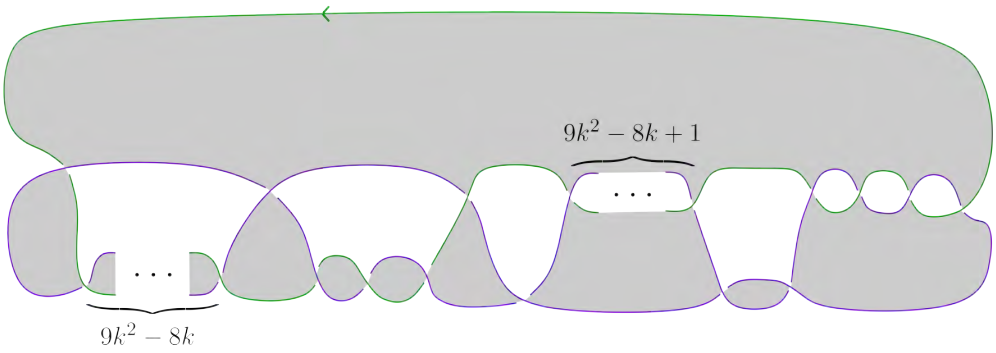

Figure 5.5: The 2-bridge link associated with $\frac{p}{p-q}$ such that $\frac{p}{q} = C^1_{3,9k^2-8k}$.

choice of quasi-orientation, o_2, yields 5 type II crossings and thus

$$d(L(p, p-q), \mathfrak{s}_{o_2}) = \frac{-9k^2 + 8k - 2}{4},$$

which never equals $\pm\frac{1}{4}$ when k is odd. Once again, it follows from our earlier discussion that we need to consider whether the lattice on $\frac{p}{q} = C^1_{3,9k^2-8k}$ admits an embedding satisfying Proposition 3.9. This turns out to be the case, and the embedding required was found in Chapter 4. Hence $L(26^2, 243)$ is unobstructed from embedding in $\mathbb{C}P^2$.

§ 5.2.3 | String $C^2_{s,t}$

For the string $C^2_{s,t}$, we need to analyse two infinite families of lens spaces. The first family we consider is that of lens spaces with $\frac{p}{q} = C^2_{k^2-2,0} = [2, 2, k^2 + 1, 4, 2^{[k^2-1]}]$, with $k \neq \pm 1$ odd. The 2-bridge link associated with this family of lens spaces is shown in Figure 5.6. It has $2k^2+4$ crossings, and the signature of the associated Goeritz matrix is k^2+2.

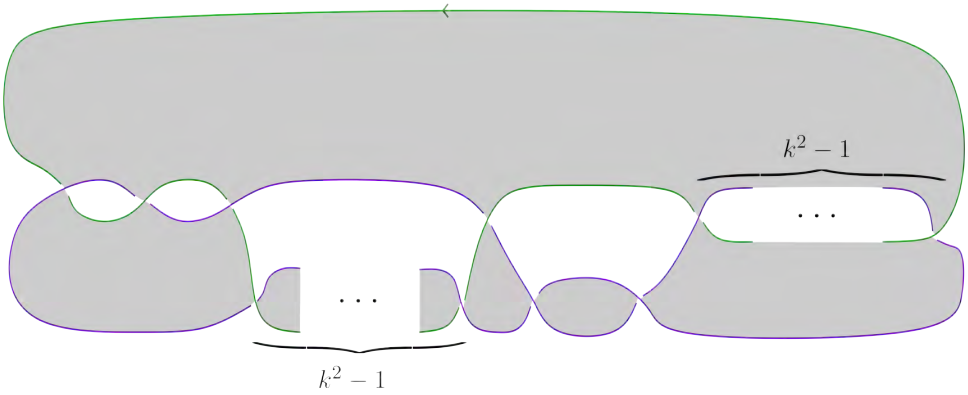

Figure 5.6: The 2-bridge link associated with $\frac{p}{p-q}$ such that $\frac{p}{q} = C^2_{k^2-2,0}$.

Let us now compute the d-invariants for each quasi-orientation of the link. One choice of

quasi-orientation, o_1, yields $2k^2+2$ type II crossings, and hence we have

$$d(L(p,p-q),\mathfrak{s}_{o_1}) = \frac{k^2}{4},$$

which is always different from $\pm\frac{1}{4}$, since $k \neq \pm 1$. The second choice of quasi-orientation, o_2, yields no type II crossings, thus

$$d(L(p,p-q),\mathfrak{s}_{o_2}) = -\frac{k^2+2}{4},$$

which is never equal to $\pm\frac{1}{4}$. We conclude that lens spaces with $\frac{p}{q} = C^2_{k^2-2,0}$ and $k \neq \pm 1$ odd are obstructed from embedding in $\mathbb{C}P^2$.

Next, we consider the family of lens spaces with $\frac{p}{q} = C^2_{3,9k^2+4k-1} = [9k^2+4k+1, 2, 6, 2^{[9k^2+4k-1]}, 4, 2, 2, 2]$ with k odd. The associated 2-bridge link is shown in Figure 5.7 and it has $18k^2+8k+12$ crossings. The signature of the corresponding Goeritz matrix is $9k^2+4k+6$.

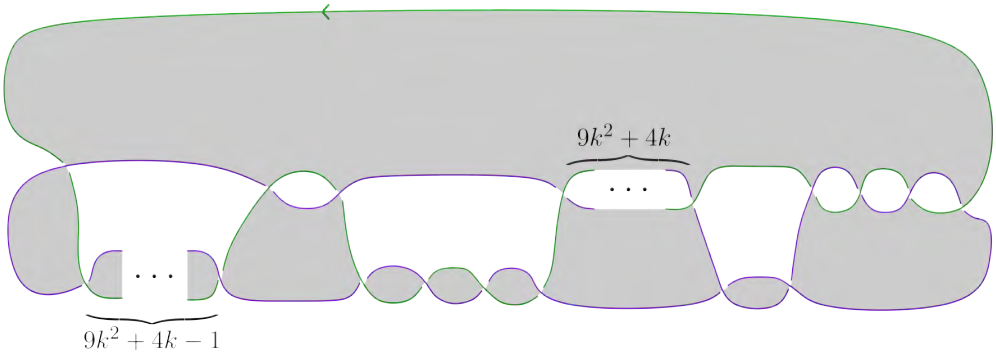

Figure 5.7: The 2-bridge link associated with $\frac{p}{p-q}$ such that $\frac{p}{q} = C^2_{3,9k^2+4k-1}$.

One choice of quasi-orientation of the link, say o_1, yields $18k^2+8k+10$ type II crossings, thus giving

$$d(L(p,p-q),\mathfrak{s}_{o_1}) = \frac{9k^2+4k+4}{4},$$

which can never equal $\pm\frac{1}{4}$ for any integer k. The second quasi-orientation, o_2, yields no type II crossings, hence

$$d(L(p,p-q),\mathfrak{s}_{o_2}) = \frac{9k^2+4k+6}{4},$$

which presents no integer solutions of k that allow the numerator to equal ± 1. We conclude that lens spaces with $\frac{p}{q} = C^2_{3,9k^2+4k-1}$ are obstructed from embedding in $\mathbb{C}P^2$.

§ 5.2.4 | String $C^3_{s,t}$

In this case, we need to analyse the infinite family of lens spaces with $\frac{p}{q} = C^3_{k^2-2,t} = [t+3, 2, k^2+1, 3, 2^{[t]}, 3, 2^{[k^2-2]}]$, with $k \neq \pm 1$ odd. Lens spaces with $\frac{p}{q} = C^3_{k^2-2,t}$ are double covers of S^3 branched over the 2-bridge link in Figure 5.8 (a) when t is odd, and (b) when t is even. The total number of crossings is $2k^2+2t+6$, and the signature of the associated Goeritz matrix is k^2+t+3.

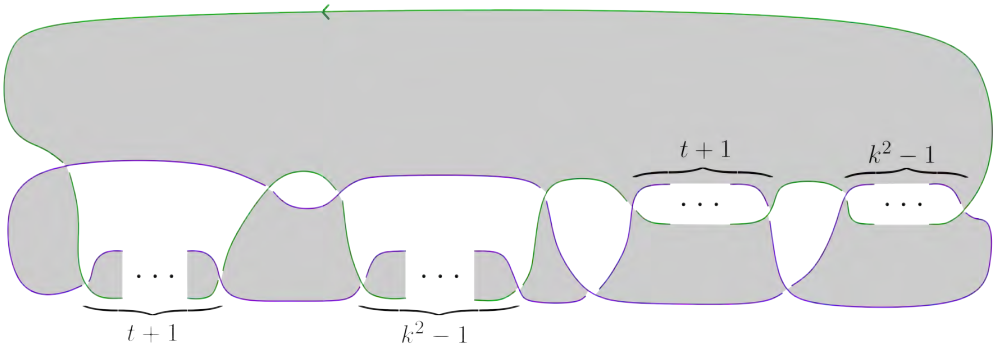

(a)

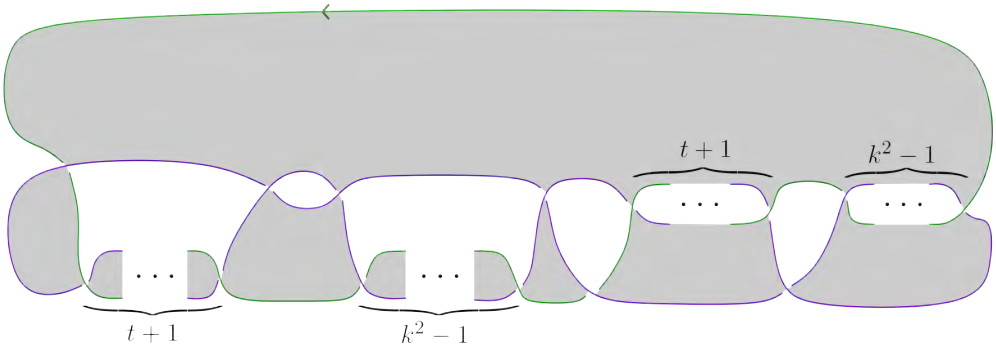

(b)

Figure 5.8: The 2-bridge link associated with $\frac{p}{p-q}$ such that $\frac{p}{q} = C^3_{k^2-2,t}$ when t is odd (a) and when t is even (b).

We shall now compute the d-invariants associated with this link. Suppose that t is odd. One choice of quasi-orientation o_1, yields $2k^2+t+3$ type II crossings, therefore

$$d(L(p, p-q), \mathfrak{s}_{o_1}) = \frac{k^2}{4},$$

which never equals $\pm\frac{1}{4}$ since $k \neq \pm 1$. The second choice of quasi-orientation, o_2, yields

$t+1$ type II crossings, and consequently

$$d(L(p,p-q),\mathfrak{s}_{o_2}) = -\frac{k^2+2}{4},$$

which once again never equals $\pm\frac{1}{4}$, for any $k \neq \pm 1$. We conclude that when t is odd, lens spaces with $\frac{p}{q} = C^3_{k^2-2,t}$ and $k \neq \pm 1$ odd are obstructed from embedding in $\mathbb{C}P^2$.

Now, assume that t is even and let us compute the d-invariants. One choice of quasi-orientation, say o_1, yields $2k^2+t+3$ type II crossings and thus

$$d(L(p,p-q),\mathfrak{s}_{o_1}) = \frac{k^2}{4},$$

with $k \neq \pm 1$. The second choice of quasi-orientation, o_2, yields $t+5$ type II crossings, and hence

$$d(L(p,p-q),\mathfrak{s}_{o_2}) = \frac{2-k^2}{4},$$

with $k \neq \pm 1$. Hence, in this case, the d-invariant is never equal to $\pm\frac{1}{4}$, with any choice of spin structure. We conclude that when t is even, lens spaces with $\frac{p}{q} = C^3_{k^2-2,t}$ and $k \neq \pm 1$ odd are obstructed from embedding in $\mathbb{C}P^2$.

Chapter 6

Future Directions

In [50], Lisca extended the work from [49] and classified which connected sums of lens spaces bound rational homology balls. Let $\mathcal{F}_n$ be the set

$$\mathcal{F}_n = \left\{ \frac{m^2 n}{mnk+1} \,|\, m > k > 0,\ \gcd(m,k) = 1 \right\} \subset \mathbb{Q}, \quad n \geq 2.$$

Theorem 6.1 (Lisca [50])**.** *Let Y be an oriented 3-manifold homeomorphic to a connected sum of lens spaces. Then Y smoothly bounds a rational homology ball if and only if Y is orientation-preserving homeomorphic to a connected sum in which each summand is (possibly orientation-reversing) homeomorphic to one of the following oriented 3-manifolds:*

(1) $L(p,q)$ *with p and q as in Theorem 3.2;*

(2) $L(p,q)\#L(p,p-q)$, *with $\frac{p}{q} > 1$;*

(3) $L(p_1,q_1)\#L(p_2,q_2)$, *with $\frac{p_i}{q_i} \in \mathcal{F}_2$, for $i = 1,2$;*

(4) $L(p,q)\#L(n,n-1)$, *with $\frac{p}{q} \in \mathcal{F}_n$ for some $n \geq 2$;*

(5) $L(p_1,q_1)\#L(p_2,p_2-q_2)$, *with $\frac{p_i}{q_i} \in \mathcal{F}_n$, $i = 1,2$, for some $n \geq 2$.*

A direct continuation of the obstruction work presented up to now would be to apply Donaldson's Diagonalisation Theorem to classify when a manifold Y as above is unobstructed from embedding in $\mathbb{C}P^2$. Indeed, note that a connected sum of lens spaces $\#_i L(p_i,q_i)$ bounds a boundary connected sum of positive-definite plumbings $\natural_i P_i$, and the corresponding plumbing graph is obtained from the disjoint union of the linear plumbing graphs corresponding to the summands [4]. Therefore, one could set up the problem in a similar fashion to what we discussed.

Note that aside from case (1), each lens space in the list above does not necessarily bound a rational homology ball, thus it cannot embed individually in $\mathbb{C}P^2$. This could be of interest, as all results known up to now concerning embeddings of connected sums of lens spaces in $\mathbb{C}P^2$ are about lens spaces which are not obstructed from embedding individually.

In order to continue the discussion, recall the definition of a Kollár manifold from the previous chapter: a compact, orientable, smooth 4-manifold M is a *Kollár manifold* if $H_1(M) = 0$, $H_2(M) \cong \mathbb{Z}$, and ∂M is a union of rational homology 3-spheres. Such a manifold is said to be *spherical* if all its boundary components are spherical 3-manifolds. If B is a rational homology ball bounded by a lens space $L(p,q)$ which smoothly embeds in $\mathbb{C}P^2$, the manifold $M = \mathbb{C}P^2 \backslash B$ is an example of a Kollár manifold. In work to appear [29], Golla–Owens look at embeddings of disjoint unions of rational homology balls in an integer homology $\mathbb{C}P^2$ to provide a source of Kollár manifolds. Their study is motivated by the following conjecture due to Kollár.

Conjecture 1 (Kollár [44])**.** *If M is a spherical Kollár manifold with boundary $Y_1 \sqcup \cdots \sqcup Y_n$, then:*

$$\sum_{i=1}^{n} \left(1 - \frac{1}{|\pi_1(Y_i)|}\right) \leq 3.$$

Lens spaces are finite cyclic quotients of S^3, and hence spherical 3-manifolds. If we consider a disjoint union of rational homology balls $B_1 \sqcup \cdots \sqcup B_n$, bounded by lens spaces $L_1 \sqcup \cdots \sqcup L_n$, and their complement M in $\mathbb{C}P^2$, we see that Kollár's conjecture together with [29, Proposition 2.4] imply that we may only embed up to three disjoint rational homology balls (and thus lens spaces) in $\mathbb{C}P^2$. This motivates research of triples of rational homology balls that disjointly embed in $\mathbb{C}P^2$. Note that this question is not equivalent to asking how many lens spaces embed disjointly, nor to considering the embedding of connected sums of lens spaces discussed earlier.

In their recent paper [28], Golla–Owens discuss smooth embeddings in $\mathbb{C}P^2$ of triples of rational homology balls bounded by lens spaces of Lisca type (1). They also describe two constructions to find rational balls bounded by lens spaces that embed in a homotopy $\mathbb{C}P^2$, and that can be implemented in a computer search, producing a variety of examples. The first construction corresponds to [28, Proposition 6.3], and it gives a criterion to build a simply-connected cobordism from $L(p_1,q_1)\#L(p_2,q_2)$ to $L(p_3,q_3)$ by attaching a single 2-handle to $(L(p_1,q_1)\#L(p_2,q_2)) \times I$ according to some constraints. The

second construction is from [28, Proposition 6.5] and instead yields a cobordism from $L(p_1, q_1)\#L(4,1)$ to $L(p_2, q_2)$, where $\frac{p_1}{q_1} = [a_1, \ldots, a_n]^-$ and $\frac{p_2}{q_2} = [b_1, \ldots, b_n]^-$, p_1 and p_2 are odd and pairwise coprime and there is an index $1 \leq j \leq n$ such that for $i \neq j$, $a_i = b_i$ and $b_j = a_j + 4$.

The computer search set up by Golla–Owens, implementing these constructions, produced many triples of lens spaces, at least one of which is of Lisca type (2) or (3). The next step in understanding these embeddings is to isolate a string arising from one of these lens spaces and shed light on any possible recurrence relations among triples that could lead to a Farey-tree type of argument, as in [28]. Currently, we are attempting to develop a Kirby calculus argument to explain some recurrence relations found in the data. As previously mentioned, these constructions yield embeddings into homotopy $\mathbb{C}P^2$, therefore it would also be natural to study when this corresponds to a standard $\mathbb{C}P^2$.

Part II

Embeddings of $\mathbb{R}P^2$ in $\mathbb{R}^4$ with Five Critical Points

Chapter 7

Introduction

In this part of the thesis, we discuss smooth embeddings of $\mathbb{R}P^2$ in $\mathbb{R}^4$. In general, studying embeddings of orientable and non-orientable surfaces in 4-space is of great interest in low-dimensional topology because of the exotic phenomena that might arise. Two embeddings are said to be *exotic* if they are topologically isotopic, but not smoothly so. The first example of this phenomenon consisted of an infinite family of embeddings of $\#_{10}\mathbb{R}P^2$ into S^4, given by Finashin–Kreck–Viro in [22]. Some additional examples are due to Finashin, who constructed an infinite family of exotic embeddings of $\#_6\mathbb{R}P^2$ in $\mathbb{R}^4$ [21], and Miyazawa, who produced a family of exotic P^2-knots [57], which are surfaces resulting from the connected sum of the standard $\mathbb{R}P^2$ and a special 2-knot obtained from a construction of Plotnick [62]. In the latter case, a key ingredient to proving that the embeddings are topologically isotopic was Lawson's result from [46] (also generalised by Conway–Orson–Powell in [13]) that every embedding of $\mathbb{R}P^2$ in S^4 with $\pi_1(S^4 \backslash \mathbb{R}P^2) \cong \mathbb{Z}/2\mathbb{Z}$ is topologically standard.

Given a smooth embedding of a surface in S^4, note that it is always possible to remove a point from the ambient manifold, thus obtaining a smooth embedding in $\mathbb{R}^4$. Similarly, one can add a point at infinity to $\mathbb{R}^4$ and consider embeddings in S^4. With this remark, we want to highlight that all discussions in this part of the thesis follow analogously, regardless of whether we are considering an embedding in $\mathbb{R}^4$ or S^4. Throughout this part of the thesis, by standard embedding of $\mathbb{R}P^2$ in $\mathbb{R}^4$, we shall mean the real projective plane obtained by gluing an unknotted disc sitting in $\mathbb{R}^3 \times [0, \infty)$ to the unknotted Möbius band in $\mathbb{R}^3 \times (-\infty, 0]$ along S^1 in $\mathbb{R}^3 \times \{0\}$ [10]. Note that there are two such standard embeddings of $\mathbb{R}P^2$ in $\mathbb{R}^4$, distinguished by their Euler numbers $e(\mathbb{R}P^2) = \pm 2$. Intuitively speaking, each embedding corresponds to a choice of half-twist of the Möbius band. When discussing whether a certain embedding of $\mathbb{R}P^2$ in $\mathbb{R}^4$ is standard, we shall

mean isotopic to one of the standard embeddings.

Consider an embedding of $\mathbb{R}P^2$ in $\mathbb{R}^4$ and a height function from $\mathbb{R}^4$ to $\mathbb{R}$ that restricts to a Morse function on $\mathbb{R}P^2$ with five critical points. The project we shall now discuss aims to prove that any such embedding must be smoothly isotopic to the standard embedding of $\mathbb{R}P^2$ in $\mathbb{R}^4$, generalising work by Bleiler–Scharlemann in [10] for the case of an embedding with three critical points. Unfortunately, the scope has not been reached. More generally, it is possible to construct embeddings of $\mathbb{R}P^2$ in $\mathbb{R}^4$ with seven critical points by taking the connected sum of a standard $\mathbb{R}P^2$ and a 2-sphere with six critical points, of which non-standard examples are known [23, Example 9]. One would expect such an embedding to be non-standard, although to the author's knowledge there is no explicit construction in the literature. Gordana Matić observed that the embeddings of exotic P^2-knots found by Miyazawa in [57] have eleven critical points, as they are obtained by the connected sum of a standard $\mathbb{R}P^2$ and a 2-knot with three minima, four saddles, and three maxima. In general, it is quite rare to find embedding descriptions explicitly stating the number of critical points throughout the literature.

Mark Powell outlined a helpful argument showing that an embedding $\varepsilon : \mathbb{R}P^2 \hookrightarrow \mathbb{R}^4$ with five critical points must have $\pi_1(\mathbb{R}^4 \backslash \varepsilon(\mathbb{R}P^2)) \cong \mathbb{Z}/2\mathbb{Z}$, thus by Lawson's work [46] must be topologically standard. Indeed, we can visualise our $\mathbb{R}P^2$ as the union of a ribbon disk D in $\mathbb{R}^3 \times [0, \infty)$ and a Möbius band M in $\mathbb{R}^3 \times (-\infty, 0]$ along a ribbon knot K in $\mathbb{R}^3 \times \{0\}$. Since we are assuming that $\mathbb{R}P^2$ has five critical points, we note that this implies that the ribbon disc D bounded by K is obtained by gluing one band to a 2-component unlink, hence it has a single saddle, and that the Möbius band M also has a single saddle and (we may assume) one minimum. Let $E_{\mathbb{R}P^2}$ denote the exterior of $\mathbb{R}P^2$ in $\mathbb{R}^4$. Then $E_{\mathbb{R}P^2} \cong E_D \underset{E_K}{\cup} E_M$, where E_D and E_M are the exteriors of D and M in $\mathbb{R}^3 \times [0, \infty)$ and $\mathbb{R}^3 \times (-\infty, 0]$, respectively, while E_K is the exterior of K in $\mathbb{R}^3$. Now note that the handle decomposition of M implies the existence of a 1-handle and a 2-handle in E_M, thus $\pi_1(E_M) \cong \mathbb{Z}/2\mathbb{Z}$, since M is non-orientable. From the fact that D is ribbon, we deduce that any loop in E_D can be pushed into E_K, and hence there is a surjection $\pi_1(E_K) \twoheadrightarrow \pi_1(E_D)$. By the Seifert Van Kampen Theorem, we know that $\pi_1(E_{\mathbb{R}P^2}) \cong \pi_1(E_M) *_{\pi_1(E_K)} \pi_1(E_D) \cong \pi_1(E_M) \cong \mathbb{Z}/2\mathbb{Z}$. Thus, we know that our $\varepsilon : \mathbb{R}P^2 \hookrightarrow \mathbb{R}^4$ with five critical points is topologically unknotted, making it interesting for us to analyse what happens on the smooth level. Note that if one can find an embedding $\varepsilon : \mathbb{R}P^2 \hookrightarrow \mathbb{R}^4$ with five critical points that is not smoothly isotopic to the standard one, this would result in a pair of exotic embeddings.

The initial motivation to address this problem was given by *Kinoshita's conjecture*, which states that every smooth embedding of $\mathbb{R}P^2$ in S^4 is isotopic to a connected sum of a standard $\mathbb{R}P^2$ and a 2-knot. This conjecture has not formally appeared in the literature, but it is known among knot theorists [41]. The author thought that proving that an $\mathbb{R}P^2$ with five critical points is standard would be an example in support of the conjecture, while proving the contrary would disprove it. An article by Viro [71] shows this is not the case, as the number of critical points of a surface is not additive under connected sum. This is shown in Example 22 of the Appendix in [71]. Therefore, it is interesting that although Kinoshita's conjecture motivated the study of this problem, it is unrelated to it in the end. Interestingly, Kinoshita's conjecture has recently been disproven by Hughes–Kim–Miller–Nahm in [38].

When working with an embedding of a surface $\varepsilon : \Sigma \hookrightarrow \mathbb{R}^4$, it can be hard to visualise $\varepsilon(\Sigma)$. Movies of surfaces were developed by Fox [23], and are a useful tool to understand such embeddings. Put $\varepsilon(\Sigma)$ in general position in $\mathbb{R}^4$ and define a height function $h : \mathbb{R}^4 \to \mathbb{R}$. Now we can slice $\varepsilon(\Sigma)$ using a family of parallel hyperplanes $\mathbb{R}^3_t$, with $-\infty < t < \infty$, perpendicular to the direction of h. If $\varepsilon(\Sigma) \cap \mathbb{R}^3_t$ is non-empty and non-singular, then it will consist of a knot or a link in $\mathbb{R}^3$. All the non-singular intersections $\varepsilon(\Sigma) \cap \mathbb{R}^3_t$ result in a finite collection of knots and links in 3-space, called a *movie* of $\varepsilon(\Sigma)$. There will be singular intersections for a finite number of values of t, for example, when a hyperplane intersects $\varepsilon(\Sigma)$ in an isolated point (like a minimum or a maximum). Alternatively, the intersection could contain a node with four arcs, corresponding to a saddle point. We can look at the collection $\varepsilon(\Sigma) \cap \mathbb{R}^3_t$ for increasing values of t: when $\varepsilon(\Sigma)$ presents a minimum, we will see the appearance of an unknotted circle in $\varepsilon(\Sigma) \cap \mathbb{R}^3_t$ as the value of t increases. Similarly, a maximum corresponds to an unknot that vanishes. As we pass through a saddle point, the number of components of the link in $\varepsilon(\Sigma) \cap \mathbb{R}^3_t$ may change, and such points are usually represented by band moves. Given a knot (or a link) γ and an embedding of $b : I \times I \hookrightarrow S^3$ such that $b^{-1}(\gamma) = I \times \partial I$, a *band attachment* (or band move in the present context) is the process of replacing $b(I \times \partial I)$ in γ with $b(\partial I \times I)$. Thorough introductions to movies of surfaces can be found in [12, 23]. In this thesis, we will often mention movie pictures of $\mathbb{R}P^2$: this should be understood as always referring to the image of an embedding that is clear from context.

Consider, as an example, a smooth embedding of $\mathbb{R}P^2$ in $\mathbb{R}^4$ on which h as above restricts to a Morse function with three critical points. Since the Euler characteristic of $\mathbb{R}P^2$ is

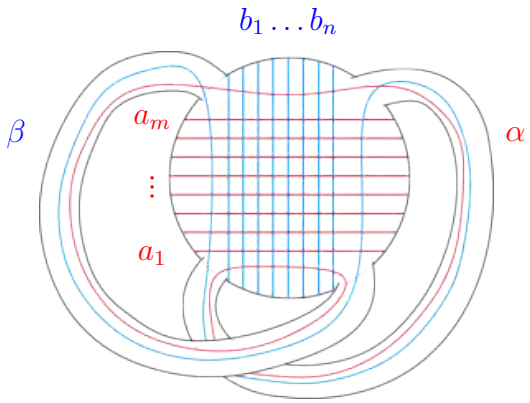

Figure 7.1: The manifold N from [10], arising as the regular neighbourhood of a movie picture of an embedding of $\mathbb{R}P^2$ in $\mathbb{R}^4$ with three critical points.

1, we can assume that the embedding of $\mathbb{R}P^2$ presents one minimum, one saddle, and a maximum (we shall see more on this in the next chapter). When looking at a movie of this embedding, as t increases, we can expect to see the appearance of an unknot representing the minimum, a band attached to it representing the saddle, and finally an unknot which eventually vanishes, representing the maximum. So a movie of an embedding of $\mathbb{R}P^2$ in $\mathbb{R}^4$ as above consists of an unknot to which we attach a band, resulting in an unknot again.

At this point, note that proving a statement about a movie picture (i.e. about knots and links) is useful because it can tell us something about the embedding we are working with. More specifically, note that movie pictures allow us to understand *smooth* embeddings, because a Morse function on a surface requires the existence of a smooth structure. The example discussed was exactly the embedding of $\mathbb{R}P^2$ in $\mathbb{R}^4$ analysed by Bleiler–Scharlemann in [10]. The result proved in their work is rephrased below.

Theorem 7.1 (Bleiler–Scharlemann [10])**.** *Any embedding of $\mathbb{R}P^2$ in $\mathbb{R}^4$ with three critical points is standard.*

This result is a consequence of the main Theorem from [10], which we may rephrase as saying that there is only one way (up to a half-twist) to attach a band to an unknot to obtain another unknot. To prove this theorem, Bleiler–Scharlemann construct a manifold arising as the regular neighbourhood of an unknot with a band attached from the movie description above, which consists of a 3-ball with two handles attached. This manifold is called N, and is depicted in Fig. 7.1.

On ∂N, they consider two families of embedded simple closed curves. The first family, A_m, consists of the curve α, which represents the boundary of the disc bounded by the

unknot γ corresponding to the minimum in the movie picture of $\mathbb{R}P^2$, together with some other curves $a_1, \ldots, a_m$ representing intersections between sheets of said disc and ∂N. The second family of curves B_n is defined similarly, but this time β is the boundary of the disc bounded by γ_b, the unknot corresponding to the maximum obtained after attaching a band b to γ in the movie picture. These two families bound embedded planar surfaces E_A and E_B in $\overline{\mathbb{R}^3 - N}$. Analysing how these surfaces intersect is key to understanding what families of A_m and B_n can appear on ∂N. This, in turn, is of use in proving the main theorem about the movie picture of $\mathbb{R}P^2$ in $\mathbb{R}^4$, see [10].

The intersection of E_A and E_B is studied via graphs of intersection. These are graphs Γ_A and Γ_B, whose vertices are discs corresponding to the curves in A_m and B_n, and hence to the boundary components of E_A and E_B, respectively. The work of Bleiler–Scharlemann in [10] employs and extends techniques from [64], in which Scharlemann proves that smooth embeddings of spheres in $\mathbb{R}^4$ with four critical points are standard. The latter article is also an important reference for this thesis. We shall not go into the details of the construction of graphs of intersection right now, but will present a thorough discussion in the next chapter in the context of our work. A good introduction to the topic by Gordon can be found in [31].

What makes working with graphs of intersection interesting is that one can produce results about embeddings of surfaces in 4-space using relatively simple machinery from graph theory, like circuits, cycles, sinks, and sources [64]. The downside is that although the techniques employed are simple, the combinatorial aspect is often elaborate.

Litherland first introduced graphs of intersection in [52], in the context of determining which knots have Property P. A knot $K \subset S^3$ satisfies Property P if the only Dehn surgery on K yielding a homotopy 3-sphere is the trivial one; it is now known that all knots except the unknot have Property P [45]. Later on, Scharlemann further developed methods using graphs of intersection in [65] to prove that knots with unknotting number equal to 1 are prime, and in [64], where he proves that smooth embeddings of spheres in $\mathbb{R}^4$ with four critical points (in the same sense discussed for our problem) are standard. We remark that the latter statement was also proved again later by Thompson in [68] and Gabai in [24] using different techniques (in which the result is derived as a corollary of a stronger statement). In [10], Bleiler–Scharlemann proved that any embedding of $\mathbb{R}P^2$ in 4-space with three critical points is standard: the technique and structure of the proof are very similar to those in [64], but the authors refined and generalised some of the graph

theoretical notions to address the additional subtlety arising from this set-up (which were also employed in [9]). A celebrated application of graphs of intersection is due to Gordon–Luecke in [33], where they proved that knots with homeomorphic complements are equivalent, thus solving the Knot Complement Problem. Graphs of intersection were mainly employed to approach problems about Dehn surgery in the 1980s-1990s. More recently, these techniques were used by Matignon–Sayari in [54, 55] to investigate Dehn surgeries creating 3-manifolds that contain a non-orientable surface, by Eudave-Muñoz–Guzmán-Tristán [19] to provide upper bounds for toroidal slopes parametrising Dehn surgeries on a knot K, and finally by Baker–Gordon–Luecke in [7, 8] to explore the relations between the bridge number of a knot K and the genus of a Heegaard splitting of a manifold resulting from surgery on K.

Overview. The second part of this thesis is divided into four chapters: in Chapter 8, we discuss the movie pictures of embeddings of $\mathbb{R}P^2$ in $\mathbb{R}^4$ with five critical points, set up the objectives we wish to prove, and construct graphs of intersection Γ_P and Γ_Q; in Chapter 9, we analyse the phenomena of band slides and band swims and how they affect Γ_P and Γ_Q; in Chapter 10, we present the unfruitful strategy employed to prove the aforementioned objectives; finally, in Chapter 11 we present a previous approach to the problem and discuss similar questions.

Chapter 8

Framework

§ 8.1 | Knots and Bands

Suppose we have an $\mathbb{R}P^2$ smoothly embedded in $\mathbb{R}^4$. Let $h : \mathbb{R}^4 \to \mathbb{R}$ be a height function such that it restricts to a Morse function $h_{|\mathbb{R}P^2}$ with five critical points on $\mathbb{R}P^2$. We want to show that such $\mathbb{R}P^2$ is isotopic to the "standard" real projective plane in $\mathbb{R}^4$, which is obtained from gluing together the boundaries of an unknotted Möbius band in $\mathbb{R}^3 \times \{0\}$ and an unknotted disc in $\mathbb{R}^3 \times [0, \infty)$.

The Euler characteristic of the real projective plane is $\chi(\mathbb{R}P^2) = 1$. The Morse inequalities tell us that $\chi(\mathbb{R}P^2)$ is an alternating sum of the number of critical points of each index of a Morse function on $\mathbb{R}P^2$ [56]. As we are interested in Morse functions with five critical points, we immediately deduce that there are only two possibilities:

1. $h_{|\mathbb{R}P^2}$ has two minima, two saddles, and a maximum; or
2. $h_{|\mathbb{R}P^2}$ has a minimum, two saddles, and two maxima.

Since a Morse function can always be "turned upside-down", we may, without loss of generality, assume we are in case 1. According to the earlier discussion about movie pictures, we deduce that in a movie picture of such $\mathbb{R}P^2$ we expect to see an unlink of two components with two bands attached to it, resulting in an unknot.

At this point, we shall more generally try to understand diagrammatically the number of ways two bands can be attached to a split 2-component link and yield a knot.

Proposition 8.1. *Suppose we have a split 2-component link, with two bands attached so that the result is a knot. Then at least one of the bands must join the two components of*

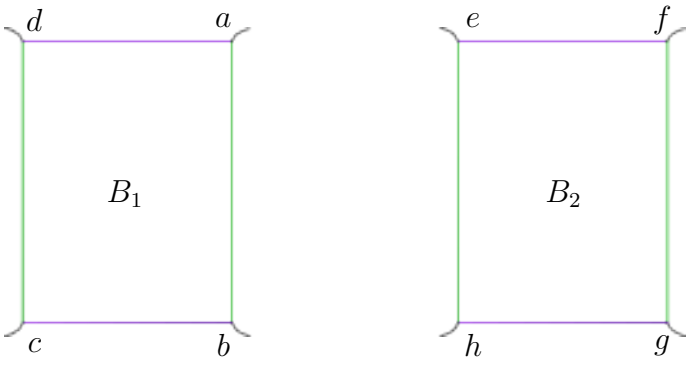

Figure 8.1: Two bands with purple attaching regions.

the link, and one of the bands must be non-oriented.

A band move or attachment is *oriented* if the attaching regions of the band have orientations that either both agree or disagree with the orientations of the arcs they are being attached to, inherited from the knot (or link) orientation. A band move is *non-oriented* otherwise [26].

Proof. Draw two rectangles B_1 and B_2 representing the bands, as in Figure 8.1. Suppose the attaching region of the bands corresponds to the top purple segments and that the resulting knot will have the remaining green segments on its arcs. We need to understand all the possible ways to draw arcs joining the vertices of the bands.

As the bands have to yield a knot, we know that there will be at least two arcs joining B_1 and B_2. Assume without loss of generality that a first arc has ends $c - h$. We shall now focus on the corner d and consider all the other vertices it can join.

Let us start by supposing that the corner d is joined by an arc connecting B_1 and B_2. Immediately observe that such an arc cannot be $d - e$, since it would force the band attachment to yield a link rather than a knot.
Consider what happens instead when we have the arc $d - g$: then all the possible arcs joining f do not respect the conditions stated earlier because either the initial split 2-component link is forced to be a knot, or the final knot is forced to be a 2-component link. Hence, it is not possible to join d and g.
Finally, suppose we have an arc joining the corners d and f. The vertex g cannot join e because the band attachments would fail to yield a knot. Similarly, g cannot join a, since the split 2-component link would be forced to be a knot. However, we may draw

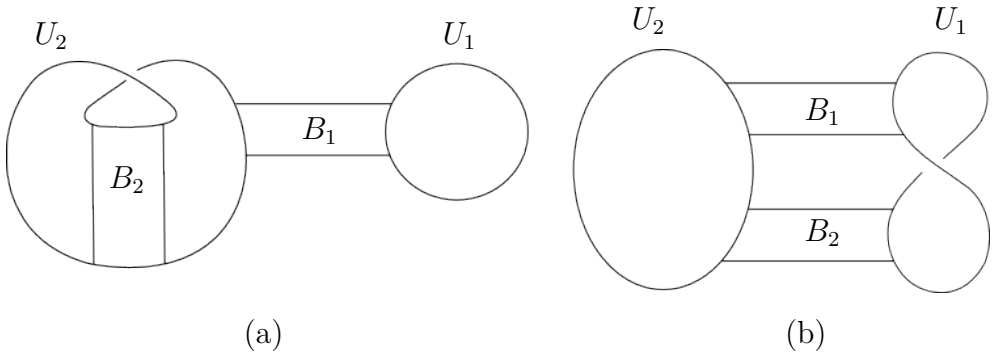

Figure 8.2: Two ways to attach two bands to a 2-component unlink resulting in an unknot.

the arc $b-g$, which then forces us to join a and e. We now have two bands attached to a 2-component link, yielding a knot. Note, however, that some care needs to be taken with the crossings of the arcs in order to ensure we are actually attaching the bands to a *split* 2-component link and thus have a valid configuration.

Now suppose that the corner d is joined by an arc that stays on B_1.
Suppose we have the arc $b-d$. Then a cannot join e, since the band attachments would not yield a knot. If a joins f instead, then the arc $e-g$ is forced, making the 2-component link an unknot, hence giving rise to an invalid configuration. If a joins g we must also have the arc $e-f$. Thus, we have a valid configuration joining the corners of B_1 and B_2, taking care to respect the condition that bands should be attached to a split 2-component link.
Suppose instead that we have the arc $a-d$. It is not possible to join b and e, as the result of attaching the bands would be a 2-component link. Similarly, we cannot join b and g because it would force the bands to attach to a 3-component link. However, we may join the corners $b-f$ and $e-g$ and obtain a valid band configuration which mirrors the one discussed in the previous case. □

For the problem we are considering we are more specifically interested in a 2-component unlink (which is split by definition), resulting in an unknot once the bands are attached.

Before proceeding with the set-up of the problem, it is important to observe an interesting issue which arises from the fact that we are working with two bands. Suppose we have a movie of $\mathbb{R}P^2$, i.e. a 2-component unlink yielding an unknot after attaching two bands, as in either picture of Figure 8.2. In general, these bands may interact with each other, something which did not happen in any of the cases considered by Scharlemann [64] and

Bleiler–Scharlemann [10] because there was always a single band involved.

The first type of possible interaction is a *band slide*, which consists of sliding one band's attaching region over the whole length of the other band's side [67]. Some band slides will take us from one configuration of Figure 8.2 to the other, establishing a relation between them. We shall later discuss band slides in major depth, and will also see that we must always work with both configurations of Figure 8.2, so it is not possible to discard one in favour of the other.

The second issue comes from band swims. Using the terminology introduced by Swenton in [67], a *band swim* essentially consists of passing one band's width lengthwise through another band's interior, as shown in Figure 8.3.

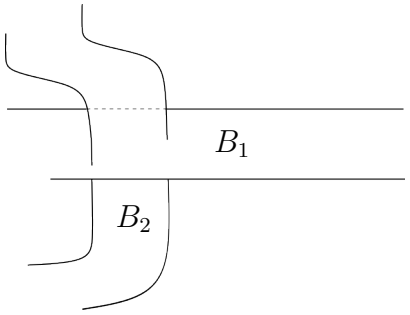

Figure 8.3: A band swim.

In order to illustrate the issue arising from band swims, let us look for instance at Fig. 8.2 (a). We have two knots and two bands, and we can obtain an embedding of $\mathbb{R}P^2$ by attaching the bands in either order, or simultaneously. However, suppose we attach B_1 first. After this attachment we can isotope the width of B_2 through the ghost of the length of B_1, that is, we can perform a band swim. We can now attach the newly placed B_2 and denote it B_2', after which we can undo the attachment of B_1. At this point, the band B_1 is the same, but B_2 is no longer isotopic to B_2'. However, the resulting embedding of $\mathbb{R}P^2$ is isotopic to the one we started with. What emerges from this example is that we have a more complicated way to attach the bands. Suppose we are looking at a movie of such an $\mathbb{R}P^2$, but are only given two very complicated bands attached to a 2-component unlink such that the resulting attachment is the unknot. This information determines an embedding of $\mathbb{R}P^2$, but the next step is to determine whether it is unknotted. In particular, we need a way to detect band slides and swims, in order to "undo" them and make the bands we are working with isotopic to the standard bands in Fig. 8.2. The problems arising from slides and swims add a non-trivial amount of complexity to the

problem, and will be further discussed in subsequent chapters. We highlight that band slides and band swims preserve the isotopy type of the embedding we are working with [67].

Keeping the movie pictures from Figure 8.2 in mind, we want to prove a statement about the possible knot configurations, which then implies something about the embedded $\mathbb{R}P^2$ we are studying. This strategy is essentially the same as that employed in [10] and in [64] in the main theorems. We want to prove that, up to band slides and band swims, any two bands attached to a 2-component unlink which yield an unknot are isotopic to the standard bands of Figure 8.2. Note that pictures (a) and (b) are related to each other via band slides. In particular, we want to prove that any movie picture from Fig. 8.2 (a) can be modified to a movie picture where the band sum of U_1 and U_2 via B_1 is simply a connected sum. This would allow us to use what Swenton in [67] calls a *cup move* to reduce B_1 and U_1. In Morse theoretical terms, B_1 and U_1 would correspond to a cancelling pair of critical points. To summarise, we want to show that any 2-component unlink with two bands attached, resulting in an unknot, is related via band slides, swims and isotopies to a single unknot with a band attached, yielding an unknot again. The latter is the picture from the original Bleiler–Scharlemann case in [10], so the aim is to reduce the problem of $\mathbb{R}P^2$ with five critical points to that of $\mathbb{R}P^2$ with three critical points, solved by Bleiler–Scharlemann.
The objective is to prove the statement below.

Objective 8.1.1. *Suppose we have a 2-component unlink to which we attach two bands that will yield an unknot. Then, up to band slides and swims, the bands are isotopic to the standard bands from Figure 8.2.*

In order to tackle the proof of such an objective, we will consider two oriented surfaces: a separating sphere $\hat{P}$ for the 2-component unlink, and a 2-disc $\hat{Q}$ bounded by the unknot resulting from the two band attachments. Let us now focus on Fig. 8.2 (a): note that the bands can intersect sheets coming from $\hat{Q}$ an arbitrary number of times; they can also cross the separating sphere $\hat{P}$, however, B_1 has to do so an odd number of times, since it has to connect the two link components, while B_2 has to do so an even number of times, since it has both ends on U_2. Using band slides and swims, we aim to prove that any embedding of $\mathbb{R}P^2$ with such a movie picture can be reduced to an embedding where B_1 crosses $\hat{P}$ once. By sliding from one knot configuration to the other in an appropriate way, we may recast this statement in terms of Fig. 8.2 (b); this time we require both B_1

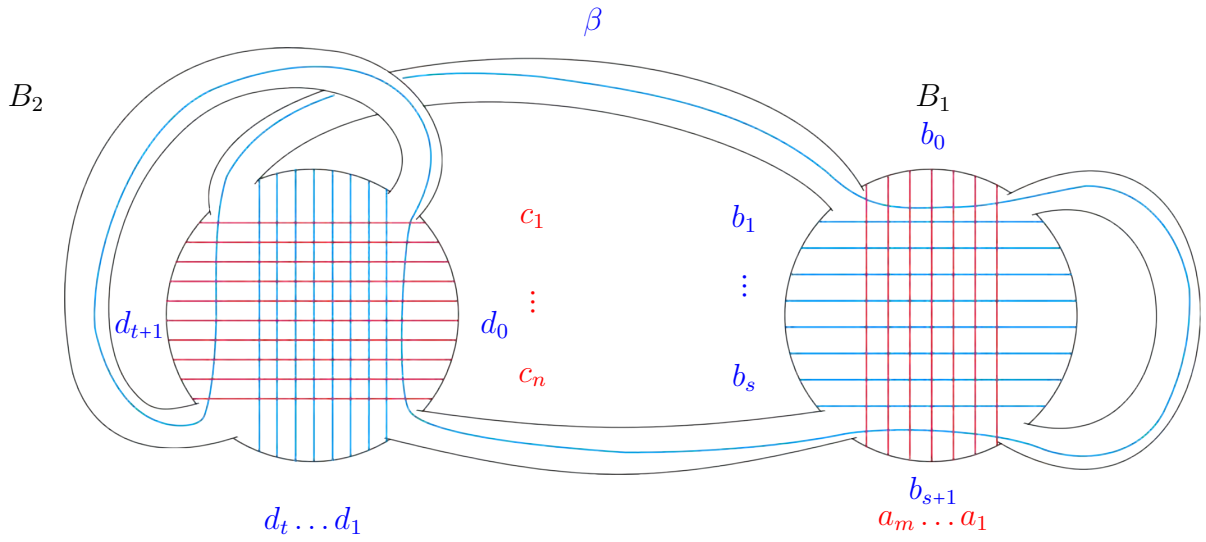

Figure 8.4: Manifold M.

and B_2 to cross $\hat{P}$ an odd number of times, and aim to show that such an embedding can be reduced to one where one of the bands only crosses $\hat{P}$ once.

We shall construct two 3-manifolds with the specific aim of proving Objective 8.1.1, closely following the Bleiler–Scharlemann approach. First, let us take a regular neighbourhood of the two unknots together with the two bands in Fig. 8.2 (a): the resulting 3-manifold $M \subset \mathbb{R}^3$ consists of two 3-balls with four 1-handles and is shown in Figure 8.4. Observe that there are two families of embedded simple closed curves in ∂M. The first family, $\mathcal{R}_{m,n}$, consists of curves $a_1, \dots, a_m, c_1, \dots, c_n$. These curves arise from the intersection of the bands with $\hat{P}$, and hence are the boundary components of the punctured 2-sphere $P = \hat{P} \cap (\overline{\mathbb{R}^3 - M})$. Based on our previous discussion, we require m to be odd and n to be even. The second family, $\mathcal{B}_{s,t}$, consists of β, which bounds $\hat{Q}$, and curves $b_1, \dots, b_s, d_1, \dots, d_t$ arising from the intersection of sheets of $\hat{Q}$ with B_1 and B_2. Let $Q = \hat{Q} \cap (\overline{\mathbb{R}^3 - M})$ be the punctured 2-disc bounded by $\mathcal{B}_{s,t}$, and note that there are no parity restrictions on s and t.

Take a regular neighbourhood of the two unknots together with the two bands in Fig. 8.2 (b) to construct N, the second 3-manifold of interest, represented in Figure 8.5. Once again, there are two families of embedded simple closed curves in ∂N which arise as before and are denoted in the same way $\mathcal{R}_{m,n}$ and $\mathcal{B}_{s,t}$. However, observe that the parity requirements are now different, as m and n must both be odd; as for s and t, there are again no parity restrictions.

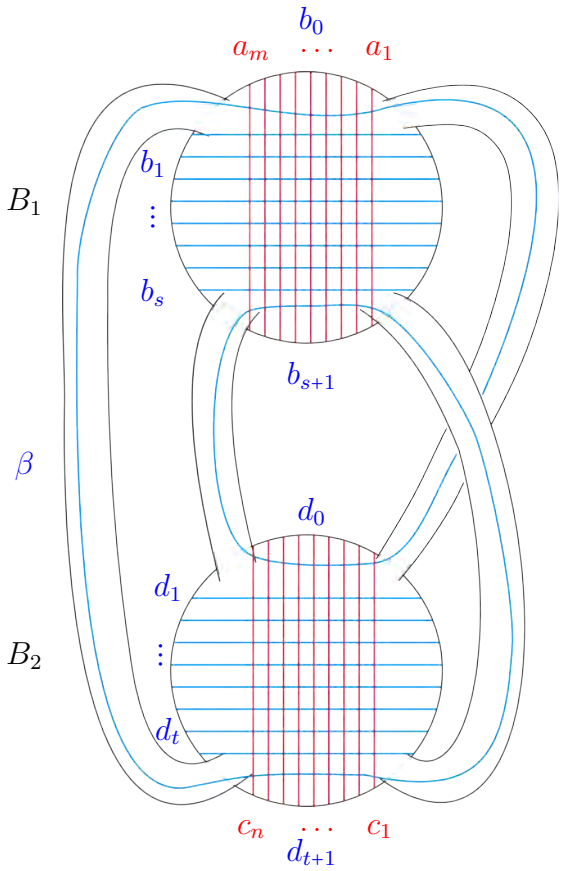

Figure 8.5: Manifold N.

We remark that in both cases the number of times the curve β wraps around the 1-handles is left unspecified.

It was previously observed that Fig. 8.2 (a) and (b) are related by band slides; analogously, the manifolds M and N are related by handle slides. In particular, a band slide that relates the underlying movie pictures corresponds to two handle slides that relate the manifolds. It is important to note that band sliding affects the number of curves on the relevant manifold. This means that if we start from M with curves $\mathcal{R}_{m,n}$ and $\mathcal{B}_{s,t}$, and then slide to N, the families $\mathcal{R}_{m,n}$ and $\mathcal{B}_{s,t}$ will now have a different number of curves. In order to avoid notational clutter we will keep using the same indices to describe the different families of curves, but it should be understood that these are different for M and N, though it will always be clear from context. We also remark that in both Fig. 8.4 and Fig. 8.5 we kept the same notation for the 3-balls arising from the corresponding bands. This is to avoid introducing new notation, but it will always be clear which one

is being referred to in subsequent discussions.

After constructing M and N as above, the aim is to prove the following statement.

Objective 8.1.2 (Main Objective)**.** *Suppose that M as above is embedded in $\mathbb{R}^3$ in such a way that some $\mathcal{R}_{m,n}$ and $\mathcal{B}_{s,t}$ bound planar surfaces P and Q in $\overline{\mathbb{R}^3 - M}$. Then, after a sequence of modifications of the planar surfaces, we may obtain that P is bounded by $\mathcal{R}_{1,n}$.*

Remark 8.2. By modification of the surfaces, we mean any modification that does not change the isotopy type of the embedding of $\mathbb{R}P^2$ in $\mathbb{R}^4$. This includes modifications arising from band slides, band swims, movie isotopies, and reductions of the boundary components of P (and Q) using compressing discs. In particular, note that we may slide between the movie configurations underlying M and N in order to perform such modifications of P and Q.

The attempt to prove the statement above is the focus of this part of the thesis. The importance is due to the fact that if it were true, it would imply Objective 8.1.1, as illustrated below.

Proof of Objective 8.1.1, assuming Objective 8.1.2. Suppose we have a 2-component unlink L in $\mathbb{R}^3$, consisting of unknots U_1 and U_2. Let $\hat{P}$ be the 2-sphere separating U_1 and U_2. Attach bands B_1 and B_2 to L in such a way that we obtain an unknot U which bounds a disc $\hat{Q}$. From a combinatorial standpoint, we must either have that both B_1 and B_2 connect U_1 and U_2, or that, say, B_1 connects the two components and B_2 is only attached to U_2. These are the two possibilities depicted in Figure 8.2. Start by considering the latter case, depicted in Fig. 8.2 (a).

Let M be the regular neighbourhood of $U_1 \cup B_1 \cup U_2 \cup B_2$, homeomorphic to two 3-balls with four 1-handles attached. By general position $\hat{P}$ can be isotoped so that $\hat{P} \cap B_1 = B_1(\{a_i\} \times I)$, for $\{a_i\} \subset I$, $i = 1, \dots, m$, m odd, and $\hat{P} \cap B_2 = B_2(\{c_j\} \times I)$, for $\{c_j\} \subset I$, $j = 1, \dots, n$, n even. Similarly, by a general position argument, $\hat{Q}$ can be isotoped so that $\hat{Q} \cap B_1 = B_1(\mathring{I} \times \{b_k\})$, where $\{b_k\}$, $k = 1, \dots s$, is a finite subset of I, and so that $\hat{Q} \cap B_2 = B_2(\mathring{I} \times \{d_l\})$, where $\{d_l\}$, $l = 1, \dots t$, is also a finite subset of I. Note that the requirements about the parity of m and n arise from the fact that B_1 crosses $\hat{P}$ to connect U_1 and U_2, while B_2 stays on U_2.

At this point, it is possible to arrange the complements P and Q of $\mathring{M}$ in $\hat{P}$ and $\hat{Q}$ to

satisfy the hypotheses of Objective 8.1.2. Suppose we can find some $\mathcal{R}_{1,n}$, intersecting B_1 only once. This implies that the band sum $U_1 \#_{B_1} U_2$ is actually a connected sum $U_1 \# U_2$. However, since U_1 is an unknot, we can perform a cup move as in [67] and cancel B_1 and U_1. This leaves us with U_2 and B_2 attached to it, which must still result in an unknot. At this point we can apply Bleiler and Scharlemann's result from [10], which tells us that B_2 must be a half-twisted band. Alternatively, we can find a slide to a manifold N as above, find some $\mathcal{R}_{1,n}$ (or $\mathcal{R}_{m,1}$) and proceed as in the next case.

Suppose now that both B_1 and B_2 are attached to U_1 and U_2 instead, as in Fig. 8.2 (b). Let N be the regular neighbourhood of $U_1 \cup B_1 \cup U_2 \cup B_2$, homeomorphic once again to two 3-balls with four 1-handles attached. By a general position argument we can arrange that $\hat{P} \cap B_1 = B_1(\{a_i\} \times I)$, for $\{a_i\} \subset I$, $i = 1, \dots, m$, m odd, and $\hat{P} \cap B_2 = B_2(\{c_j\} \times I)$, for $\{c_j\} \subset I$, $j = 1, \dots, n$, n odd. Similarly, isotope $\hat{Q}$ so that $\hat{Q} \cap B_1 = B_1(\mathring{I} \times \{b_k\})$, where $\{b_k\}$, $k = 1, \dots s$, is a finite subset of I, and so that $\hat{Q} \cap B_1 = B_1(\mathring{I} \times \{d_l\})$, where $\{d_l\}$, $l = 1, \dots t$, is also a finite subset of I. Note that the parity requirements for m and n are now different from the previous case, reflecting the different configuration.
It is once again possible to arrange the complements P and Q of $\mathring{M}$ in $\hat{P}$ and $\hat{Q}$ to satisfy the hypotheses of Objective 8.1.2. Suppose we can find some $\mathcal{R}_{1,n}$, intersecting B_1 only once. Again this means that the band sum $U_1 \#_{B_1} U_2$ is just a connected sum $U_1 \# U_2$. Once again then B_2 is attached to the unknot $U_1 \# U_2$ and results in an unknot again, so we can apply the result from [10] to deduce there is a unique way to attach it (up to a half-twist). Note that we could have alternatively performed a band slide of B_2 over the (former) B_1 to end up in the configuration from the previous case. The argument could have equally followed from there. Alternatively, we can find a slide to the manifold M and find some $\mathcal{R}_{1,n}$ and proceed as in the previous case. The case with $\mathcal{R}_{m,1}$ is symmetric. □

§ 8.2 | Graphs of Intersection

This section aims to set up the machinery we will use to approach Objective 8.1.2. The aim is to understand the intersections of the surfaces P and Q previously introduced. The manifolds M and N play a role in constructing the graphs Γ_P and Γ_Q, which can help us keep track of the boundary components of P and Q and their intersections. These are the graphs of intersection mentioned in Chapter 7.

§ 8.2.1 | Constructing Γ_P and Γ_Q

We start by considering the manifold M. Recall that P and Q are planar surfaces with boundary components $\mathcal{R}_{m,n}$ and $\mathcal{B}_{s,t}$, respectively. Assume that $m + n + s + t$ has been minimised, and put P and Q in general position so that their intersections consist of arcs

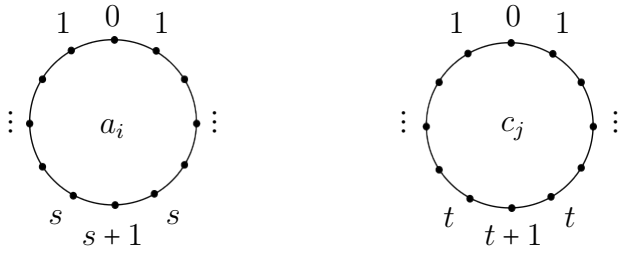

Figure 8.6: Vertices in Γ_P.

— starting and ending at the boundary components — and circles. Assume that we have reduced as much as possible the number of components in the intersection of P and Q. This also implies that we have removed all circles in $P \cap Q$ except those essential in both surfaces [10, 64].

Look at the intersections of $\mathcal{R}_{m,n}$ and $\mathcal{B}_{s,t}$ to derive the data needed to construct the planar graphs. We begin constructing the graph Γ_P, which lives on the sphere $\hat{P}$. Its vertices correspond to the curves $a_1, \ldots, a_m, c_1, \ldots, c_n$ in $\mathcal{R}_{m,n}$, and we shall often call them *disc* or *fat vertices*. Keeping in mind Figure 8.4, observe that each curve of $\mathcal{R}_{m,n}$ on a given 3-ball intersects each relevant curve of $\mathcal{B}_{s,t}$ twice – on the front and on the back of M– with the only exception being the curve β. Let us break down the latter in segments and associate labels b_0, b_{s+1}, d_0 and d_{t+1} to the ones lying on the 3-balls of M, as in Figure 8.4. Each point of intersection may be referred to as $f(i,k)$ or $r(i,k)$ if it lies on the front or on the back, respectively. When the distinction does not matter, we may simply denote it by (i,k). Record these intersections of $\mathcal{R}_{m,n}$ and $\mathcal{B}_{s,t}$ by decorating the vertices of Γ_P with labels corresponding to the relevant indices of the curves of $\mathcal{B}_{s,t}$, as shown in Figure 8.6. Note that each vertex of Γ_P coming from B_1 has valence $2s+2$, while those from B_2 have valence $2t+2$. The edges of Γ_P correspond to the arcs of $P \cap Q$. Any edge may be oriented from higher to lower labels with the convention that edges connecting B_1 and B_2 are oriented from the former to the latter. Edges which stay on the same 3-ball and whose ends have the same label are unoriented, and we shall call them *level edges*. This makes Γ_P a semi-directed graph.

The graph Γ_Q is defined in a similar way. It lives on the disc $\hat{Q}$ bounded by β, with vertices given by b_0, $b_1, \ldots, b_s$, b_{s+1}, d_0, $d_1, \ldots, d_t$, d_{t+1}. The vertices $b_1, \ldots, b_s$ have valence $2m$, while $d_1, \ldots, d_t$ have valence $2n$. Figure 8.7 shows what these vertices look like. The vertices arising from β instead lie on $\partial\hat{Q}$. They look like half discs and have valence m for b_0, b_{s+1}, and valence n for d_0, d_{t+1}. If we go along the curve β clockwise, these vertices

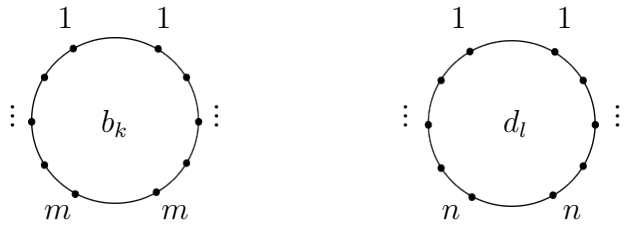

Figure 8.7: Vertices in Γ_Q.

will appear in this order on the boundary of $\hat{Q}$. Edges in Γ_Q have an assigned orientation depending on their labels, following the same rule as the previous graph. Therefore, Γ_Q is a semi-directed graph as well.

Until now, we have discussed how Γ_P and Γ_Q arise from P and Q when working with M. The construction of these graphs starting from N is completely analogous; the only differences are the order of appearance of the boundary vertices of Γ_Q, which will be b_0, d_0, b_{s+1}, d_{t+1}, and the parity of n, which is odd.

In either case, observe that there is a bijection between Γ_P and Γ_Q, as an edge in one graph corresponds to an edge in the other with labels and vertices swapped.

We shall now provide some key graph-theoretical definitions, which mostly follow the terminology employed by Scharlemann and Bleiler–Scharlemann in their work. There will be some minor modifications in order to allow us to translate some lemmas and propositions from [10, 64] into this setting. We begin with the notion of a circuit as presented in [10], which is a generalisation of the one from [64].

Definition 8.3. *A* circuit *γ in Γ_P or Γ_Q is a (not necessarily embedded) closed path such that for a regular neighbourhood $\eta(\gamma)$ of γ there is a boundary component γ' of $\eta(\gamma)$ such that γ' is homotopic to γ in $\eta(\gamma)$ and bounds a single disc component of $\hat{P} - \eta(\gamma)$ ($\hat{Q} - \eta(\gamma)$) called the* interior *of γ.*

Remark 8.4. As the graph Γ_P is constructed on a 2-sphere, we might face some ambiguity in defining the interior of a circuit. If we have a circuit that corresponds to an embedded closed path, then there are two boundary components of $\eta(\gamma)$ homotopic to γ and bounding discs in $\hat{P} - \eta(\gamma)$. We may circumvent this issue by fixing a point x in $\hat{P} - \Gamma_P$ so that for any circuit presenting ambiguities we choose as interior the component of $\hat{P} - \eta(\gamma)$ which does not contain x.

According to this definition, sometimes the interior of a circuit can correspond to areas that may seem counterintuitive. For instance, suppose we have a circuit in Γ_P arising from a path with a "figure-eight" shape. The interior of the circuit corresponds to what we would intuitively picture as the outside of the figure-eight curve, which is instead the disc component mentioned in the definition, since Γ_P lives on a sphere.
Note that according to the definition, this sub-graph is not a circuit in Γ_Q, as no boundary component of its neighbourhood splits off a disc component. This is because Γ_Q lives in a disc $\hat{Q}$.

The scope of this example was to highlight that the notion of a circuit should not be exclusively tied to the picture of an immersed curve, but rather to whether a certain configuration of edges gives rise to an interior. This indicates that caution should be employed when arguing or discussing examples with circuits in Γ_P or Γ_Q, although most of the time we will be discussing innermost circuits and therefore will avoid many such complexities.

We shall define a *loop* to be a circuit with just one edge, whose vertex is the *base* of the loop. A *chord* of a circuit is an edge in the circuit interior with ends lying in the circuit. A *spoke* is a chord that is not a loop. A vertex with no edge oriented away from it is a *sink*, while one with no edge oriented into it is a *source*. A vertex with no labels is called a *puncture* and is neither a sink nor a source.

Since the interior of a circuit is an embedded disc in $\hat{P}$ or $\hat{Q}$, we can define a label sequence as in [64].

Definition 8.5. *The interior of a circuit allows us to define a sequence of labels as follows. Choose a path going once through every edge of the circuit and such that at each vertex it contains the segment of the circle that lies in the interior of the circuit. Read off the labels of the ends of the edges which the path either traverses or crosses transversally. This sequence of integers is called the* label sequence *of the circuit.*
Remark 8.6. The label sequence depends on the choice of starting point and on the orientation chosen to go around the circuit. When the latter is a cycle or semi-cycle (to be defined below), there is a natural choice of orientation [64].

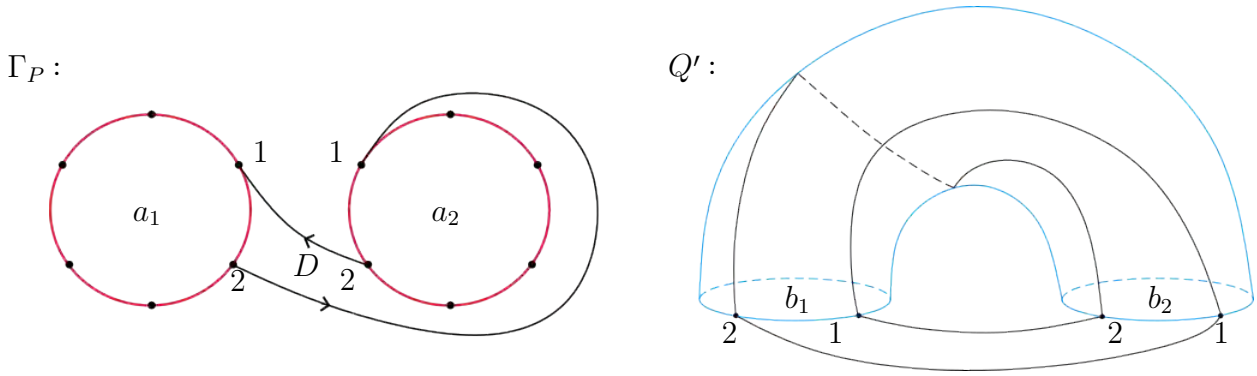

Figure 8.8: A Scharlemann cycle.

Definition 8.7. *A* cycle *is a circuit with all its edges oriented so that it is possible to follow a path around it, always consistent with such orientations.*
A semi-cycle *is a circuit with at least one oriented edge such that there is a path around it never inconsistent with orientations.*
Remark 8.8. Given the orientation we have assigned to the edges of Γ_P and Γ_Q, there can be no cycles or semi-cycles whose vertices belong to different 3-balls of M or N. Note that every cycle is a semi-cycle.

Circuits and cycles are key elements in almost every argument about graphs of intersection. In particular, there is a special type of cycle which is of great relevance, defined below.

Definition 8.9. *A* Scharlemann cycle *is a disc face of P or Q, bounded by vertices and edges of Γ_P or Γ_Q, such that each edge starts at a label i and ends on a label $i+1$.*

Note that a Scharlemann cycle stays on one 3-ball of M (or N), hence the labels i and $i+1$ are referring to labels of the same set of curves. Such cycles are important because their existence implies we can construct a 3-manifold of codimension 0 in $\mathbb{R}^3$ (or S^3) with non-trivial torsion in first homology, giving rise to a contradiction. More about this can be found in [34, 53]. These cycles first appeared in [64], where they are used to define a new surface on which surgery is applied to reduce the number of minimised boundary components, giving rise to a contradiction. The next example provides useful insights.

Example 8.10. Suppose we have a Scharlemann cycle in Γ_P, as shown in Figure 8.8. Here we see a disc face D of P bounded by the vertices a_1 and a_2, and two edges. Now consider the graph Γ_Q in Q. The edges of Γ_P appear here as well, this time connecting the vertices b_1 and b_2 of Γ_Q.

Construct a new surface Q' by attaching to Q the annulus in ∂M (or ∂N) between b_1 and b_2. Then Q' is a punctured torus with boundary $\mathcal{B}_{s-2,t}$. Now note that D lies on one side of Q', and ∂D is a simple closed curve in Q' that crosses the annulus a non-trivial number of times (in this specific example twice). Surgery on Q' using D yields a punctured disc in the closure of the complement of M (or N) with boundary $\mathcal{B}_{s-2,t}$. In [10, 64], this type of argument is used to reach a contradiction about the minimal number of boundary components of planar surfaces in the complement of M.

A closely related argument showcasing the importance of Scharlemann cycles is presented by Luecke in [53]. A Scharlemann cycle, as in Figure 8.8, can be used to construct a 3-manifold L which has the following handle decomposition:

- The 0-handle corresponds to the regular neighbourhood of $\hat{Q}$;
- The 1-handle is the 3-ball bounded by the annulus from ∂M between b_1 and b_2;
- The 2-handle is the regular neighbourhood of D.

As ∂D traverses the annulus twice, we deduce that $H_1(L) \cong \mathbb{Z}/2\mathbb{Z}$. Then L is a manifold with non-trivial torsion in first homology which embeds in $\mathbb{R}^3$, giving rise to a contradiction.

This is only a simple example of a Scharlemann cycle. In general, the number of times a label i appears determines the order of the torsion of $H_1(L)$ as above. Hence, this is a problematic configuration, and we will make use of it to exclude or reduce some graph configurations in our arguments.

It is useful to generalise such a notion, as shown below.

Definition 8.11. *A* Scharlemann collection *is a collection of disc faces of P or Q such that each disc face has a label sequence of the form $(l_1, l_1 \pm 1, \ldots, l_\alpha, l_\alpha \pm 1)$ for possibly different values of α, and labels l_α and $l_{\alpha'}$ not necessarily belonging to the same set of curves.*

Remark 8.12. In this case, each label sequence is not required to alternate between the same two labels, therefore each disc face is bounded by a circuit, not necessarily a cycle.

Scharlemann collections are useful because they can be used in the same ways as Scharlemann cycles.

Example 8.13. Suppose we have a Scharlemann collection in Γ_Q, as shown in Figure 8.9. Here we see two disc faces $\mathcal{F}_1$ and $\mathcal{F}_2$ of Q. These are bounded by circuits, and not cycles, as the vertices joined by the edges belong to B_1 and B_2.

Γ_Q :

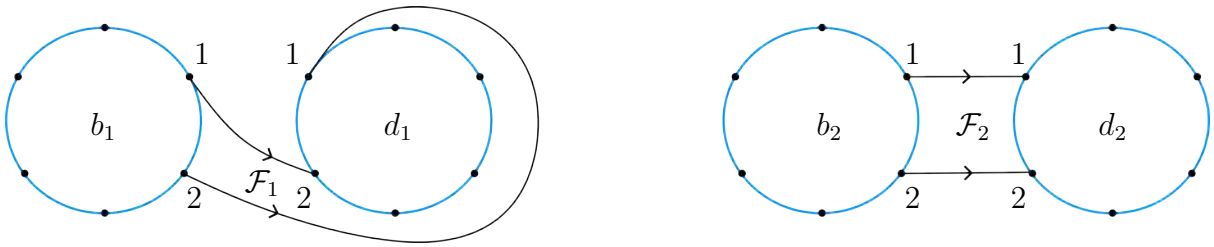

Figure 8.9: A Scharlemann collection in Γ_Q.

Construct a new surface P' by attaching to P the annuli from ∂M (or ∂N) between a_1 and a_2, c_1 and c_2, respectively, as shown in Figure 8.10. The boundaries of the faces $\mathcal{F}_1$ and $\mathcal{F}_2$ are shown as the green and orange simple closed curves, respectively. Both faces lie on the same side of P', and observe that $\mathcal{F}_1$ goes over both annuli once in the same direction, while $\mathcal{F}_2$ traverses each annulus once in opposite directions.

P' :

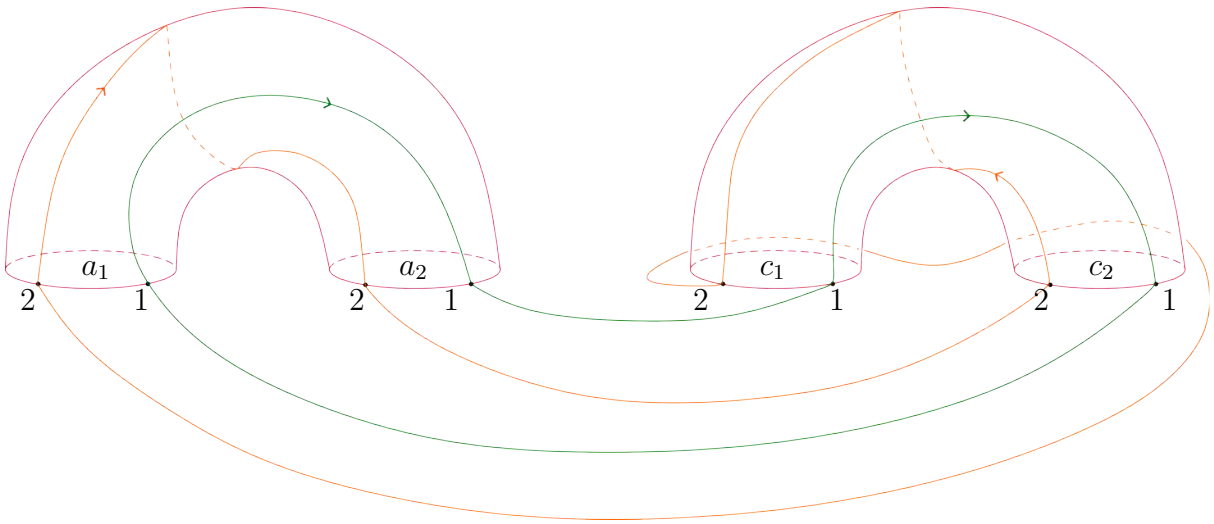

Figure 8.10: Constructing a manifold P' from P using the Scharlemann collection from Fig. 8.9.

It is now possible to apply the same argument by Luecke [53] as in Example 8.10. Construct a new 3-manifold L using a 0-handle obtained by thickening $\hat{Q}$, two 1-handles

coming from the 3-balls bounded by the annuli attached to P, and two 2-handles obtained from the thickening of the disc faces $\mathcal{F}_1$ and $\mathcal{F}_2$. The first homology of L is generated by the 1-handles modulo the relations introduced by the 2-handles, the latter resulting from the signed number of times each disc face traverses each annulus. Thus,

$$H_1(L) \cong \frac{\mathbb{Z} \oplus \mathbb{Z}}{\langle (1,1), (1,-1) \rangle},$$

and since

$$\begin{vmatrix} 1 & 1 \\ 1 & -1 \end{vmatrix} = -2,$$

we deduce that $H_1(L) \cong \mathbb{Z}\backslash 2\mathbb{Z}$. Once again, we have constructed a codimension 0 submanifold of $\mathbb{R}^3$ with non-trivial torsion in first homology, a contradiction.

§ 8.2.2 | Parity Rule

The graphs Γ_P and Γ_Q also carry information about the orientation of the boundary components of P and Q. This information can be used to rule out graph configurations that contradict the requirement that P and Q are oriented surfaces. In order to make use of such data we introduce a "parity rule" for our graphs, which is a generalisation of the one presented by Scharlemann in [64].

The first step in order to introduce this rule is to define front and back of the manifolds M and N, as shown in Fig. 8.4 and Fig. 8.5, respectively. We start with M.

Let ξ be a unit normal vector field to Q in $\overline{\mathbb{R}^3 - M}$, chosen so that it points upwards at b_0, downwards at b_{s+1} and westwards at d_0 and d_{t+1}. Call the *front* of M the hemisphere of B_1 outside of which ξ points at b_0 and b_{s+1}, and the hemisphere of B_2 between d_0 and d_{t+1} into which d_0 points. The remaining hemispheres will be called the *back* of M.
We also define η to be the unit normal vector field to P in $\overline{\mathbb{R}^3 - M}$ that points west at a_1 and consequently upwards at c_1.

Now focus on N. In an analogous way, define ξ' to be a unit normal vector field to Q in $\overline{\mathbb{R}^3 - N}$, chosen so that it points upwards at b_0, b_{s+1} and downwards at d_0, d_{t+1}. Call the *front* of N the hemisphere of B_1 between b_0 and b_{s+1} into which ξ' points at b_{s+1}, and the hemisphere of B_2 between d_0 and d_{t+1} into which it points at d_0.
Analogously define η' as the unit vector field to P in $\overline{\mathbb{R}^3 - N}$ that points west at a_1 and c_1.

We now associate a sign to the graph vertices. Start by focusing on the graphs arising from M. As the vertices of Γ_P arise from boundary components of a separating sphere, η will be pointing in opposite directions on any two adjacent vertices. Thus we say that a_i and c_j are positive vertices for i, j odd, and are negative for i, j even. The portion of vertex corresponding to the front of M will be the right hemisphere for positive vertices and the left hemisphere for negative ones. As for the vertices of Γ_Q, we say that b_0 is a positive vertex, b_{s+1}, d_0 and d_{t+1} are negative vertices. These are boundary vertices of Γ_Q and we assume all of them to belong to the front of M. The sign of the remaining vertices of Γ_Q cannot be determined a priori. However, we remark that on B_1 the portion of a positive vertex corresponding to the front will be the right hemisphere. For positive vertices on B_2 it will be the left hemisphere instead. In future examples, we will shade the relevant hemisphere of a vertex to indicate the portion that belongs to the front of M or N.

Repeat the same process and associate a sign to the graph vertices arising from N. For the vertices of Γ_P we will use the same convention as above. For the vertices of Γ_Q we say that b_0 and b_{s+1} are positive, while d_0 and d_{t+1} are negative. As in the previous setting, assume they are on the front of N. The sign of remaining vertices cannot be determined a priori; however, for positive vertices, we assume that the front is the portion corresponding to the right hemisphere, regardless of whether they belong to B_1 or B_2.

Associating signs to every vertex gives rise to the following notion: we say an edge is *synchronous* if it connects vertices of the same sign, *asynchronous* if it connects vertices of opposite sign. We can now establish a parity rule.

Proposition 8.14 (Parity Rule)**.** *Let e be an edge in Γ_P. Suppose e connects vertices on the same side of M (or N). Then e is synchronous in Γ_P if and only if it is asynchronous in Γ_Q. Now suppose e connects the front and back of M (or N). Then e is synchronous in Γ_P if and only if it is synchronous in Γ_Q.*

Proof. The following proof is adapted from Greene's notes [34]. Suppose e is an arc of $P \cap Q$ staying on the same side of M (or N), running from some $f(i,k)$ to $f(j,l)$ (or any same side combination). Then e must connect points of $\partial P \cap \partial Q$ of opposite sign. Let us examine an endpoint x of e, which is a point of intersection of $P \cap Q \cap M$. We develop a frame at this endpoint by taking the triple consisting of the relevant vectors from ξ, η — which we may take to be tangent to ∂M (or ∂N) — and the normal resulting from the

first two vectors. Suppose, without loss of generality, it is the outward one. Now advance the frame along e: at the opposite endpoint y we obtain the frame given by ξ, η and the resulting normal, which is now pointing inwards. As these frames arise from the same orientation on M, the sign of intersection of P and Q at x must be opposite to the sign at y. In terms of graphs this means that if e is synchronous in, say, Γ_P, then it must be asynchronous in Γ_Q.
Now suppose that e connects the front and back of M (or N). Take the frame defined as before at the endpoint x on the front. Suppose this frame defines the outward normal of M at x. Now move the frame along e to the endpoint y. At this point the normal will be pointing inwards. However, since we are now at the back of our manifold, we have changed the sign of the frame twice, and hence it is still the same. That means that x and y are points of the same sign. Translated into graph theory this tells us that e is synchronous in Γ_P if and only if it is synchronous in Γ_Q. □

The purpose of defining a Parity Rule is to add further restrictions on the graph configurations that can arise from Γ_P and Γ_Q.

Corollary 8.15. *No boundary vertex of Γ_Q presents loops with labels i and i' such that $i \equiv i' \mod 2$ (similarly for labels j, j').*

Proof. This is a direct consequence of the Parity Rule. Suppose we did have such a loop. Then this would be a synchronous edge in Γ_Q, on the front of the relevant manifold. The corresponding edge in Γ_P would be synchronous as well, giving rise to a contradiction.
A combinatorial proof is possible as well. Such a loop in Γ_Q would contain an odd number of labels in its interior, giving rise to a contradiction since each edge has two endpoints. □

Corollary 8.16. *There can be no level edges between the boundary vertices d_0 and d_{t+1} of Γ_Q arising from M.*

Proof. Any level edge between d_0 and d_{t+1} is on the front of M and is synchronous. This edge corresponds to a synchronous loop based at some c_j, hence giving rise to a contradiction. A combinatorial proof is possible as well, since a level edge cuts off two components of the graph with an odd number of labels. □

A similar corollary can be deduced for the graphs arising from N.

Corollary 8.17. *There can be no level edges between the boundary vertices b_0 and b_{s+1}, or d_0 and d_{t+1} of Γ_Q arising from N.*

Proof. Same argument as for Corollary 8.16. □

§ 8.2.3 | Basic Properties

This section presents some properties of Γ_P and Γ_Q which follow directly from the graph theoretical notions previously introduced. Unless specified, these are valid regardless of whether the graphs arise from M or N. The following results are readapted from [10, 64].

Lemma 8.18. *Γ_P and Γ_Q have no level loops.*

Proof. Suppose we have a level loop in Γ_P based at a_i. Between any two equal labels of a_i in Γ_P lie an odd number of labels. Any vertex in the interior of this loop has either $(2s+2)$ or $(2t+2)$ ends of edges incident to it. In total, there is an odd number of labels in the interior of the circuit, each at the end of an edge. But this is impossible since each edge has two ends.

Recall the bijection existing between Γ_P and Γ_Q and note that a level loop in one graph corresponds to a level loop in the other. Hence, both Γ_P and Γ_Q have no level loops. □

Proposition 8.19. (1) *Any chord of an innermost cycle or semi-cycle is a level spoke.*

(2) *An innermost semi-cycle has no chords.*

Proof. (1) Suppose the (semi-)cycle contains a chord. If this chord is a loop, note that it must be oriented because of Lemma 8.18, and thus it is a cycle in an innermost (semi-)cycle, a contradiction. If the chord is an oriented spoke, then it divides the interior of the (semi-)cycle into two components belonging to the interior of a circuit. One of these components would then be a (semi-)cycle contained in an innermost (semi-)cycle, again a contradiction. Therefore, only level spokes are possible.

(2) Suppose we have an innermost semi-cycle which has a chord. By *(1)*, this chord must be a level spoke. Then it divides the interior of the semi-cycle into two components, at least one of which is still a semi-cycle interior to the supposed innermost one, resulting in a contradiction.

□

Note that statements (1) and (2) above are stronger than the corresponding ones in [64, Proposition 2.5.2].

Proposition 8.20. *Let $\mathcal{R}_{m,n}$ and $\mathcal{B}_{s,t}$ be such that they do not give rise to punctures. If an innermost cycle or semi-cycle has an interior vertex, it must have an interior source or sink.*

Remark 8.21. We want to avoid a situation in which the interior vertices of an innermost (semi-)cycle are punctures. When Γ_P and Γ_Q arise from M, this means that we need to exclude the case $\mathcal{R}_{m,0}$ and $\mathcal{B}_{s,t}$ with $t \neq 0$. Note that punctures cannot arise on N: this is because $\mathcal{R}_{m,n}$ is such that m and n are odd, and thus any curve from $\mathcal{B}_{s,t}$ intersects at least a curve from $\mathcal{R}_{m,n}$.

Proof. Assume that the innermost (semi-)cycle lives on B_1. We shall consider two cases.

Suppose that all interior vertices are from B_1 and that none of them is a source or sink. This means that each vertex has an edge pointing in and another pointing out. Then we can start at a vertex v and construct a path through the interior oriented edges, which is always consistent with the orientations. This path cannot hit the same vertex twice, or it would create a cycle contained in an innermost (semi-)cycle, so it must end on one of the vertices of the existing innermost (semi-)cycle. Using the same reasoning, one can construct another path starting at v, through the interior oriented edges and always inconsistent with orientations. Similarly, this path cannot hit the same vertex twice, so it must terminate at a vertex of the innermost (semi-)cycle. Then the union of these two paths divides the interior of the innermost (semi-)cycle into two components, one of which is again the interior of a (semi-)cycle, giving a contradiction.

Now suppose that the interior vertices are from either B_1 and B_2, or only from B_2, and that none of them is a source or a sink. Consider an interior vertex v belonging to B_2. Since we assumed it is not a sink, then there must be at least one edge pointing away from it. This edge must necessarily end on another vertex from B_2, because of the orientations imposed. Let us construct a path through the interior vertices which starts at v and is always consistent with orientations. This path can only hit vertices from B_2 (because of the orientations), and it cannot hit the same vertex twice, otherwise it would create a cycle. Follow the path until we reach the last vertex w available from B_2 (which we know will happen since there are finitely many). Because we are assuming that w is not a sink, we know that there is an edge going out from w. We already observed that this edge

cannot be incident to another interior vertex from B_2. Similarly, it cannot be incident to vertices from B_1 (either from the circuit or its interior), as it would not be an edge going out of w. Thus there is no edge going out of w, a contradiction.

Observe that in this argument, we did not need to assume there were no sources. So we have proved something stronger, namely that in this case we must have a sink.

If the innermost (semi-)cycle we are considering lives on B_2, the proof follows in the same way, swapping the roles of sources and sinks in the second part (hence we would prove we must always have a source if we have interior vertices from B_1 and B_2, or from B_2 only). □

The following lemma and proof are the same as in [64], with the exception that we are not restricting ourselves to the interior of a circuit.

Lemma 8.22. *If α is a level edge in either Γ_P or Γ_Q, then the labels that precede and follow those of α in a label sequence (or are on the same side of the vertices joined by the level edge) are the same.*

Remark 8.23. When referring to labels l_1, l_2 that are on the same side of a level edge α, we shall mean that it is possible to connect l_1 and l_2 via an arc which is a normal push-off of α in Q that does not intersect α.

Proof. First note that if α is a level edge, then it must connect vertices belonging to the same 3-ball. Without loss of generality, assume that α belongs to B_1.

Suppose α joins vertices v and v' in Γ_P with label l. The argument for Γ_Q is identical. Notice that the pair of adjacent labels to l in v is the same as that in v'. If $l \in \{0, s+1\}$ in Γ_P, both adjacent labels are always equal, thus concluding the proof.

If l does not belong to the aforementioned set, then the labels adjacent to l are different on any vertex. If this is the case, there must be a label k adjacent to l on both v and v'. Suppose that k is on opposite sides of the edge α. We can then trace an arc β from v to v', close to α and joining the ends of v and v' between l and k, crossing α once. This arc has ends in ∂M (or ∂N) lying near the same component b_l of ∂Q, between b_l and b_k. The ends of β can be connected by an arc β' in the neighbourhood of b_l in ∂M, resulting in a simple closed curve $\beta \cup \beta'$. Recall that Q is an oriented surface, hence its regular neighbourhood $\nu(Q)$ is homeomorphic to $Q \times I$. In particular, we say that Q is two-sided, because its neighbourhood has two boundary components or, equivalently,

$\nu(Q) - Q$ is disconnected. Now, $\beta \cup \beta'$ is a simple closed curve living in $\nu(Q)$ as a normal push-off of the simple closed curve given by the union of α and the relevant portion of b_l, intersecting Q only once. This is a contradiction, because it would imply that Q is one-sided, which means that $\nu(Q) - Q$ is connected.

The same proof can be applied to the vertices of B_2. □

Note that Corollary 8.16 can be obtained as a direct consequence of Lemma 8.22. Corollary 8.17 can also be deduced from Lemma 8.22.

As previously mentioned, the results presented in this subsection are of the same flavour as those in [10, 64], and follow directly from the set-up of the graphs. However, it is interesting to note that the modifications to the graph constructions introduce enough complications that we were not able to deduce any more results for the most general setting. Any further results which appear will, in fact, only apply to specific configurations of $\mathcal{R}_{m,n}$ and $\mathcal{B}_{s,t}$.

Chapter 9

Band Slides and Band Swims

The current chapter aims to discuss in detail the issue of band interactions, specifically for the movie decomposition of $\mathbb{R}P^2$ we are working with. It was observed in Chapter 8 that such a movie picture presents two bands which may interact with each other in two different ways, either via band slides or band swims. These phenomena can give rise to very complicated movies of $\mathbb{R}P^2$, and consequently elaborate graph configurations. It is therefore crucial to understand and identify these band interactions, in order to "undo" them in some way. This would simplify configurations in Γ_P and Γ_Q and the underlying movie picture describing the embedding. In this chapter we present what was understood about the phenomena, together with some examples and issues.

§ 9.1 | Band Slides

We start by discussing band slides, that is, the sliding of one band's end lengthwise along another band's side, as described in [67]. In order to do so, focus on Figure 8.2. It is possible to go from (a) to (b) by either sliding the top of B_2 to the left, or by sliding its bottom to the right. Sliding B_1 over either side of B_2 instead does not affect the knot configuration, as the result of this particular slide can be isotoped to a picture that is symmetric to (a). Note that there are four admissible slides when starting in this configuration.

When starting from Fig. 8.2 (b), it is possible to slide either side of B_1 over either side of B_2 to obtain (a) (or a mirrored picture), only with the roles of the two bands swapped. Similarly, sliding either side of B_2 over either side of B_1 takes us to Fig. 8.2 (a). Therefore, when starting from (b), there are eight admissible slides.

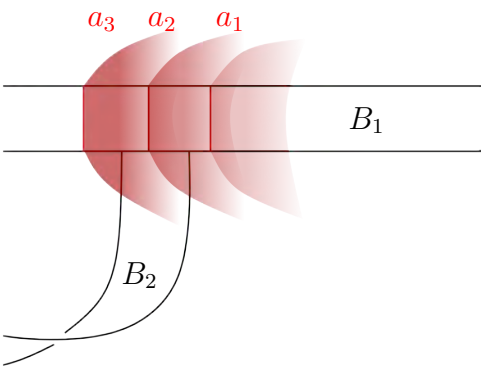

Figure 9.1: A band B_2 intersects $\hat{P}$ when sliding over B_1.

In general, note that some of the aforementioned slides take us to the mirrors of the configurations represented in Fig. 8.2, or swap the front and back of the bands. While this is not an issue in terms of the movie picture, it is definitely something to take into consideration when we are trying to use the graphs to detect a band slide. Finally, observe again that the relation via slides between the two knot configurations in Fig. 8.2 directly translates into a relation via handle slides between the manifolds M and N, which arise from their regular neighbourhoods.

To fully understand how sliding affects the embedding $\mathbb{R}P^2 \hookrightarrow \mathbb{R}^4$, it is not enough to look at the underlying kind of knot configuration, but we need to understand the image of the related embedding of Fig. 8.2 in $\mathbb{R}^3$. This is described by how the bands interact with the planar surfaces $\hat{P}$ and $\hat{Q}$, hence it is fundamental to consider what happens to the families of simple closed curves $\mathcal{R}_{m,n}$ and $\mathcal{B}_{s,t}$ on the manifolds M and N, and to their intersection.

We start by remarking that sliding affects the number of closed curves of $\mathcal{R}_{m,n}$ and $\mathcal{B}_{s,t}$. Let us zoom in on the band B_2 sliding over B_1, as in Figure 9.1. Observe that, during the slide over B_1, B_2 will intersect disc portions of $\hat{P}$ which come from $a_m, \dots, a_1$, and record how many times B_1 intersects $\hat{P}$. Consequently, each time B_2 slides over each curve (or line segment, in this picture), it will cross $\hat{P}$ as well. Hence, B_2 will also pick up m curves (or line segments).

Let us now think about how sliding affects the intersection of the bands with $\hat{Q}$. First of all, observe that the boundary of $\hat{Q}$ includes the sides of B_1 and B_2, hence by sliding we are isotoping this boundary. Recall that before the slide the bands can also intersect $\hat{Q}$ in its interior. Suppose B_2 intersects $\hat{Q}$ in an arc d_1 (which will correspond to a simple

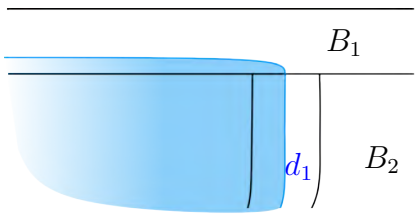

Figure 9.2: A band B_2 sliding over B_1 introduces intersections with $\hat{Q}$.

closed curve on M or N). This arc is part of a sheet coming from $\hat{Q}$, and it gets dragged over B_1 during the slide, as in Figure 9.2. Hence, sliding introduces an intersection of B_1 with $\hat{Q}$. As in the previous case, this can be generalised: if B_2 intersects $\hat{Q}$ in $d_1, \ldots, d_t$ segments, then sliding will introduce t new intersections of B_1 with $\hat{Q}$.

Given M or N, with $\mathcal{R}_{m,n}$ and $\mathcal{B}_{s,t}$ families of curves, it is clear from the discussion above that sliding bands in the underlying movie picture will affect the number of curves. We provide a summary of the effects of sliding below.

Suppose that we are starting from Fig. 8.2 (a), and that on the related manifold M we have $\mathcal{R}_{m,n}$ and $\mathcal{B}_{s,t}$ curves. When sliding B_1 over B_2 we obtain a mirror image of Fig. 8.2 (a) and $\mathcal{R}_{m,n}$ and $\mathcal{B}_{s,t}$ are modified as follows:

- B_1 picks up n curves from B_2, and thus we have $\mathcal{R}_{m+n,n}$;
- B_2 picks up s curves from B_1, and thus we have $\mathcal{B}_{s,s+t}$.

Similarly, when sliding B_2 over B_1 we obtain Fig. 8.2 (b) and:

- B_2 picks up m curves from B_1, and thus we have $\mathcal{R}_{m,m+n}$;
- B_1 picks up t curves from B_2, and thus we have $\mathcal{B}_{s+t,t}$.

The situation is analogous when starting from Fig. 8.2(b), but any slide will result in Fig. 8.2(a) (with the roles of the bands potentially swapped) or a mirror image.

Note that the parities of m and n are always coherent with the slides. As slides affect the number of curves in $\mathcal{R}_{m,n}$ and $\mathcal{B}_{s,t}$, they will directly affect the graphs Γ_P and Γ_Q by introducing new vertices, labels, and edges. At this point, it is important to understand what they will look like, and the aforementioned distinctions between the front and back of a band become extremely relevant. The reason is that a simple count of vertices cannot

help us detect when a slide has taken place, nor provide any information about how to find an inverse slide.

In the next section, we will present a simple example of a band slide to familiarise ourselves with the patterns and issues arising in Γ_P and Γ_Q. The aim is to be able to detect slides and understand how to reduce some elements in the graphs by performing a reverse slide.

§ 9.1.1 | Slide Example

Suppose we are in the configuration of Fig. 8.2 (a), and that $m = t = 1$, $n = s = 0$. There is only one possible arc of intersection of P and Q: in Γ_P it corresponds to a loop based at a_1 with labels 0 and 1; in Γ_Q it is a level edge between b_0 and b_1 with label 1. Now slide the lower bottom of B_2 over B_1, as shown in Figure 9.3. This takes us to the configuration in Fig. 8.2 (b) with $m = n = s = t = 1$.

Observe that during the intermediate steps of the band slide, B_2 intersects a portion of P near a_1: when the band is sliding over B_1 and the curve c_1 starts forming, the arc starting at $a_1 \cap b_0$ is now forced to join $c_1 \cap d_0$. Once c_1 is completely formed, and B_2 is sliding to the end of B_1, there is an arc of $P \cap Q$ joining $a_1 \cap b_1$ and $c_1 \cap d_1$. The remaining vertices and edges are obtained analogously.

The graphs in Fig. 9.4 represent the intersections arising from this slide. The shading on each vertex indicates the part lying on the front of the corresponding manifold N. Recall that b_0 and b_2 are both assumed to be of positive sign, while d_0 and d_2 are assumed to be negative. The parity rule forces b_1 and d_1 to be of the same sign, which in this case we assumed to be positive (negative signs would have worked as well). Additional notation regarding the orientation of the edges has been omitted to avoid clutter. This is a good point to observe that slides are not a local move because, aside from taking us between the configurations of Fig. 8.2, they also affect existing edges of a graph.

We may now attempt to undo a slide. Slide B_2 over B_1 over the reversed path from the previous slide, as in Figure 9.5. We will end up in our original knot configuration, but with $m = t = 1$ and $n = s = 2$, with new vertices and edges arising in the same fashion previously described.

We analyse the new arcs introduced in $P \cap Q$ via the graphs, shown in Figure 9.6. Once

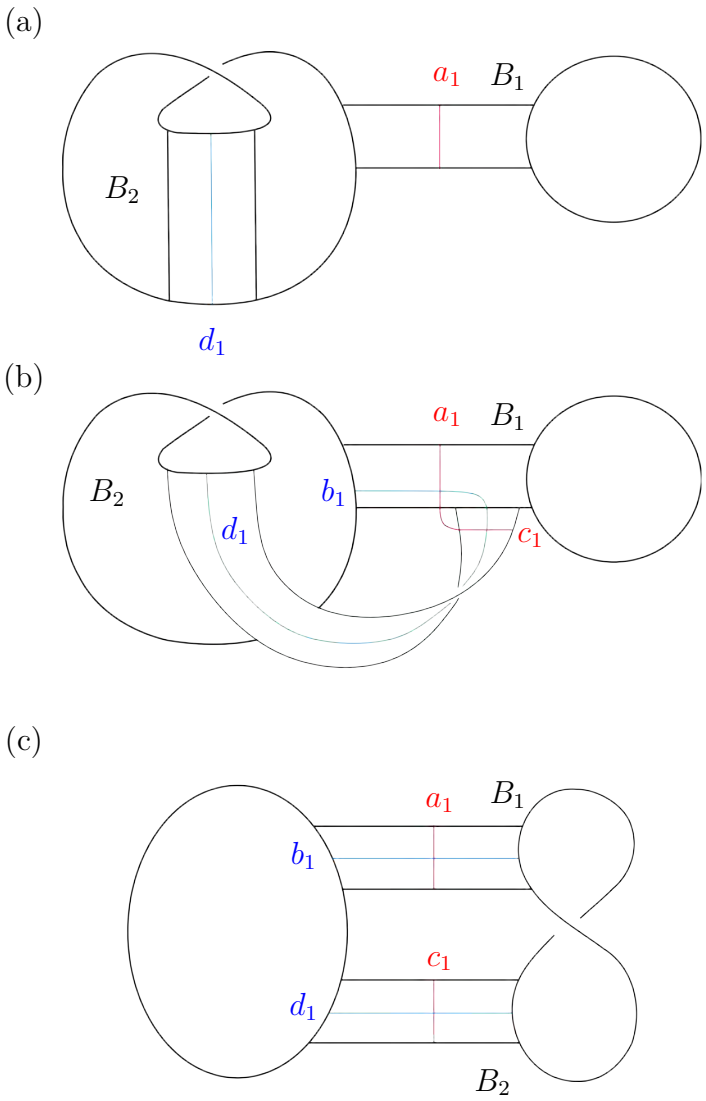

Figure 9.3: Stages of sliding B_2 over B_1.

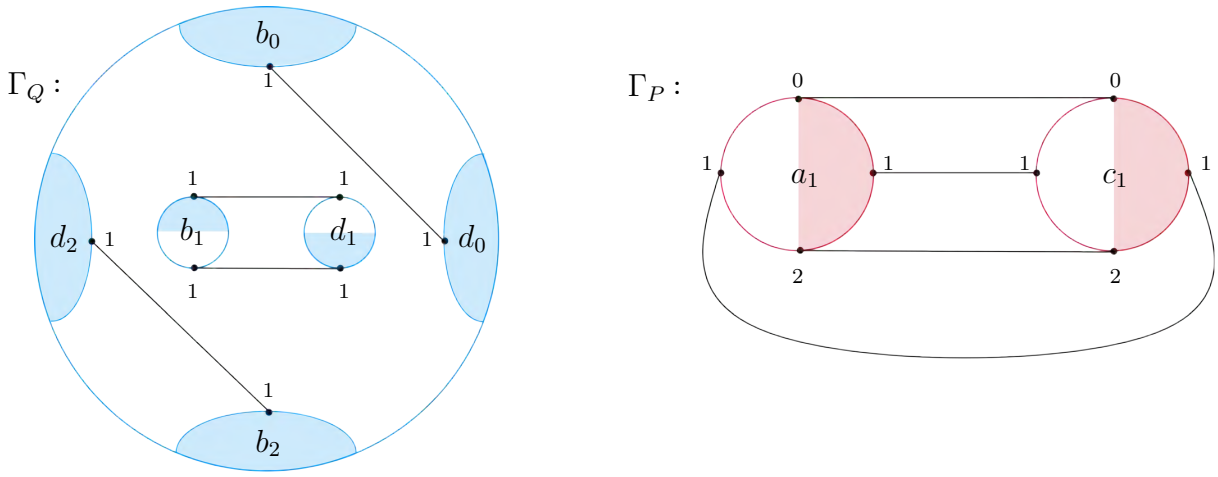

Figure 9.4: The graphs Γ_Q and Γ_P after one slide.

again, the shaded areas represent the portion of the vertices on the front of M, the graphs are coherent with the parity rule, and we have omitted orientations of edges and vertex signs to avoid clutter. Now observe that Γ_Q presents a loop based at d_2 bounding a compressing disc in Q, which can be used to eliminate c_1 and c_2, thus reducing n to zero. This in turn reduces Γ_P to a single vertex a_1 which is the base of all the edges (loops) of the graph. It is possible to start from an innermost one and observe that it bounds a compressing disc in P, which can be used to reduce b_1 and b_2. After this sequence of reductions, we are back to the starting point of Figure 9.3, hence we have undone the slide.

Remark 9.1. The undoing of the slide in this example required a reduction of $\mathcal{R}_{m,n}$ and $\mathcal{B}_{s,t}$. For this purpose, the existence of the loop based at d_2 bounding a disc portion of Q was fundamental. Note that the loop alone is not sufficient to reduce the number of labels (or curves). Indeed, that is not possible if the loop contains vertices in its interior. In general, it is important to understand how and where the slides introduce new vertices and edges in Γ_P and Γ_Q, in order to make statements about the possibility of finding loops that enable reductions. Note that graph elements arising from a slide also appear in a certain order. This can be seen by focusing on Figure 9.5 (a) and (b): if we draw the intermediate steps between the two pictures, we can observe that the loop based at d_2 appears before c_2 is "completely formed" (this is because of how B_1 intersects P). Although this is a simple example, it is not clear if this is enough to deduce that the loop will always bound a disc face of Q. It might be that one needs to take into account additional factors, like what the original edge between a_1 and c_1 with label 2 looks like.

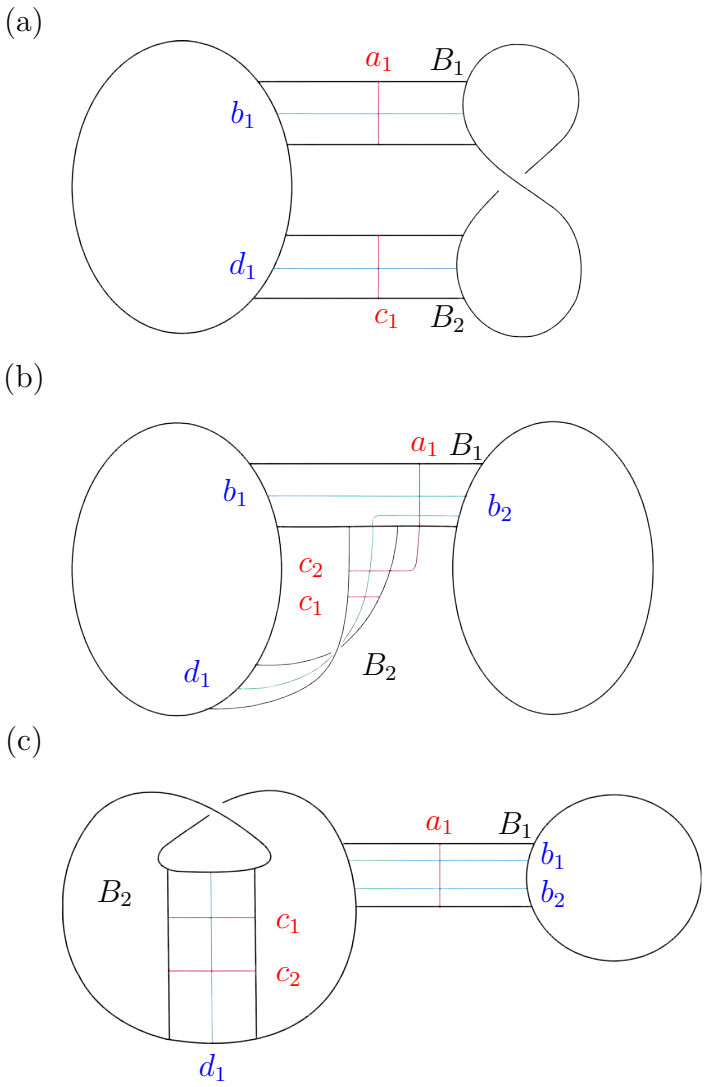

Figure 9.5: Stages of sliding B_2 back over B_1.

In more complicated examples, this could be part of a circuit containing punctures in its interior, for instance. This issue illustrates that although slides are an intuitive concept, a good amount of caution is required when working with them.

It is clear that to undo a slide we must find a suitable loop in one of the graphs, which can present its challenges. We also note that in general it can be quite difficult to determine what graph configurations arise from sliding. It seems plausible to expect "concentric" circuits to appear in Γ_P, but no rigorous notion of it was produced during the time spent working on this project. This is a direction worth pursuing because of the fact that the new vertices introduced from a slide in either graph always connect to pre-existing ones through some, if not all, of the edges. Hence it seems reasonable to expect the circuits of

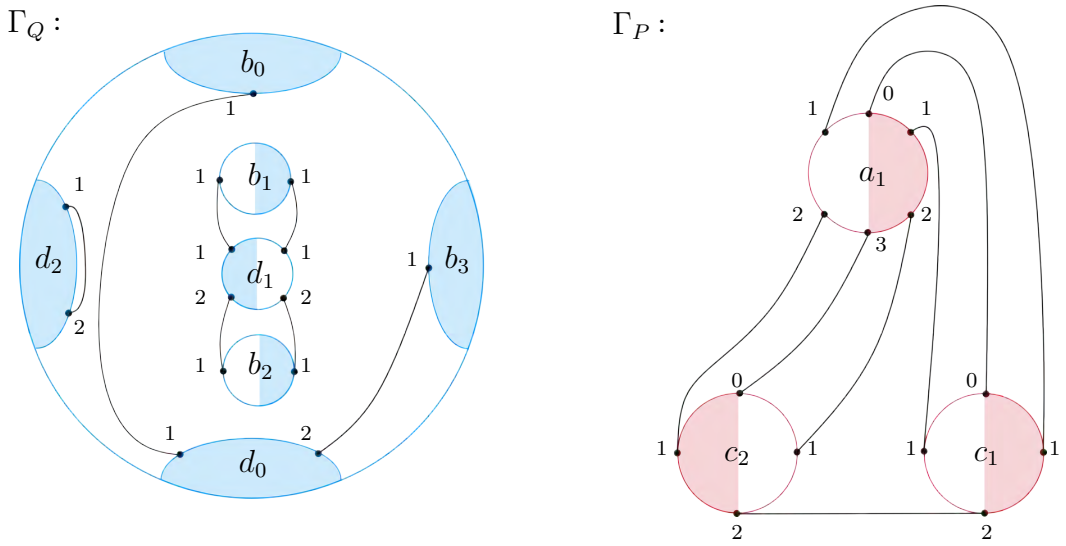

Figure 9.6: The graphs Γ_Q and Γ_P after two slides.

our graphs to contain sinks and sources, but a precise statement can only be made once the circuits arising from a slide are understood in a precise sense.

The problem can be summarised as follows: suppose we are looking at the graphs Γ_P and Γ_Q. Is there a specific configuration that can tell us whether a slide has happened? If that is the case, does the configuration contain a loop as in Fig. 9.6 which can immediately be used to reduce $\mathcal{R}_{m,n}$ and $\mathcal{B}_{s,t}$? If not, is there enough information in the graphs to understand how to perform a slide that cancels the previous one? If so, can we always guarantee that we will find a loop bounding a reducing disc?

§ 9.2 | Band Swims

The second possible interaction between the bands is called a band swim, introduced in Chapter 8, which consists of dragging the width of a band through the length of another band. It is important to note that during this interaction, the ends of the band that swims remain fixed. In particular, this implies that Figure 8.2 (a) and (b) are not related by a band swim.

As in the previous case, it is important to understand what happens to the image of the embedding of a movie from Fig. 8.2 in $\mathbb{R}^3$ during a swim. In particular, we need to determine how the intersection of the bands B_1 and B_2 with $\hat{P}$ and $\hat{Q}$ changes. In general, a swim is more complicated than a slide since it can happen in several elaborate ways, based on how one band is isotoped before actually passing through the other one.

This process can be broken into two parts, first the isotopy and then the actual swim. Consider any of the configurations in Fig. 8.2 and let B_2 swim through B_1. We shall describe the process as follows: choose a point on one side of B_2 and a framed arc starting at that point and ending at a point on one end of B_1. Such a framed arc gives a complete description of the isotopy and swim of B_2 through B_1. In general, we may assume this framed arc not to have endpoints on any c_j or b_k. Sometimes, it might be useful to make a different assumption, which will be discussed later on.

Let us now focus on understanding what a band swim looks like, ignoring for the moment any isotopy taking place before it. Figure 9.7 provides a close look at what happens during a swim (note that in this image we are assuming $m = t = 1$ and $n = s = 0$). It is crucial to note that this is only one of the possible ways to swim B_2 through B_1. Recall

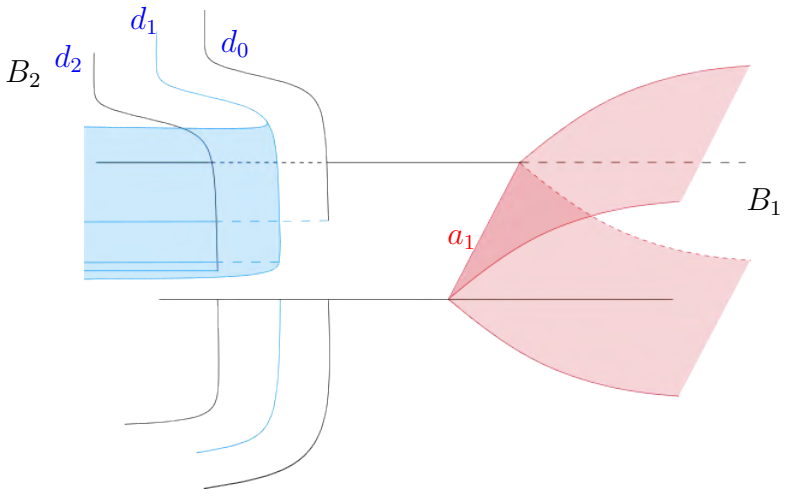

Figure 9.7: A close look at a swim of B_2 through B_1.

that the red and blue segments represent the intersection of the bands with $\hat{P}$ and $\hat{Q}$, respectively, so we should always imagine a portion of these surfaces around them. In this case, the portion of $\hat{P}$ around a_1 is represented as a fold, which will intersect B_1 in two segments once the swim is complete. Similarly, the disc sheet of $\hat{Q}$ near d_1 is represented as a fold as well, and observe that as B_2 swims through B_1, this fold will intersect B_1 in two segments. The sides of the band B_2 correspond to the boundary of $\hat{Q}$ and should be pictured as dragging sheets of this disc behind them when swimming through B_1 (Fig. 9.7 does not show all these disc sheets to reduce clutter). Note that one of the segments introduced by a side of B_2 will sit between the segments introduced by the fold. Which one it will be depends on the direction that the disc sheet containing d_1 folds in. Finally, observe that during a swim like the one in Figure 9.7, any red segments on B_2 are unaffected (because one can always place an end of the framed arc between

two such segments), as well as any blue segments on B_1.

We now present a summary of the effect of swimming on the families $\mathcal{R}_{m,n}$ and $\mathcal{B}_{s,t}$ (ignoring any isotopies before this move). Suppose we are in any configuration of Fig. 8.2 and are swimming B_1 through B_2. Then $\mathcal{R}_{m,n}$ and $\mathcal{B}_{s,t}$ are modified as follows:

- B_1 picks up $2n$ curves from B_2, and thus we have $\mathcal{R}_{m+2n,n}$;
- B_2 picks up $2s+2$ curves from B_1, and thus we have $\mathcal{B}_{s,t+2s+2}$.

Similarly, when swimming B_2 through B_1:

- B_2 picks up $2m$ curves from B_1, and thus we have $\mathcal{R}_{m,2m+n}$;
- B_1 picks up $2t+2$ curves from B_2, and thus we have $\mathcal{B}_{s+2t+2,t}$.

Once again, note that parities of m and n stay coherent.

Let us now consider a band swim of B_1 through B_2 where we assume $\mathcal{B}_{s,t}$ to be such that $t \neq 0$. We previously mentioned that there are some occasions in which we may want to assume that the framed arc describing this swim terminates at a point on an end of B_2 belonging to some d_l. Let us consider the case where we have $\mathcal{R}_{3,0}$ and $\mathcal{B}_{0,1}$ on M. Suppose there is a loop in the graph Γ_Q based at b_0 with labels 3 and 2, which contains in its interior the puncture d_1. This loop cannot be used to reduce the number of vertices of Γ_P as in the Slide Example, because it does not bound a disc face of Q. However, it is possible to draw a framed arc in Γ_Q starting at the boundary vertex b_0 and ending at the puncture d_1. This arc also lives in $\mathbb{R}^3$ and can be used to guide a band swim of B_1 through B_2, which guides B_1 over the puncture from d_1. Figure 9.8 shows two steps of this process. Picture (a) depicts the bands before swimming, and the orange arc corresponds to the framed arc that guides the swim and arises from Γ_Q. The blue areas around the sides of B_1 and d_1 represent portions of Q in $\overline{\mathbb{R}^3 - M}$. Picture (b) shows what happens halfway through the swim: one side of B_1 has already swum through B_2, and pushed d_1 out of Q. The latter can be seen as dragging the puncture towards b_0 using the framed arc in Γ_Q. The next step, which is not shown in Fig. 9.8, is to complete the band swim by dragging b_1 through B_2. This will now introduce a new puncture in Γ_Q, which we may call d_1 again and which can be connected to b_1 via a framed arc. This swim resulted in moving d_1 out of the loop in Γ_Q, which can now be used to reduce the number of vertices of Γ_P.

Note that this argument works in the same way if there are $b_1, \ldots, b_s$ segments on B_1:

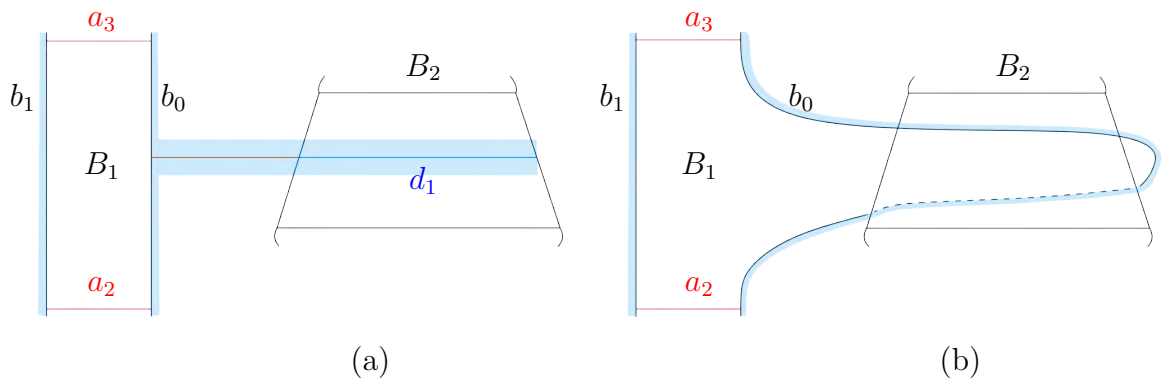

Figure 9.8: Intermediate steps of swimming B_1 through a puncture d_1 of B_2.

the only difference is that the swim will push the puncture out of the loop and introduce additional punctures outside of it. Moreover, in this example we consider a loop based at b_0, but the same argument works more generally for a loop based at a vertex $b_0, b_1, \dots, b_s, b_{s+1}$. Recall that the graphs Γ_P and Γ_Q also contain circles from $P \cap Q$ which are essential in both surfaces. Most of the times this causes no issues, and the circles can be ignored. However, in a situation like the one above, it might happen that the loop considered contains in its interior a circle from $P \cap Q$ and the puncture inside of it. Then the framed arc in Γ_Q describing the swim crosses the circle, and in particular, this implies that the band B_1 intersects $\hat{P}$ in two arcs during the swim. This local intersection, however, can be undone once the swim is completed, and the circle from $P \cap Q$ will appear around the new puncture d_1, which can be connected to B_1 via a framed arc that intersects it.

The type of swim discussed is extremely interesting because it can be used to push punctures outside of circuit interiors under specific conditions. Note that this only applies to punctures, which are vertices with no labels (and hence can only really arise from B_2 on M). Observe that if in the example discussed $\mathcal{B}_{s,t}$ had $s \neq 0$, the band swim would introduce additional punctures. We would still manage to swim d_1 out of the aforementioned loop, but at the cost of introducing more punctures. When working in more general settings, such as with circuits containing punctures in their interior, this can hinder us from pushing out all the punctures, as new ones could be introduced inside the circuit every time.

Up to this point, we have avoided thinking about the isotopy that happens before an actual swim and have only focused on the effects of the latter. Suppose we have a framed

arc γ describing a swim of B_1 through B_2: this arc contains information about the isotopy that precedes the swim as well. The arc γ lives in $\mathbb{R}^3$ and connects a side of B_1 to an end of B_2. It is likely that somewhere in its interior, γ will intersect Q or P. We consider four cases:

- γ intersects P: then we can push B_1 through P, introducing new intersections. Thus, P is now bounded by $\mathcal{R}_{m+2,n}$, and we may proceed with the swim;
- γ intersects Q: in this case we can push this sheet of Q along γ and in front of B_1, introducing two intersections of B_2 with Q, which is now bounded by $\mathcal{B}_{s,t+2}$, before proceeding with the swim;
- γ intersects P first, then Q: this is a combination of the two previous cases, which will introduce two intersections of B_1 with P and two intersections of B_2 with Q, all before the swim;
- γ intersects Q first, then P: then one can push Q in front of B_1 along γ, which will create a circle of intersection with P, as well as introduce two new curves on B_2. When pushed along γ, B_1 will intersect P in two new curves. All of this happens before starting the actual swim.

Any other intersection of γ with P and Q is a combination of the aforementioned cases. The observations above tell us that isotopies can introduce many complications even before a swim starts. In particular, we face two main problems. The first is that all we know about P and Q comes from Γ_P and Γ_Q, which only record their intersections with the 3-balls arising from B_1 and B_2. Hence, we do not know how P and Q sit in $\overline{\mathbb{R}^3 - M}$ (or $\overline{\mathbb{R}^3 - N}$), and in particular, we do not know if and how a framed arc γ is going to encounter these surfaces when specifying a swim. The second issue is that swims and isotopies do not necessarily commute, hence once the swim is performed, it is not possible to "undo" the initial isotopy and reduce the number of curves introduced by it.

§ 9.2.1 | Swim Examples

In this section, we present some examples of band swims. It is important to note that we shall only portray the effect of a swim and not of the isotopy happening before it, as the previous discussion showed that we don't have any means to detect what happens at that stage. Therefore, each example cannot be taken as a complete description of a swim, but only of a part of it.

Example 9.2. Suppose we have a movie picture of $\mathbb{R}P^2$ as in Fig. 8.2 (a) with $m = 1$,

$n = s = t = 0$. The graph Γ_P presents the obvious loop based at a_1, while Γ_Q presents an edge between b_0 and b_1. Consider a swim of B_2 through B_1 that looks like the one in Figure 9.7, without d_1 and associated fold. The resulting graphs are shown in Figure 9.9 (as usual, we have omitted to orient edges). The swim is consistent with the parity rule, so note that b_1 and b_2 are positive vertices.

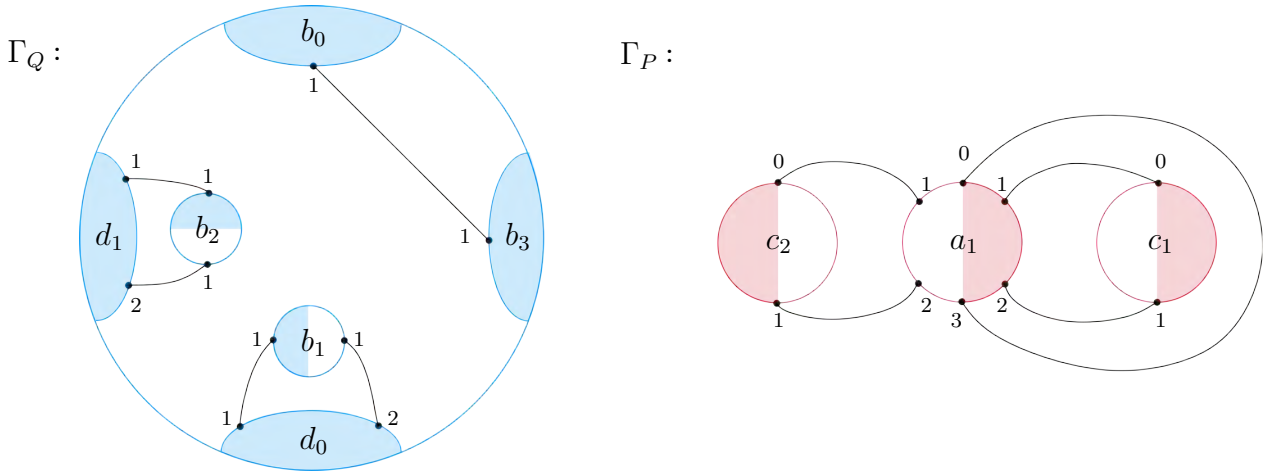

Figure 9.9: Graphs resulting from the swim of B_2 through B_1 in Example 9.2.

At this stage, we can also remark on a fundamental difference between swims and slides: unlike the latter, swims are a local move. This is evident from the fact that the knot configuration underlying the movie remains unchanged, and that introducing new vertices and edges in the graphs does not affect pre-existing ones.

Unlike for slides, it is not immediately clear what the inverse of a swim should be. It is natural to imagine that we can reduce the vertices and edges in Γ_P and Γ_Q by "swimming back", but it is quite difficult to make this idea precise. One reason is that swims can happen in several ways, so it is not enough to swim B_2 through B_1 in the opposite direction. Indeed, we need a specific framed arc to define this swim. The second reason is that swimming back will introduce more vertices and edges locally, and it is not immediately clear how they would lead to a reduction (unlike the loops resulting from sliding). The issue of defining an inverse of a swim was never solved, but below we report some observations which could potentially be of use.

It can be seen from Fig. 9.9 that this swim has given rise to a collection of disc faces in P and Q. We have two disc faces coming from Γ_Q: the first one is bounded by a portion of b_1 and d_0 and the edges connecting them, while the second one is bounded by a portion of b_2 and d_1 and the respective edges. Similarly there are two disc faces coming from

Γ_P: the one bounded by a_1, c_1, and the relevant edges, and the one bounded by a_1, c_2 and the edges between them. Together with the relevant disc portions of ∂M enclosed by b_1, b_2, a_1 on B_1 and by d_0, d_1, c_1, c_2 on B_2, the disc faces form a cube C which lives in $\overline{\mathbb{R}^3 - M}$ by construction. Such a cube is homeomorphic to an S^2 embedded in $\mathbb{R}^3$, which by Alexander's Theorem bounds a 3-ball [5] that intersects ∂M only in two disc faces. Now, such a 3-ball is contractible, and the idea is that understanding the effect of the contraction should provide a way to undo the band swim. The issue is understanding what this looks like on M and on the underlying movie, and how to make this contraction precise. Some questions worth considering concern how C and its interior sit in $\overline{\mathbb{R}^3 - M}$ and how to deduce which curves survive the contraction and why.

One would like to be able to determine that a swim has happened and to undo it just by looking at the graphs. In this specific case, the contraction of the 3-ball bounded by C should lead to the reduction of b_1, b_2, c_1, c_2. We expect the cube C to represent the framed arc with ends on ∂M that specifies how to undo the swim performed. However, no topological argument was developed to address the subtleties of this move.

Example 9.3. Suppose we have a movie of $\mathbb{R}P^2$ as in Fig. 8.2 (a), with $m = 1$, $n = 2$, $s = t = 0$. There are several different ways to draw the edges of Γ_P and Γ_Q, so whenever we picture the graphs, we shall leave the relevant labels empty to account for the various possibilities. Let us now perform a swim of B_1 through B_2 as shown in Fig. 9.10, where we are picturing the swim as starting at the bottom of B_2 and moving upwards. The

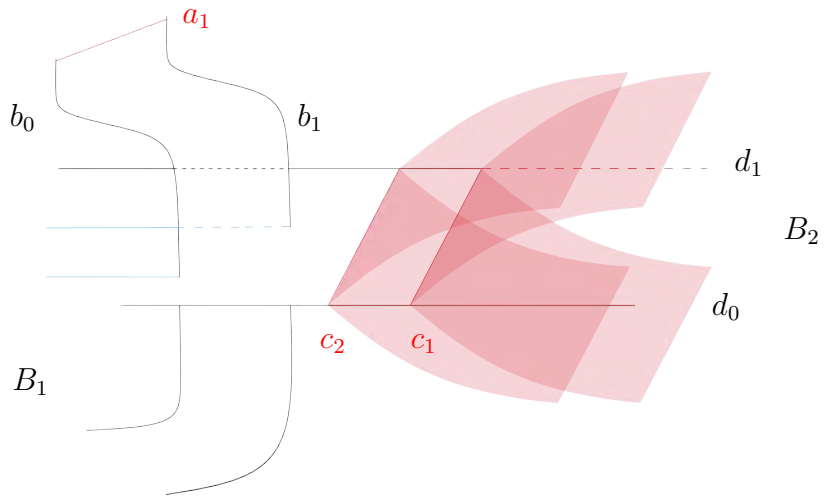

Figure 9.10: A close look at the swim of B_1 through B_2 in Example 9.3.

movie picture will now correspond to Fig. 8.2 (a) with $m = 5$, $n = 2$, $s = 0$, $t = 2$. We remark that, upon intersection with B_1, the fold from c_2 introduces a_2 and a_5, while the

fold from c_1 introduces a_3 and a_4. The labelling was chosen to be consistent with the usual notation. The graphs after the swim are represented in Fig. 9.11.

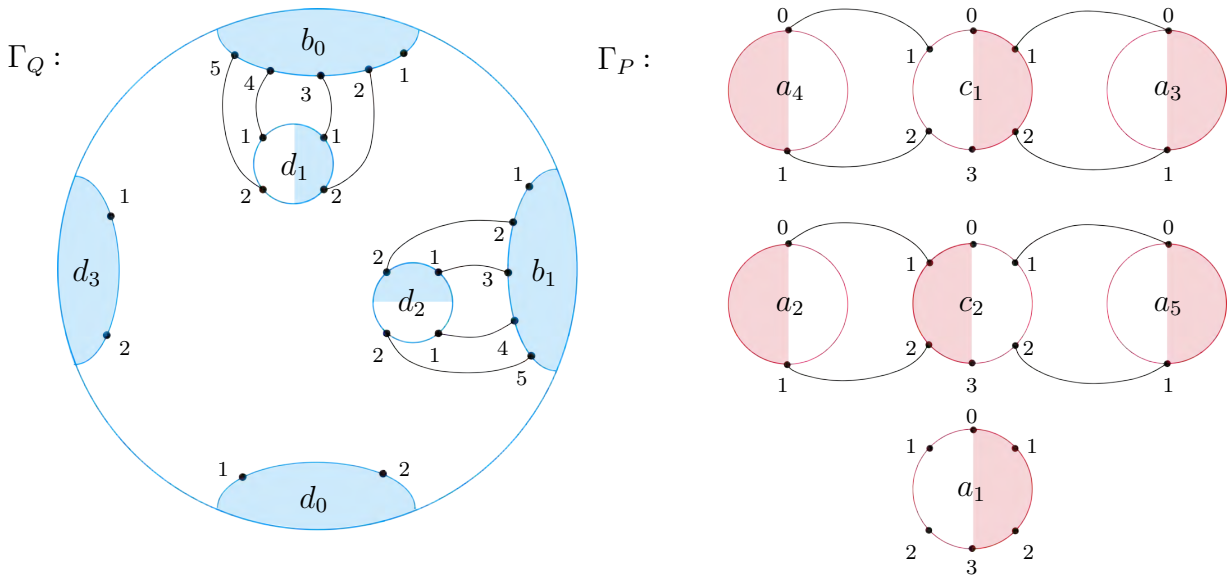

Figure 9.11: Graphs resulting from the swim of B_1 through B_2 in Example 9.3.

Once again, we observe that the swim has given rise to a collection of disc faces in P and Q, which together with portions of ∂M, allow us to construct two nested cubes. The inner cube C_I may be constructed using the two disc faces from Γ_Q contained between the labels 3 and 4, the two disc faces of Γ_P with boundary on c_1, and the relevant portions of ∂M (note that in this example they will be on the back of the manifold). Similarly, the outer cube C_O can be constructed by taking the disc faces from Γ_Q bounded by b_0 and b_1, contained between the labels 2 and 5 (ignoring the edges inside), together with the disc faces from Γ_P with boundary on c_2, and the relevant faces of ∂M (once again on the back). Both C_I and C_O are homeomorphic to an S^2 living in $\mathbb{R}^3$ (and more specifically in $\overline{\mathbb{R}^3 - M}$), therefore they bound nested 3-balls that are contractible. As in the previous example, it would be desirable for this contraction to guide the inverse swim. An additional layer of difficulty comes from the fact that we are working with nested cubes, so, for instance, one needs to understand topologically how a contraction of the 3-ball bounded by C_I guides a contraction of the 3-ball bounded by C_O, and which vertices of Γ_P and Γ_Q survive it.

Example 9.4. This final example is very similar to the previous one. Suppose we are working with the movie picture from Figure 8.2 (a) with $m = s = 1$, $n = 2$, $t = 0$. Suppose we swim B_1 through B_2, as shown in Fig. 9.10 with the addition of a fold coming from

b_1. After the swim, the movie picture will have $m = 5$, $n = 2$, $s = 1$, and $t = 4$ curves, and the graphs Γ_P and Γ_Q are shown in Figure 9.12. Note that in this case, we have assumed that the vertices d_2 and d_4 arise from disc sheets dragged by the sides of B_1, while d_1 and d_3 come from the fold associated with b_1 (and which in this case is pictured as folding towards d_0). In general, when dealing with cases where $s > 0$ (or $t > 0$), we will always have to choose how to partition the folds resulting from our curves to study the relevant graphs.

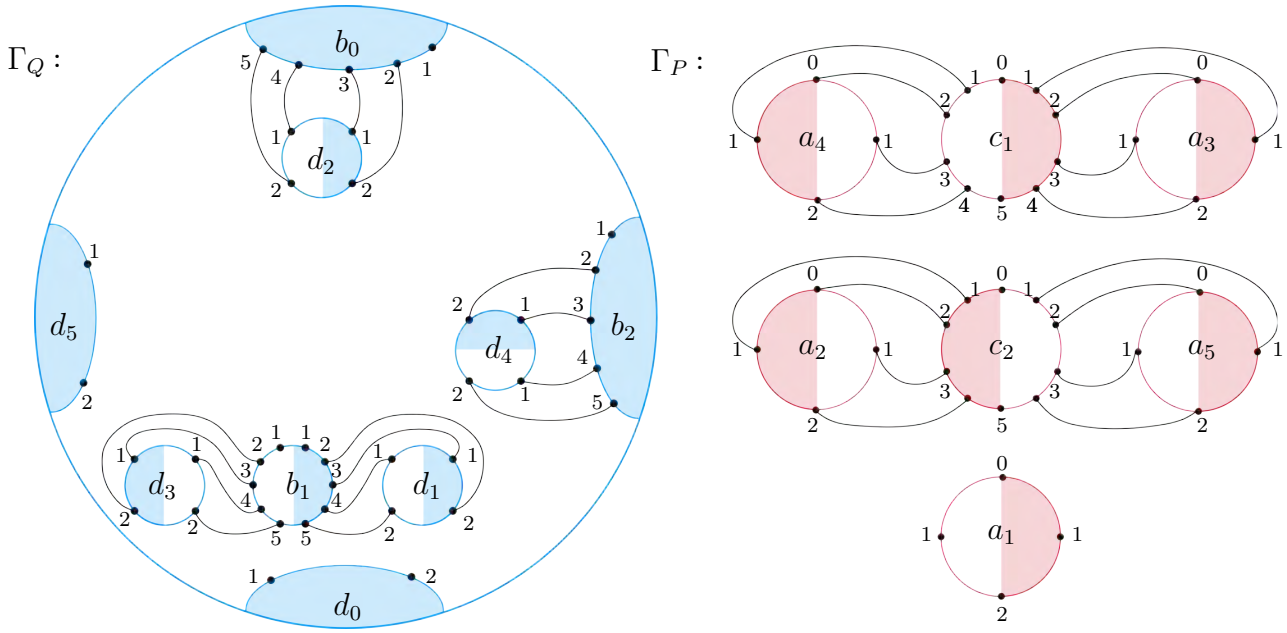

Figure 9.12: Graphs resulting from the swim of B_1 through B_2 in Example 9.4.

The graph Γ_P only differs from the one in Example 9.3 by the number of edges coming out of c_1 and c_2, due to the overall increased number of labels. The graph Γ_Q also differs from the previous example for the same reason (with vertices being relabelled) and for the fact that we have three new vertices, arising from b_1 and the intersections with Q introduced by the swim.

Following the principle of the previous examples, one can construct cubes living in $\overline{\mathbb{R}^3 - M}$. In this case we can construct more than just two cubes (and indeed we can construct 12 cubes): some of these are nested, while some others are intersecting each other. This adds further complications to the issue of understanding which cubes should guide the reduction of curves and how.

In general, swims will give rise to graph configurations similar to the ones shown in these

examples, with the only difference being the number of vertices and edges introduced. This means that in Γ_P (and often in Γ_Q) we expect to see two new vertices "coming out" of a central one, forming the triples we have seen in the various examples. Finally, it is interesting to observe that, while the concept of undoing a swim is less intuitive than the corresponding one for a slide, it seems easier to deduce that a swim has happened by examining the graphs.

§ 9.3 | Swims and Slides

Up to now, we have presented band slides and band swims individually, so the next step is to investigate their relation with each other. Based on the discussions from the previous sections, we can immediately remark that no combination of slides can represent a swim, and vice versa. Hence we cannot express one phenomenon in terms of the other. This reflects the fundamental distinction that swims are a local move, while slides are not, as they affect pre-existing edges and vertices in the graphs.

It is natural to ask whether swims and slides commute. The answer in general is negative, and it is easy to produce many examples proving this. However, there are some cases in which commutativity does hold.

Recall that a swim can be described by a framed arc. In $\mathbb{R}^3$ we can construct a 3-ball D_1 which contains this framed arc, as well as the width of the band swimming and the length of the band that is being swum through. Similarly, we can construct a 3-ball $D_2 \subset \mathbb{R}^3$ which contains the end of the band that is sliding, and the portion of the knot and band that are being slid on. The 3-balls D_1 and D_2 represent the support of the band swim and of the band slide, respectively. We have that the slide and swim commute if and only if their supports are disjoint. This means we need to be cautious when combining slides and swims, however understanding the occasions in which they do commute could be useful in working with the graphs.

Chapter 10

Strategy Behind Objective 8.1.2

In this chapter we outline the strategy employed to tackle the proof of Objective 8.1.2. The approach attempted was of the same flavour as the one presented in [10] and [64].

We begin by considering some specific cases for $\mathcal{R}_{m,n}$ and $\mathcal{B}_{s,t}$, arising on either M or N. For each of these cases, we discuss modifications of P and Q that eventually satisfy the conclusion of Objective 8.1.2. Afterwards, we wish to show that given any $\mathcal{R}_{m,n}$ and $\mathcal{B}_{s,t}$, it is possible to modify P and Q so that we are in one of the cases for which we know that Objective 8.1.2 holds. This is to be done via a proof by contradiction. Given any $\mathcal{R}_{m,n}$ and $\mathcal{B}_{s,t}$, we assume that no modification of P and Q can take us to one of the aforementioned cases. We would then wish to prove a series of topological and combinatorial results that lead to a contradictory statement.

The author did not manage to show that Objective 8.1.2 holds for each special case of $\mathcal{R}_{m,n}$ and $\mathcal{B}_{s,t}$ considered, on either M or N. In this chapter, we present the work undertaken and discuss the issues that prevented the completion of the proof.

§ 10.1 | Special Cases for M

§ 10.1.1 | Case $n = 0$, $s = 0$

We begin by proving that Objective 8.1.2 holds for M with $\mathcal{R}_{m,0}$, $m \geq 3$, and $\mathcal{B}_{0,t}$, shown in Figure 10.1. Consider the graph Γ_Q, where the only vertices presenting labels are b_0 and b_1. Suppose that Γ_Q contains no loops: then the only edges are parallel level edges between b_0 and b_1. In Γ_P, this corresponds to n vertices, with each one being the base of a loop. Then an innermost loop in Γ_P can be used to compress Q, replacing it by a new surface Q', which can be isotoped to have boundary disjoint from P. Observe that Q'

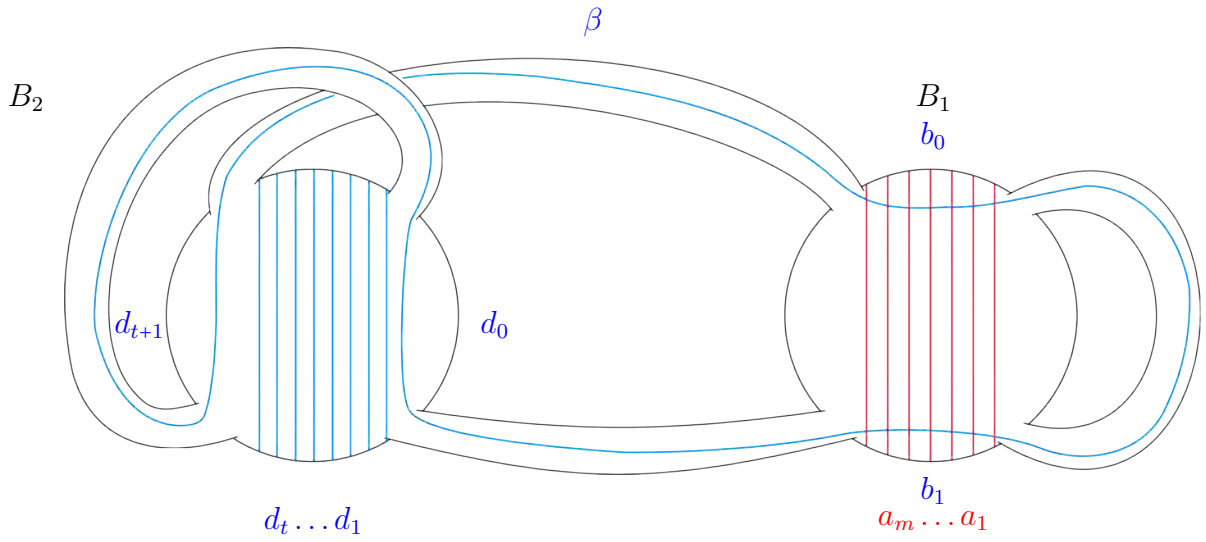

Figure 10.1: Manifold M with $\mathcal{R}_{m,0}$ and $\mathcal{B}_{0,t}$.

consists of the disjoint union of two possibly punctured discs, Q_1 and Q_2. Let Q_1 be the disc whose boundary is U_1 from Fig. 8.2 (a), and Q_2 the disc whose boundary is U_2 from the same figure. Since $n = 0$, we know that B_2 does not cross the separating sphere $\hat{P}$, therefore it stays in one component of $\overline{\mathbb{R}^3 - \hat{P}}$. Moreover, note that punctures in Q' arise from intersections of the surface with B_2, hence we must have that Q_2 is a punctured disc. Observe that if Q_1 had any punctures, these would arise from intersections of Q with either B_1 or B_2. Since B_2 does not intersect $\hat{P}$, and B_1 has $s = 0$, we deduce that Q_1 has no punctures. The band B_1 intersects $\hat{P}$ in m segments, and we know it does not intersect any component of the interior of Q', since $s = 0$. Then the band B_1 can be isotoped to intersect $\hat{P}$ only once and thus represent a cancelling pair of critical points together with the unknot U_1. Cancelling this pair, we obtain a movie picture of an $\mathbb{R}P^2$ with three critical points, which is standard by [10].

Suppose now that there are loops in Γ_Q. In this case, we may choose an innermost one, which will necessarily have labels k and $k+1$. If this loop contains no puncture in its interior, we can use the disc face it bounds in Q to compress P and reduce m by two. If the loop contains a puncture, then we can push it out by swimming B_1 through B_2 as described in Chapter 9 and then proceed to reduce m by two. This process can be iterated until we are left with $m = 1$, or we are forced to have all parallel level edges between b_0 and b_1, in which case we proceed as above.

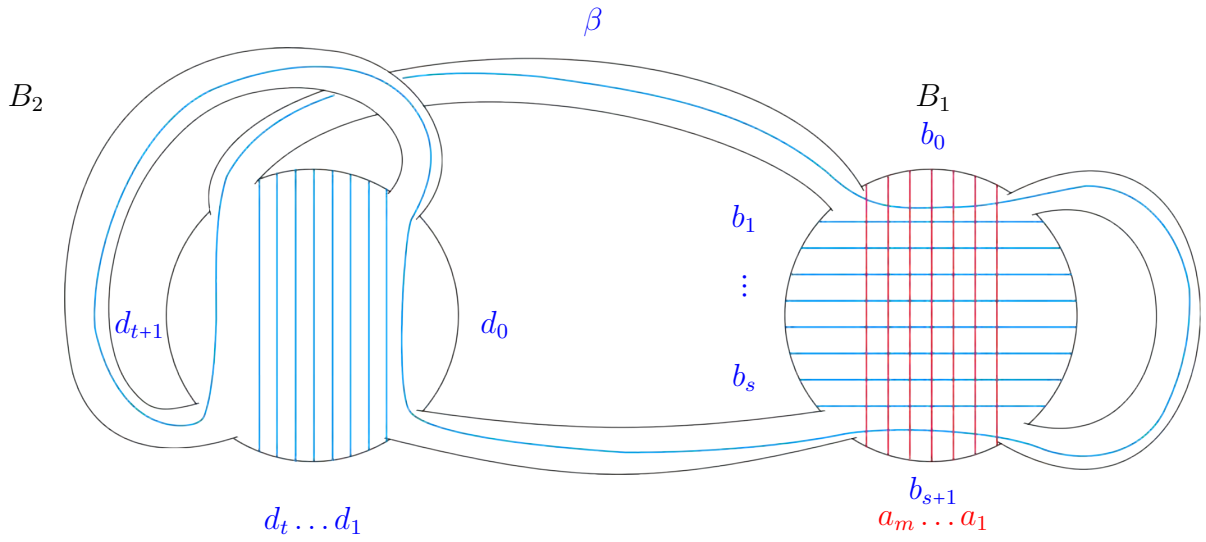

Figure 10.2: Manifold M with $\mathcal{R}_{m,0}$ and $\mathcal{B}_{s,t}$.

§ 10.1.2 | Case $n = 0$

This case is a generalisation of the previous one, represented in Figure 10.2. We shall assume that $\mathcal{R}_{m,0}$ and $\mathcal{B}_{s,t}$ are such that $m \geq 3$ and $s \geq 1$ (so that we are not in the previous case) and that $m + s$ is minimal, in the sense that there are no modifications of P and Q that can reduce this sum. We aim to relate this case to the general case discussed in [64], and use a proof by contradiction to show that $m + s$ can be reduced until Objective 8.1.2 is satisfied. Note that all the results about Γ_P and Γ_Q derived in this subsection only hold for this case.

We now present a list of results from [64] that remain valid in this case, with some minor modifications. It is important to note that this is only possible because the vertices of Γ_Q arising from B_2 are punctures.

Lemma 10.1. *Any loop in Γ_P or Γ_Q has interior vertices. Moreover, for a loop Γ_Q, we may suppose that at least one of the interior vertices is not a puncture.*

Proof. Suppose we have a loop in Γ_P or Γ_Q with no interior vertices. An innermost loop with this property has adjacent labels l and $l + 1$ (recall we cannot have level loops by Lemma 8.18). Then the disc face in the interior of the loop can be used to compress P or Q, reducing the value of m or s by at least one, contradicting the minimality of $m + s$.

If an innermost loop in Γ_Q contains a puncture in its interior, then it can be pushed out by swimming B_1 through B_2 appropriately. This process can be repeated as many times as needed, but it increases the value of t by at least $2s$. Once all punctures have

been pushed out of such a loop, we may compress P and reduce m by two, contradicting minimality of $m + s$ again. □

Corollary 10.2. *No vertex in Γ_P or Γ_Q is incident only to level edges.*

Proof. We begin by proving the statement for Γ_P. Suppose there is a loop in Γ_Q and choose an innermost one. By Lemma 10.1, we know it has at least two interior vertices that are not punctures (if we had only one such vertex, then it would be the base of another loop). Among these interior vertices, pick a vertex b_k which is not the base of any loop. Then for any a_i in Γ_P, the edges incident to the label k cannot be level. If Γ_Q contains no loop instead, then Γ_P contains no level edge.

The proof for Γ_Q is analogous. □

The result below is from [64, Proposition 4.7].

Proposition 10.3. *An innermost semi-cycle in Γ_Q contains at least one interior vertex which is not a puncture.*

Proof. We begin by considering an innermost semi-cycle. Suppose an innermost semi-cycle in Γ_Q only contains punctures at most. By Prop. 8.19, we know the semi-cycle contains no chords. Consider two edges of the circuit that are incident to the same vertex: their ends must have adjacent labels. Start at the head of an oriented edge and let $e_1, e_2, \ldots, e_{2r}$ be the label sequence. The latter satisfies all the hypotheses of Lemma 3.1 in [64]. Therefore, we know that the label sequence is composed of segments of at most two kinds:

(1) $(e_{2i}, \ldots, e_{2i+2}) = (k, k-1, k)$ of length three;

(2) $(e_{2i}, \ldots, e_{2i+4}) = (k, k, k-1, k-1, k)$ of length five,

where k is the highest label appearing in the semi-cycle. In particular, note that the semi-cycle presents only two labels, k and $k-1$. Let D be the interior of the semi-cycle: note that it is a potentially punctured disc face. Let P' be the surface obtained by attaching to P the annulus in ∂M between a_k and a_{k-1}. We have that ∂D is a simple closed curve crossing the annulus as many times as terms of type (1) appear in the label sequence, thus non-trivially. If the semi-cycle is not a loop, then we can use a homology argument as in Example 8.10 (ignoring the punctures) to obtain a contradiction. If the semi-cycle is a loop, then we can use a swim to push the punctures out and then use a

surgery argument as in Example 8.10 to contradict minimality of $m+s$. In any case, we conclude that an innermost semi-cycle in Γ_Q must contain interior vertices which are not punctures.

□

Proposition 10.4. *An innermost cycle in Γ_P has interior vertices.*

Proof. The proof of this exact statement is provided in [64, Proposition 4.8]. It is of the same flavour as the proof of the previous proposition, and makes use of the contradiction arising from the presence of Scharlemann cycles. Note that in this case we do not have to worry about punctures. □

Proposition 10.5. *Either there is a cycle in Γ_P or there is a cycle in Γ_Q.*

Proof. See [64, Proposition 5.1]. □

Proposition 10.6. *If an innermost cycle in Γ_P or Γ_Q has an interior vertex, it must have an interior source or sink.*

Proof. By Prop. 10.3 and 10.4, we know that any innermost cycle must have interior vertices (and in the case of Γ_Q we also know that they cannot all be punctures). Then it is possible to apply the proof of [64, Proposition 2.5 (3)] (a slightly modified version of which is presented in Prop. 8.20). □

Proposition 10.7. *The following are equivalent:*

(a) Γ_P *contains a cycle;*

(b) Γ_P *contains a sink or a source;*

(c) Γ_Q *contains an oriented loop;*

(d) Γ_Q *contains a cycle;*

(e) Γ_Q *contains a sink or a source on which no loop is based;*

(f) Γ_P *contains an oriented loop.*

Proof. See [64, Proposition 5.2]. □

From this point onwards, one can simply follow Scharlemann's article [64] step by step. The first difference in our case arises from the fact that Γ_Q lives on a disc and b_0 and b_{s+1} are split into two half-vertices. However, this does not prevent us from applying the same

arguments, and we have accounted for this difference in the results stated above. The second (and more prominent) issue arises from the presence of punctures in Γ_Q. However, using band swims, it is possible to adapt many of the original results as in this section, so that one may proceed with the combinatorial part of the argument.

The next step in [64] is to define a partial ordering on the vertices of Γ_P, which induces a partial ordering on the vertices of Γ_Q. Punctures are excluded from this process. Therefore, the combinatorial arguments in Section 6 of [64] are valid, and we will reach the point of proving that an innermost semi-cycle in Γ_Q has at most only punctures in its interior, contradicting Prop. 10.3. Hence, whenever we have $\mathcal{R}_{m,0}$ and $\mathcal{B}_{s,t}$ on M with $s \neq 0$, it is always possible to modify P and Q so that either we are in the case $\mathcal{R}_{m,0}$ and $\mathcal{B}_{0,t}$ discussed above, or $\mathcal{R}_{1,0}$ and $\mathcal{B}_{s,t}$. In either case, Objective 8.1.2 holds.

§ 10.1.3 | Case $s = 0$, $t = 0$

We shall prove that Objective 8.1.2 holds for $\mathcal{R}_{m,n}$ and $\mathcal{B}_{0,0}$, with $m \geq 1$ and $n \geq 2$, shown in Figure 10.3. We assume there are no loops in Γ_Q, because if there were they would guide a reduction of curves until we are in one of the situations below.

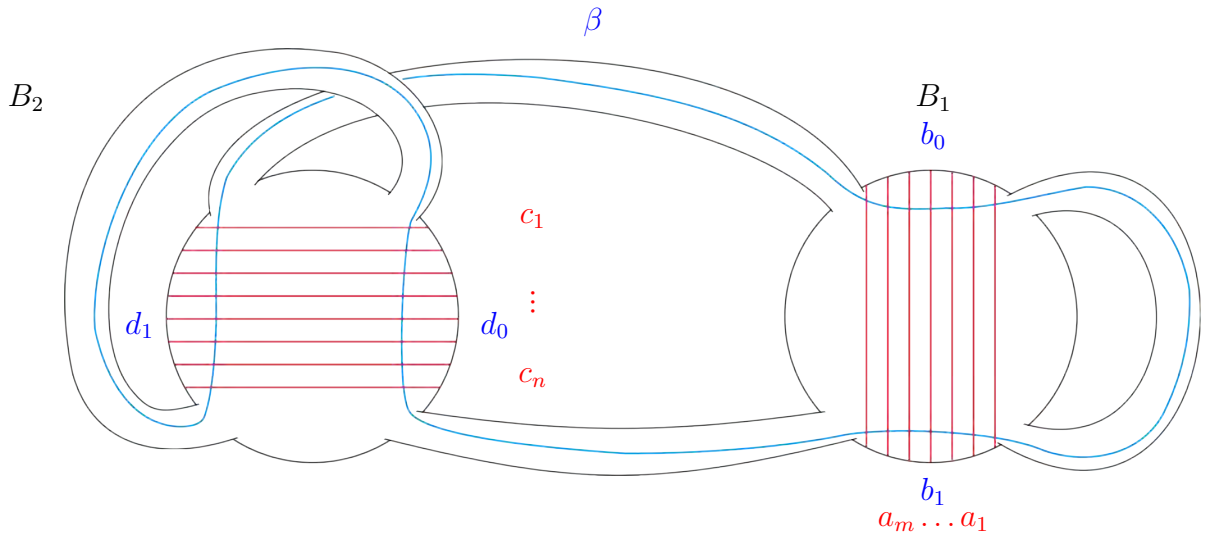

Figure 10.3: Manifold M with $\mathcal{R}_{m,n}$ and $\mathcal{B}_{0,0}$.

Focus on Γ_Q and consider the situation in which all edges with one end on b_0 have the other end on b_1, and similarly, all edges on d_0 terminate on d_1. Hence, all edges with the same ends are parallel. Note that those with ends on b_0 and b_1 are parallel level edges, so they correspond to loops in Γ_P. However, at this stage, we cannot ensure that at least one of these loops bounds a disc face of P, because their interiors might contain circuits

consisting of the vertices from B_2. Therefore, we cannot guarantee that these loops can be used to reduce the number of curves of $\mathcal{R}_{m,n}$. Note that the edges between d_0 and d_1 have ends labelled l and $n-l+1$ for $1 \leq l \leq n$. Then we can find a Scharlemann cycle with labels $[\frac{n}{2}, \frac{n}{2}+1]$ and we can iteratively apply the surgery argument of Chapter 8 until we obtain $n = 0$ and are left only with level edges between b_0 and b_1. Now Γ_P consists of m vertices each the base of a loop, so we can find an innermost one bounding a disc face of P and use it to compress Q as in the case $n = 0$, $s = 0$.

Now assume that each edge with an end on b_0 has the other end on d_1, and that those with an end on b_1 have the other end on d_0.

If $m < \frac{n}{2}$, then we can find a Scharlemann cycle between d_0 and d_1 with labels $[\frac{n}{2}, \frac{n}{2}+1]$ and use a surgery argument like in the previous case to reduce n until $m = \frac{n}{2}$.

Assume this is the case and that b_0 is connected to d_1 by parallel edges, while b_1 is connected to d_0 in the same way, as shown in Figure 10.4.

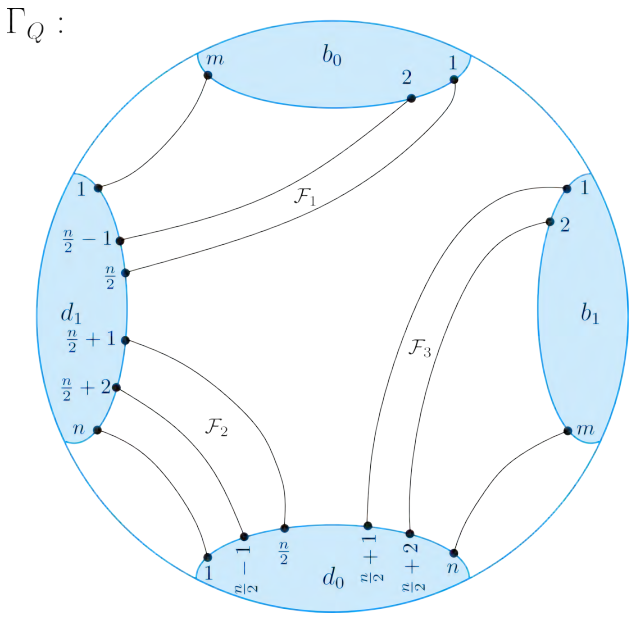

Figure 10.4: A configuration of Γ_Q when $s = 0$, $t = 0$, $m = \frac{n}{2}$ on M.

Then we will always find a Scharlemann collection $\{\mathcal{F}_1, \mathcal{F}_2, \mathcal{F}_3\}$ of three disc faces. The face $\mathcal{F}_1$ has labels $[1,2]$ on b_0 and $[\frac{n}{2}-1, \frac{n}{2}]$ on d_1; $\mathcal{F}_2$ has labels $[\frac{n}{2}-1, \frac{n}{2}]$ on d_0 and $[\frac{n}{2}+1, \frac{n}{2}+2]$ on d_1; finally, $\mathcal{F}_3$ has labels $[1,2]$ on b_1 and $[\frac{n}{2}+1, \frac{n}{2}+2]$ on d_0. However, these faces are linearly dependent in the sense that they cannot be used as in Example

8.13 to construct a sub-manifold of $\mathbb{R}^3$ of codimension 0 with non-trivial torsion in first homology, and obtain a contradiction. At this point we can focus on the underlying movie picture and slide B_2 along the bottom of B_1 as in Figure 10.5 (a), introducing m new curves on B_2 and m loops in Γ_Q. Note that after sliding, we are working with N

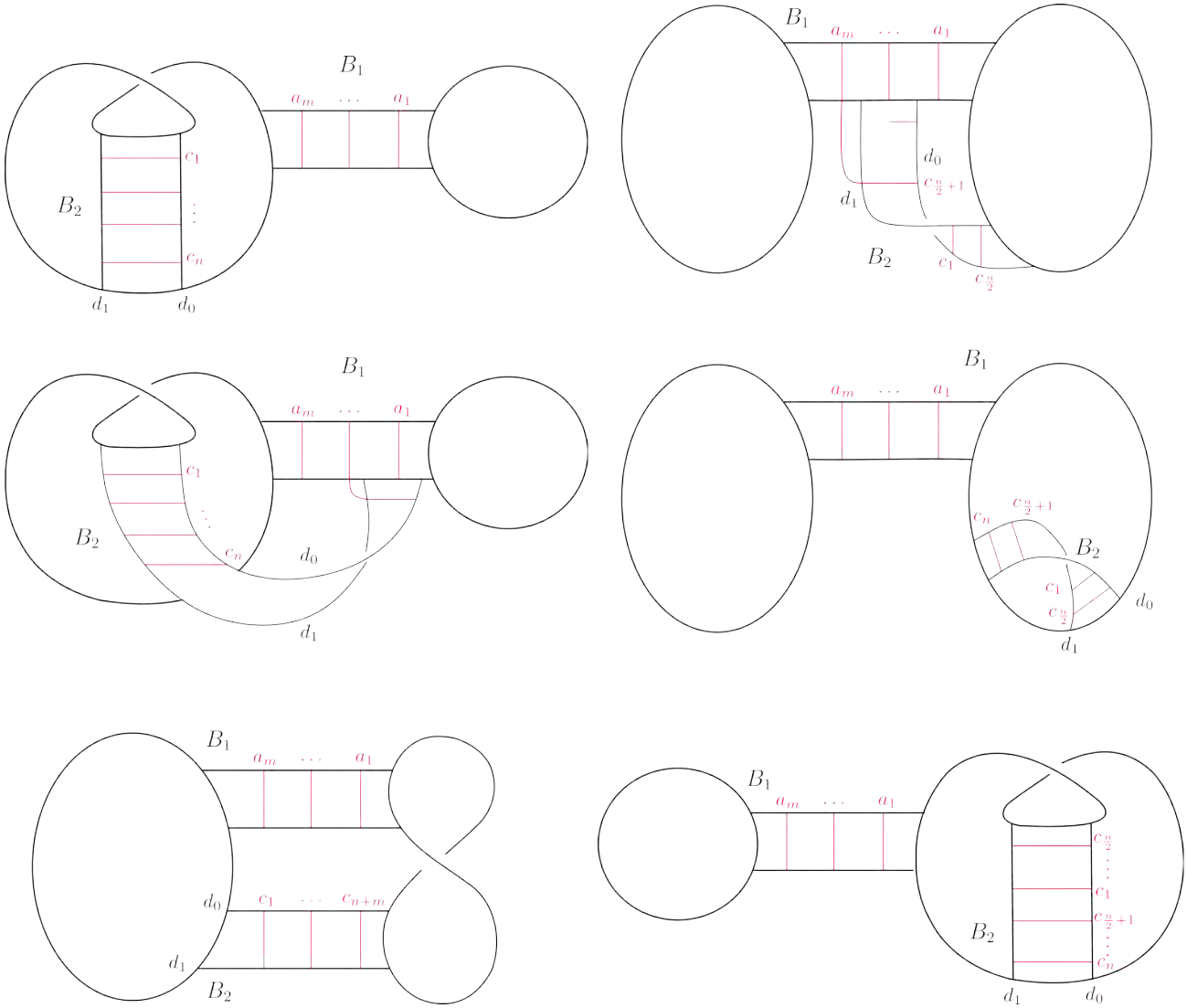

Figure 10.5: Sliding the bottom of B_2 over the bottom of B_1 (a), and sliding the left end of B_2 over the bottom of B_1 (b).

and its underlying movie picture, hence this shows that we cannot ignore one manifold completely in favour of the other, as there is a level of interdependency between them due to band sliding. The m loops introduced by the slide are based at d_0, as shown in Figure 10.6 (a), and can be used to reduce the number of curves on B_2 to $\frac{n}{2}$. The graph Γ_Q (now arising from N) after the reduction contains parallel edges between b_0 and d_1 and

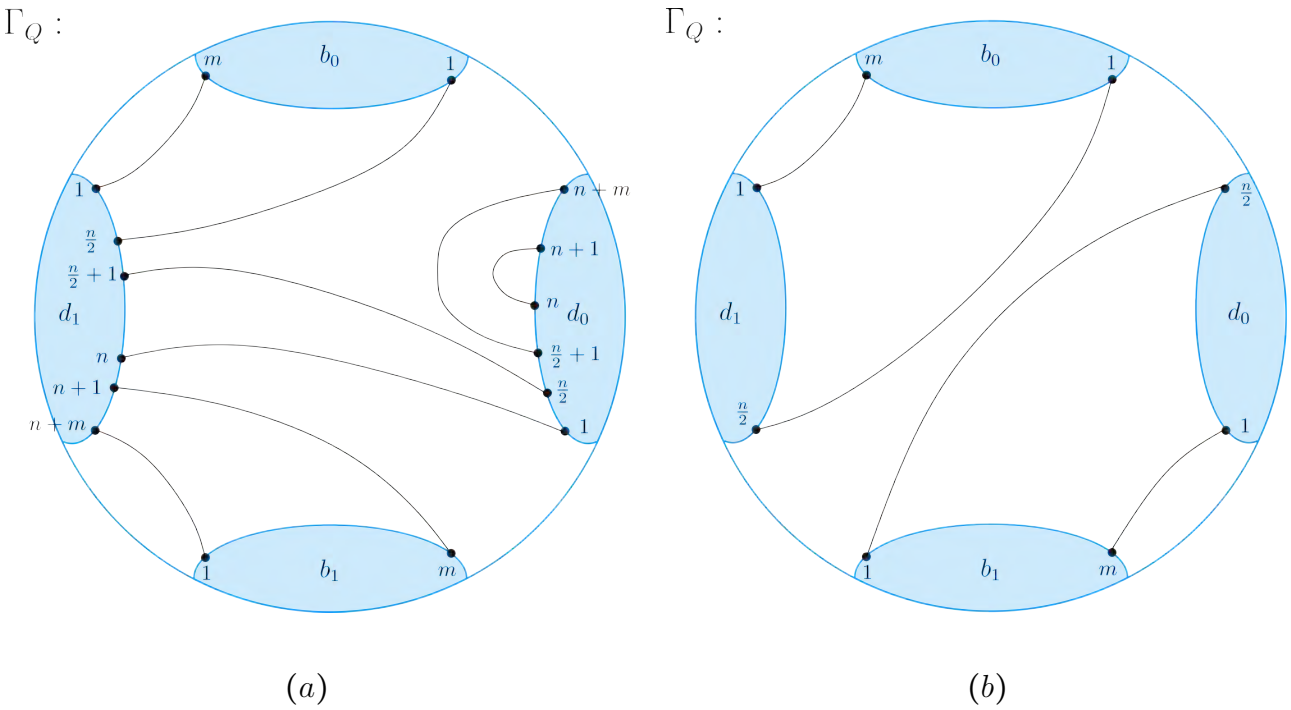

Figure 10.6: The graph Γ_Q after performing the first slide from Fig. 10.5 (a); the graph Γ_Q after using loops to reduce labels (b).

between b_1 and d_0, and is shown in Figure 10.6 (b). Once again, we can find a Scharlemann collection $\{\mathcal{F}_1', \mathcal{F}_2'\}$ of disc faces such that $\mathcal{F}_1'$ $(\mathcal{F}_2')$ has labels $[1, 2]$ from b_0 (b_1) and $[\frac{n}{2} - 1, \frac{n}{2}]$ from d_1 (d_0). This collection cannot be used to construct a 3-manifold with non-trivial torsion in its first homology. Thus, slide the left side of B_2 over the bottom of B_1 as in Figure 10.5 (b) and obtain a manifold mirroring M. During this process B_2 picks up m curves from B_1 and Γ_P presents m loops based at d_0. The graph Γ_Q is shown in Figure 10.7 (a). After reducing the loops, we eliminate all curves on B_2 and are left only with parallel level edges between b_0 and b_1, as shown in Figure 10.7 (b). At this point, the graph Γ_P consists of m vertices, each the base of a loop. We can find an innermost one bounding a disc face of P and use it to compress Q as in the case $n = 0$, $s = 0$.

Now consider the case $\frac{n}{2} < m < n$ and continue assuming that each label on b_0 is joined to a label on d_1, while each label of b_1 is joined to a label of d_0. Note that there will be $n-m$ edges between d_0 and d_1, but no Scharlemann cycle can arise between these vertices because $m > \frac{n}{2}$. Consider the movie picture underlying M and slide B_2 along the bottom of B_1. After the slide, we obtain a movie underlying N, and B_2 picks up m additional curves. Note that this induces m loops based at d_0: these can be used to reduce the labels on d_0 until we are left with $n - m$ of them. We remark that $0 < n - m < \frac{n}{2}$, and if

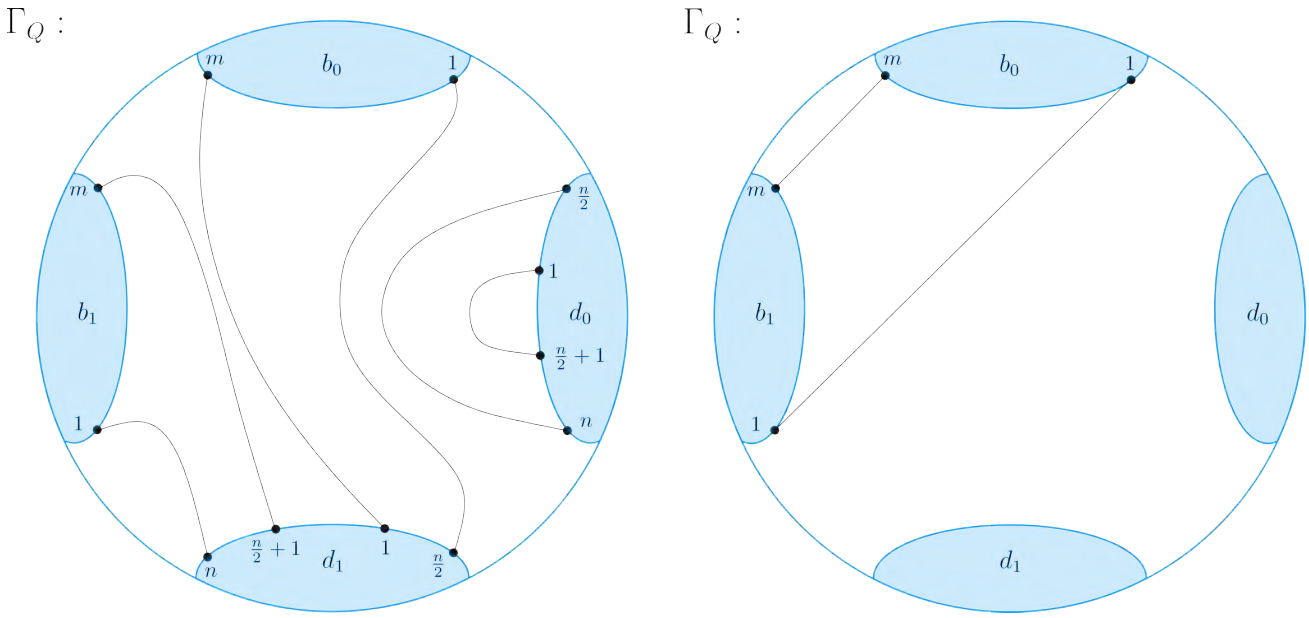

Figure 10.7: The graph Γ_Q after performing the second slide from Fig. 10.5 (a); the graph Γ_Q after using loops to reduce labels (b).

$n-m=1$ then we already satisfy Obj. 8.1.2 for N. After reducing the loops (assuming $n-m\neq 1$), we are left with $2m-n$ edges between b_0 and b_1 (note that these are even), with ends labelled k and $2m-n-k+1$. The remaining labels of b_1 are joined to d_0, while those of b_0 are joined to d_1. At this point, note that we must have a Scharlemann cycle between b_0 and b_1 with labels $m-\frac{n}{2}$ and $m-\frac{n}{2}+1$. The surgery argument can be applied repeatedly until we are left with no edges joining b_0 and b_1. The only edges of Γ_Q are now between b_0 and d_1, and b_1 and d_0. Note that all vertices now have the same number of labels, namely $n-m$. Observe that this is now an instance of the case $s=0$, $t=0$ with $m'=n'$ (in this instance $m'=n'=n-m$) for the manifold N, showing how interdependent these configurations are. How to approach the reduction of curves from this point onwards can be found in the section for the corresponding case for N.

Now suppose that $m>n$ and that every edge with an end on d_1 (d_0) has the other end on b_0 (b_1), leaving $m-n$ (odd) edges between b_0 and b_1. Slide B_2 along the bottom of B_1 to get to the movie picture for N. Now B_2 has $n+m$ curves with n loops: these can be reduced until B_2 only has $m-n$ curves. After the reduction, there are n (even number of) edges between b_0 and b_1, with labels k and $2m-k-n+1$, for $m-n+1\leq k\leq m$. Once again, this means we can find Scharlemann cycles with labels $[m-\frac{n}{2}, m-\frac{n}{2}+1]$, which

can be used to reduce the labels of b_0 until there are $m-n$ left. After this reduction, we are in the case $s=0$, $t=0$ for N, discussed in the relevant subsection.

Let us now consider the most general configuration in this case, assuming there are no loops in Γ_Q. This is shown in Figure 10.8. We are assuming there are e edges between b_0 and d_1, and consequently between b_1 and d_0. Then there are $m-e$ edges between b_0 and b_1, and $n-e$ edges between d_0 and d_1. Let us assume that $n>m>e$ and that $e \geq \frac{n}{2}$. The latter condition is to exclude the existence of Scharlemann cycles between d_0 and d_1, which would enable us to reduce n until this condition is satisfied. The case $m>n>e$ is symmetric, hence shall not be discussed. Note that the cases $e=m$ and $e=0$ have already been discussed.

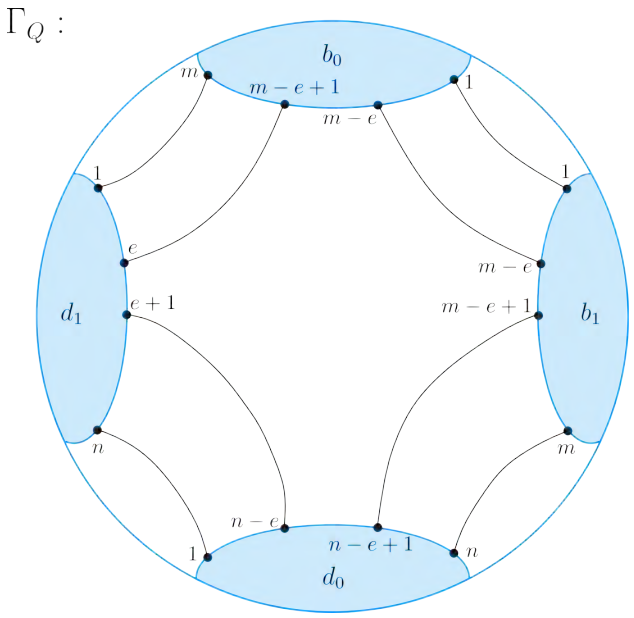

Figure 10.8: A general configuration of Γ_Q when $s=0$, $t=0$ on M.

Once again, we slide the bottom of the band B_2 along the bottom of B_1 to obtain a movie picture for N, as in Fig. 10.5 (a). After the slide, B_2 has $n+m$ curves, $2e$ of which correspond to labels paired into loops based at d_0. The graph Γ_Q after the slide is shown in Figure 10.9. The Slide Example in Chapter 9 is useful towards understanding how edges are created or modified. Observe that we still have $n-e$ edges between d_0 and d_1 with no Scharlemann cycle. Starting from the innermost one, the loops at d_0 guide a reduction of $2e$ labels, which shall simultaneously disappear from d_1 as well. The result of this reduction is shown in Figure 10.10 (a). Let us think about what happens to the loop with ends n and $n+1$: it bounds a disc in Q which can be used to compress P, eliminating the labels

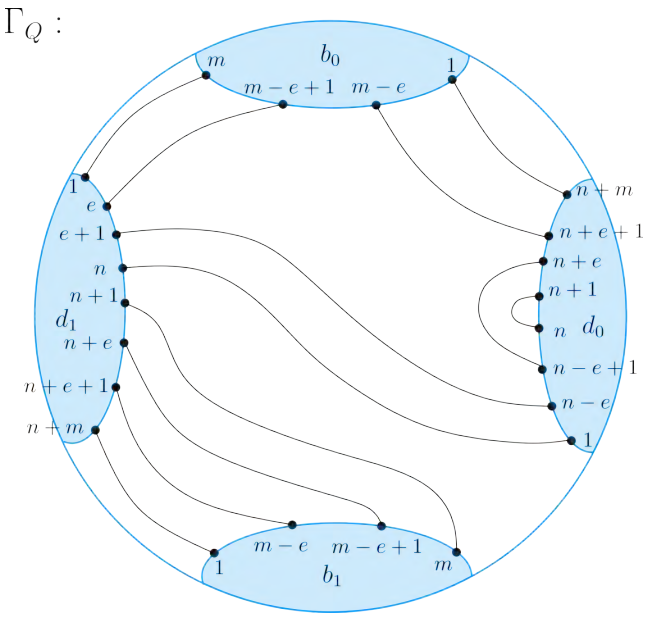

Figure 10.9: The graph Γ_Q of Fig. 10.8 after performing a band slide to N.

n and $n+1$; these labels also disappear from d_1, and the edges ending on said labels on d_1 are then joined together; this process is iterated for every loop. In particular, observe that the lowest label to disappear on d_1 is $n-e+1$: since $e \geq \frac{n}{2}$, then $n-e+1 \leq \frac{n}{2}+1 \leq e+1$, so the edges between d_1 and b_0 may be modified as well, introducing some edges between b_0 and b_1. When this is the case we have $2e-n$ (an even number of) edges between b_0 and b_1, with ends labelled k and $2m-n-k+1$. Note that this implies the existence of a Scharlemann cycle with labels $[m-\frac{n}{2}, m-\frac{n}{2}+1]$, allowing the reduction of two labels on b_1 and b_0. This process can be iterated until there are no edges left between b_0 and b_1. After performing all the reductions we may relabel the graph Γ_Q as in Figure 10.10 (b).

At this point we may slide the left end of B_2 along the bottom of B_1, as in Figure 10.5 (b), which will take us to a configuration that is symmetric to that of Fig. 8.2 (a). Consequently, we shall work with a manifold that mirrors M, and this is reflected in Γ_Q, shown in Figure 10.11 (a). After the slide, B_2 has $2n+2m-4e$ curves, $n-e$ loops based at d_0, and $m-e$ edges between d_0 and d_1. We remark that the labels of B_2 now do not appear completely in order: this is because the band slide introduces the new curves on the left of c_1. As in previous cases, the loops may be reduced so that Γ_Q appears as in Figure 10.11 (b). At this point observe that b_0 and b_1 have $m+n-2e \leq m$ labels, while d_0 and d_1 have $2m-2e < n$ labels. The combination of slides discussed can thus be iterated until we are left with no curves on B_2 and eventually with one curve on B_1, satisfying Objective 8.1.2.

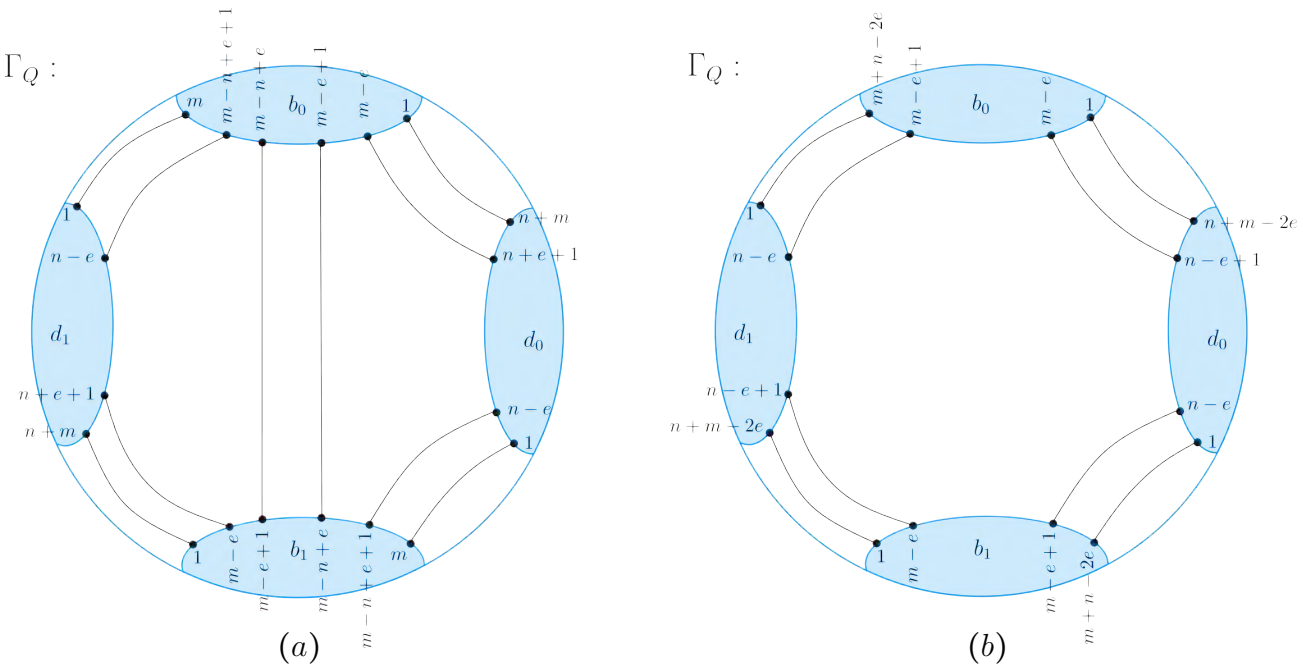

Figure 10.10: The graph Γ_Q of Fig. 10.9 after reducing loops (a) and after reducing Scharlemann cycles and relabelling (b).

§ 10.1.4 | Case $s = 0$

This case, represented in Figure 10.12, is a generalisation of the one presented in the previous section. As for the case $n = 0$, we would wish to develop an argument (perhaps even directly appealing to [10, 64]) to prove that whenever $t \geq 1$, this configuration can always be reduced to one of the cases already discussed, via appropriate modifications of P and Q. This scope was not reached. The main challenge was the fact that the vertices in Γ_P coming from B_1 are not punctures. Consider an innermost cycle or semi-cycle in Γ_P which contains interior vertices. These vertices can come from either B_1 or B_2 (or both), and we must have either a source or a sink. However, the fact that we are potentially working with interior vertices from different 3-balls is not enough to guarantee the existence of a loop in Γ_Q. In the case $n = 0$ (and in [10, 64]), the existence of a source or a sink is enough to imply the existence of a loop in the other graph and continue the argument. This implication does not necessarily hold in this case.

There are two ideas worth exploring to tackle this case.
The first one is to reduce m to 1 using slides: we would like to repeatedly slide B_1 over B_2, end up in a configuration that is either M or mirrors it, and pick up a number $n_l \leq n$ of loops which can be used to reduce the curves of B_1 by $2n_l$ until we are left with only one and satisfy Objective 8.1.2. One key problem with this approach is that we cannot

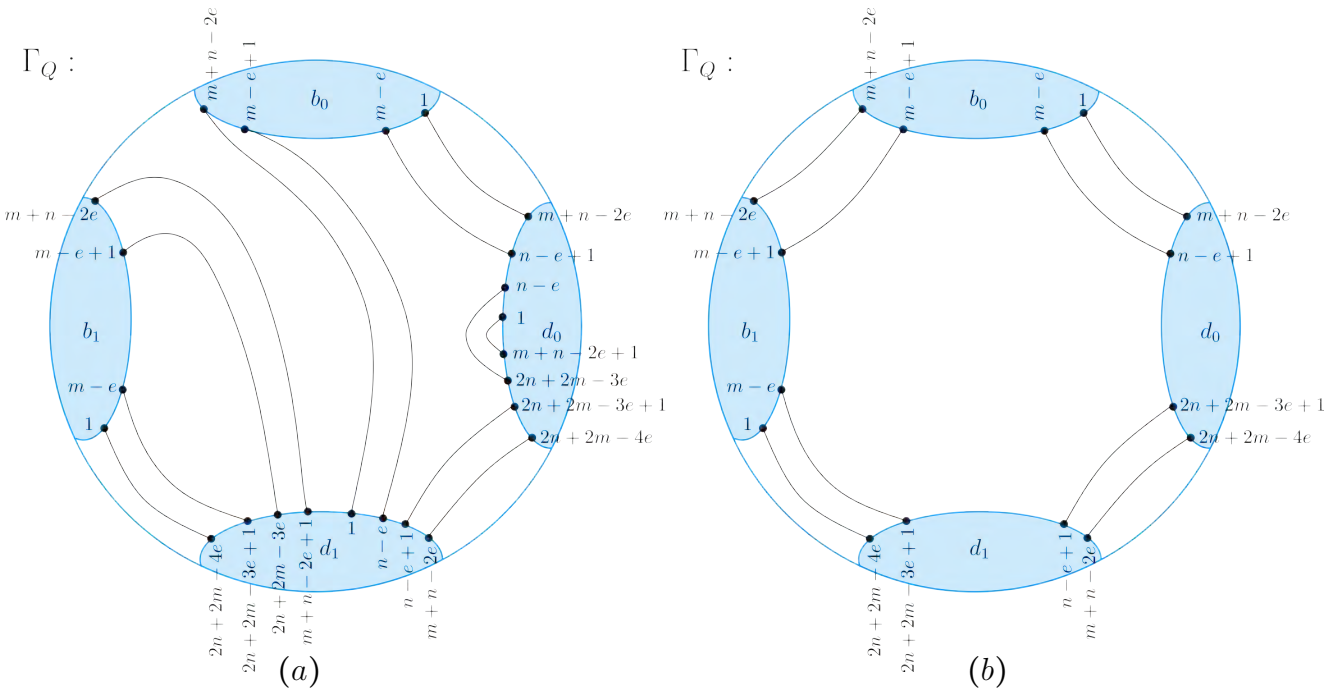

Figure 10.11: The graph Γ_Q of Fig. 10.9 after sliding (a) and reducing loops (b).

determine which way B_1 should slide over B_2, nor how (or whether) the required loops arise. This is because we have no a priori restrictions on the configurations arising from the graphs.

The second idea worth considering involves trying to follow as closely as possible the work by Bleiler–Scharlemann in [10]. This would involve interpreting b_0 and b_1 from Γ_Q as the "bad vertices" described in [64]. If this were possible, then we would work towards proving that such a configuration can always be reduced to one of the previous cases, either $n = 0$ or $t = 0$.

§ 10.1.5 | Case $t = 0$

This case is symmetric to the one discussed in the previous subsection, and it presents the same problems. Once again, there are two ideas to explore.

We can consider using band slides to make $n = 0$. We would then be left with a situation almost analogous to the one in [64], wanting to prove that P and Q can be modified such that either $m = 1$ or $s = 0$. Alternatively, we can try to follow Bleiler–Scharlemann and interpret d_0 and d_1 in Γ_Q as the "bad vertices" in [10].

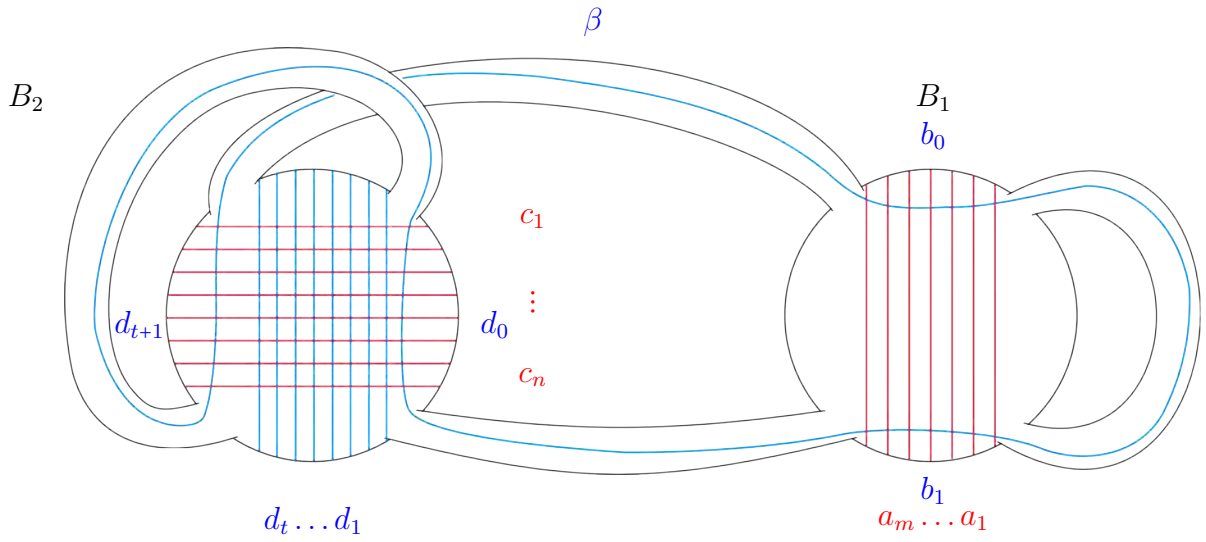

Figure 10.12: Manifold M with $\mathcal{R}_{m,n}$ and $\mathcal{B}_{0,t}$.

In either case, the problems arising are the same discussed in the previous subsection.

§ 10.2 | Special Cases for N

The symmetric nature of the manifold allows us to reduce the number of cases to consider. We would like to show that in the case $s = 0$ (or $t = 0$), P and Q can be modified so that we may have either $m = 1$ ($n = 1$) or $t = 0$ ($s = 0$). The issues arising are the same discussed for M, hence this case remains unsolved.

Below, we discuss the case $s = 0$, $t = 0$. The approach employed is analogous to the one discussed for M.

§ 10.2.1 | Case $s = 0$, $t = 0$

The manifold N with $s = 0$, $t = 0$ and $m \geq 1$, $n \geq 1$ is shown in Figure 10.13. The approach to this case once again relies on band sliding. Assume that there are no loops in Γ_Q, because if there were, they could be used to reduce labels until we are in one of the situations below.

Suppose that $m = n$ and that each edge with one end on b_0 (b_1) has the other end on d_1 (d_0).
We can slide the left end of B_2 along the bottom of B_1 to obtain a knot configuration that is symmetric to that of Fig. 8.2 (a) (Figure 10.5 (b) provides a helpful reference for the band slide). During the slide, B_2 picks up m curves, and afterwards we introduce $2m$ loops on d_0. Starting from an innermost one, we can use these loops to reduce all the

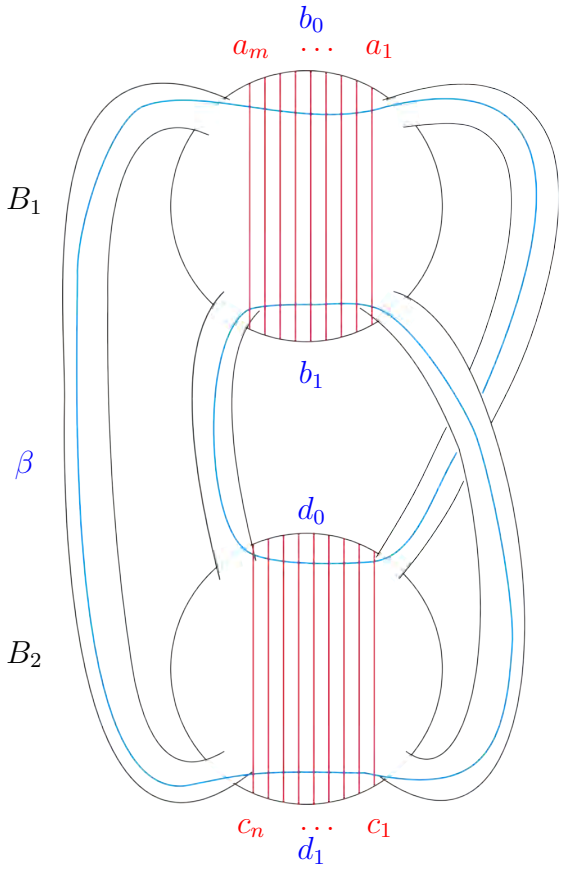

Figure 10.13: Manifold N with $\mathcal{R}_{m,n}$ and $\mathcal{B}_{0,0}$.

labels of d_0 until there are none left. The result of this operation is that Γ_Q now only consists of a series of parallel level edges between b_0 and b_1, which correspond to loops in Γ_P. The configuration is equivalent to the one for M when $n = 0$, $s = 0$, hence we know that Objective 8.1.2 is satisfied. Observe that if we instead assumed the edges of Γ_Q to be connecting b_0 (b_1) and d_0 (d_1) the proof would work in the same way, sliding in the opposite direction.

Suppose that $m > n$ and that edges from d_1 (d_0) end on b_0 (d_1). Note that there is an even number of $m - n$ edges between b_0 and b_1, with labels k and $m - n - k + 1$. Then, there exists a Scharlemann cycle with labels $[\frac{m-n}{2}, \frac{m-n}{2} + 1]$, which can be used to reduce the labels of b_0 by 2. This process can be applied iteratively until the number of labels of b_0 is the same as d_0, and we are thus in the situation discussed for the previous case. This argument works analogously if we assume that the edges from d_1 (d_0) join b_1 (b_0). The case $m < n$ is symmetric to the one just discussed.

Finally, let us consider a general configuration for this case shown in Figure 10.14. We assume there are no loops in Γ_Q and no Scharlemann cycles, hence we must have $m = n$. Note that there are e edges between b_0 (b_1) and d_1 (d_0), and without loss of generality, we may assume that $e \geq \frac{m+1}{2}$. We expect to tackle this case by performing a series of band

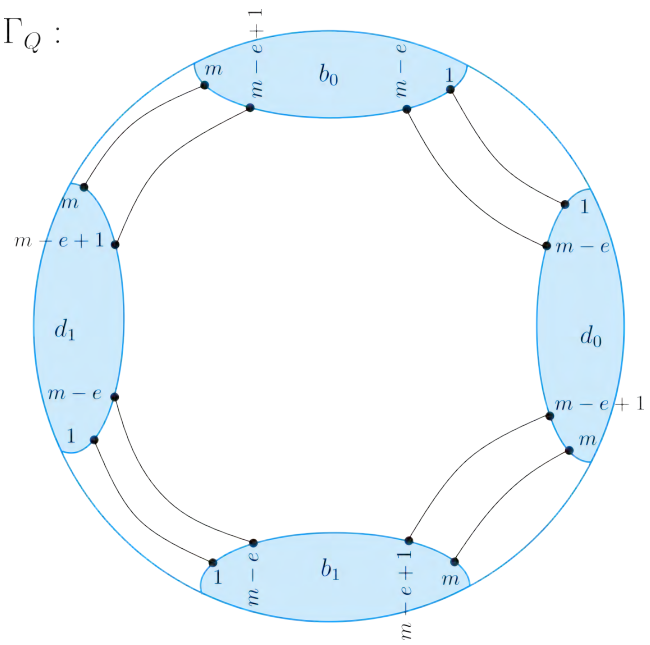

Figure 10.14: A general configuration of Γ_Q when $s = 0$, $t = 0$ on N.

slides, as in the analogous one for M. Indeed, we can prove that Objective 8.1.2 holds for this case by simply sliding to the general configuration for M when $s = 0$, $t = 0$ and reduce the boundary components of P and Q from there, using the methods previously discussed.

Chapter 11

Conclusion

§ 11.1 | Previous Attempt

In this section, we discuss our initial approach to the $\mathbb{R}P^2$ problem, highlighting some of the issues arising from it and that led to the set-up discussed in previous chapters. In this framework, the aim remains to prove Objective 8.1.1. In particular, we are still working with the movie configurations arising from Figure 8.2, which involve a 2-component unlink, two bands, and an unknot resulting from the band attachments. The manifolds M and N arise as the regular neighbourhoods of these movie pictures, so they remain the same in this case as well. The difference involves the planar surfaces whose intersections we want to analyse.

Keeping in mind Fig. 8.2, we consider the discs D_A bounded by U_1, D_B bounded by U_2, and D_C bounded by the unknot resulting from U_1 and U_2 with B_1 and B_2 attached. The bands from Fig. 8.2 may intersect these discs in many different ways. These intersections are recorded as segments on the bands in the movie pictures, and as embedded simple closed curves on the boundaries of M and N in the familiar way.

Let $\mathcal{A}_{m,n}$ be the family of simple closed curves consisting of $\alpha, a_1, \ldots, a_n, a_{n+1}, \ldots, a_m$, shown in Figures 11.1 on M and 11.2 on N. This family is the boundary of the surface A obtained by puncturing the disc D_A. Similarly, the family $\mathcal{B}_{p,q}$ consists of $\beta, b_1, \ldots, b_p, b_{p+1}, \ldots, b_q$, and is the boundary of B, the surface obtained after puncturing D_B. Finally, $\mathcal{C}_{s,t}$ consists of $\gamma, c_1, \ldots, c_s, c_{s+1}, \ldots, c_t$, and is the boundary of C, the surface obtained after puncturing D_C. Observe that A, B, and C are oriented planar surfaces in $\overline{\mathbb{R}^3 - M}$ (or $\overline{\mathbb{R}^3 - N}$), and that there are no parity requirements on the number of curves

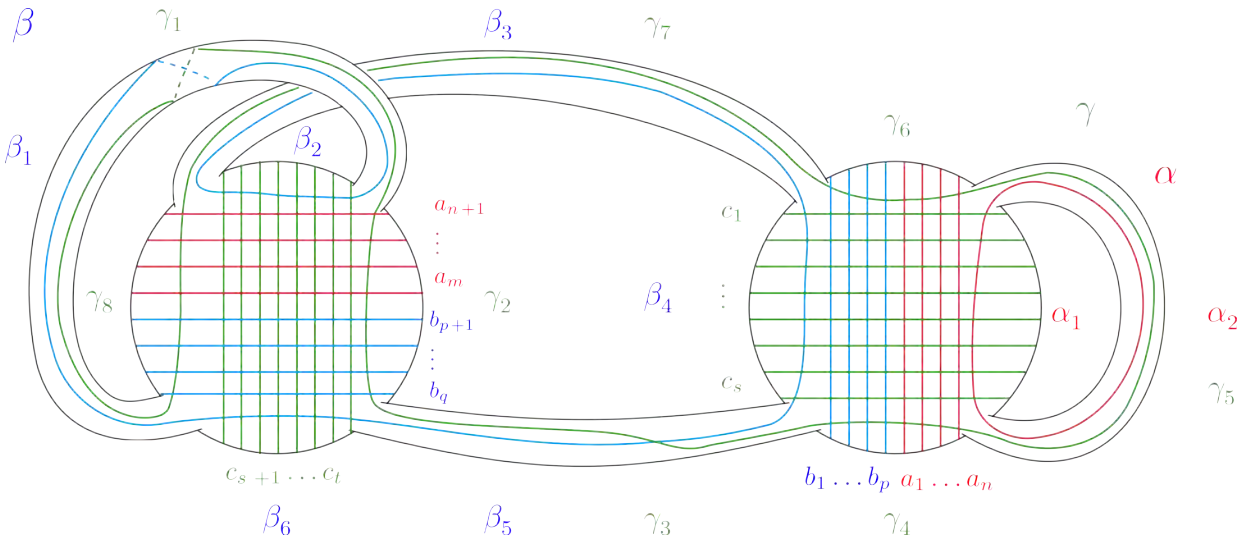

Figure 11.1: Manifold M with $\mathcal{A}_{m,n}$, $\mathcal{B}_{p,q}$, $\mathcal{C}_{s,t}$ from first approach.

from each family, since we are not considering any separating surface this time. Finally, it is vital to note that we have no control over the order in which curves from $\mathcal{A}_{m,n}$ and $\mathcal{B}_{p,q}$ appear on B_1 and B_2. In Figures 11.1 and 11.2, these curves are presented as always adjacent to curves of the same family (except in the extremal cases), but this is simply a stylistic choice of representation to illustrate the indices of these curves, and should in no way be thought of as a representation of a general case.

Already at this point, some complications arise. We need to formulate an objective to prove, similar to Obj. 8.1.2, but it is not immediately clear what this objective should be. One possibility considered is stated below.

Objective 11.1.1 (Old Objective)**.** *Suppose that M is embedded in $\mathbb{R}^3$ in such a way that some $\mathcal{A}_{m,n}$, $\mathcal{B}_{p,q}$, $\mathcal{C}_{s,t}$ as above bound planar surfaces A, B, and C in $\overline{\mathbb{R}^3 - M}$. Then it is possible to modify the planar surfaces so that they are respectively bounded by $\mathcal{A}_{0,0}$, $\mathcal{B}_{0,0}$, $\mathcal{C}_{0,0}$.*

The issue with this objective is that we might be imposing a condition that is too strong on the families of curves (one can compare this with Obj. 8.1.2 to get a sense of it). However, it is not clear how to relax the requirement imposed and still obtain families $\mathcal{A}_{m,n}$, $\mathcal{B}_{p,q}$, $\mathcal{C}_{s,t}$ that can be of help in the proof of Objective 8.1.1. It also seems possible that one might have to consider different cases based on the family of curves whose requirements one wishes to relax.

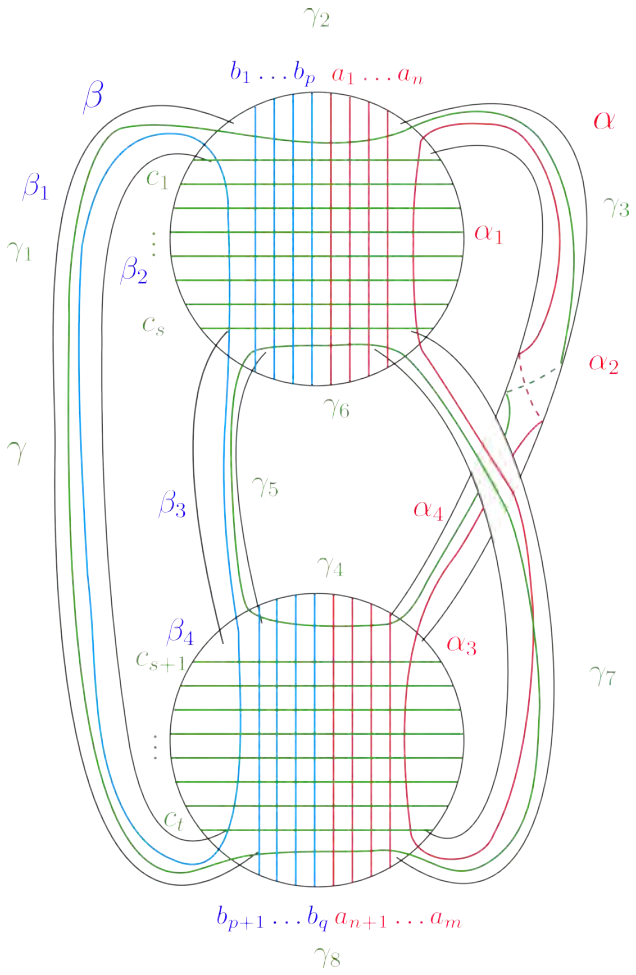

Figure 11.2: Manifold N with $\mathcal{A}_{m,n}$, $\mathcal{B}_{p,q}$, $\mathcal{C}_{s,t}$ from first approach.

Let us now discuss the construction of the appropriate graphs of intersection for M. The construction for N works in the same way. The graph Γ_A is constructed in the 2-disc D_A with boundary $\partial D_A = \alpha$, and each $a_1, \dots, a_n, a_{n+1}, \dots, a_m$ corresponds to a fat vertex. Let α_1, α_2 (or $\alpha_1, \alpha_2, \alpha_3, \alpha_4$ for N) be the portions of α lying on B_1 (and B_2): they correspond to half vertices lying on ∂D_A. The edges of this graph correspond to the arc components of $A \cap C$. Note that the number of times α and γ wrap around the 1-handles of M is unspecified. Moreover, any points of intersection between α and γ can be pushed into the 1-handles. These intersections will appear on ∂D_A and are unlabelled. The labels at the endpoints of each edge specify the curves on which the edge starts or ends. All vertices of Γ_A, except for the ones on ∂D_A, intersect curves from $\mathcal{C}_{s,t}$ (except for γ) twice: on the front and on the back of M.

The graph Γ_B arising from $\mathcal{B}_{p,q}$ is constructed in the disc D_B with $\partial D_B = \beta$ in the same way, with its edges being the arc components of $B \cap C$.

Finally, the graph Γ_C is constructed in the disc D_C, also in the same way as the others. However, it differs from the previous graphs because it carries additional information, since it records arcs in $A \cap C$ and in $B \cap C$. Except for boundary vertices, this graph still contains fat vertices; however, the labels now belong to two different families, $\mathcal{A}_{m,n}$ and $\mathcal{B}_{p,q}$, and based on our previous discussion, we have no way of knowing a priori how they are distributed around a vertex of Γ_C. We remark that the discs D_A and D_B (and consequently A and B) are disjoint, so there are no edges in Γ_C connecting labels associated to $\mathcal{A}_{m,n}$ to those associated to $\mathcal{B}_{p,q}$.

There exist surjections $\Gamma_C \twoheadrightarrow \Gamma_A$ and $\Gamma_C \twoheadrightarrow \Gamma_B$ on the edges of the graphs. Indeed, every edge in Γ_A (Γ_B) corresponds to an edge in Γ_C with vertices and labels swapped. Note that there is no relation between Γ_A and Γ_B. The absence of a bijective relation between the graphs means that the only graph that gives a full picture of the intersections of the planar surfaces A, B, C is Γ_C. In general, this forces us to work with three graphs at the same time, which quickly becomes very complicated and limits our ability to deduce general properties as in previous chapters. Moreover, band slides and swims can still happen, and it is now even harder to understand how they impact the graphs and how to undo these moves. The difficulty of producing more than a couple of very simple examples of valid graph configurations in this setting is the reason for changing our approach to the $\mathbb{R}P^2$ problem.

§ 11.2 | Further Problems

Movie pictures and graphs of intersection can be employed to approach several questions about smooth embeddings of surfaces in 4-space, similar to the one discussed in this thesis.

Consider a smooth embedding of a sphere S^2 in $\mathbb{R}^4$ on which there is a Morse function with six critical points; this set-up is closely related to the one analysed by Scharlemann in [64]. One can ask if any such embedding of a sphere in 4-space is standard. In this case, the six critical points could correspond either to two minima, two saddles and two maxima; or to three minima, two saddles and one maximum (up to turning the Morse function "upside-down"). As there exist non-trivial examples of the first type of embedding (see [23, Example 9]), the answer to the question is no in general. However, one can investigate what happens when the embedding is of the second type. A movie picture of such an embedding consists of a 3-component unlink with two bands attached, resulting in an unknot. The fact that both bands are constrained to join the three different

components of the unlink could make this case slightly easier than ours, as there is a unique knot configuration underlying a movie picture, and one might hope to reduce this problem to the one discussed by Scharlemann in [64]. Once again, the presence of more than one band signifies that band sliding and swimming can take place, giving rise to the same type of issues discussed in this thesis.

Another similar question is presented in Kirby's problem list [42]. It concerns smooth embeddings of a torus T^2 in $\mathbb{R}^4$ with four critical points and whether they are standard or not. A movie representation of such a torus would consist of a single unknot to which two bands are attached, resulting in an unknot again. Band swims and band slides are always a concern, although it is interesting to point out that the latter do not alter the knot configuration underlying the movie picture. One possible way to approach this problem is by studying the intersections of the two discs resulting from the unknots. However, at first glance, it seems that this model does not always detect band slides. In the case in which the bands do not intersect the two discs (apart from their attaching areas), it seems that sliding only introduces additional twisting in the bands, which cannot be detected by the graphs constructed in the usual way. Solving this problem may be more complicated than the previous one, because it requires a completely new set-up and a way to detect the unknottedness of the torus.

Finally, another possible application of the techniques presented can be to links of knotted surfaces, suggested by Arunima Ray. For instance, we may consider how a sphere with two critical points and one with four embed in $\mathbb{R}^4$. These are both known to be individually standard, but one could investigate whether they can link with each other and thus give rise to non-standard embeddings. For embeddings of non-orientable surfaces, such as $\mathbb{R}P^2$, similar questions can be asked, although one needs to define an appropriate notion of linking. In all these cases one would work with movie representations of the relevant embeddings and the usual issues that come with them. For a case like the one presented for the spheres, one would not have to worry about band slides, so it seems that it might still be possible to tackle simple enough cases and isolate various issues.

Graphs of intersections have been and still are very valuable tools in 3-dimensional topology, and are worth considering when tackling smooth embedding problems in 4-space, although the combinatorics may often be challenging.

Bibliography

[1] Paolo Aceto, Marco Golla, and Kyle Larson. Embedding 3-manifolds in spin 4-manifolds. *J. Topol.*, 10(2):301–323, 2017. doi:10.1112/topo.12010.

[2] Paolo Aceto, Marco Golla, Kyle Larson, and Ana G. Lecuona. Surgeries on torus knots, rational balls, and cabling, 2020. URL: https://arxiv.org/abs/2008.06760, arXiv:2008.06760.

[3] Paolo Aceto, Duncan McCoy, and JungHwan Park. A survey on embeddings of 3-manifolds in definite 4-manifolds, 2024. URL: https://arxiv.org/abs/2407.03692, arXiv:2407.03692.

[4] Paolo Aceto, Duncan McCoy, and JungHwan Park. Definite fillings of lens spaces. *J. Differential Geom.*, 131(1):1–41, 2025. doi:10.4310/jdg/1755541518.

[5] James W. Alexander. On the subdivision of 3-space by a polyhedron. *Proceedings of the National Academy of Sciences of the United States of America*, 10(1):6–8, 1924. URL: http://www.jstor.org/stable/84201.

[6] Kenneth L. Baker, Dorothy Buck, and Ana G. Lecuona. Some knots in $S^1 \times S^2$ with lens space surgeries. *Communications in Analysis & Geometry*, 24(3):431–470, January 2016. doi:10.4310/CAG.2016.v24.n3.a1.

[7] Kenneth L. Baker, Cameron McA. Gordon, and John Luecke. Bridge number, Heegaard genus and non-integral Dehn surgery. *Trans. Amer. Math. Soc.*, 367(8):5753–5830, 2015. doi:10.1090/S0002-9947-2014-06328-9.

[8] Kenneth L. Baker, Cameron McA. Gordon, and John Luecke. Bridge number and integral Dehn surgery. *Algebr. Geom. Topol.*, 16(1):1–40, 2016. doi:10.2140/agt.2016.16.1.

[9] Steven Bleiler and Martin Scharlemann. Tangles, property P, and a problem of J. Martin. *Math. Ann.*, 273(2):215–225, 1986. doi:10.1007/BF01451402.

[10] Steven Bleiler and Martin Scharlemann. A projective plane in $\mathbb{R}^4$ with three critical points is standard. Strongly invertible knots have property P. *Topology*, 27(4):519–540, 1988. doi:10.1016/0040-9383(88)90030-4.

[11] Gerhard Burde, Heiner Zieschang, and Michael Heusener. *Knots*, volume 5 of *De Gruyter Studies in Mathematics*. De Gruyter, Berlin, extended edition, 2014.

[12] J. Scott Carter and Masahico Saito. *Knotted surfaces and their diagrams*, volume 55 of *Mathematical Surveys and Monographs*. American Mathematical Society, Providence, RI, 1998. doi:10.1090/surv/055.

[13] Anthony Conway, Patrick Orson, and Mark Powell. Unknotting nonorientable surfaces, 2024. URL: https://arxiv.org/abs/2306.12305, arXiv:2306.12305.

[14] Andrew Donald. Embedding Seifert manifolds in S^4. *Trans. Amer. Math. Soc.*, 367(1):559–595, 2015. doi:10.1090/S0002-9947-2014-06174-6.

[15] Andrew Donald and Brendan Owens. Concordance groups of links. *Algebr. Geom. Topol.*, 12(4):2069–2093, 2012. doi:10.2140/agt.2012.12.2069.

[16] Simon K. Donaldson. The orientation of Yang-Mills moduli spaces and 4-manifold topology. *J. Differential Geom.*, 26(3):397–428, 1987. URL: http://projecteuclid.org/euclid.jdg/1214441485.

[17] Allan L. Edmonds and Charles Livingston. Embedding punctured lens spaces in four-manifolds. *Comment. Math. Helv.*, 71(2):169–191, 1996. doi:10.1007/BF02566415.

[18] David B. A. Epstein. Embedding punctured manifolds. *Proceedings of the American Mathematical Society*, 16(2):175–176, 1965. URL: http://www.jstor.org/stable/2033837.

[19] Mario Eudave-Muñoz and Araceli Guzmán-Tristán. Toroidal surgeries and the genus of a knot. *Osaka J. Math.*, 56(3):549–575, 2019. URL: https://projecteuclid.org/euclid.ojm/1563242424.

[20] Jonathan D. Evans and Ivan Smith. Markov numbers and Lagrangian cell complexes in the complex projective plane. *Geom. Topol.*, 22(2):1143–1180, 2018. doi:10.2140/gt.2018.22.1143.

[21] Sergey M. Finashin. Exotic embeddings of $\#6\mathbb{R}\mathrm{P}^2$ in the 4-sphere. In *Proceedings of Gökova Geometry-Topology Conference 2008*, pages 151–169. Gökova Geometry/Topology Conference (GGT), Gökova, 2009.

[22] Sergey M. Finashin, Matthias Kreck, and Oleg Ya. Viro. Nondiffeomorphic but homeomorphic knottings of surfaces in the 4-sphere. In *Topology and geometry—Rohlin Seminar*, volume 1346 of *Lecture Notes in Math.*, pages 157–198. Springer, Berlin, 1988. doi:10.1007/BFb0082777.

[23] Ralph H. Fox. A quick trip through knot theory. In *Topology of 3-manifolds and related topics (Proc. The Univ. of Georgia Institute, 1961)*, pages 120–167. Prentice-Hall, Inc., Englewood Cliffs, NJ, 1961.

[24] David Gabai. Genus is superadditive under band connected sum. *Topology*, 26(2):209–210, 1987. doi:10.1016/0040-9383(87)90061-9.

[25] The GAP Group. *GAP – Groups, Algorithms, and Programming, Version 4.15.1*, 2025. URL: https://www.gap-system.org.

[26] Nakisa Ghanbarian and Stanislav Jabuka. Band-unknotting numbers and connected sums of knots, 2025. URL: https://arxiv.org/abs/2512.06299, arXiv:2512.06299.

[27] Patrick M. Gilmer and Charles Livingston. On embedding 3-manifolds in 4-space. *Topology*, 22(3):241–252, 1983. URL: https://www.sciencedirect.com/science/article/pii/0040938383900113, doi:10.1016/0040-9383(83)90011-3.

[28] Marco Golla and Brendan Owens. The farey tree and embeddings of lens spaces and rational balls in $\mathbb{CP}^2$, 2025. URL: https://arxiv.org/abs/2512.09183, arXiv:2512.09183.

[29] Marco Golla and Brendan Owens. On a class of 4-manifolds, after Kollár – Unpublished, 2026.

[30] Robert E. Gompf and András I. Stipsicz. *4-manifolds and Kirby calculus*, volume 20 of *Graduate Studies in Mathematics*. American Mathematical Society, Providence, RI, 1999. doi:10.1090/gsm/020.

[31] Cameron McA. Gordon. Combinatorial methods in Dehn surgery. In *Lectures at KNOTS '96 (Tokyo)*, volume 15 of *Ser. Knots Everything*, pages 263–290. World Sci. Publ., River Edge, NJ, 1997. URL: https://doi.org/10.1142/9789812796097_0010, doi:10.1142/9789812796097_0010.

[32] Cameron McA. Gordon and Richard A. Litherland. On the signature of a link. *Invent. Math.*, 47(1):53–69, 1978. doi:10.1007/BF01609479.

[33] Cameron McA. Gordon and John Luecke. Knots are determined by their complements. *J. Amer. Math. Soc.*, 2(2):371–415, 1989. doi:10.2307/1990979.

[34] Joshua Evan Greene. Combinatorial methods in low-dimensional topology, 2019. URL: https://sites.google.com/bc.edu/joshua-e-greene/home/mt-832-combinatorial-methods-in-low-dimensional-topology.

[35] Paul Hacking and Yuri Prokhorov. Smoothable del Pezzo surfaces with quotient singularities. *Compos. Math.*, 146(1):169–192, 2010. doi:10.1112/S0010437X09004370.

[36] Walter Hantzsche. Einlagerung von Mannigfaltigkeiten in euklidische Räume. *Math. Z.*, 43(1):38–58, 1938. doi:10.1007/BF01181085.

[37] Morris W. Hirsch. The imbedding of bounding manifolds in euclidean space. *Annals of Mathematics*, 74(3):494–497, 1961. URL: http://www.jstor.org/stable/1970293.

[38] Mark Hughes, Seungwon Kim, Maggie Miller, and Gheehyun Nahm. An irreducible real projective plane in the 4-sphere, 2026. URL: https://arxiv.org/abs/2605.12921, arXiv:2605.12921.

[39] Woohyeok Jo, Jongil Park, and Kyungbae Park. On lens spaces bounding smooth 4-manifolds with $\boldsymbol{b_2 = 1}$, 2024. URL: https://arxiv.org/abs/2410.22719, arXiv:2410.22719.

[40] Woohyeok Jo, Jongil Park, and Kyungbae Park. Algebraic Montgomery-Yang problem and smooth obstructions. *Trans. Amer. Math. Soc.*, 378(4):2969–3003, 2025. doi:10.1090/tran/9364.

[41] Atsuko Katanaga, Osamu Saeki, Masakazu Teragaito, and Yuichi Yamada. Gluck surgery along a 2-sphere in a 4-manifold is realized by surgery along a projective plane. *Michigan Math. J.*, 46(3):555–571, 1999. doi:10.1307/mmj/1030132479.

[42] Robion Kirby. Problems in low-dimensional topology, 1995. URL: https://people.brandeis.edu/~ruberman/K2.pdf.

[43] Robion C. Kirby. *The topology of* 4*-manifolds*, volume 1374 of *Lecture Notes in Mathematics*. Springer-Verlag, Berlin, 1989. doi:10.1007/BFb0089031.

[44] János Kollár. Is there a topological bogomolov–miyaoka–yau inequality? *arXiv: Algebraic Geometry*, 2006. URL: https://api.semanticscholar.org/CorpusID:18236693.

[45] Peter B. Kronheimer and Tomasz S. Mrowka. Witten's conjecture and property P. *Geom. Topol.*, 8:295–310, 2004. doi:10.2140/gt.2004.8.295.

[46] Terry Lawson. Detecting the standard embedding of $\mathbf{R}\mathrm{P}^2$ in S^4. *Math. Ann.*, 267(4):439–448, 1984. doi:10.1007/BF01455961.

[47] Tye Lidman, Allison H. Moore, and Mariel Vazquez. Distance one lens space fillings and band surgery on the trefoil knot. *Algebr. Geom. Topol.*, 19(5):2439–2484, 2019. doi:10.2140/agt.2019.19.2439.

[48] Francesco Lin. The surgery exact triangle in Pin(2)-monopole Floer homology. *Algebr. Geom. Topol.*, 17(5):2915–2960, 2017. doi:10.2140/agt.2017.17.2915.

[49] Paolo Lisca. Lens spaces, rational balls and the ribbon conjecture. *Geom. Topol.*, 11:429–472, 2007. doi:10.2140/gt.2007.11.429.

[50] Paolo Lisca. Sums of lens spaces bounding rational balls. *Algebr. Geom. Topol.*, 7:2141–2164, 2007. doi:10.2140/agt.2007.7.2141.

[51] Paolo Lisca and Andrea Parma. On stein rational balls smoothly but not symplectically embedded in $\mathbb{C}\mathbb{P}^2$. *Bulletin of the London Mathematical Society*, 54(3):949–960, 2022. URL: https://londmathsoc.onlinelibrary.wiley.com/doi/abs/10.1112/blms.12607, arXiv:https://londmathsoc.onlinelibrary.wiley.com/doi/pdf/10.1112/blms.12607, doi:10.1112/blms.12607.

[52] Richard A. Litherland. Surgery on knots in solid tori. II. *J. London Math. Soc. (2)*, 22(3):559–569, 1980. doi:10.1112/jlms/s2-22.3.559.

[53] John Luecke. Notes on the knot complement problem – Unpublished, 1989.

[54] Daniel Matignon and Nabil Sayari. Non-orientable surfaces and Dehn surgeries. *Canad. J. Math.*, 56(5):1022–1033, 2004. doi:10.4153/CJM-2004-046-9.

[55] Daniel Matignon and Nabil Sayari. Klein slopes on hyperbolic 3-manifolds. *Math. Proc. Cambridge Philos. Soc.*, 143(2):419–447, 2007. doi:10.1017/S0305004107000229.

[56] John Milnor. *Morse theory*, volume No. 51 of *Annals of Mathematics Studies*. Princeton University Press, Princeton, NJ, 1963. Based on lecture notes by M. Spivak and R. Wells.

[57] Jin Miyazawa. A gauge theoretic invariant of embedded surfaces in 4-manifolds and exotic p^2-knots. 2023. URL: https://arxiv.org/abs/2312.02041, arXiv:2312.02041.

[58] Brendan Owens. Equivariant embeddings of rational homology balls. *Q. J. Math.*, 69(3):1101–1121, 2018. doi:10.1093/qmath/hay016.

[59] Brendan Owens. Smooth, nonsymplectic embeddings of rational balls in the complex projective plane. *Q. J. Math.*, 71(3):997–1007, 2020. doi:10.1093/qmathj/haaa013.

[60] Peter Ozsváth and Zoltán Szabó. Absolutely graded Floer homologies and intersection forms for four-manifolds with boundary. *Adv. Math.*, 173(2):179–261, 2003. doi:10.1016/S0001-8708(02)00030-0.

[61] Peter Ozsváth and Zoltán Szabó. On the Heegaard Floer homology of branched double-covers. *Adv. Math.*, 194(1):1–33, 2005. doi:10.1016/j.aim.2004.05.008.

[62] Steven P. Plotnick. Fibered knots in S^4—twisting, spinning, rolling, surgery, and branching. In *Four-manifold theory (Durham, N.H., 1982)*, volume 35 of *Contemp. Math.*, pages 437–459. Amer. Math. Soc., Providence, RI, 1984. doi:10.1090/conm/035/780592.

[63] Daniel Ruberman. Imbedding punctured lens spaces and connected sums. *Pacific J. Math.*, 113(2):481–491, 1984. URL: http://projecteuclid.org/euclid.pjm/1102709207.

[64] Martin Scharlemann. Smooth spheres in $\mathbf{R}^4$ with four critical points are standard. *Invent. Math.*, 79(1):125–141, 1985. doi:10.1007/BF01388659.

[65] Martin Scharlemann. Unknotting number one knots are prime. *Invent. Math.*, 82(1):37–55, 1985. doi:10.1007/BF01394778.

[66] Alexandru Scorpan. *The wild world of 4-manifolds*. American Mathematical Society, Providence, RI, 2005.

[67] Frank J. Swenton. On a calculus for 2-knots and surfaces in 4-space. *J. Knot Theory Ramifications*, 10(8):1133–1141, 2001. doi:10.1142/S0218216501001359.

[68] Abigail Thompson. Property P for the band-connect sum of two knots. *Topology*, 26(2):205–207, 1987. doi:10.1016/0040-9383(87)90060-7.

[69] Vladimir G. Turaev. Classification of oriented Montesinos links by means of invariants of spin structures. volume 143, pages 130–146, 178. 1985. Studies in topology, V.

[70] Kurt van Reidemeister. Homotopieringe und linsenräume. *Abhandlungen aus dem Mathematischen Seminar der Universität Hamburg*, 11:102–109, 1935. URL: https://api.semanticscholar.org/CorpusID:124078064.

[71] Oleg Ja. Viro. Local knotting of sub-manifolds. *Mat. Sb. (N.S.)*, 90(132):173–183, 325, 1973.

[72] Charles T. C. Wall. All 3-manifolds imbed in 5-space. *Bull. Amer. Math. Soc.*, 71:564–567, 1965. doi:10.1090/S0002-9904-1965-11332-5.

[73] E. Christian Zeeman. Twisting spun knots. *Trans. Amer. Math. Soc.*, 115:471–495, 1965. doi:10.2307/1994281.